The Thesis Committee for Adolfo Lozano III
Certifies that this is the approved version of the following thesis:

Analysis of a Novel Thermoelectric Generator in the Built Environment

APPROVED BY
SUPERVISING COMMITTEE:

Supervisor:

Michael E. Webber

Philip S. Schmidt

Analysis of a Novel Thermoelectric Generator in the Built Environment

by

Adolfo Lozano III, B.S.M.E.

Thesis

Presented to the Faculty of the Graduate School of

The University of Texas at Austin

in Partial Fulfillment

of the Requirements

for the Degree of

Master of Science in Engineering

The University of Texas at Austin

August 2011

Dedication

To Dad, Mom, Steve, and my favoritest little sister in the whole wide world, Lily.

Acknowledgements

This body of work could not have been produced without the help of many bright individuals along the way. I was fortunate enough to have crossed paths with every single one of the following people.

First, I would like to thank *Two Seven Ventures LLC*, a private investment company based in Aspen, Colorado, for their financial support of this research. Additionally, I would like to thank Mr. Mike Helms of *Nextek Power Systems*, a DC power company based in Detroit, Michigan, and Mr. Garth Schultz of *Power Panel Inc.*, a solar panel manufacturer also based in Detroit, Michigan, for answering all my questions throughout this research.

I am also indebted to Dr. Gary C. Vliet for his extensive guidance on my thermodynamic analysis of the solar-thermal energy system (Chapter 3), as well as to Dr. Philip S. Schmidt for his advice on my thermodynamic analysis of the thermoelectric generator itself (Chapter 4). (In fact, Dr. Schmidt gets two mentions, as he served as a mentor to me during my graduate school career, and was an excellent and invaluable supervisor to me during my first year of graduate school as his teaching assistant.) They were extremely helpful and insightful, did not hesitate spending considerable time helping me. These two professors essentially served as secondary advisors to me during this study.

Mr. Phillip C. Watts of *Watts Thermoelectric LLC*, patent application holder of the novel thermoelectric generator that this study was centered on, certainly deserves a great deal of recognition. Mr. Watts is one of the most intelligent and humble people I've ever met and have the utmost respect for him. He and his wife opened their doors to me during my two-day travel to Longmont, CO in November 2010, the trip of which was

graciously supported by *Two Seven Ventures LLC*. Throughout this project's timeline, Mr. Watts provided me with the technical advice and support that was absolutely essential to me completing this study. He spent many hours on the phone with me discussing this project, answered hundreds of emails in a timely fashion—and most importantly—was happy to help every step of the way.

Throughout the progression of this study, I also consulted with several graduate school peers for technical help. These individuals were: Mr. Ravi I. Singh, who provided me with useful input while constructing my numerical model; Dr. Sanjiv E. Shah, who gave me useful input during the initial stages of my thermodynamic analyses; and Mr. Felix Gutierrez Jr., who gladly and clearly answered all my kindergarten-level electrical-related questions.

I must also thank my colleagues of the *Webber Energy Group* for their intellectual contributions to this research: Mr. Stuart M. Cohen and Mr. John R. Fyffe, for their considerable help and direction on my emissions analysis (Section 5.1); Ms. Melissa C. Lott, Mr. Aaron K. Townsend, Mr. Charles M. Upshaw, and Mr. Jared B. Garrison, for their advice and guidance on my economic analysis (Section 5.2); Mr. David M. Wogan, for pointing me to the proper insolation data source; Mr. Jared B. Garrison (receives two mentions), for his direction and advice on writing this body of work; and finally Mrs. Anne C. Lynch and Ms. Tina S. Vazquez, who both graciously helped me with 1,001 administrative items throughout the year, and were happy to do so. All of these individuals are very helpful people that genuinely care for their peers' progress and success. Further, their technical expertise essentially made them unofficial advisors to me during this study; I could not have completed this study without their collective input.

I am also greatly indebted to Dr. Michael E. Webber, who not only was my advisor during this year-long study, but also a mentor to me during my graduate school

career. I have had many amazing opportunities exclusively because of Dr. Webber, for which I am immensely grateful for, including: attending the AAAS 2011 Annual Meeting in Washington, D.C.; meeting with distinguished representatives from various organizations such as the White House Council on Environmental Quality (CEQ), NASA, and Citizens for Affordable Energy; touring a local power plant and recycling facility; and most importantly, presenting this research at the AIAA 9th International Energy Conversion Engineering Conference (IECEC) in San Diego, CA in August 2011. After a year of working with him, I learned that aside from being a great and successful advisor and leader, Dr. Webber is sincerely one of the nicest and most caring human beings I have ever met. It is for these reasons that I was truly lucky to have been part of the *Webber Energy Group*.

I also thank Dad, Mom, my younger brother, Steve, and my little sister, Lily. They are my neverending sources of love and support, and have been there *for* me and *with* me every step of the way. I love them with all my heart, and always will. Had it not been for them, there is no doubt in my mind that I would not be where I am today.

Finally, and most importantly, I give the utmost gratitude to The Creator, who sustains me on a daily basis. I have been extremely blessed in every aspect of my life, and give all the glory to Him. My few successes and accomplishments have come through Him and Him alone:

"I am strong, when I am on Your shoulders,
You raise me up to more than I can be."

Abstract

Analysis of a Novel Thermoelectric Generator in the Built Environment

Adolfo Lozano III, M.S.E.

The University of Texas at Austin, 2011

Supervisor: Michael E. Webber

This study centered on a novel thermoelectric generator (TEG) integrated into the built environment. Designed by *Watts Thermoelectric LLC*, the TEG is essentially a novel assembly of thermoelectric modules whose required temperature differential is supplied by hot and cold streams of water flowing through the TEG. Per its recommended operating conditions, the TEG nominally generates 83 Watts of electrical power. In its default configuration in the built environment, solar-thermal energy serves as the TEG's hot stream source and geothermal energy serves as its cold stream source. Two systems-level, thermodynamic analyses were performed, which were based on the TEG's upcoming characterization testing, scheduled to occur later in 2011 in Detroit, Michigan.

The first analysis considered the TEG coupled with a solar collector system. A numerical model of the coupled system was constructed in order to estimate the system's annual energetic performance. It was determined numerically that over the course of a sample year, the solar collector system could deliver 39.73 megawatt-hours (MWh) of

thermal energy to the TEG. The TEG converted that thermal energy into a net of 266.5 kilowatt-hours of electricity in that year. The second analysis focused on the TEG itself during operation with the purpose of providing a preliminary thermodynamic characterization of the TEG. Using experimental data, this analysis found the TEG's operating efficiency to be 1.72%.

Next, the annual emissions that would be avoided by implementing the zero-emission TEG were considered. The emission factor of Michigan's electric grid, RFCM, was calculated to be 0.830 tons of carbon dioxide-equivalent (CO_2e) per MWh, and with the TEG's annual energy output, it was concluded that 0.221 tons CO_2e would be avoided each year with the TEG. It is important to note that the TEG can be linearly scaled up by including additional modules. Thus, these benefits can be multiplied through the incorporation of more TEG units.

Finally, the levelized cost of electricity (LCOE) of the TEG integrated into the built environment with the solar-thermal hot source and passive ground-based cold source was considered. The LCOE of the system was estimated to be approximately $8,404/MWh, which is substantially greater than current generation technologies. Note that this calculation was based on one particular configuration with a particular and narrow set of assumptions, and is not intended to be a general conclusion about TEG systems overall. It was concluded that while solar-thermal energy systems can sustain the TEG, they are capital-intensive and therefore not economically suitable for the TEG given the assumptions of this analysis. In the end, because of the large costs associated with the solar-thermal system, waste heat recovery is proposed as a potentially more cost-effective provider of the TEG's hot stream source.

Table of Contents

List of Tables

List of Figures

Nomenclature

a_s	Solar azimuth angle
a_w	Solar collector azimuth angle
A	Aperture area of solar collector; Surface area
B	Equation of time angle
c_P	Isobaric specific heat capacity (assumed to be $c_P =$ 4,190 J/kg-K for water)
C	Empirical sky diffuse factor; Arbitrary constant
CAP	Capacity
$CAPEX$	Capital expense
CF	Capacity factor
D	Depth; Diameter
$\dot{E}_{GEN}$	Change in time of energy generated in control volume
$\dot{E}_{IN}$	Heat transfer rate entering control volume
$\dot{E}_{OUT}$	Heat transfer rate exiting control volume
$\dot{E}_{STOR}$	Change in time of energy stored in control volume
E	Electrical energy
EF	Emission factor
ET	Equation of time
f( )	A function of
F, F'	Insolation factor
$G_T(t)$	Insolation incident on tilted collector (time-dependent)
h	Enthalpy
h_s	Solar hour angle

H	Height
i	Incidence angle; Interest/discount rate
I	Insolation
k	Thermal conductivity
$\dot{L}$	Thermal power load
LAT	Geographic latitude
$LCOE$	Levelized cost of electricity/energy
$LONG$	Geographic longitude
$\dot{m}$	Mass flow rate
m	Mass; Slope of solar efficiency curve
n	Number of solar collectors; Day number; n^{th} time step; Number of interest periods
$OPEX$	Operational and maintenance expenses
P	Electrical power output; Pump; Emissions; Price per Watt
$\dot{Q}$	Heat transfer rate
$\dot{Q}_U$	Useful energy collected by collector (over a time interval)
R	Insolation tilt factor
S	Seebeck coefficient
STM	Standard Time Meridian
t	Time; Thickness
T	Temperature
U	Overall heat transfer coefficient
V	Volume
$\dot{V}$	Volumetric flow rate
W	Width

ZT	Figure of merit

Greek Letters

α	Solar altitude angle
β	Solar collector tilt angle
δ_s	Solar declination angle
Δ	Differential or change in (defined as $OUT - IN$)
η_0	Maximum insolation efficiency of solar collector
η_{MAX}	Maximum efficiency of a thermoelectric device
λ	Eigenvalue of ODE
ρ	Density (assumed to be $\rho = 1{,}000\ \mathrm{kg/m^3}$ for water); Radiation reflectance
σ	Electrical conductivity

Subscripts

AMB	Ambient
B, b	Beam (direct) insolation
C	Cold stream; Collected
C,L	Cold stream convective losses
D, d	Diffuse insolation
GEN	Generated
GHP	Geothermal heat pump
$GSHP$	Ground source heat pump
H	Hot stream; Horizontal collector surface
HE	Heat engine

H,L	Hot stream convective losses
IN	Inlet (of stream or loop); Entering
$LOSS$	Convective loss
LM	Log mean
N	Normal insolation
OUT	Outlet (of stream or loop); Exiting
R, r	Reflected insolation
S	Thermal storage tank; Summer
SC	Solar collector
SYS	System
T	Tilted collector surface
U	Useful; Used
TEG	Thermoelectric generator (TEG)
TOT	Total
W	Winter

Acronyms, Abbreviations, and Units

AHRI	Air Conditioning, Heating, and Refrigeration Institute
ASHRAE	American Society of Heating, Refrigerating, and Air-Conditioning Engineers
CPI	Consumer Price Index
CV	Control volume
DC	Direct current
DXHP	Direct geoexchange heat pump
EERE	Office of Energy Efficiency and Renewable Energy

EIA	U.S. Energy Information Administration
EPA	U.S. Environmental Protection Agency
gpm	Gallons per minute
GHP	Geothermal heat pump
GSHP	Ground source heat pump
kWh	Kilowatt-hour
LCOE	Levelized cost of electricity/energy
MW	Megawatt
MWh	Megawatt-hour
NERC	North American Electric Reliability Corporation
NOAA	National Oceanic and Atmospheric Administration
NREL	National Renewable Energy Laboratory
O&M	Operational and Maintenance
PE	Polyethylene
PSI	Pounds per square inch
PVT	Photovoltaicthermal
RFCM	Reliability First Corporation–Michigan Electric Grid
TEG	Thermoelectric generator
Vdc	Voltage from a direct current
W	Watt

Chapter 1: Introduction

1.1 Survey of Renewable Energy for Electricity Generation

1.1.1 Renewable Energy and Fossil Fuels Defined

Renewable energy refers to any source of energy that is either naturally and continually replenished (in short geologic time scales) or simply inexhaustible and can therefore be sustained indefinitely [1]. Examples of renewable energy sources include biomass (i.e., organic matter), water (hydropower), hydrogen, the earth's subsurface (geothermal), wind, and solar radiation [1, 2]. (Note that nuclear energy is not considered a renewable energy source by this definition.) Biomass sources (e.g., wood, crops, and waste) can either be used to produce biofuels like ethanol or biodiesel, or can be combusted directly for electricity generation; flowing waters can be dammed for hydropower, whereas oceans' large temperature gradients across their depth can be harnessed for electricity generation; fuel cells produce electricity with a constant supply of hydrogen; geothermal temperature gradients are exploited by ground source heat pumps to heat or cool spaces; wind can be harnessed via wind turbines; and finally, solar radiation can be used to generate electrical energy via photovoltaics, or thermal energy via solar-thermal energy systems [1, 2].

In contrast to renewable energy sources, there exist conventional or nonrenewable energy sources, namely fossil fuels. Note that the term "fossil fuel" is a broad term that chiefly includes coal, petroleum, and natural gas. In particular, fossil fuels refer to organic matter (i.e., plants or animals) that existed millions of years ago and have since been buried in the subsurface and preserved between layers of sediment as a result of geologic processes. Over time, said fossils are exposed to intense temperatures and pressures, resulting in the breakdown of the organic matter via biochemical processes.

Depending on factors like the age of the fossils and range of temperatures and pressures they have been subjected to, these fossils exist today as combustible hydrocarbons in either solid form (coal), liquid form (petroleum), or in gaseous form (natural gas), all of which are burned for energy generation. In fact, the majority of petroleum (i.e., oil) and natural gas (i.e., methane) available today is from organic matter dating back to the Early Cretaceous and Late Jurassic Periods—that is, 88.5–119 and 144–169 millions of years ago, respectively [3, 4].

1.1.2 A Motivation for Renewable Energy: Emissions and Environmental Considerations

One of the key problems with fossil fuels is their emission of greenhouse gases when burned. Not all fossil fuels produce equal emissions per unit volume or mass of fossil fuel burned; coal, for example, is more carbon-intensive than natural gas and thus emits much more pollution. (In fact, natural gas is generally hailed as a much "cleaner" fossil fuel than coal or petroleum.) Principal air pollutants include CO_2 (carbon dioxide), CH_4 (methane), N_2O (nitrous oxide), and fluorinated gases (hydrofluorocarbons, perfluorocarbons, and sulfur hexafluoride) [5]. Of these emissions, CO_2 has been historically responsible for more than 80% of the total emissions[1], while CH_4 has been responsible for roughly 10% [6]. Other pollutants include CO (carbon monoxide), NO_x (nitrogen oxides), SO_x (sulfur oxides), Hg (mercury), and particulate matter. Moreover, these gases each have different global warming potentials; fluorinated gases, for example, have a severely greater global warming potential than CH_4, which in turn has a greater global warming potential than CO_2.

[1] Over the past two decades; based on per unit mass of pollutants' carbon dioxide equivalent emissions, where all gases have been normalized in order to compare their emissions based on global warming potentials

The negative environmental impacts of emissions are well-documented. For example, sulfur dioxide (SO_2), the nitrogen oxides, and particulates are known to cause serious respiratory illnesses, while mercury can contaminate bodies of water and result in severe environmental hazards [7]. In addition to these detrimental environmental effects, global climate change is no longer a disputable phenomenon as it was in the past. The scientific consensus now holds that the burning of fossil fuels increases the concentration of greenhouse gases in the atmosphere, which in turn has unequivocally raised the global temperature [8].

Although there exist solutions to our emissions dilemma like cap and trade or carbon taxation, these are only temporary solutions that simply mitigate the emissions problem rather than fix it. In fact, this is one of the greatest benefits of renewable energy sources—they produce zero emissions (with the exception of biomass). As a result, renewable energy generation technologies are generally considered to be environmentally-friendly. This is one of the motivations for utilizing renewable energy sources, and this study is centered on such an energy generation technology.

1.1.3 Limitations to Renewable Energy Sources

Of course, renewable energy sources have their limitations. First, they are intermittent sources of energy subject to meteorological conditions. For example, wind fluctuates throughout the day and can even be minimal on certain days; similarly, the solar radiation incident on the earth's surface is dependent on cloudiness, and droughts reduce the amount of water available [1]. Therefore, although sustainable energy sources, renewable energy sources are not continuously available in the same capacity.

More importantly, energy generation technologies that utilize renewable energy sources are traditionally more expensive than their fossil fuel counterparts [1]. Renewable energy sources are well-known for their high capital costs and thus generally regarded as capital-intensive. In fact, levelized costs per unit energy generated are generally two- to three-times greater on average for power plants utilizing renewable energy sources than fossil fuels [9]. As a result, although renewable energy generation is an attractive option, prices will have to decrease in order to be economically competitive with traditional fossil fuel energy generation.

1.1.4 Survey of U.S. Annual Energy Consumption and the Electric Power Sector by Energy Source

Of the 98 Quadrillion BTU ($98 \cdot 10^{15}$ BTU) of energy consumed by the U.S. across all sectors[2] in 2010, more than 80% was supplied by fossil fuels [1], as shown in Figure 1.1. In contrast, renewable energy sources only accounted for 8%; and of this 8%, biomass and hydropower constituted 84% of renewable energy sources.

[2] As categorized by the EIA, sectors include residential, commercial, industrial, transportation, and electric power generation

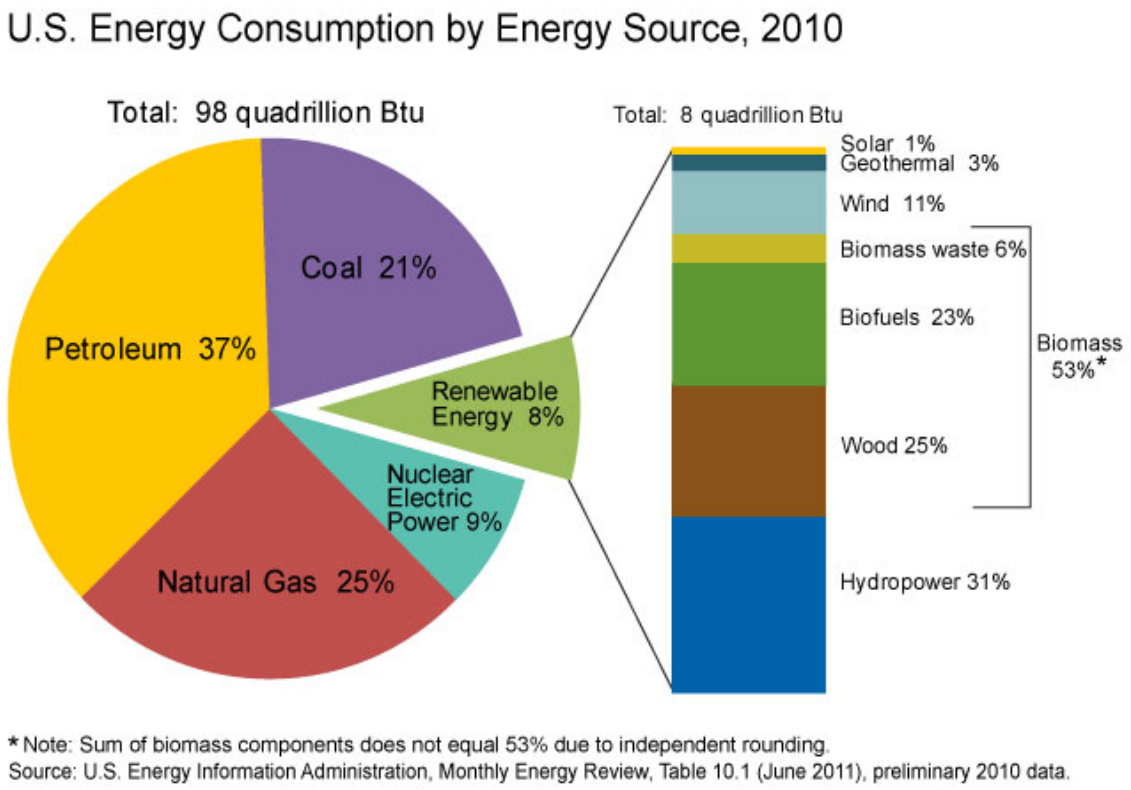

Figure 1.1: U.S. energy consumption by energy source across all sectors in 2010 [1]. The vast majority of the nation's energy was supplied by fossil fuels—namely petroleum, coal, and natural gas. (Note that the correct source is Table 2.1 of the EIA's June 2011 Monthly Energy Review.)

Furthermore, since this study revolved around electricity generation, the U.S. electric power sector was of particular interest. As shown in Figure 1.2, fossil fuels—namely coal and natural gas—also dominate the electric power sector, supplying nearly three-quarters of the electricity generated [10]. In contrast, renewable energy sources only constitute roughly 10%.

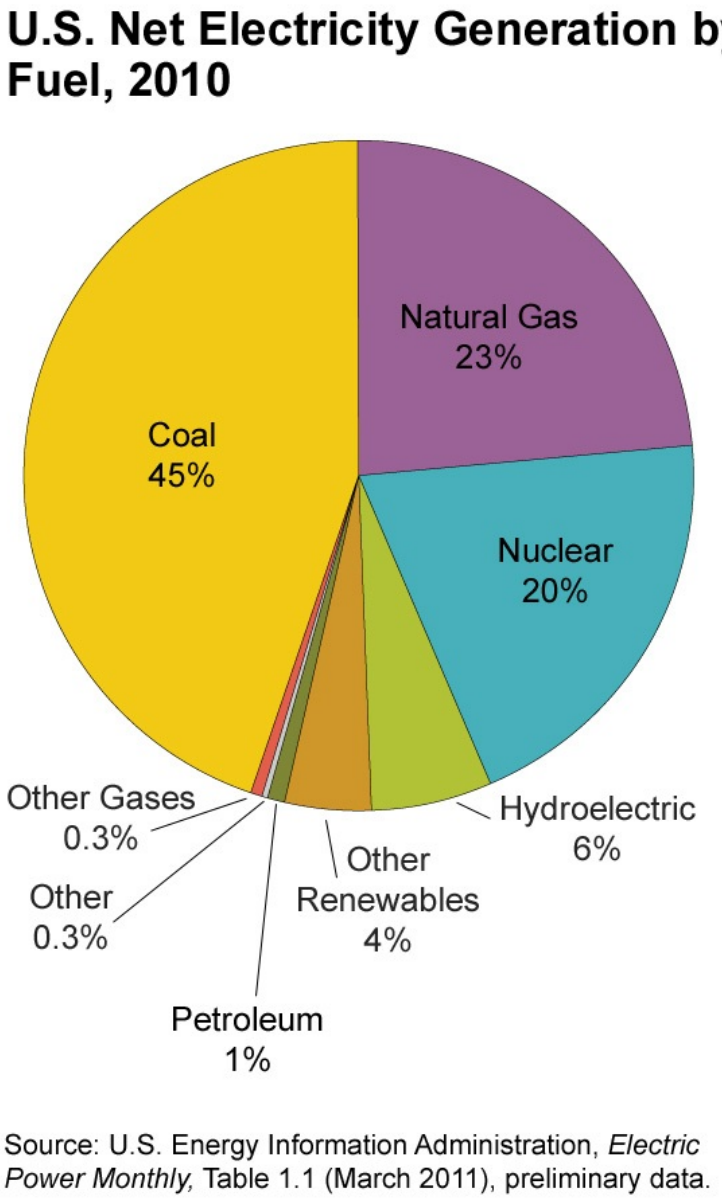

Figure 1.2: U.S. net electricity generation by fuel in 2010 [10]. In the electric power sector, coal has historically been the most common energy source, followed by natural gas and nuclear energy.

In their Annual Energy Outlook 2011, the U.S. Department of Energy's Energy Information Administration (EIA) predicts that electricity generation from renewable energy sources will increase by a staggering 72% from 2009 until 2035 [11]. In

particular, wind and biomass will be responsible for the majority of renewable energy sources. This rapid growth will be primarily the result of state renewable portfolio standards and federal tax credits. However, renewables will still constitute a small percentage of the nation's overall generation mix, from 11% in 2009 to 14% in 2035.

Accordingly, coal is expected to remain the largest contributor to electricity generation in 2035, as can be deduced from Figure 1.2. Generation from coal is expected to increase by 25% but its overall contribution to the nation's fuel mix will drop from 45% in 2009 to 43% in 2035. Additionally, natural gas will also have substantial growth, rising from 23% in 2009 to 25% in 2035. (Interestingly, natural gas-fired plants will have the largest growth in capacity, responsible for 60% for capacity additions between 2010 and 2035; this growth rate compares to 25% for renewables, 11% for coal-fired plants, and 3% for nuclear plants. This is in part driven by low natural gas prices and relatively low capital costs, making it more attractive than coal.) Finally, nuclear energy is expected to grow by 9%, but will drop in its overall contribution to the fuel mix from 20% in 2009 to 17% in 2011.

These expected trends are depicted in Figure 1.3.

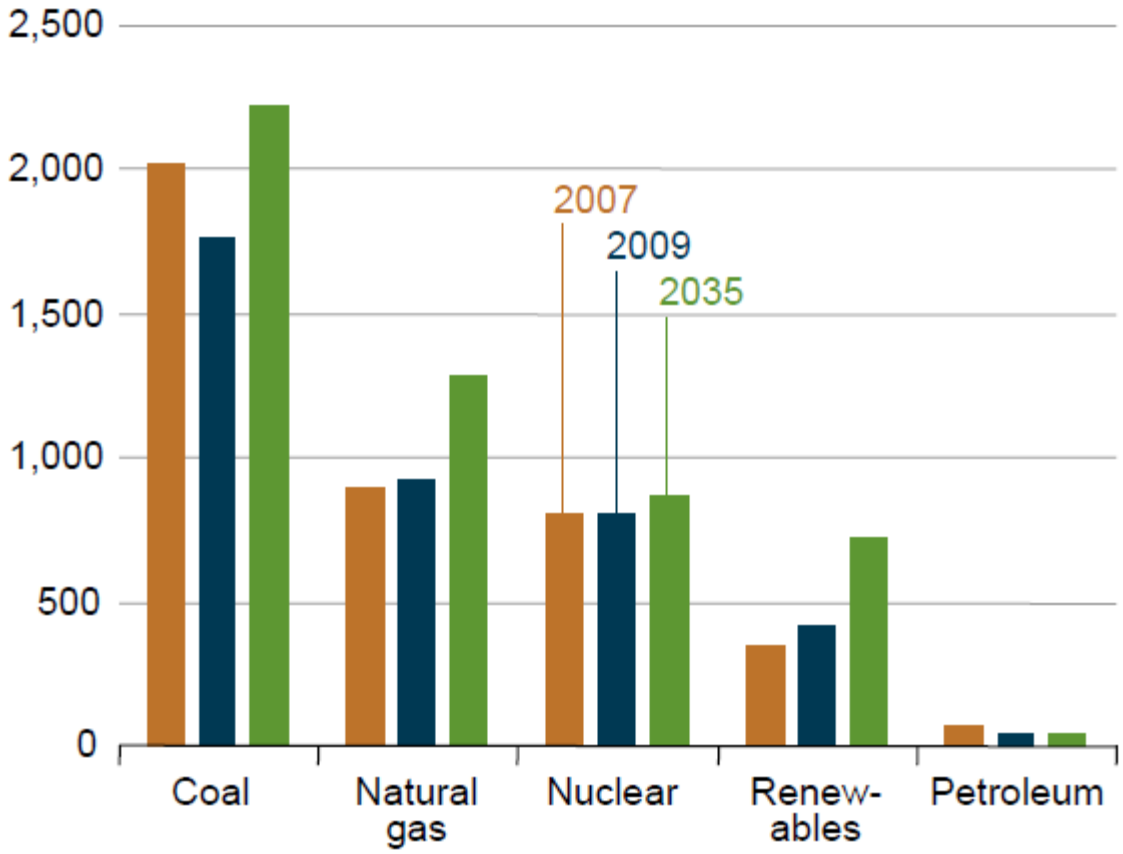

Figure 1.3: Expected trends to 2035 in electricity generation by fuel source [11]. Of all energy sources in the U.S. electric power sector, renewables are expected to have the most rapid growth due to state policies and federal tax credits. However, in spite of this growth, coal is expected to still be the predominant fuel source at least until 2035.

1.2 SCOPE AND ROADMAP OF STUDY

This study is centered on a novel thermoelectric generator (TEG) integrated into the built environment, in which renewable energy sources served as the TEG's hot and cold sources. Solar-thermal energy served as the TEG's hot source and geothermal energy served as the TEG's cold source. In this default configuration in the built environment, a systems-level, first-order, first law thermodynamic analysis was performed on two different systems.

The first analysis (Chapter 3) focused on the solar-thermal energy system as it operated while coupled with the TEG. The goal of this analysis was to quantify the annual electricity generated, as well as to calculate the annual amount of thermal energy collected by the solar-thermal system. This was accomplished by performing a control volume analysis on the solar collector system and constructing a numerical model.

The second thermodynamic analysis (Chapter 4), which focused on the TEG itself, had the goal of thermodynamically characterizing the novel TEG during operation. This preliminary characterization of the TEG was realized by performing various control volume analyses in order to determine expressions for the internal heat transfer taking place within the TEG during operation. Heat transfer parameters were quantified via experimental data.

Additionally, although the TEG was designed to operate with a geothermal energy system while integrated in the built environment, this system was not considered in this study (Section 3.6). Although geothermal energy systems are briefly outlined and quantified based on experimental data, an in-depth analysis of the same breadth as the previous two analyses was not performed.

An emissions analysis followed (Section 5.1), where the environmental impact of the zero-emission TEG was considered. This analysis resulted in determining the amount

of carbon dioxide-equivalent emissions that would be avoided by implementing any number of TEGs.

The final analysis considered the economics of the TEG in the built environment (Section 5.2). The goal of this analysis was to evaluate the cost-competitiveness of the TEG as an energy generation technology by determining its levelized cost of electricity (LCOE). In this analysis, the LCOEs of all three subsystems—the solar-thermal energy system, the TEG itself, and the geothermal energy system—were calculated and summed to provide a levelized cost of the integrated system operating in the built environment.

Figure 1.4 provides a high-level flow chart of the four major analyses performed in this study.

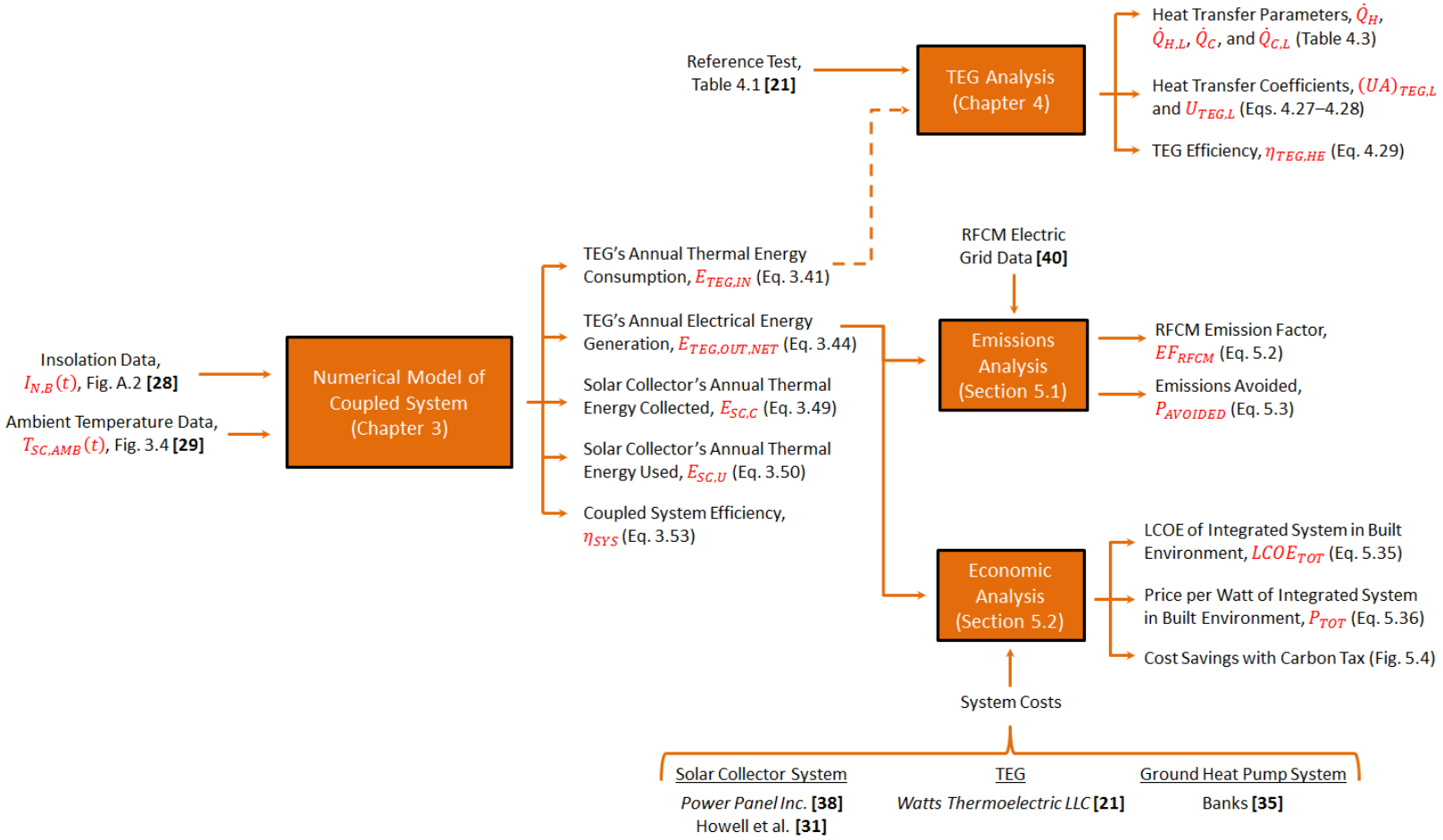

Figure 1.4: Roadmap of analyses performed in this study. All results are summarized in Chapter 6. Note how different energy terms correspond to thermal or electrical energy.

Chapter 2: The Novel Thermoelectric Generator

2.1 INTRODUCTION TO THERMOELECTRICS

2.1.1 The Thermoelectric Effect

The thermoelectric effect is the underlying scientific phenomenon that provides the underpinning for this work. It is collectively attributed to three separate but related observed phenomena: the Seebeck Effect, the Peltier Effect, and the Thomson Effect.

The Seebeck Effect, credited to Thomas Johann Seebeck, can be effectively summarized as the resulting voltage generated from establishing a temperature difference across a semiconductor (or conductor). In the case where only one semiconductor is used (as implied in the aforestated definition), the voltage difference is independent of the established temperature difference [12]. If, on the other hand, two dissimilar semiconductors are connected in series and a temperature differential is applied across their two junctions, then the resultant voltage is a function of the temperature difference. This effect is in fact the same operating principle for thermocouples. Thus, the Seebeck Effect can be considered to be the generation of an electric current from establishing a temperature differential across the junctions [13].

The Peltier Effect, discovered by Jean-Charles Peltier, is illustrated by considering a closed circuit made of two dissimilar semiconductors (or conductors). If current is allowed to flow through the circuit from an external source (i.e., an externally-applied EMF, like a battery), then the temperature at one junction will rise and the other will fall [13]. This phenomenon is called the Peltier Effect. As current flows through the semiconductor, the quantity of heat that must be removed from (or added to) the junction in order to maintain a constant junction temperature is known as the reversible Peltier

Heat. This quantity should not to be confused with normal heat conduction by electrons [12] or I^2R Joule heating [14], both of which are irreversible.

Finally, the Thomson Effect, discovered by William Thomson (Lord Kelvin), is illustrated by considering a single semiconductor for which a temperature and voltage difference has been established. As current flows through the semiconductor, three components of heat exist, similar to the Peltier Effect: the irreversible normal heat conduction by electrons [12], the irreversible I^2R Joule heating [12, 14], and finally the reversible Thomson Heat.

2.1.2 Thermoelectric Devices

The thermoelectric couple is the basic building block of all thermoelectric devices (see Figure 2.1) and consists of two semiconductors (n-type and p-type), connected electrically in series and thermally in parallel with metallic junctions to form a closed circuit. A thermoelectric device is comprised of hundreds of thermoelectric couples connected in series to produce a significant current. Thermoelectric devices can be operated in power generation mode, per the Seebeck Effect, or in reverse in cooling mode, per the Peltier Effect. In this study, only the former mode was of interest.

2.1.2.1 Physical Mechanism

In conventional power generation mode, heat is applied to one junction of a thermoelectric couple, thus establishing a temperature differential across its two junctions (see Figure 2.1). Upon heating, electron/hole pairs are formed at the hot end, absorbing heat [15]. These charge carriers diffuse across their respective semiconductors (electrons in the n-type and electron holes in the p-type) to the cold junction, carrying heat with

them. This transfer causes a charge accumulation at the cold side, building an internal electric field that resists diffusion [12], thereby generating an electric potential. The electron/hole pairs finally recombine at the cold junction, rejecting heat [15]. Thus, the end result of charge carriers' direction of motion is the generation of a clockwise direct current (DC) in the circuit.

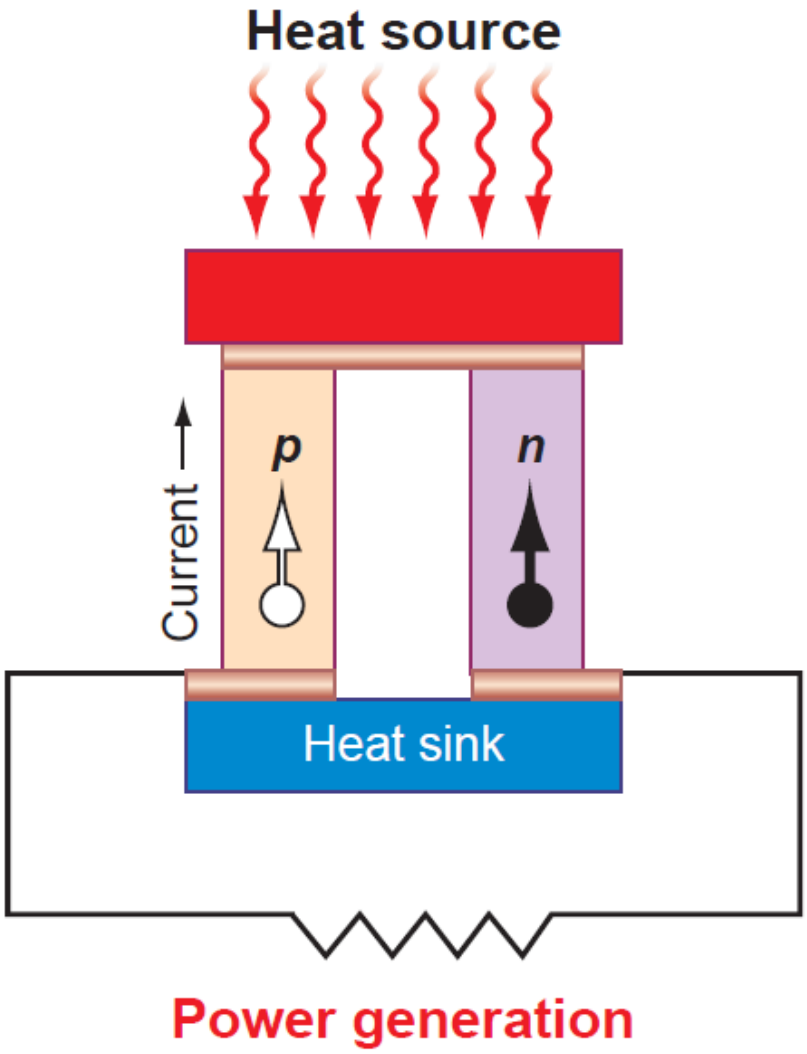

Figure 2.1: Schematic of a thermoelectric couple in power generation mode [16]. A thermoelectric couple is comprised of a p-type and n-type semiconductor with metallic junctions.

Accordingly, many thermoelectric couples can be assembled to form a thermoelectric module (see Figure 2.2), and many thermoelectric modules can be assembled to form a thermoelectric generator (TEG). These generators can be used as a provider of electrical power when configured with a way to apply a temperature differential across each module.

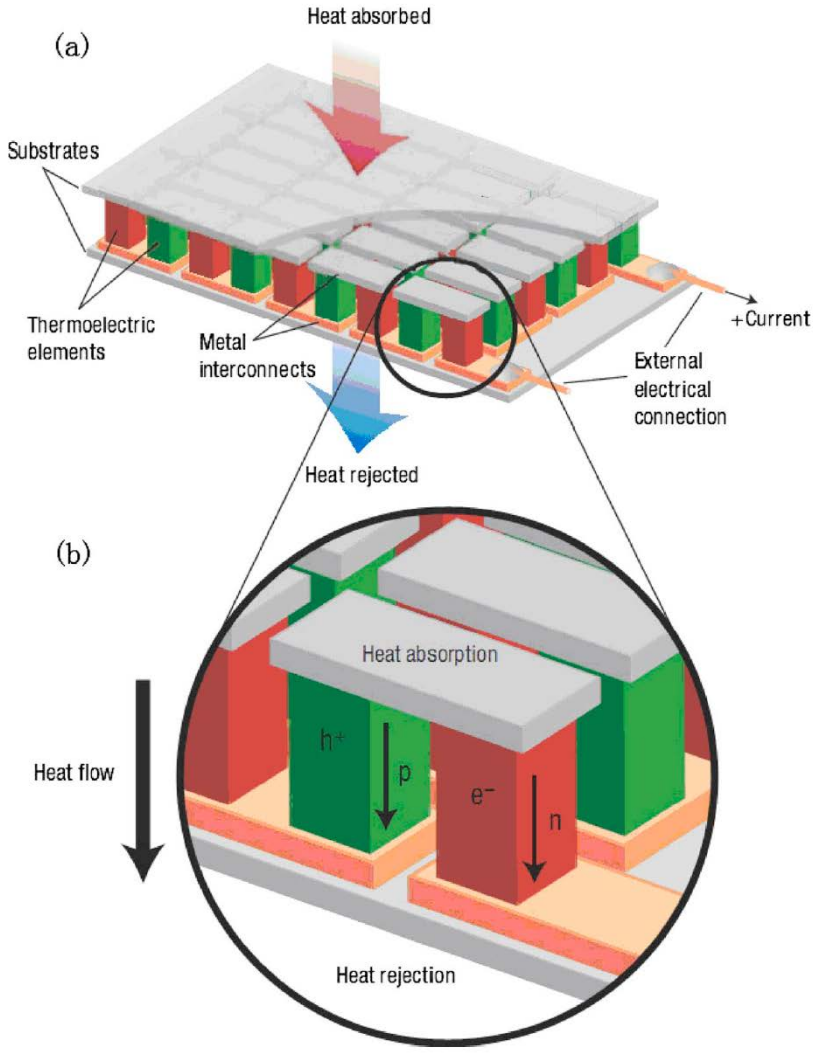

Figure 2.2: Illustration of a thermoelectric module [17]. A thermoelectric module consists of many thermoelectric couples connected electrically in series in order to generate a significant current.

2.1.2.2 Efficiency of Thermoelectric Devices

The efficiency of thermoelectric devices is measured via a dimensionless parameter called the figure of merit, ZT. This parameter is inherent to the thermoelectric material's electrical and thermal transport properties [16], and is strictly a function of the material properties of the semiconductors constituting the device, including thermal conductivity, k, electrical conductivity, σ, and the Seebeck Coefficient S:

$$ZT = \frac{S^2\sigma}{k}T \tag{2.1}$$

The efficiency of the device is a function of the figure of merit, along with different relevant temperatures: T_C, T_H, and T_M, which are the temperatures of the cold source, hot source, and the mean of these two temperatures, respectively:

$$\eta_{MAX} = \frac{(T_H - T_C)\left(\sqrt{1+ZT_M}-1\right)}{T_H\left(\sqrt{1+ZT_M}+\frac{T_C}{T_H}\right)} \tag{2.2}$$

2.1.2.3 Pros and Cons of Thermoelectric Devices

The many pros and cons of thermoelectric power generation technologies are well-documented in literature. Benefits of thermoelectrics include the following: they are solid-state power generation devices [15] with no moving parts [16], and are therefore silent, reliable [18], and less prone to failure than mechanical power generation devices [19]; they do not require the use of bulk fluids (e.g., CFCs or HCFCs) for operation [19]; and finally, they produce no greenhouse gas emissions [16].

However, thermoelectric devices have historically been plagued by very low conversion efficiencies, usually reported at 5% or less [15, 16, 18, 19]. Thermoelectrics have been stuck at a ZT value of approximately unity for several decades [15, 16, 19]. In order for thermoelectrics to be commercially viable and economically competitive with

current technologies, this value must rise substantially; this target value varies across industry, but ranges from $ZT = 3$-10 [16, 17, 19].

2.2 THE NOVEL THERMOELECTRIC GENERATOR

This study centered on a novel thermoelectric generator (TEG), invented by Phillip C. Watts, manager of *Watts Thermoelectric LLC*. The TEG is described fully in Patent Application No. 20090301541, filed in December 2009 [20].

The TEG is essentially a novel assembly of thermoelectric modules whose required temperature differential is driven by hot and cold streams of fluid flowing through the generator.

Figure 2.3: Three pictorial views of the novel thermoelectric generator [21]. A single rack (pictured) was the thermoelectric generator studied in this study. Hot and cold streams of water drive the required temperature differential in the TEG.

2.2.1 Description of the Thermoelectric Generator

The TEG can consist of one or more "racks" (see Figure 2.3), each of which serves as an independent, autonomous unit of the TEG. In this study, however, only a single rack was considered, and all references to the "TEG" herein refer to a single rack.

A rack is comprised of 16 banks (4 rows x 4 columns) of thermoelectric modules. Each bank contains 12 thermoelectric modules separated by 13 aluminum heat spreaders. These thermoelectric modules were bismuth telluride modules. A single hot stream and a single cold stream of water (the nominal operating fluid) drive the rack's temperature differential as they flow through each bank and through channels within each of the heat spreaders of each bank (see Figure 2.4). As the streams flow through the entire TEG, every module of each bank is exposed to the hot stream on one side and the cold stream on the opposite side, and therefore generates electricity from the temperature differential.

In terms of electrical design, the thermoelectric modules are connected in series within each bank. This arrangement produces a single output voltage of approximately 12 Volts in direct current (Vdc) per bank, per the default operating conditions outlined in the proceeding section (see 2.2.2). By default, all of a rack's banks are connected in parallel so as to maintain uniformity in voltage output among banks. However, this electrical design can be altered based on the specific end-user's needs; for example, rather than 16 banks producing 12 Vdc in a rack, banks can be paired such that 8 pairs produce 24 Vdc, or 4 can be connected in series to prodce 48 Vdc, etc. [21]. This versatility in the rack's output voltage was one goal of *Watts Thermoelectric LLC*, as there exist various applications where varying voltages are desired; the primary example dwells in automotives, where passenger vehicles feature 12 Volt electrical systems, whereas military vehicles employ 24 Volt systems. (The TEG's operating conditions are outlined in 2.2.2.)

In terms of mechanical design, each thermoelectric module (within each bank) is sandwiched between two heat spreaders. The stream flowing through each heat spreader alternates between hot and cold water in order to expose each module to the temperature differential; it also alternates direction through each heat spreader. Therefore, each module is thermally assembled in a parallel-flow configuration, as illustrated in Figure 2.4. Additionally, a rack has a dry weight of 75 pounds and measures 32 inches in height, 13.5 inches in width, and 20 inches in depth.

Moreover, a rack is comprised of 4 water reservoirs, which are located at the inlet and outlet of each stream, 2 recirculation pumps, which are located at the inlet of the hot water stream and outlet of the cold water stream, and 4 air removal devices, which were incorporated in order to prevent air from becoming trapped within the heat spreaders' water channels. And finally, endplates, harnesses, nuts, clamps, springs, and other parts constitute the ancillary equipment used to assemble the rack in its final form.

Further assembly and design details, along with more images, can be found in the patent application [20].

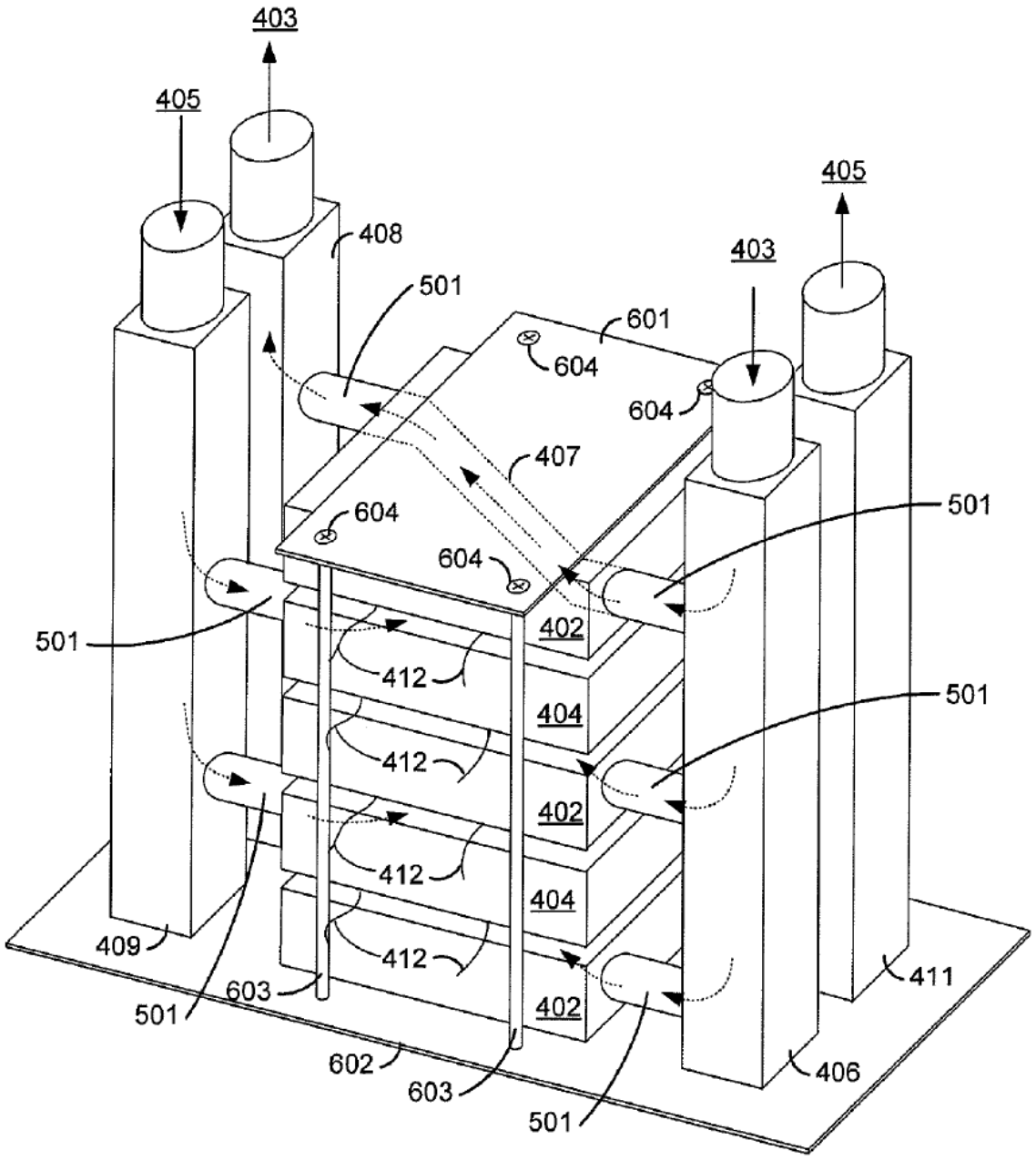

FIG. 6

Figure 2.4: Schematic of a portion of one bank [20]. Each thermoelectric module within the TEG is sandwiched between two heat spreaders—metal blocks with interior water channels as pictured. Hot water flows through one spreader, then cold water on the next spreader, etc.

There are various points of measurement that are used to characterize the TEG in operation: the hot stream's inlet ($T_{H,IN}$) and outlet ($T_{H,OUT}$) temperatures, the cold stream's inlet ($T_{C,IN}$) and outlet ($T_{C,OUT}$) temperatures, volumetric flow rates for both streams ($\dot{V}_H$, $\dot{V}_C$), and finally the actual TEG's power output (P_{OUT}).

2.2.2 The Default Operating Conditions of the Thermoelectric Generator

From previous unpublished testing, it was ascertained by *Watts Thermoelectric LLC* that a rack (TEG) nominally generates 83 Watts of electrical power at an inlet temperature differential of $\Delta T = 75$ °F between the hot and cold streams. These specific conditions produce an average output voltage per bank of 12.5 Vdc, which is viewed as the operational target voltage per bank. These conditions—namely the voltage per bank and overall electrical power output—are considered the nominal parameters that describe the TEG's default mode of operation, as listed in Table 2.1.

Parameter	Nominal Value
P_{OUT}	83 W
$T_{H,IN}$ $(T_{H,MIN})$	130 °F
$\dot{V}_H$	1.3 gpm
$T_{C,IN}$	55 °F
$\dot{V}_C$	6 gpm
Voltage (avg. per bank)	12.5 Vdc
Current (total per rack)	6.64 A

Table 2.1: TEG default operating conditions [21]. Note that the unit "gpm" refers to gallons per minute.

The hot stream volumetric flow rate of $\dot{V}_H = 1.3$ gpm is equivalent to a mass flow rate of $\dot{m}_H = 0.082$ kg/s, assuming a constant water density of $\rho = 1{,}000$ kg/m^3 (as done through this entire study). Similarly, the cold stream volumetric flow rate of $\dot{V}_C = 6$ gpm is equivalent to a mass flow rate of $\dot{m}_C = 0.379$ kg/s.

Because the TEG would produce more than 83 Watts of power if the hot stream inlet temperature ($T_{H,IN}$) were to be raised above 130 °F while maintaining the same cold stream inlet temperature, $T_{H,IN}$ is thus treated as a minimum hot stream inlet temperature, $T_{H,MIN}$; thus $T_{H,MIN} = 130$ °F. Nevertheless, 83 Watts was considered to be the TEG's nominal electrical output with the expectation that the working fluid temperatures would be held steady. Along the same lines, the TEG's maximum hot stream inlet temperature,

$T_{H,MAX}$, is governed by the materials used to construct the TEG, and was limited to $T_{H,MAX} = 176$ °F for the prototype TEG analyzed in this study [21].

Predictably, as both water streams flow through the TEG, they begin to equalize in temperature, similar to a heat exchanger, via the thermodynamic processes taking place within the TEG. That is, the hot stream cools as it flows though the TEG, while the cold stream warms. Thus, the streams' inlet temperatures, $T_{H,IN}$ and $T_{C,IN}$, are not constant throughout the process. However, note that the streams' outlet temperatures are nowhere near equal (see 4.1 for experimental data).

Furthermore, racks can be combined in series to provide more power based on the end-user's specific needs. For example, an array of 3 racks provides 250 W, while 12 racks provide 1 kW. Despite the scalability and modularity of the racks, this analysis centered on a single rack, as noted previously.

2.2.3 The Thermoelectric Generator in the Built Environment

2.2.3.1 The Default Configuration

Per the patent application, the TEG can be integrated into the built environment as seen in Figure 2.5 [20]. In this default configuration, renewable energy sources serve as the TEG's hot and cold sources: solar-thermal energy serves the TEG's hot stream source, and geothermal energy serves as the TEG's cold stream source. This default configuration in the built environment was the basis for all analyses presented herein. Additionally, the upcoming Characterization Test, discussed in detail in 4.4, resembled this configuration.

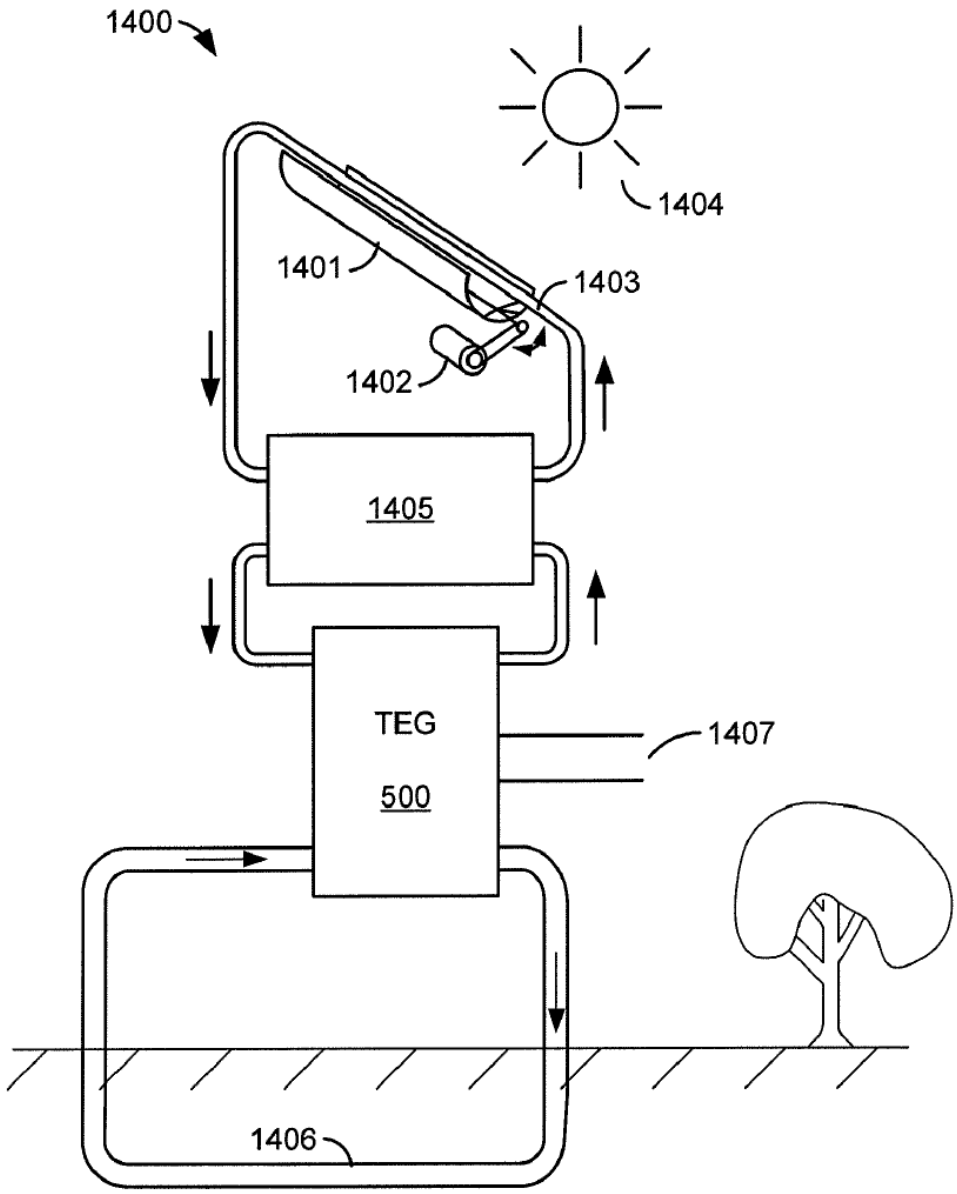

FIG. 14

Figure 2.5: Schematic of the TEG in its default configuration in the built environment [20]. Here, the TEG uses a solar collector system as its hot stream source and a geothermal heat pump system (operating in reverse for a cooling application) as its cold stream source.

It is of critical importance to note that the solar-thermal energy and geothermal energy systems supply (or draw) *thermal* energy to (or from) the TEG, while the TEG itself produces *electricity* (electrical energy).

Continuing, solar-thermal energy and geothermal energy systems were chosen in particular primarily because they are reliable sources of renewable energy [21]. As indicated in 2.1.2.3, thermoelectric generators are zero-emission devices, and therefore integrating the TEG with similar zero-emission technologies in the built environment made for a symbiotic matchup. Of course, the TEG need not be coupled with these two sources in particular; any sources that supply and draw thermal energy to and from the TEG—renewable or not—can conceivably be used.

Further, according to *Watts Thermoelectric LLC*, the motivation for integrating their novel TEG with these two renewable energy sources in particular was that the integrated system could potentially be purchased and maintained at a low cost. This in turn would allow the TEG to be implemented in regions with limited access to electricity that is often found in underdeveloped communities. In fact, this was the primary motivation for *Watts Thermoelectric LLC*—to promote and advance widespread low-cost access to electricity to those without it.

2.2.3.2 A Prospective Hot Stream Source: Waste Heat Recovery

Needless to say, the TEG's integration in the built environment need not be limited to solar-thermal energy as its hot stream source. There exist many alternatives for the hot source—the most promising of which is waste heat recovery.

Opportunities to recover waste heat present themselves in an extremely broad range of applications and can in turn be used as "free" sources of fuel when paired with

thermoelectric power generation technologies. These potential applications are typically categorized based on their temperature grade and include: automotive applications, where the high inefficiency of internal combustion engine is targeted [15, 22]; industrial/manufacturing plant applications, which feature many promising applications typically in the form of high-temperature flue gases from furnaces found in many processing industries, including those of glass, aluminum, steel, cement, paper, petrochemicals, and many more [22, 23]; and most intriguingly, even waste heat from the human body can potentially be utilized [22]! The potential of electricity generation by recovering waste heat across these industries are quantified in detail in the report authored by Hendricks and Choate [23], which serves as an excellent survey of opportunities for waste heat recovery across many industries.

However, considering waste heat recovery as a prospective hot source for the TEG was outside of the scope of the analyses presented herein. At the time of writing, *Watts Thermoelectric LLC* considered waste heat recovery to be the most promising hot source—more so than solar-thermal energy—and was investigating ways to implement such applications to their novel TEG.

Chapter 3: Thermodynamic Analysis of the Solar Collector-Thermoelectric Generator Coupled System Operating in the Built Environment

This chapter considers a systems-level thermodynamic analysis of the novel thermoelectric generator (TEG) coupled with a solar collector system as it operated in the built environment. Recall that solar-thermal energy serves as the TEG's hot stream source in its default configuration. It is of critical importance to note that the solar collector system supplies the TEG with *thermal* energy, while the TEG produces *electrical* energy (electricity); this is an underlying assumption throughout the analysis. Further, this chapter excludes the systems-level analysis of the internal thermodynamics of the TEG itself, which is presented in Chapter 4. Additionally, recall that geothermal energy serves as the TEG's cold stream source. As indicated in 1.2, a thermodynamic analysis of this system was not part of the scope of this study.

The primary motivation for this portion of the analysis was to quantify the electricity generated, in kilowatt-hours (kWh), by the TEG during operation over the course of a year. This analysis also aimed at quantifying the annual thermal energy collected by the solar collector in that year. The latest year for which solar radiation (i.e., insolation) data were available from the U.S. Departments of Energy's National Renewable Energy Laboratory (NREL) was 2005 and was therefore selected as a test case. Using insolation, plus information about the TEG's behavior during operation, a thermodynamic analysis of the TEG in the built environment was conducted in order to estimate its annual energetic performance in the built environment.

Finally, the last section of this chapter provides a general outline of the geothermal energy system (the TEG's cold stream source) that was excluded from the scope of this analysis.

3.1 A BRIEF OVERVIEW OF SOLAR-THERMAL ENERGY

A solar collector system is comprised of a type of collector (flat-plate or evacuated-tube), a heat transfer fluid (water or antifreeze), and finally a thermal storage tank.

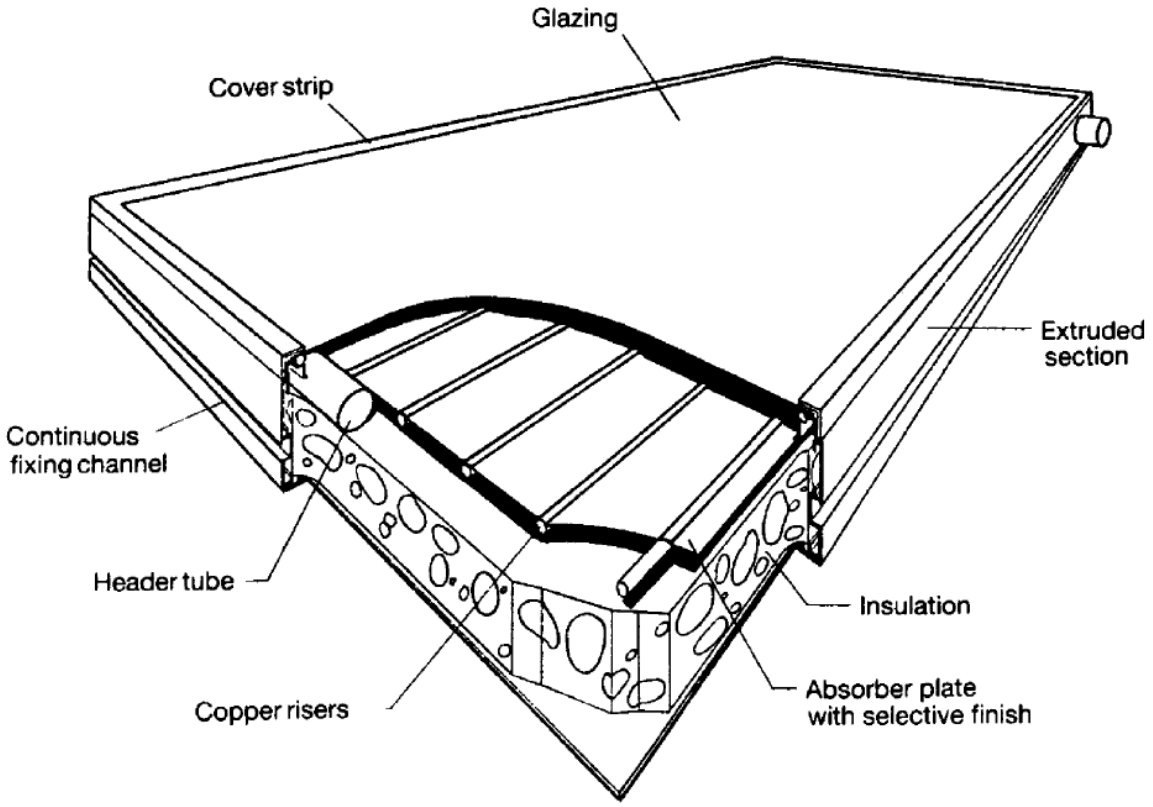

Figure 3.1: Pictorial view of a flat-plate collector [24]. Insolation is trapped as heat in the flat-plate solar collector, which serves to heat the heat transfer fluid (typically water or antifreeze) as it flows through the tubes within the collector.

There are two types of solar-thermal energy systems: active and passive. Active systems feature circulating pumps whereas passive systems do not; passive systems are also usually not as efficient as active systems [25] and were not the focus of this study. Within active systems, there are direct/open-loop systems and indirect/closed-loop systems. In the former, water is used as the heat transfer fluid, and is circulated through

the collector itself (see Figure 3.1) and deposited in the storage tank directly. In the latter, antifreeze (a water-glycol mixture) is used as the heat transfer fluid, and after being circulated through the collector, flows through a heat exchanger inside the storage tank rather than being directly deposited into it. These two types of active systems are illustrated in Figure 3.2.

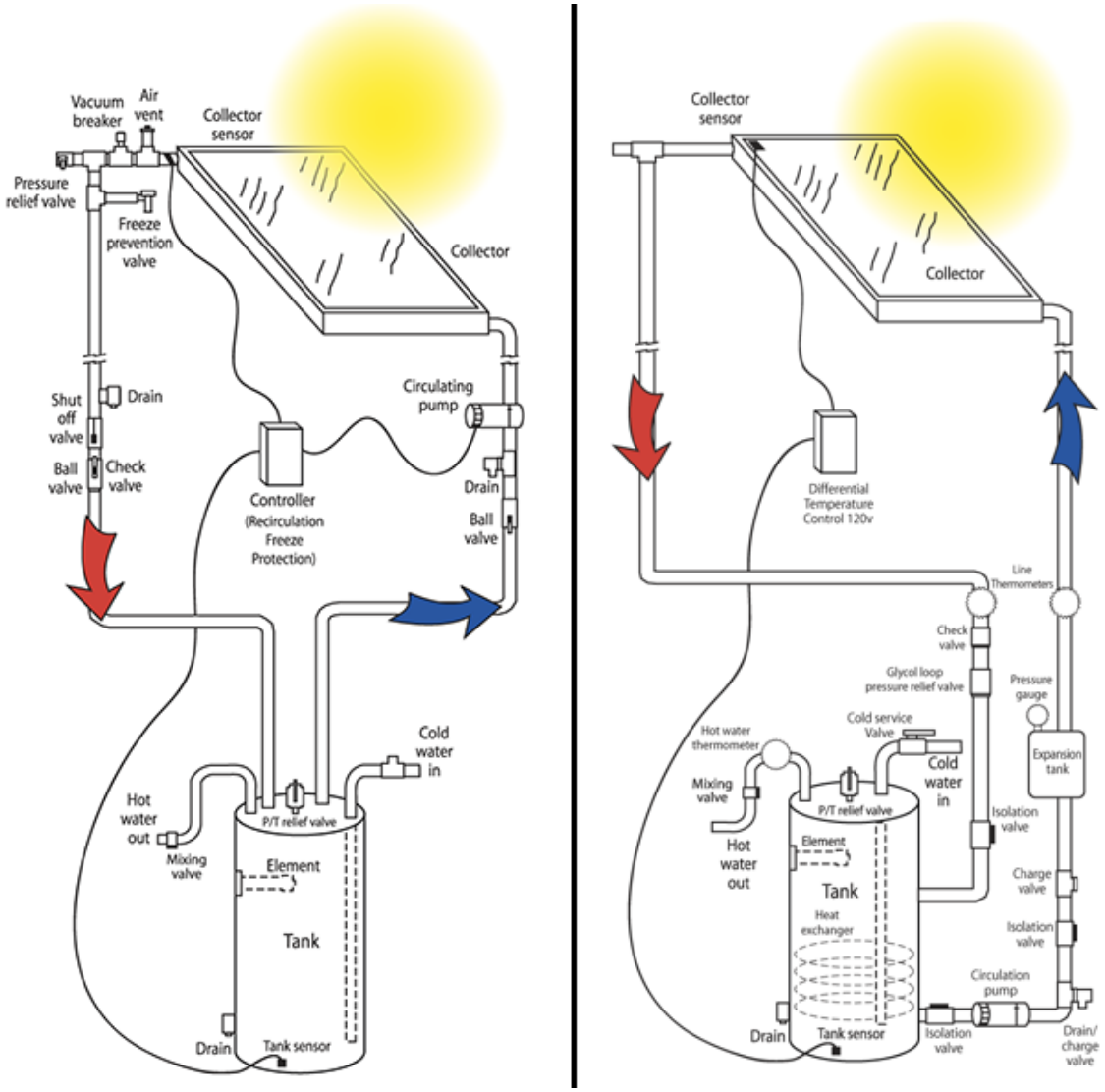

Figure 3.2: Schematic of direct/open-loop and indirect/closed-loop solar-thermal energy systems [26]. An open-loop system (left) uses water as its heat transfer fluid, whereas a closed-loop system (right) uses antifreeze and requires heat exchange to occur within the thermal storage tank.

Climate is usually the deciding factor as to what type of system is used, based on whether freezing temperatures are typical or not. It is reported that open-loop systems are more efficient than closed-loop systems [27]. Such a distinction is reasonable, as water's specific heat capacity is reduced when mixed with a type of glycol (thereby making

antifreeze). Should freezing temperatures be expected to commonly occur, antifreeze makes for the best fluid because of its reduced freezing point; otherwise, water is the preferred medium.

The thermodynamic analysis presented in this chapter was based on the upcoming Characterization Test (see 4.4). In this particular case, the solar-thermal energy system used was an active, direct/open-loop system, and featured a fixed-position, flat-plate solar collector with a thermal storage tank in which to store the heated working fluid. Its analysis is presented in the following sections.

3.2 CONTROL VOLUME ANALYSIS OF THE THERMAL STORAGE TANK

The purpose of performing an energy balance on the thermal storage tank was to determine the storage tank temperature, T_S, as it fluctuated throughout a typical day. The storage tank temperature was of particular interest because the TEG drew fluid (water) from the storage tank as its hot loop source (see Figure 2.5). Thus, the TEG's hot loop inlet temperature, and subsequently its power output, was governed by the storage tank temperature.

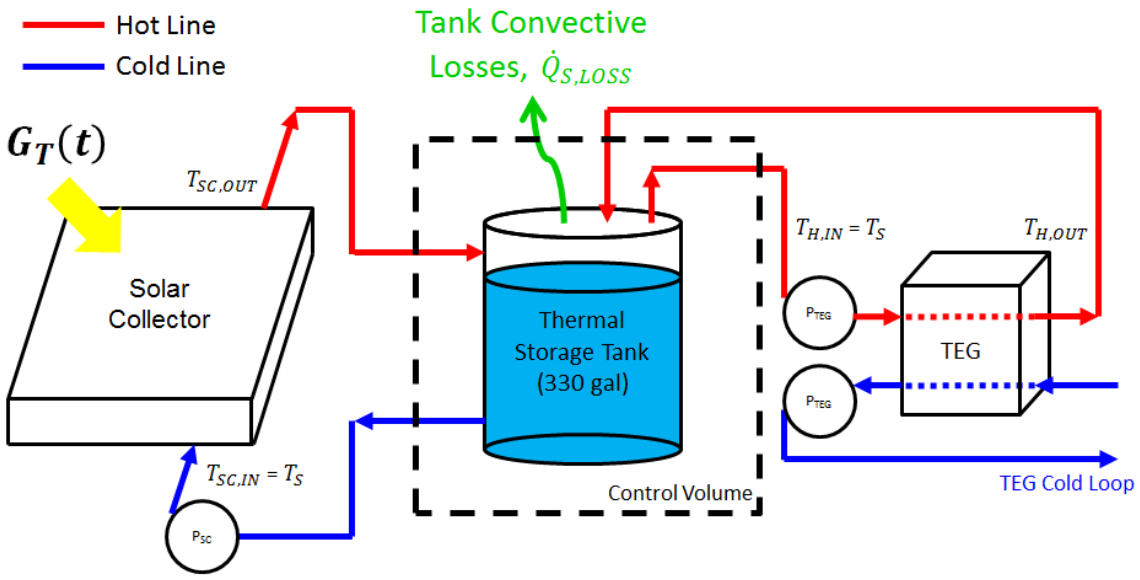

Figure 3.3: A control volume analysis of the thermal storage tank was performed, to solve for the tank's temperature, T_S. The setup shown was based on the TEG's upcoming Characterization Test (see 4.4). Note that the TEG's cold loop was not part of the analysis of the coupled system covered in this chapter.

Following Figure 3.3, the following relationships are expected under normal operating conditions: the collector outlet temperature is greater than the collector inlet temperature; the collector inlet temperature is equivalent to the storage tank temperature, which in turn is equivalent to the TEG's hot loop inlet temperature; and the TEG's hot loop inlet temperature is greater than the TEG's hot loop outlet temperature. That is:

$$T_{SC,OUT} > T_{SC,IN} = T_S = T_{H,IN} > T_{H,OUT} \tag{3.1}$$

Therefore, ΔT_H, which is defined as the difference between the hot stream's outlet and inlet temperatures (i.e., $\Delta T_H = T_{H,OUT} - T_{H,IN}$), is a negative quantity. These relative relationships are denoted in Figure 3.3 by the red- and blue-colored lines.

3.2.1 Assumptions

For purposes of this analysis, it was assumed that both of the pumps (P_{SC} and P_{TEG} as shown in Figure 3.3) are thermally negligible. That is, they each exhibited a negligible fluid temperature change (i.e., they were isothermal) because of the relatively small change in pressure. The size of the solar collector pump, P_{SC}, is approximately 16 PSI (pounds per square inch), while the TEG's two pumps, P_{TEG}, are each sized at 6 PSI. Hence, their thermal effects were approximated as zero in the thermodynamic analysis. However, the electrical power requirements for each of these pumps were not neglected. In particular, P_{SC} was considered during the analysis (see 3.4.2.1), while the effect of P_{TEG} was considered in the post-analysis (see 3.5.3.2). Additionally, pipe losses in the coupled system were not accounted for, but are non-zero in a real system.

Most importantly, it was assumed that the TEG had a constant electrical power output of 83 Watts (W) at any time during operation (i.e., anytime it was ON) per its default operating conditions (see Table 2.1). Here, there are two assumptions implied: first, the TEG's cold stream inlet temperature, $T_{C,IN}$, continuously remained at a constant temperature of 55 °F; and second, 83 W was achieved regardless of what the TEG's hot stream inlet temperature, $T_{H,IN}$, was, as long as it was above a minimum temperature of $T_{H,IN} = 130$ °F. More information is provided in 3.6 regarding the first assumption. With regard to the second assumption: in actuality, the TEG produces *at least* 83 W of electrical power for conditions of $T_{C,IN} = 55$ °F and $T_{H,IN} > 130$ °F. However, scaling the actual power production based on greater temperature differentials required an empirical characterization of the system that was not available to this study, as explained in the following chapter (see 4.1). Hence, this major assumption was made.

3.2.2 Energy Balance Derivation of the Thermal Storage Tank

From the first law of thermodynamics (i.e., conservation of energy), the general energy balance equation for an open system (control volume) is based on the heat transfer inputs and outputs, as well as the energy stored and generated in the control volume over time. That is,

$$\dot{E}_{IN} - \dot{E}_{OUT} = \dot{E}_{STOR} - \dot{E}_{GEN} \tag{3.2}$$

The heat transfer input and output terms ($\dot{E}_{IN}$ and $\dot{E}_{OUT}$) are functions of the streams' mass flow rates and enthalpies. Here, the kinetic and potential energy effects of each stream were neglected, and the storage tank's convective loss term, $\dot{Q}_{S,LOSS}$, was included as a heat transfer output term ($\dot{E}_{OUT}$). The energy storage term is a function of the control volume's mass, working fluid's specific heat capacity, and change in storage tank temperature over time. Further, there was no energy generation in the control volume. Evaluating Equation 3.2 term-by-term (and paying special attention to the nomenclature used in Figure 3.3), the following is obtained:

$$\begin{aligned}\left(\dot{m}_{SC}h_{SC,OUT} + \dot{m}_H h_{H,OUT}\right) - \left(\dot{m}_{SC}h_{SC,IN} + \dot{m}_H h_{H,IN} + \dot{Q}_{S,LOSS}\right) \\ = m_S c_P \frac{\mathrm{d}T_S}{\mathrm{d}t} - 0\end{aligned} \tag{3.3}$$

Rearranging,

$$m_S c_P \frac{\mathrm{d}T_S}{\mathrm{d}t} = \dot{m}_{SC}\left(h_{SC,OUT} - h_{SC,IN}\right) + \dot{m}_H\left(h_{H,OUT} - h_{H,IN}\right) - \dot{Q}_{S,LOSS} \tag{3.4}$$

$$\rho V_S c_P \frac{\mathrm{d}T_S}{\mathrm{d}t} = \dot{m}_{SC}\Delta h_{SC} + \dot{m}_H \Delta h_H - \dot{Q}_{S,LOSS} \tag{3.5}$$

Now, the solar collector stream's heat transfer term, $\dot{m}_{SC}\Delta h_{SC}$, is replaced with $\dot{Q}_U$, which represents the useful power gained from the collector (see 4.4.2.2); it is a quantity calculated directly from the solar collector's efficiency curve (and not from the $\dot{m}_{SC}\Delta h_{SC}$ term) and was provided by the manufacturer in this study. Similarly, the TEG hot stream's heat transfer term, $\dot{m}_H \Delta h_H$, is substituted with $\dot{L}_{TEG}$, which is short-hand

notation that represents the load that the TEG bears on the solar collector-TEG coupled system. Thus, Equation 3.5 becomes:

$$\rho V_S c_P \frac{\mathrm{d}T_S}{\mathrm{d}t} = \dot{Q}_U + \dot{L}_{TEG} - \dot{Q}_{S,LOSS} \tag{3.6}$$

The $\dot{Q}_U$ term is defined by the following: number of solar collectors used in the system, n_{SC}, and their aperture area, A_{SC}; the time-dependent solar insolation incident on the tilted collector, $G_T(t)$, and maximum efficiency, η_0; the efficiency curve's slope, m_{SC} (which is a negative value), solar collector stream inlet temperature, $T_{SC,IN}$, and finally time-dependent solar collector ambient temperature, $T_{SC,AMB}(t)$. Further, the $\dot{L}_{TEG}$ term's definition remained the same. Additionally, the storage tank's convective loss term is defined by the overall heat transfer coefficient, U_S, surface area, A_S, storage tank temperature, T_S, and storage tank ambient temperature, $T_{S,AMB}$. Summarizing,

$$\dot{Q}_U = n_{SC} A_{SC} \left\{ \eta_0 G_T(t) + m_{SC} \left(T_{SC,IN} - T_{SC,AMB}(t) \right) \right\} \tag{3.7}$$

$$\dot{L}_{TEG} = \dot{m}_H \Delta h_H \tag{3.8}$$

$$\dot{Q}_{S,LOSS} = U_S A_S \left(T_S - T_{S,AMB} \right) \tag{3.9}$$

However, note from the diagram (Figure 3.3) that the solar collector stream's inlet temperature, $T_{SC,IN}$, is the storage tank temperature, T_S. (In contrast, note that the TEG's hot stream inlet temperature, $T_{H,IN}$, was not considered as such; see discussion in 3.4.2.) Thus, $T_{SC,IN}$ is defined as:

$$T_{SC,IN} = T_S \tag{3.10}$$

Therefore, $\dot{Q}_U$ becomes:

$$\dot{Q}_U = n_{SC} A_{SC} \left\{ \eta_0 G_T(t) + m_{SC} \left(T_S - T_{SC,AMB}(t) \right) \right\} \tag{3.11}$$

Further, since specific heats are approximately constant for a fluid in the liquid state not undergoing a phase change, the following relationship was assumed for the working fluid in order to work with temperatures rather than enthalpies and in turn simplify the analysis:

$$\Delta h = c_P \Delta T \tag{3.12}$$

Thus, the coupled system's load term, $\dot{L}_{TEG}$, is redefined as:

$$\dot{L}_{TEG} = \dot{m}_H c_P \Delta T_H \tag{3.13}$$

3.2.3 Summary of Important Equations Resulting from Energy Balance

This section summarizes the important equations resulting from the energy balance. The governing equation was:

$$\rho V_S c_P \frac{\mathrm{d}T_S}{\mathrm{d}t} = \dot{Q}_U + \dot{L}_{TEG} - \dot{Q}_{S,LOSS} \tag{3.6}$$

Where:

$$\dot{Q}_U = n_{SC} A_{SC} \left\{ \eta_0 G_T(t) + m_{SC} \left(T_S - T_{SC,AMB}(t) \right) \right\} \tag{3.11}$$

$$\dot{L}_{TEG} = \dot{m}_H c_P \Delta T_H \tag{3.13}$$

$$\dot{Q}_{S,LOSS} = U_S A_S \left(T_S - T_{S,AMB} \right) \tag{3.9}$$

Here, note that the coupled system's load, $\dot{L}_{TEG}$, will always be a negative quantity during operation, since $T_{H,IN} > T_{H,OUT}$ as indicated in Equation 3.1.

3. 3 INSOLATION AND AMBIENT TEMPERATURE DATA

Here, note that per Equation 3.11, $\dot{Q}_U$ is a function of insolation incident on the tilted collector, $G_T(t)$, and the solar collector's ambient temperature, $T_{SC,AMB}(t)$. That is, $\dot{Q}_U = \mathrm{f}\left(G_T(t), T_{SC,AMB}(t) \right)$. Solar insolation data that were used to determine the insolation incident on the collector, $G_T(t)$, were obtained from an NREL database [28] at the appropriate location (see 4.4.1). In the NREL database, the latest year for which insolation data are available is 2005, so it was decided to use data from that particular year as a test case for this analysis. As such, numerical results will not be identical to those observed during the Characterization Testing (see 4.4) because of the discrepancy

in insolation data. However, they will serve as an appropriate approximation. Additionally, ambient temperature data, $T_{SC,AMB}(t)$, were obtained from the National Oceanic and Atmospheric Administration (NOAA) [29]. Further information is discussed is the following sections.

For both data sets, data were available on an hourly basis. However, for this analysis, quarter-hourly data were desired for higher resolution. Because each hourly data point within each data set was in close proximity with its neighboring data points, linear interpolation was used to convert the hourly data into quarter-hourly estimates. Ambient temperature data are shown in Figure 3.4, whereas insolation data are explained in 3.3.3.

3.3.1 Selecting 12 Representative Days in 2005

Further, in order to approximate the TEG's performance throughout the year, 12 "representative" days of 2005 were selected as sample cases for the numerical model. Effectively, one day of each month was used to represent that month as a whole. 12 days were chosen instead of all 365 days of the year simply to facilitate the analysis. These dates would ultimately be used to collectively represent 2005 as a year.

In order to avoid randomly selecting dates, the following procedure was implemented. First, four "special solar event" days of 2005 were chosen: the summer solstice, fall equinox, winter solstice, and spring equinox. Then, the remaining eight representative days were equally spaced out among these fixed dates (two between each solar event) and can thus be considered "equitemporal" between the four fixed dates. Table 3.1 lists the dates selected.

Representative Date Chosen	Month Represented	Day No. of Year 2005 (out of 365)	Note
01/20/2005	January	20	--
02/18/2005	February	49	--
03/20/2005	March	79	Vernal Equinox
04/20/2005	April	110	--
05/21/2005	May	141	--
06/21/2005	June	172	Summer Solstice
07/22/2005	July	203	--
08/22/2005	August	234	--
09/22/2005	September	265	Autumnal Equinox
10/22/2005	October	295	--
11/21/2005	November	325	--
12/21/2005	December	355	Winter Solstice

Table 3.1: 12 representative days in 2005 were selected to represent their respective months. Solar insolation and ambient temperature data would be gathered for these dates. These 12 days would go on to represent 2005 as a whole in this study.

3.3.2 Ambient Temperature Data

For each representative day chosen, ambient temperature data were obtained from NOAA [29] at the appropriate location (see 4.4.1). This data would serve as the solar collector's ambient temperature, $T_{SC,AMB}(t)$. See Figure 3.4 for ambient temperature data.

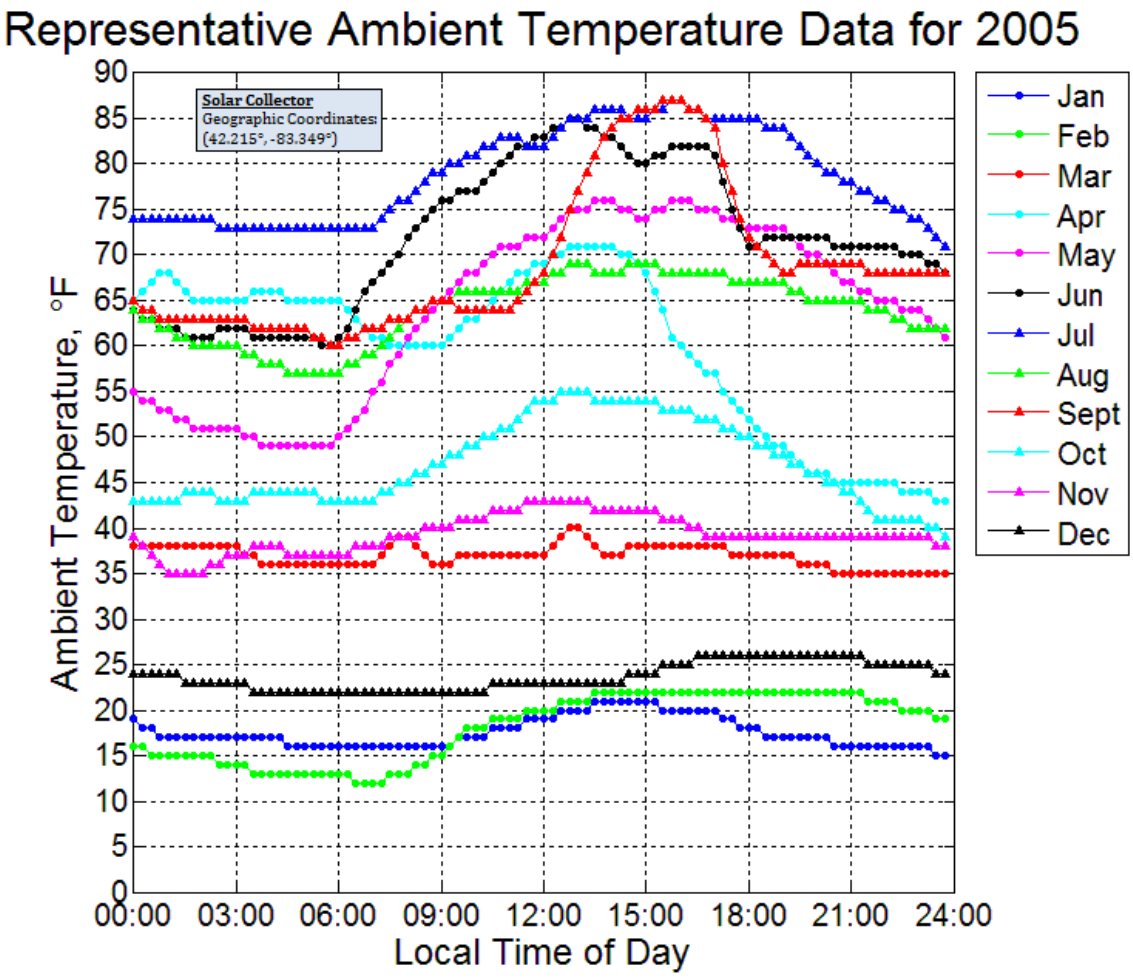

Figure 3.4: Ambient temperature data for the representative days from each month in 2005 at the appropriate site were used for $T_{SC,AMB}(t)$ [29].

3.3.3 Calculating the Insolation Incident on the Tilted Solar Collector

Only two kinds of recorded insolation data were available from NREL [28] at the appropriate location (see 4.4.1): extraterrestrial insolation incident on a horizontal surface, $I_{H,B}$, and extraterrestrial insolation incident on a surface normal to the sun, $I_{N,B}$, both of which were measured at the top of the atmosphere (per the NREL User's Manual for the insolation database) [28]. In this study, these data sets are referred to as

"horizontal insolation data" and "normal insolation data," respectively. (Plots for both data sets are shown in Appendix A.1.) Here, note that meteorological conditions like cloudiness were not accounted for in the insolation data sets (per the User's Manual) [28].

Due to the physical configuration of the system, it was necessary to convert these data sets into insolation incident on a tilted surface (i.e., the solar collector). The solar trigonometric equations (as well as values) required for this calculation are detailed in Appendix A.2.1 and follow both Goswami et al. [30] and Howell et al. [31]. Essentially, the insolation incident on the tilted collector $G_T(t)$ was defined as the sum of the beam/direct, diffuse, and reflected radiation components:

$$G_T = I_{T,B} + I_{T,D} + I_{T,R} \tag{3.14}$$

Equation 3.14 was expressed in terms of solar angles (see Nomenclature for symbol definitions):

$$G_T = I_{N,B}\left(\cos(i) + C\cos^2\left(\frac{\beta}{2}\right) + \rho_{SC}(\sin(\alpha) + C)\sin^2\left(\frac{\beta}{2}\right)\right) \tag{3.15}$$

Further, G_T can be expressed in terms of the insolation factor, F_{TOT}, which was defined by the beam/direct tilt factor R_b and insolation multipliers F_d and F_r (see Appendix A.2.1):

$$G_T = I_{N,B}F_{TOT} \tag{3.16}$$

Where:

$$F_{TOT} = R_b + F_d + F_r \tag{3.17}$$

$$R_b = \cos(i) \tag{3.18}$$

$$F_d = \mathrm{C}\cos^2\left(\frac{\beta}{2}\right) \tag{3.19}$$

$$F_r = \rho_{SC}(\sin(\alpha) + C)\sin^2\left(\frac{\beta}{2}\right) \tag{3.20}$$

Instead of using normal insolation data, $I_{N,B}$, (as shown), horizontal insolation data, $I_{H,B}$, *could be* used via the following relation:

$$I_{N,B} = \frac{I_{H,B}}{\sin(\alpha)} \tag{3.21}$$

However, this approach causes a singularity at $\alpha = 0°$, which in nature corresponds to sunrise and sunset times, and as a result adversely affected G_T. However, using normal insolation data circumvented this issue. See Appendix A.2.1 for derivation. These calculations were incorporated into the numerical model described in the following section. The resulting insolation incident on the collector curves are shown in Figure 3.5.

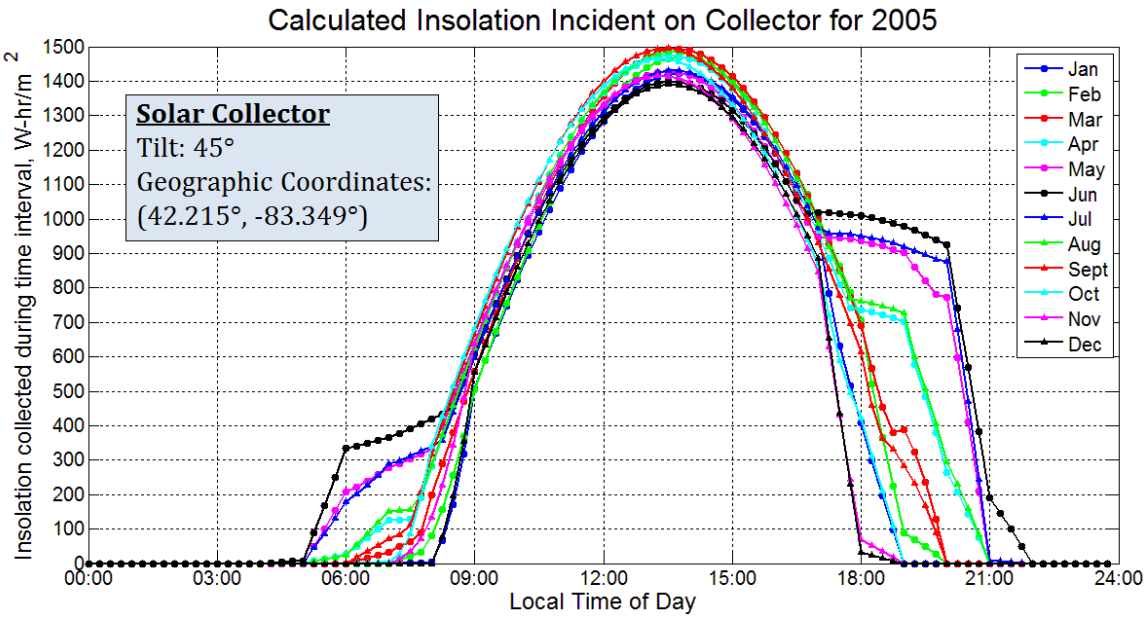

Figure 3.5: Normal insolation data, $I_{N,B}$, for the representative days from each month in 2005 at the appropriate site [28] were used to calculate the insolation incident on the tilted collector, $G_T(t)$, shown here (see Appendix A.1).

3.4 NUMERICAL ANALYSIS OF THE SOLAR COLLECTOR-THERMOELECTRIC GENERATOR COUPLED SYSTEM

3.4.1 Motivation and Numerical Equations

Recall that the governing equation from the control volume analysis on the thermal storage tank was a first-order ordinary differential equation (ODE) for T_S (see Equation 3.6). Further, recall that $\dot{Q}_U = \mathrm{f}\left(G_T(t), T_{SC,AMB}(t)\right)$. Each of these time-dependent terms—insolation incident on the tilted collector, $G_T(t)$, and collector ambient temperature, $T_{SC,AMB}(t)$—were only available as data in discrete time intervals, based on local meteorological conditions. Hence, these discrete data sets (see Figure 3.4 and 3.5) that were part of the ODE necessitated a numerical solution for storage tank temperature, T_S. Although an analytical solution could be obtained if the discrete data sets could be expressed as analytical, continuous functions, it proved much more practical to keep the discrete data sets and instead opt for a numerical solution.

The motivation for the numerical analysis was to obtain a solution of the storage tank temperature, T_S, from the ODE over the course of a day, since this was the TEG's hot stream inlet temperature (i.e., $T_S = T_{H,IN}$) as shown in Figure 3.3. Writing the derivative in finite-difference form [32],

$$\frac{\mathrm{d}T_S}{\mathrm{d}t} = \frac{T_S^n - T_S^{n-1}}{\Delta t} \tag{3.22}$$

Substituting into the ODE and solving resulted in a first-order forward Euler explicit scheme [32, 33]:

$$T_S^n = T_S^{n-1} + \left\{\frac{1}{\rho V_S c_P}\left[\dot{Q}_U^n + \dot{L}_{TEG} - \dot{Q}_{S,LOSS}^n\right]\right\}\Delta t \tag{3.23}$$

Where, expressed at the nth time step, Equations 3.11 and 3.9 were respectively rewritten as Equations 3.24 and 3.25:

$$\dot{Q}_U^n = n_{SC} A_{SC}\left\{\eta_0 G_T^n(t) + m_{SC}\left(T_S^{n-1} - T_{SC,AMB}^n(t)\right)\right\} \tag{3.24}$$

$$\dot{L}_{TEG} = \dot{m}_H c_P \Delta T_H \tag{3.13}$$

$$\dot{Q}_{S,LOSS}^{n} = U_S A_S \left(T_S^{n-1} - T_{S,AMB} \right) \tag{3.25}$$

As described in 3.3, quarter-hourly data were obtained from hourly data. Although it is most common in the field to march in time (i.e., integrate) with an hourly time step [33], a quarter-hourly time step was instead selected here:

$$\Delta t = 0.25 \text{ hr } \left| \frac{3{,}600 \text{ s}}{1 \text{ hr}} \right| \tag{3.26}$$

The following brief discussion is an attempt to explain the concept of numerical time integration. Essentially, in order to solve the ODE, one marches in time and determines the value of T_S for the next time step based on parameter values at the current time step. T_S will therefore be a vector of values throughout the course of a day. This procedure is illustrated with the following table [33]:

n	**Time HRS [LST]**	$\boldsymbol{G_T^n(t)}$ **[W]**	$\boldsymbol{T_{SC,AMB}^n(t)}$ **[°C]**	$\boldsymbol{\dot{Q}_U^n(T_S, G_T(t), T_{SC,AMB}(t))}$ **[W]**	$\boldsymbol{\dot{Q}_{S,LOSS}^n(T_S)}$ **[W]**	$\boldsymbol{T_S^{n-1}}$ **[°C]**	$\boldsymbol{T_S^n}$ **[°C]**
1	0:00	#	#	--	--	$T_{S,AMB}$	$T_{S,AMB}$
2	0:15	#	#	# (use $T_S^{(1)}$)	# (use $T_S^{(1)}$)	$T_{S,AMB}$	$T_S^{(2)}$
3	0:30	#	#	# (use $T_S^{(2)}$)	# (use $T_S^{(2)}$)	$T_S^{(2)}$	$T_S^{(3)}$
4	0:45	#	#	# (use $T_S^{(3)}$)	# (use $T_S^{(3)}$)	$T_S^{(3)}$	$T_S^{(4)}$
…	…	…	…	…	…	…	…
96	23:45	#	#	# (use $T_S^{(95)}$)	# (use $T_S^{(95)}$)	$T_S^{(95)}$	$T_S^{(96)}$
97	0:00	#	#	# (use $T_S^{(96)}$)	# (use $T_S^{(96)}$)	$T_S^{(96)}$	$T_S^{(97)}$

Table 3.2: Illustration of numerical time integration based on an Euler explicit scheme.

As illustrated in Table 3.2, note that in the numerical model, a single day was defined from 0:00–23:45 HRS (LST), with 96 data points to represent the quarter-hourly time steps.

3.4.2 Design Parameters and Controls of the Numerical Model

This section refers to design parameters needed to be addressed and controls needed to be created after the numerical model of the solar collector-TEG coupled system had been constructed. The numerical model of the coupled system was constructed to closely resemble the TEG's upcoming Characterization Test (see 4.4) in terms of type and number of solar collectors used, heat transfer fluid used (water), type and size of thermal storage tank used, etc. Appendix B.2 includes the MATLAB script created for the numerical model.

3.4.2.1 Numerical Design Parameters

Simulation of Representative Days

To begin, once one day of the 12 representative days was selected (see 3.3.1), the numerical model was constructed to allow up to 7 iterations of this same date; that is, up to 7 consecutive 01/20/2005's could be simulated, or 7 05/21/2005's, etc. The number "7" was arbitrarily chosen simply to allow sufficient time for the coupled system to reach steady state, although it was later determined that 2 iterations would have sufficed, based on the test setup chosen for the Characterization Test. Thus, note that the input data sets—insolation incident on the tilted collector, $G_T(t)$, and ambient temperature, $T_{SC,AMB}(t)$—were identical for each day simulated, whereas other parameters—such as

storage tank temperature, T_S, and useful power collected from the solar collector, $\dot{Q}_U$—were not.

Modeling the TEG as a Thermal Load

Recall Equation 3.13:

$$\dot{L}_{TEG} = \dot{m}_H c_P \Delta T_H \equiv \dot{m}_H c_P \left(T_{H,OUT} - T_{H,IN}\right) \tag{3.13}$$

From Figure 3.3 and Equation 3.1, note that $T_{H,IN} = T_S$. Thus, $T_{H,IN}$ could have been defined accordingly as:

$$\dot{L}_{TEG} = \dot{m}_H c_P \left(T_{H,OUT} - T_S\right), \tag{3.27}$$

However, it was not considered as such. That is, $\dot{L}_{TEG}$ was *not* considered to be a function of T_S (i.e., $\dot{L}_{TEG} = \text{f}(T_S)$). Instead, $\dot{L}_{TEG}$ was quantified in this numerical analysis based on the measured value for $\dot{m}_H c_P \Delta T_H$ (per Equation 3.13) from the Reference Test—which is explained in detail in 4.1. The same hot stream mass flow rate, $\dot{m}_H$, measured in the Reference Test was used. For specific heat capacity of water, the constant $c_P = 4{,}190$ J/kg-K was used, as was done for all analyses in this study (see Nomenclature and 4.4.4). However, for the hot stream temperature differential, ΔT_H, a constant negative value of $\Delta T_H = $ -20°C ≈ -36°F was assumed in the numerical model (recall Equation 3.1). Note that this ΔT_H value was a conservative modeling assumption from experimental data; it was not derived using the log mean temperature difference approach, which is introduced in 4.2.2.4 as Equation 4.20.

Thus, in the numerical model, $\dot{L}_{TEG}$ was assumed to be a constant thermal load on the solar collector-TEG coupled system of:

$$\dot{L}_{TEG} = \text{-}6{,}925.9 \text{ W} \tag{3.28}$$

The reason for assuming a value for ΔT_H rather than creating an empirical function where $T_{H,OUT} = \text{f}\left(T_{H,IN}\right)$ and calculating the temperature differential

accordingly (which would certainly be preferable) was the limited availability in experimental data (see Chapter 4). The entire analysis presented in this chapter revolved around this assumption.

Thermal Storage Tank

Additionally, it was assumed that the storage tank was, at all times, fully mixed (i.e., unstratified) in order to simplify the numerical analysis. And, as discussed in 3.2.1, the numerical model of the coupled system did not explicitly model or consider the cold stream's geothermal energy system.

Electrical Power Requirement for Pumps

As indicated in 3.2.1, the electrical pumping power requirement, P_{SC}, for the coupled system of 300 Watts (see 4.4.2.2) was incorporated into the numerical model. This was done by simply reducing $\dot{Q}_U$ by 300 W at every instant (or, in this model, every quarter-hour). This reduction parenthetically simulated diverting 300 W of thermal power from the collector, somehow converting it to electrical power (assuming 100% conversion efficiency for simplicity, although in practical systems, the efficiency will need to be accounted for), and feeding it to the pump, thereby making the solar collector-TEG coupled system completely self-autonomous. In reality, the pump actually plugs into an electrical outlet, thereby requiring an external source for power. Here, however, the coupled system is treated as being self-autonomous and as not depending on any external sources for electrical power.

Other Numerical Parameters

Finally, since the numerical model resembled the upcoming Characterization Test (see 4.4), the properties and parameters listed in 4.4.4 were incorporated into the numerical model. And, while numerical results are later graphically shown in U.S. Customary Units (i.e., temperatures in °F), the numerical model performed all iterations and calculations in SI units (i.e., with temperatures in °C) to ensure accuracy.

3.4.2.2 Numerical Controls

Three primary controls were added to the numerical model to accurately simulate the TEG during operation:

1. Solar collector only ON for $\dot{Q}_U > 0$; this criterion ensured that the solar collector was operated only when it was advantageous.
2. Solar collector shut OFF just below $T_{S,MAX}$, at $T_S \geq 78$ ℃ (172.4 °F); this criterion ensured that the storage tank temperature did not surpass its maximum allowable temperature of $T_{S,MAX} = 80$ ℃ (176 °F) (see 4.4 for more storage tank details).
3. TEG only ON just above $T_{H,MIN}$, at $T_S > 56.4$ ℃ (133.6 °F); this criterion ensured that the TEG was operated per its operating conditions and outputted its nominal power of 83 W (see 2.2.2).

It is important to note that based on numerical controls (2) and (3), the TEG's operating temperature window was effectively set to be:

$$56.4 \text{ ℃ } (133.6 \text{ °F}) < T_S \leq 78 \text{ ℃ } (172.4 \text{ °F}) \tag{3.29}$$

This was a slightly conservative window of the TEG's actual operating window per its default operating conditions (see 2.2.2):

$$T_{H,MIN}\ (130\ °\text{F}) < T_S \leq T_{S,MAX}\ (176\ °\text{F}) \tag{3.30}$$

Other operating windows were not considered in this analysis. Further, note that the TEG's minimum hot stream inlet temperature, $T_{H,MIN}$, governed the lower operating temperature limit, whereas the maximum storage tank temperature, $T_{S,MAX}$, governed the upper operating temperature limit.

See Appendix B.2 for the MATLAB script.

3.4.3 Numerical Stability and Accuracy

As with any numerical model, two of the biggest concerns of the numerical scheme selected to solve the governing differential equation deal with the scheme's stability and accuracy. Numerical instability is best exemplified by unbounded growth or oscillations in the numerical solution and are usually indicative of using too large of a time step. Here, recall that a forward Euler explicit finite difference scheme (Equation 3.23)—a conditionally stable scheme based on the time step chosen—was selected for time integration. Additionally, recall that the governing equation that resulted from the control volume analysis was a first-order ordinary differential equation (ODE) (see 3.2.3). (Generally speaking, also recall that a first-order ODE only has a single eigenvalue, λ.)

Consideration of the numerical scheme's stability entails a stability analysis, in which the amplification factor of the particular scheme is quantified and graphed on a stability diagram [32]. The amplification factor (as part of the stability analysis) is a function of the ODE's eigenvalue(s), and its absolute value must be less than unity for numerical stability [32].

A forward Euler explicit finite difference scheme is always unstable for purely imaginary λ, whereas for real λ, it is stable only for certain values of $\lambda\Delta t$ [32]. As a result, the time step size, Δt, for numerically solving a first-order ODE via a forward Euler explicit finite difference scheme, is limited to [32]:

$$\Delta t \leq \frac{2}{|\lambda|} \tag{3.31}$$

Thus, in order to determine the minimum time step size required, the eigenvalue of the ODE must be determined and quantified. The simplest approach to accomplish this is simply to express the governing ODE in the following form:

$$\frac{\mathrm{d}T_S}{\mathrm{d}t} = \lambda T_S + C \tag{3.32}$$

Here, C is a non-relevant value which may be time-dependent. Following this approach, the ODE was expressed in Equation 3.32-form:

$$\frac{\mathrm{d}T_S}{\mathrm{d}t} = \left(\frac{n_{SC}A_{SC}m_{SC} - U_S A_S}{\rho V_S c_P}\right) T_S + \left(\frac{n_{SC}A_{SC}\eta_0 G_T(t) - m_{SC}n_{SC}A_{SC}T_{SC,AMB}(t) + \dot{L}_{TEG} + U_S A_S T_{S,AMB}}{\rho V_S c_P}\right) \tag{3.33}$$

Therefore, the eigenvalue of the ODE was algebraically determined to be:

$$\lambda = \frac{n_{SC}A_{SC}m_{SC} - U_S A_S}{\rho V_S c_P} \tag{3.34}$$

(Interestingly, each of the discrete data set terms, $G_T(t)$ and $T_{SC,AMB}(t)$, did not affect the eigenvalue of the ODE, but rather C, the nonhomogeneous portion of the ODE. Further, notice that the eigenvalue of the ODE is real and negative; this indicates that if an analytical solution were obtained, it would decay over time with nonoscillatory behavior.)

Quantifying Equation 3.34 with the appropriate parameters (see 4.4.4), the following eigenvalue is obtained:

$$\lambda = -1.371 \cdot 10^{-5} \left[\mathrm{s}^{-1}\right] \tag{3.35}$$

Thus, per Equation 3.31, the time step for integration is limited to:

$$\Delta t \leq 40.52 \text{ hr} \tag{3.36}$$

As Equation 3.26 lists, time integration was advanced with a quarter-hourly step size, i.e., $\Delta t = 0.25$ hr. Thus, it was clear that the quarter-hour time step was well within the numerical scheme's region of stability. This was in fact corroborated by running the numerical model with an hourly time step and obtaining the exact same results.

Finally, regarding accuracy, the finite difference scheme selected for time integration was of the first order. The order refers to the level of accuracy associated with the numerical scheme. Higher-order time integration schemes exist, most famously Runge-Kutta schemes [32]. In this case, a forward Euler finite difference scheme was elected for its relative ease in implementation.

3.5 RESULTS OF NUMERICAL ANALYSIS

This section includes the following 5 solution plots:

- Beam/direct tilt factor, R_b, and insolation multipliers, F_d and F_r, (see 3.3.3), which were calculated from normal insolation data
- Insolation incident on the tilted collector, G_T, which were calculated from normal insolation data
- Solar collector's $\dot{Q}_U$ and ON/OFF status
- Storage tank temperature, T_S, over the course of a day
- TEG's ON/OFF status

Collective results for all 12 representative days are included in Appendix B.1. Here, graphical solution plots from only one month (January, i.e., 01/20/2005) are presented for brevity. Additionally, the energy produced by the TEG throughout the entire year of 2005 was quantified, as well as the energy collected by the solar collector.

Moreover, Figure 3.6 shows a high-level flow chart of the results obtained in this analysis. This figure is meant to illustrate the procedure of the analysis for the reader.

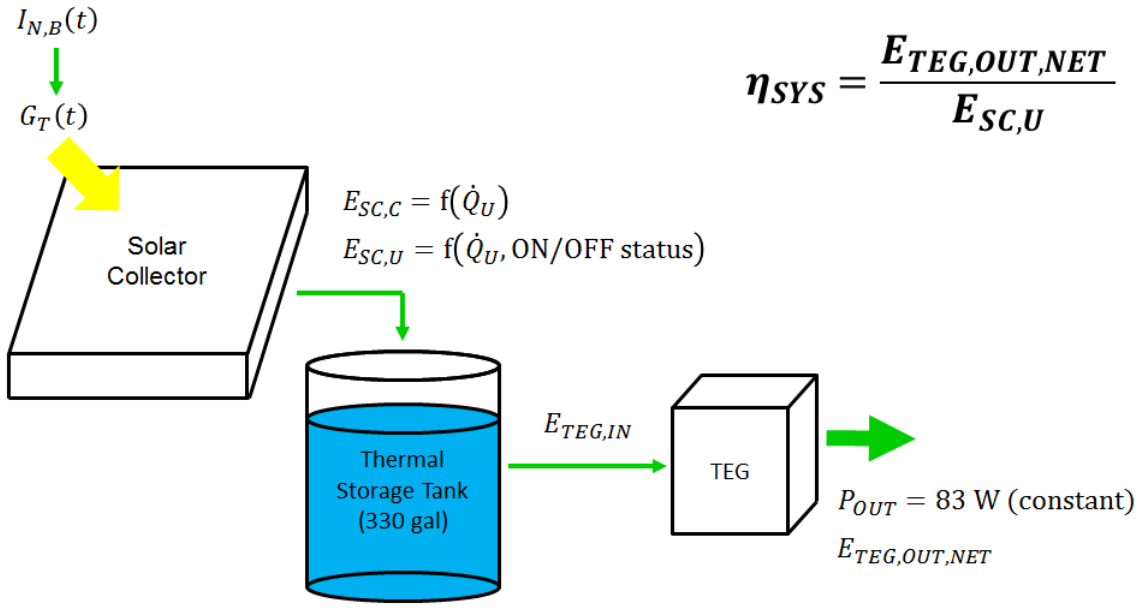

Figure 3.6: High-level flow chart of results of the thermodynamic analysis of the solar collector-TEG coupled system (Chapter 3). The numerical model accounted for all of these components. Note that the solar collector system supplies the TEG with thermal energy, while the TEG itself produces electrical energy.

3.5.1 General Methodology

Prior to presenting results, one important methodological item must be discussed. Recall that the numerical model allowed up to 7 iterations of the same date be modeled (see 3.4.2). Once a specific representative day (i.e., month) was chosen in the model, there was a difference observed in operational trends among the consecutive days (i.e., iterations) modeled. Regardless of how many consecutive days were modeled, the 1st day always exhibited behavior different than subsequent days (i.e., from the 2nd day up to the

7th day)—which featured nearly identical behavior themselves. Thus, the 1st day was always considered to be an "initial charging" day (a "cold start"), whereas any and all subsequent days were always considered to be "steady state operation" days. This operational trend is best exemplified in Figure 3.10. To summarize:

- 1st Model Day: Initial charging day (i.e., "cold start")
- Subsequent days (2nd Model Day, 3rd Model Day, etc., up to the 7th Model Day): Steady state operation days

Finally, it was observed that each date (i.e., month) only required one day of initial charging before reaching steady state operation. This was based on the particular setup of the upcoming Characterization Test. Should a different setup be modeled (e.g., fewer solar collectors or more than a single thermal storage tank), this would change accordingly.

Overall, this methodology was adopted in both the graphical presentation of solution plots, as well as the quantification of energy generated by the TEG and collected by the solar collector (3.5.2–3.5.5).

3.5.2 Graphical Solution Plots

3.5.2.1 Methodology

In the graphical presentation of solution plots, since the 2nd through 7th days were "steady state" operation days and thus nearly identical, only the first 3 consecutive days (i.e., iterations) were needed. These first three days conveyed all graphical information. Here, 01/20/2005 was the date selected for presentation. As indicated before, solution plots for all months are included in Appendix B.1.

3.5.2.2 Solution Plots for January 2005

Although 3 consecutive days were plotted for all solution plots, the first two plots presented—calculated tilt/insolation multipliers and calculated insolation data—are plotted for only a single day since insolation data were the same for all consecutive days (see discussion in 3.4.2).

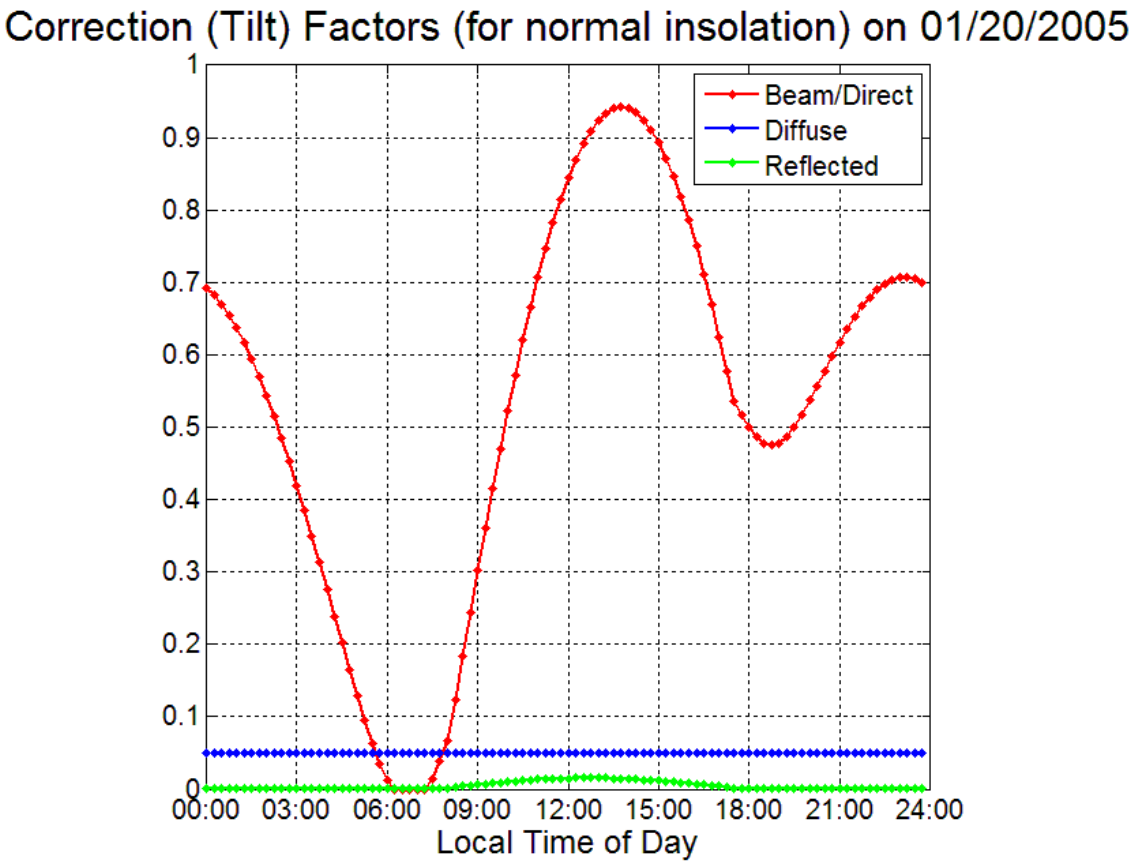

Figure 3.7: Solution plot for 01/20/2005: Calculated tilt/insolation multipliers.

The tilt factor, R_b, and insolation multipliers, F_d and F_r, were both calculated from normal insolation data (see 3.3.3). Here, the appropriate solar angle restrictions

were placed, as indicated in Appendix A.2.1. The sum of all three components defined the single insolation factor, F_{TOT}.

As expected, the diffuse and reflected insolation components incident on the tilted collector (F_d and F_r) were substantially less than the beam/direct tilt factor (R_b) incident on the tilted collector. Also, no single component was greater than unity, and peak values occurred at solar noon (usually approximately 12:45 LST), as expected.

Further, note that although R_b was relatively large in the early morning (before 06:00 HRS) and night (after 18:00 HRS) hours, it had no effect on any results since there was no insolation during these times (i.e., insolation was zero).

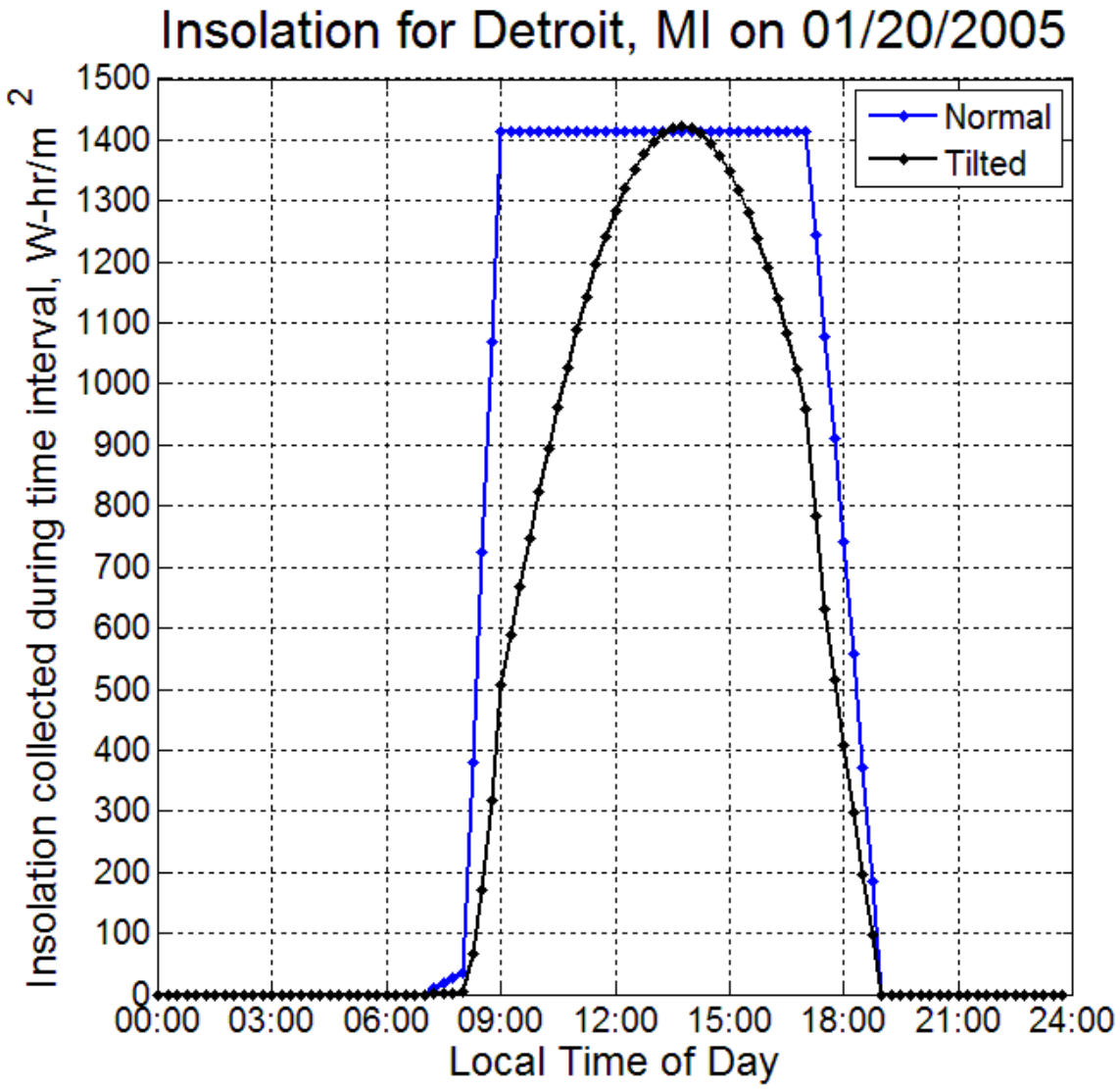

Figure 3.8: Solution plot for 01/20/2005: Insolation values incident on the tilted solar collector (calculated from normal insolation data) and the normal insolation data set itself.

The insolation incident on the tilted collector, G_T, was derived by multiplying normal insolation data, $I_{N,B}$, with the insolation factor, F_{TOT}, (see 3.3.3). Note how the insolation factor followed the shape of the beam/direct tilt factor, R_b.

Finally, these insolation values were inputs to the useful power collected from the solar collector, $\dot{Q}_U$, parameter.

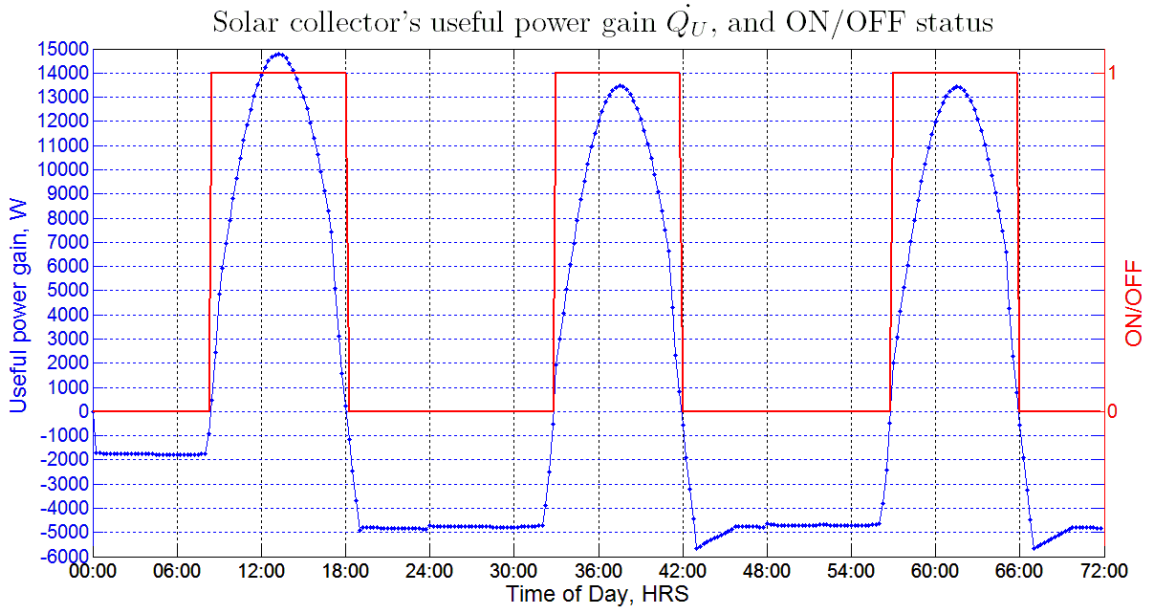

Figure 3.9: Solution plot for 01/20/2005: Solar collector results. The collector switched ON when $\dot{Q}_U$ was positive. (Note that in the right vertical axis, the placement of the "ON" binary value is arbitrary.)

Not surprisingly, running the collector in the early morning hours (00:00 through 08:15 HRS) was not advantageous, hence the negative $\dot{Q}_U$ quantities. Thus, the model kept the collector OFF during this time interval. The collector then switched ON once daybreak occurred and insolation was received on the collector, which occurred at 08:30 HRS. Finally, the collector shut OFF at sunset (at 18:15 HRS), and remained OFF until the following sunrise. This general process repeated indefinitely (or, for 2 more days as shown).

The solar collector observed a peak thermal power of roughly 15 kW during the first day (at 13:15 HRS), then roughly 13.5 kW every day thereafter. The reason that the

power decreased after subsequent days was that the storage tank convected at a much greater rate because of the greater water temperatures (see Equations 3.6 and 3.9). (Recall that insolation was identical each day and thus a constant input in the model.)

It is interesting to note that for the majority of the other representative days (not shown here), the collector was at times forced to shut OFF during daylight hours (see Appendix B.1). This occurred because the storage tank temperature, T_S, approached its maximum water temperature (see Figure 3.10), which was directly a result of the solar collector system utilizing too many solar collectors (see 3.4.2). However, in this study, since the solar collector system size was not a design variable but rather a given based on the Characterization Test (see 4.4), no action was taken.

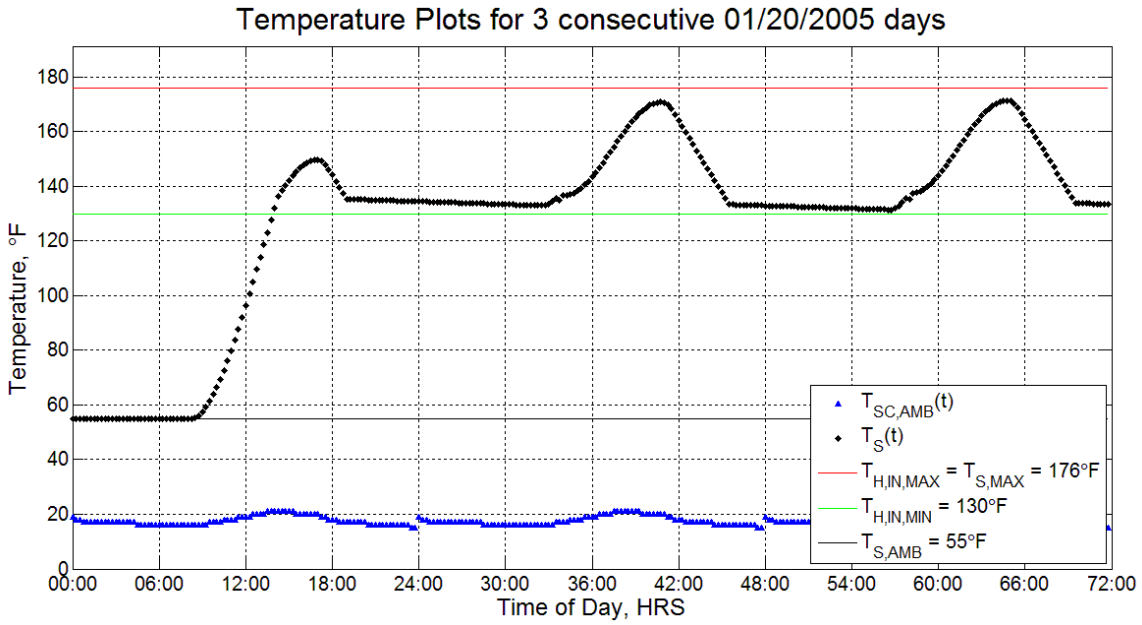

Figure 3.10: Solution plot for 01/20/2005: Storage tank temperature. In particular, notice how all days after the 1st are nearly identical, hence referred to as "steady state operation" days.

Obtaining this particular plot (Figure 3.10) was the motivation for building the numerical model in the first place, since the storage tank temperature, T_S, was the TEG's hot stream inlet temperature, $T_{H,IN}$. This temperature plot T_S was directly affected by the solar collector's ON/OFF status (which supplies power), as well as the TEG's ON/OFF status (the thermal load on the system).

On the first day, T_S started at the storage tank's constant ambient temperature of 55 °F, and remained at this temperature while the collector was OFF. Once sunrise occurred and the collector switched ON upon receiving insolation at 08:30 HRS, T_S began rising dramatically and surpassed 130 °F at 14:00 HRS. Once the TEG switched ON at 14:30 HRS (recall the conservative TEG operating window discussed in 3.4.2), the rate of T_S's increase began slowing, eventually hitting a first-day peak temperature of $T_S = 149.8$ °F at 17:00 HRS. Later, although the collector shut OFF at 18:15 HRS, the TEG remained ON, and thus T_S continued dropping. Once the TEG shut OFF at 19:15 HRS, T_S remained at a fairly constant overnight temperature of approximately 134 °F and dropped less than 2 °F through the night. The overnight temperature drop was due to the storage tank convecting to the fairly cold ambient (55 °F).

On the second day, the collector switched ON for that individual day at 33:00 HRS, resulting in an immediate but minor increase in T_S. At 33:45 HRS, the TEG switched ON, resulting in a momentary decrease in T_S. However, during this decrease, T_S reached a temperature below the lower operating limit of the TEG, and the TEG was consequently forced to shut OFF at 34:00 HRS. The TEG's shutting OFF allowed T_S to begin increasing again due to the increasing insolation incident on the collector. Then, at 34:15 HRS, the TEG was allowed to switch ON once again, and remained ON for the remainder of the day. As a result, T_S continued to rise in spite of the TEG load, hitting a peak temperature of $T_S = 170.8$ °F at 40:45 HRS. Once insolation declined, T_S began

dropping once again, since the TEG remained ON. Finally, the collector shut OFF at 42:00 HRS and the TEG shut OFF at 45:45 HRS. Then, T_S reached its constant overnight temperature of approximately 132 °F, similar to the previous night. This general pattern repeated during the third day.

It is interesting to note that T_S did not reach its upper operating limit on this particular date from January. This occurred because insolation values were relatively low, being a winter month. Had the upper limit been reached, the collector would have momentarily shut OFF in order to allow T_S to cool down, meanwhile keeping the TEG ON and operating without interruption. This occurrence typically caused various temporary ON/OFF fluctuations from the collector during daylight hours, which in turn manifested itself on the T_S solution plot as jagged peaks right at the upper operating limit (just below the maximum storage tank temperature, $T_{S,MAX}$). This behavior was observed to occur for essentially every represented month except January (presented here) and December (see Appendix B.1).

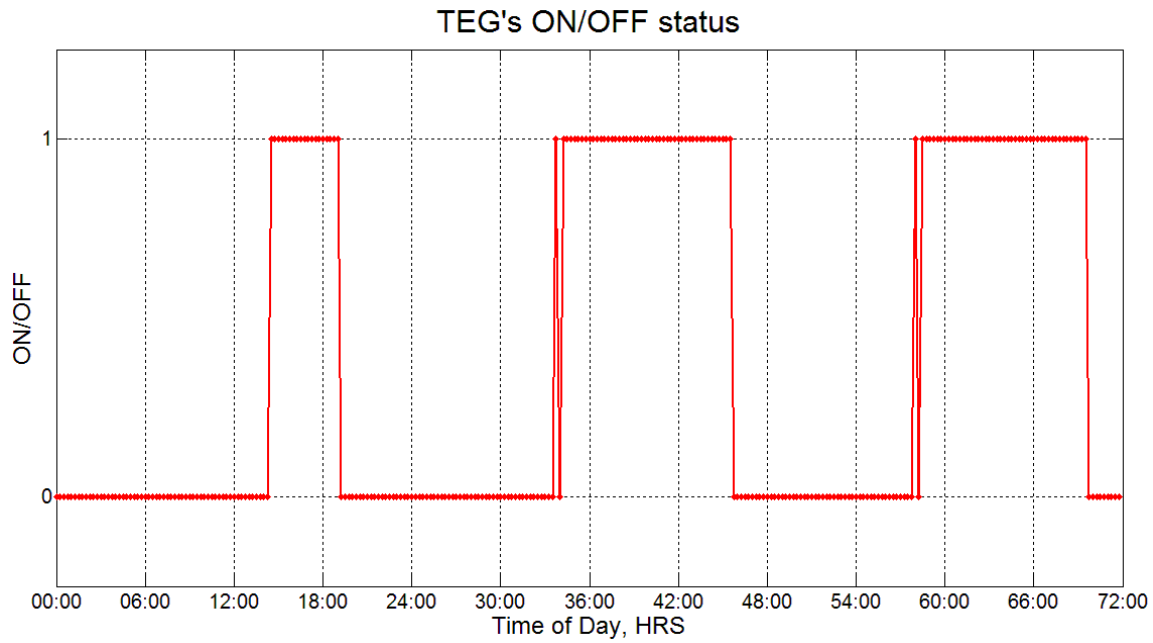

Figure 3.11: Solution plot for 01/20/2005: TEG status. The TEG's ON/OFF status was solely dependent on whether the thermal storage tank temperature was within its temperature window per Equations 3.29 and 3.30.

Recall that the storage tank temperature, T_S, was the TEG's hot stream inlet temperature, $T_{H,IN}$. As such, the ON/OFF status of the TEG was governed by T_S. Here, it was observed that the TEG was only able to switch ON after noon of the first day (due to the storage tank temperature "charging"), but was able to remain ON during daylight hours of the second and third days.

The initial ON/OFF fluctuations seen at the beginning of the second and third days were the result of the storage tank temperature, T_S, entering the TEG's operating temperature window, but being unable to sustain the TEG's thermal load (see Equation 3.28) once it switched ON. However, after this small initial "hiccup," the TEG remained ON during daylight hours thereafter.

3.5.3 Quantifying the Total Electricity Produced by the Thermoelectric Generator in 2005

As indicated at the start of this chapter, one of the motivations for this entire analysis was to quantify the electricity generated by the TEG during operation, as well as the thermal energy consumed, in the year 2005. The only caveat to be noted here was that in the numerical model, the TEG was assumed to be a constant thermal load, $\dot{L}_{TEG}$ (Equation 3.28), on the thermal storage tank.

3.5.3.1 Methodology

In order to accomplish this, the following approach as taken. There are approximately 365.25 days in a year [30]. This value was taken and divided into 12 months:

$$365.25\ {}^{\text{days}}/_{\text{year}} \div 12\ {}^{\text{months}}/_{\text{year}} = 30.4375\ {}^{\text{days}}/_{\text{month}}$$

Recall that the numerical model of the solar collector-TEG coupled system allowed up to 7 consecutive days to be simulated for each representative day (see 3.4.2). Further, recall the operational trends outlined in 3.5.1:

Model Day 1: Initial Charging

Model Days 2-7: Steady State Operation

In real-time operation, once the coupled system is installed, the initial charging only occurs once a year. That is, a “cold start” only occurs once a year, and the remainder of the days in the year will feature the coupled system in steady state operation. That is,

January 1, 2005: Initial Charging ("Cold Start") Day

Remainder of days in year 2005: Steady State Operation Days

Here, the dilemma was that in the numerical model, once a date was chosen, it always began with a cold start. For example, if the month of March were chosen (i.e.,

03/20/2005), the numerical model's results would begin with a cold start. However, in a real system, all of March would operate at steady state, since the cold start had already occurred on January 1, 2005. Thus, to circumvent the issue, the initial charging days for the months of February through December were neglected and instead converted to steady state operation days.

In order to quantify the total electrical energy produced by the TEG, the first step was to quantify the amount of time that the TEG was ON during each month. To accomplish this, the following formulas were adopted:

For January:

$$\left(\text{Time ON in Model Day 1 } [\,{}^{\text{hours}}/_{\text{day}}]\right)\left(\mathbf{1}\ {}^{\text{day}}/_{\text{month}}\right) +$$

$$\left(\text{Average Time ON in Model Days 2-7 } [\,{}^{\text{hours}}/_{\text{day}}]\right)\left(\mathbf{29.4375}\ {}^{\text{days}}/_{\text{month}}\right) =$$

$$\text{Total Time ON during Month } [\,{}^{\text{hours}}/_{\text{month}}] \qquad (3.37)$$

For February through December (remainder of months):

$$\left(\text{Time ON in Model Day 1 } [\,{}^{\text{hours}}/_{\text{day}}]\right)\left(\mathbf{0}\ {}^{\text{day}}/_{\text{month}}\right) +$$

$$\left(\text{Average Time ON in Model Days 2-7 } [\,{}^{\text{hours}}/_{\text{day}}]\right)\left(\mathbf{30.4375}\ {}^{\text{days}}/_{\text{month}}\right) =$$

$$\text{Total Time ON during Month } [\,{}^{\text{hours}}/_{\text{month}}] \qquad (3.38)$$

Note that the difference in the two formulas is how the initial charging day is considered for January but neglected for February through December. Also, note how only the steady state operation days are considered for the months of February through December. This ensured that a cold start occurred only in the first day of the year (Jan 1st), and that the remaining days in the year (Jan 2nd and on) were steady state operation days.

Next, the TEG's electrical power output was considered. Recall that it was assumed that for any time that the TEG was ON, it produced a constant 83 Watts of electrical power (see 3.2.1). Equations 3.37 and 3.38 were used to calculate the total energy produced by the TEG for each month:

$$(0.083\ \text{kW})\left(\text{Total Time ON during Month}\ [\,{}^{\text{hours}}/_{\text{month}}\,]\right) = \text{Total Energy Produced during Month}\ [\,{}^{\text{kWh}}/_{\text{month}}] \quad (3.39)$$

This formula was applied to all 12 months in order to obtain the total energy produced by the TEG during each represented month. Finally, these values were summed in order to obtain the total energy for the entire year of 2005.

3.5.3.2 Results

Following this methodology, Table 3.3 was produced.

	Time ON [hr]		Total Time TEG ON during Month, per Equations 3.37 and 3.38 [hr]	Total Electrical Energy Produced by TEG during Month, per Equation 3.39 [kWh]
	Initial Charging (Day 1)	Steady State Operation (Avg. of Days 2–7)		
Jan	4.75	11.6	345.7	28.7
Feb	--	12.3	372.9	30.9
Mar	--	12.7	386.8	32.1
Apr	--	13.8	419.8	34.8
May	--	15.6	474.3	39.4
Jun	--	16.5	501.0	41.6
Jul	--	16.0	487.0	40.4
Aug	--	14.2	432.5	35.9
Sept	--	13.3	404.6	33.6
Oct	--	12.5	380.5	31.6
Nov	--	12.0	366.5	30.4
Dec	--	11.4	346.2	28.7

Table 3.3: Summary of TEG's electrical energy output for all 12 months, based on the numerical model. It was assumed that the TEG produced a constant 83 Watts as long as the TEG was ON. See Figure 3.13 for graphical presentation of the final column.

Summing the penultimate column, it is interesting to note that of the 8,766 hours in a year (following the methodology of using 365.25 days in a year described previously), the TEG was only ON for 56.1% of the time of the year. (Therefore, this can

be viewed as a "capacity factor," which is discussed later in 5.2.) Thus the time that the TEG was ON was:

$$\text{Time TEG ON} = 4{,}917.70\ {}^{\text{hours}}/_{\text{year}} \tag{3.40}$$

Note that Equation 3.40 was obtained from the numerical model, and that it was directly a result of the thermal load that the TEG presented on the storage tank per Equation 3.28. Further, recall that this thermal load of $\dot{L}_{TEG} = \text{-}6{,}925.9\ \text{W}$ was a conservative assumption (see 3.4.2.1). Therefore, the total thermal energy consumed by the TEG in the year was therefore:

$$E_{TEG,IN} = \left(\dot{L}_{TEG}\right)(\text{Time TEG ON}) = 34.06\ \text{MWh/year} \tag{3.41}$$

Continuing, by summing the final column of values, it was concluded that the total electricity generated from the TEG for the year was:

$$E_{TEG,OUT} = 408.2\ \text{kWh/year} \tag{3.42}$$

(Alternatively, note that Equation 3.42 could have also been derived by multiplying 83 Watts with Equation 3.40, similar to Equation 3.41 above; both procedures are identical. Furthermore, note that the absolute maximum amount of annual electricity generation from the TEG is approximately 727 kWh, if it were to be operated continually throughout the year.)

Until this point, the TEG's two recirculation pumps (see 2.2.1 and Figure 3.3) have not yet been considered in the analysis. As indicated in 3.2.1, these pumps were in fact included in this analysis. So, in order to make the TEG fully self-autonomous during operation (similar to the solar collector system outlined in 3.4.2.1), it was modeled that the TEG would supply the electrical power requirement for both pumps. Each pump operated at 12 V and 1.2 A, therefore giving each a power rating of 14.4 Watts. Two pumps therefore required 28.8 Watts. (Thus, the 83 Watts was essentially reduced to 54.2

Watts.) Using the same methodology of Equation 3.39, the total energy that the two pumps consumed collectively throughout the year was calculated:

$$E_{TEG,PUMPS} = 141.6\ \text{kWh/year} \tag{3.43}$$

Note that this value was 34.7% of the energy produced by the TEG, a substantial value. Should these pumps be powered in another way (and not from the TEG), then Equation 3.42 should be used. Similarly, should lower-power pumps be used (as was being planned by *Watts Thermoelectric LLC* at the time of writing), then Equation 3.43 (and Equation 3.44) would consequently differ in a beneficial way.

Next, Equation 3.43 was deducted from Equation 3.42 to yield the net annual electricity generated by the TEG (a single rack) during the year 2005:

$$E_{TEG,OUT,NET} = E_{TEG,OUT} - E_{TEG,PUMPS} = 266.5\ \text{kWh/year} \tag{3.44}$$

This value was one of the main results of this portion of the analysis, and was used as the input for the subsequent Emissions and Economic Analyses (see Chapter 5).

The final step to this analysis was considering the energy produced by implementing more than one TEG. With each TEG producing 266.5 kWh, TEGs could conceivably be stacked for a linear increase in energy output, as shown in Figure 3.12.

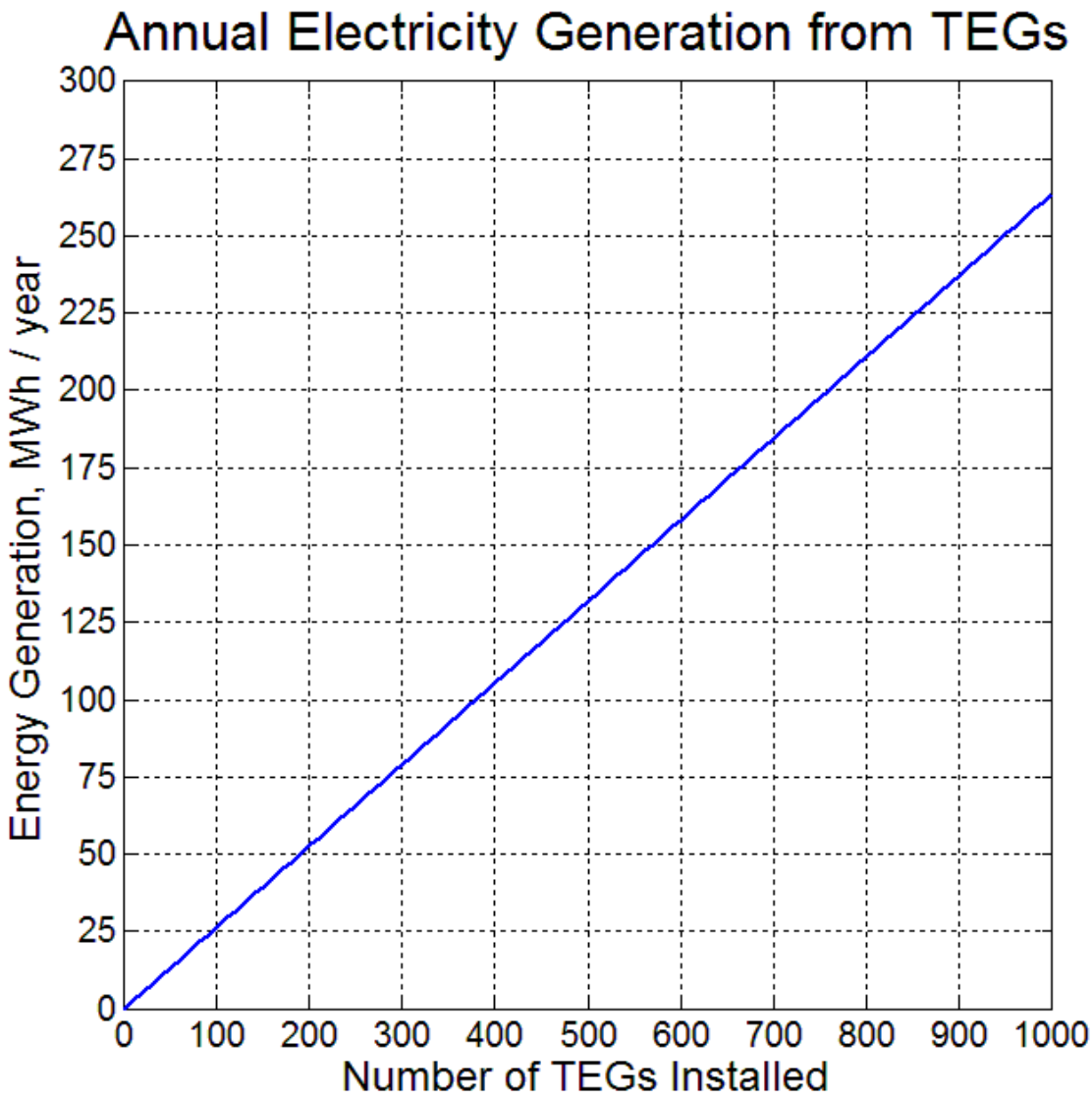

Figure 3.12: The implementation of more than one TEG would likely be most practical in a real setting. According to numerical results, each TEG produced a net annual 266.5 kWh of electricity in its default configuration.

3.5.4 Quantifying the Total Energy Collected and Used by the Solar Collector System in 2005

As indicated at the start of this chapter, the other primary motivations for this entire analysis were to quantify both the thermal energy *collected* by the solar collector, as well as the thermal energy actually *used* in the coupled system, in the year 2005.

In order to distinguish between the two parameters—thermal energy *collected*, $E_{SC,C}$, and thermal energy *used*, $E_{SC,U}$—recall that the solar collector was not always ON during daylight hours; the collector was at times forced to shut OFF (see 3.5.2.2). However, the numerical model was constructed such that it was able to calculate the thermal energy collected independently of whether the solar collector system was ON or OFF. Thus, the $E_{SC,C}$ parameter assumed that the collector was always ON, whereas the $E_{SC,U}$ parameter accounted for the collector's ON/OFF status. The $E_{SC,C}$ parameter is therefore a hypothetical parameter, while $E_{SC,U}$ is a realistic parameter. This versatility in the numerical model allowed both parameters to be quantified in this analysis. Of course, it should be noted that in a real system, only the $E_{SC,U}$ parameter would exist, as it is based on whether the solar collector were ON or OFF.

To summarize,

- Thermal energy *collected* by the solar collector, $E_{SC,C}$, hypothetically assumes the collector is always ON; thus, $E_{SC,C} = \mathrm{f}(\dot{Q}_U)$
- Thermal energy *used* by the solar collector, $E_{SC,U}$, is realistically based on the collector's ON/OFF status; thus, $E_{SC,U} = \mathrm{f}(\dot{Q}_U, \mathrm{ON/OFF\ status})$

3.5.4.1 Methodology

In order to quantify the amount of thermal energy collected by the solar collector throughout the year, $E_{SC,C}$, the $\dot{Q}_U$ curve (see Figure 3.9) was numerically integrated

versus time. This integration was accomplished by calculating the trapezoidal area for every pair of data points (i.e., first the *n* and *n+1* data points, then *n+1* and *n+2*, etc.) for each date modeled. In contrast, to calculate the actual energy *used*, $E_{SC,U}$, the $\dot{Q}_U$ curve was simply multiplied by its ON/OFF status (a binary vector of 1s and 0s) and integrated. Then, a similar approach as explained in 3.5.3.1 was followed.

As before, the year was broken up into:

January 1, 2005: Initial Charging ("Cold Start") Day

Remainder of days in year 2005: Steady State Operation Days

In order to quantify the thermal energy collected by the collector during each month, the following formula was adopted:

For January:

$$\left(\text{Energy Collected in Day 1 } [\,{}^{\text{kWh}}/_{\text{day}}\,]\right)\left(\mathbf{1}\ {}^{\text{day}}/_{\text{month}}\right)+$$

$$\left(\text{Average Energy Collected in Days 2-7 } [\,{}^{\text{kWh}}/_{\text{day}}\,]\right)\left(\mathbf{29.4375}\ {}^{\text{days}}/_{\text{month}}\right)=$$

$$\text{Total Energy Collected for that Month } [\,{}^{\text{kWh}}/_{\text{month}}] \qquad (3.45)$$

For February through December (remainder of months):

$$\left(\text{Energy Collected in Day 1 } [\,{}^{\text{kWh}}/_{\text{day}}\,]\right)\left(\mathbf{0}\ {}^{\text{day}}/_{\text{month}}\right)+$$

$$\left(\text{Average Energy Collected in Days 2-7 } [\,{}^{\text{kWh}}/_{\text{day}}\,]\right)\left(\mathbf{30.4375}\ {}^{\text{days}}/_{\text{month}}\right)=$$

$$\text{Total Energy Collected for that Month } [\,{}^{\text{kWh}}/_{\text{month}}] \qquad (3.46)$$

Similarly, the energy actually used (as opposed to collected) was calculated in the same fashion:

For January:

$$\left(\text{Energy Used in Day 1 } [\,{}^{\text{kWh}}/_{\text{day}}\,]\right)\left(\mathbf{1}\ {}^{\text{day}}/_{\text{month}}\right)+$$

$$\left(\text{Average Energy Used in Days 2-7 } [\,{}^{\text{kWh}}/_{\text{day}}\,]\right)\left(\mathbf{29.4375}\ {}^{\text{days}}/_{\text{month}}\right) =$$

$$\text{Total Energy Collected for that Month } [\,{}^{\text{kWh}}/_{\text{month}}] \qquad (3.47)$$

For February through December (remainder of months):

$$\left(\text{Energy Used in Day 1 } [\,{}^{\text{kWh}}/_{\text{day}}\,]\right)\left(\mathbf{0}\ {}^{\text{day}}/_{\text{month}}\right) +$$

$$\left(\text{Average Energy Used in Days 2-7 } [\,{}^{\text{kWh}}/_{\text{day}}\,]\right)\left(\mathbf{30.4375}\ {}^{\text{days}}/_{\text{month}}\right) =$$

$$\text{Total Energy Collected for that Month } [\,{}^{\text{kWh}}/_{\text{month}}] \qquad (3.48)$$

These formulas were applied to all 12 months in order to obtain the total energy collected and used by the solar collected during each represented month. Finally, these values were summed in order to obtain the total energy for the entire year of 2005.

3.5.4.2 Results

Following this methodology, Table 3.4 was produced.

	Energy Collected [kWh]		Energy Used [kWh]		Total Thermal Energy Collected during Month, per Equations 3.45 and 3.46 [kWh]	Total Thermal Energy Used during Month, per Equations 3.47 and 3.48 [kWh]
	Initial Charging (Day 1)	Steady State Operation (Avg. of Days 2–7)	Initial Charging (Day 1)	Steady State Operation (Avg. of Days 2–7)		
Jan	98.9	84.0	98.9	84.0	2,570.8	2,570.8
Feb	--	91.2	--	88.8	2,776.6	2,702.7
Mar	--	100.6	--	92.0	3,061.0	2,799.9
Apr	--	115.4	--	99.5	3,513.8	3,027.7
May	--	128.2	--	111.1	3,900.9	3,381.7
Jun	--	137.5	--	117.4	4,186.5	3,572.9
Jul	--	136.3	--	114.0	4,149.7	3,469.9
Aug	--	119.9	--	101.8	3,650.8	3,097.2
Sept	--	116.1	--	95.9	3,534.0	2,918.0
Oct	--	102.0	--	90.6	3,105.3	2,757.6
Nov	--	91.1	--	87.0	2,771.6	2,649.1
Dec	--	82.5	--	82.5	2,510.7	2,510.7

Table 3.4: Summary of thermal energy collected and used by the solar collector for all 12 months, based on the numerical model. Note that the energy collected and used was identical only for the months of January and December. See Figure 3.13 for graphical presentation of the final two columns.

Summing the final column of values, it was concluded that the total energy *collected* by the solar collector for the year was (note the unit change):

$$E_{SC,C} = 39.73 \text{ MWh/year} \tag{3.49}$$

Similarly, it was concluded that the total energy actually *used* by the solar collector for the year was:

$$E_{SC,U} = 35.46 \text{ MWh/year} \tag{3.50}$$

Here, it was expected for Equation 3.50 to be identical to the total thermal energy consumed by the TEG, $E_{TEG,IN}$ (Equation 3.41). However, there was a difference of 1.40 MWh. The discrepancy was attributed to the trapezoidal integration procedure used to quantify the $E_{SC,U}$ parameter, as explained in 3.5.4.1.

Finally, as an aside, these two values were divided by the number of collectors (20; see 4.4.2) in order to obtain a Watt-per-collector (per year) value. Here, it is assumed that each collector in the system had an equal contribution to the overall output:

$$E_{SC,C} = 1.99 \text{ MWh/collector/year} \tag{3.51}$$

$$E_{SC,U} = 1.77 \text{ MWh/collector/year} \tag{3.52}$$

3.5.5 The Efficiency of the Solar Collector-Thermoelectric Generator Coupled System

The previous two sections quantified the net annual energy generated by the TEG (Equation 3.44), as well as the total annual energy both collected and used by the solar collector (Equations 3.49 and 3.50, respectively). Using two of these equations (Equations 3.44 and 3.50), the overall efficiency of the coupled system operating over the course of the year was estimated to be:

$$\eta_{SYS} = \frac{E_{TEG,OUT,NET}}{E_{SC,U}} = \frac{0.267 \text{ MWh/year}}{35.46 \text{ MWh/year}} = 0.75\% \tag{3.53}$$

Additionally, the operating efficiency of the TEG itself *could have* been calculated, since the following parameters were known:

$$E_{TEG,IN} = 34.06 \text{ MWh/year} \tag{3.41}$$

$$E_{TEG,OUT,NET} = 266.5 \text{ kWh/year} \tag{3.44}$$

And since $E_{TEG,IN}$ was a function of $\dot{L}_{TEG}$, recall that $\dot{L}_{TEG}$ was defined as:

$$\dot{L}_{TEG} = \dot{m}_H c_P \Delta T_H \tag{3.13}$$

However, there were two problems with defining the TEG's operating efficiency via Equations 3.41 and 3.44. First, recall that per Equation 3.28, $\dot{L}_{TEG}$ was assigned a value based on a conservative assumption (see 3.4.2), and defining efficiency based on this would result in an erroneous value. Second, the $\dot{m}_H c_P \Delta T_H$ term that constitutes $\dot{L}_{TEG}$ (Equation 3.13) was not entirely used as the heat source for the thermoelectric modules in the TEG, as a portion of the $\dot{m}_H c_P \Delta T_H$ heat transfer term was a convective loss of the hot stream (see Equation 4.7). Thus, in order to determine an accurate and empirical operating efficiency for the TEG, a thermodynamic analysis of the TEG itself and experimental data were required. (This analysis is presented in Chapter 4.)

3.5.6 Summary of Results

To summarize, the preceding sections provided the following results:

$$\text{Time TEG ON} = 4{,}917.70 \ {}^{\text{hours}}/_{\text{year}} \tag{3.40}$$

$$E_{TEG,IN} = 34.06 \text{ MWh/year} \tag{3.41}$$

$$E_{TEG,OUT,NET} = 266.5 \text{ kWh/year} \tag{3.44}$$

$$E_{SC,C} = 39.73 \text{ MWh/year} \tag{3.49}$$

$$E_{SC,U} = 35.46 \text{ MWh/year} \tag{3.50}$$

$$\eta_{SYS} = 0.75\% \tag{3.53}$$

Thus, it was observed that the 20 solar collectors collectively collected (and used) a high amount of thermal energy from insolation throughout the year. However, when coupled with the TEG in order to convert this energy into electrical energy, the coupled system's efficiency was low, and the resultant energy was reduced by two orders of

magnitude. That is, Equations 3.49 and 3.50 were to the order of 10^{1} MWh of thermal energy, and yet Equation 3.44 was to the order of 10^{-1} MWh of electrical energy. These energies are shown graphically in Figure 3.13.

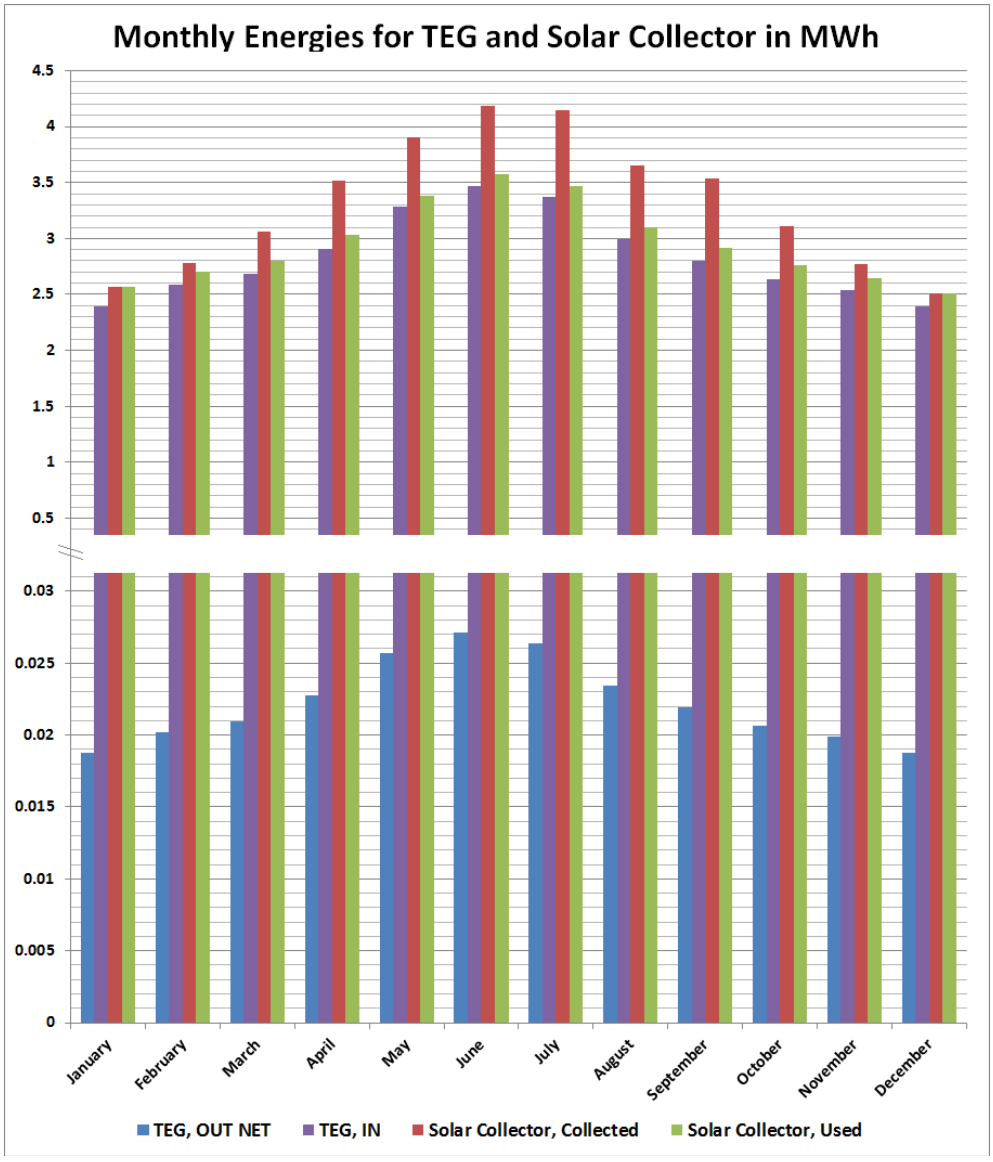

Figure 3.13: The monthly energies associated with the coupled system based on results from the numerical model. Note that all units are in MWh, hence the large discrepancy in values (two orders of magnitude). Further, recall that only a single day of each month represents the entire month (see 3.3.1).

3.6 GEOTHERMAL ENERGY, THE THERMOELECTRIC GENERATOR'S COLD STREAM SOURCE

3.6.1 A Brief Overview of Geothermal Heat Pump Systems

In its default configuration in the built environment, the TEG uses a geothermal energy system as its cold stream source. Geothermal energy systems typically feature a geothermal heat pump (GHP)[3], which draws heat from the earth and deposits it into a space. Accordingly, GHP systems are most commonly used in space heating applications. Thermodynamically, heat pumps (and refrigeration cycles) commonly operate via a vapor compression cycle, whose components consist of an evaporator (heat exchanger), compressor, condenser (heat exchanger), and an expansion valve, with a refrigerant as the working fluid [34, 35].With GHP systems, the evaporator is thermally coupled (i.e., placed in intimate contact) with a ground source, which may be an underground water source or simply the subsurface itself, depending on the particular type of system considered [35]. It is well-documented that below the earth's frost line—a depth that varies 4–6.5 feet below the earth's surface depending on region—the temperature remains at a reliable 50 °F [35]. Thus, the subsurface can be used as a reliable thermal reservoir, as done with GHP systems.

Furthermore, there are two types of GHP systems available—open- and closed-loop systems. Open-loop systems use groundwater sources like aquifers (or wells, springs, flooded mines, rivers, seas, or lakes) as the geothermal source. Open-loop systems draw water from these sources via a borehole and replenish it after using it for a heating or cooling application [35]. Comparatively, as Banks [35] illustrates in Figure 6.11 of his textbook, the cost per installed kilowatt for borehole open-loop systems is

[3] Also commonly referred to a ground-source heat pump (GSHP)

generally greater than horizontally-trenched closed-loop systems (which are discussed in detail in 4.4.3). As a result, open-loop systems were not considered in this study.

Closed-loop systems, on the other hand, operate as vapor-compression cycles, and feature either a refrigerant or an antifreeze solution as the working fluid based on the particular type of system. In such systems, the piping is buried below the surface; the purpose of this is to use geothermal energy as a heat source in place of the system's evaporator in a space heating application [35]. Further, of the four classifications of GHP systems that exist by the Air Conditioning, Heating, and Refrigeration Institute (AHRI), two of these classes refer to closed-loop systems: ARI-330, which refers to a ground source heat pump (GSHP) system, and ARI-870, which refers to a direct geoexchange heat pump (DXHP) system [36].

3.6.2 System in the Default Configuration in the Built Environment

In this particular case, however, the reverse thermodynamic effect was desired. Rather than using the earth as a geothermal heat source, it was necessary to use it as a geothermal heat sink. This is because the TEG's cold stream gains heat as it flows through the TEG (see 2.2.2), and therefore the goal was to extract heat from the cold stream and reject it into the earth. Generally, this is realized via a GHP system operating in reverse, as typically done in space cooling applications [35]. Such a process ensures that the cold stream inlet temperature, $T_{C,IN}$, continuously remains at a constant temperature—a temperature nominally targeted for 55 °F (see Table 2.1). The primary assumption made here was that the geothermal heat sink maintains its temperature over time because this was a small-scale system. However, it was understood that large-scale

systems operating over long time periods could affect the equilibrium subsurface temperature.

More information regarding the geothermal energy system, including the actual setup planned for the upcoming Characterization Test—which differs from the systems outlined here—is discussed in 4.4.3.

3.6.3 System Analysis Excluded from Scope of Study

Finally, as mentioned in 1.2, a comprehensive analysis of this system was not considered. In the thermodynamic analysis of the solar collector-TEG coupled system presented earlier in this chapter, it was simply assumed that the subsurface was as a reliable thermal reservoir and the TEG's cold stream inlet temperature, $T_{C,IN}$, therefore continually remained at a constant 55 °F, as indicated in 3.2.1. This constant-$T_{C,IN}$ assumption was all that was necessary to wholly include the thermodynamic effect of the entire geothermal energy system into the solar collector-TEG coupled system's analysis.

Further, while the electrical requirement of the solar collector's pump was accounted for in the numerical model of the solar collector-TEG coupled system (see 3.4.2), the electrical requirement for the GHP system's compressor was not. Conceivably, the numerical model could have been improved by reducing the solar collector system's thermal power output by exactly the compressor's electrical requirement (and in the process assuming 100% conversion efficiency from thermal to electrical energy), similar to the way that the solar collector's pump was accounted for in the model. (Recall that the TEG's two recirculation pumps were in fact accounted for, per Equation 3.44.) Nevertheless, since the numerical model was originally designed to only model the solar

collector-TEG coupled system, and since the geothermal energy system was beyond the scope of the study, this point was left as a future improvement on the numerical model.

Chapter 4: Thermodynamic Analysis and Characterization of the Thermoelectric Generator during Operation

This chapter considers the systems-level thermodynamic analysis of the novel thermoelectric generator (TEG) itself during operation. This analysis differed from the analysis outlined in the preceding chapter in that now the internal thermodynamics of the TEG itself during operation—decoupled and separate from its hot and cold stream sources—were the focus of the analysis. This analysis was based on a single experimental test of the TEG (referred to as the "Reference Test"), which allowed for a preliminary thermodynamic characterization of the TEG.

This chapter also introduces the upcoming "Characterization Test" on which the numerical model was based on. The Characterization Test is an elaborate experimental test of the TEG operating in the built environment (i.e., coupled with a solar-thermal energy system and geothermal energy system for the hot and cold stream sources, respectively, as in Figure 2.5), and is meant to fully empirically characterize the TEG during operation in the built environment. At the time of writing, this test was in its planning stages and was scheduled to take place later in 2011.

4.1 REFERENCE TEST

Because the TEG was relatively new, it had not undergone rigorous experimental characterization at the time of writing, hence the planning of the upcoming Characterization Test mentioned above. As a result, the TEG's operating conditions were not fully understood. Thus, for purpose of aiding this study, *Watts Thermoelectric LLC* ran a single experimental test—herein referred to as the "Reference Test"—that provided this study with a preliminary operating point for the TEG while the upcoming

Characterization Test (see 4.4) was being planned. The primary purpose for this test was to ascertain a nominal temperature drop across the hot water stream, ΔT_H, in order to accurately model the TEG as a thermal load on the storage tank in the numerical model (see Equation 3.28).

It is important to note that the Reference Test was a single test conducted in an isolated environment on the benchtop—not in the built environment. Hot water from a water heater was used as the hot stream source, and water just slightly below the ambient temperature was used as the cold stream source.

This test was conducted by *Watts Thermoelectric LLC* on April 18, 2011 and its results are listed in Table 4.1.

Parameter	**Measured Value**
P_{OUT}	84 W
$T_{H,IN}$	165.1 °F
$T_{H,OUT}$	132.2 °F
$\dot{V}_H$	1.31 gpm
$T_{C,IN}$	47.0 °F
$T_{C,OUT}$	53.1 °F
$\dot{V}_C$	3.76 gpm
Voltage (avg. per bank)	12.4 Vdc
Ambient Temperature	50 °F

Table 4.1: Reference Test results, performed by *Watts Thermoelectric LLC* on 04/18/2011, where the TEG was operated in an isolated environment [21]. Note that the unit “gpm” refers to gallons per minute.

Here, note that the hot stream volumetric flow rate of $\dot{V}_H = 1.31\,\text{gpm}$ is equivalent to a mass flow rate of $\dot{m}_H = 0.083\,\text{kg/s}$, assuming a constant water density of $\rho = 1{,}000\,\text{kg/m}^3$ (as done through this entire study). Similarly, the cold stream volumetric flow rate of $\dot{V}_C = 3.76\,\text{gpm}$ is equivalent to a mass flow rate of $\dot{m}_C = 0.237\,\text{kg/s}$.

While this test was not performed at the same test conditions as those listed as the TEG's nominal operating conditions (see 2.2.2), approximately the same power output was obtained, as shown by comparing Table 4.1 with Table 2.1. This similarity in performance is attributed to the fact that although the cold stream flow rate is much lower than the nominal flow rate, the hot stream inlet temperature was raised substantially, which in turn countered the effect of the lower flow rate.

Results from this test would go on to thermodynamically characterize the TEG, whose analysis is outlined in the proceeding section.

4.2 Control Volume Analysis of the Thermoelectric Generator during Operation

To begin, the TEG was analyzed as a black box. The primary reason for this was to simplify the analysis and consider only the thermal effects of the TEG. For this analysis, the TEG was modeled as a heat engine rather than as a heat exchanger; the control volume analysis of the TEG therefore reflected this approximation.

Additionally, the TEG was greatly simplified in this analysis, particularly the hot and cold streams. In actuality, hot and cold streams flow through the entire TEG, through heat spreaders in each bank (see 2.2.1), so that each individual thermoelectric module within the TEG is exposed to a hot and cold stream in a counterflow configuration. Thus, in order to facilitate the analysis, only the essential design criteria were taken: the TEG

essentially operated as a heat engine with counterflow streams, similar to a heat exchanger.

Finally, the equations derived from this analysis were quantified in subsequent sections based on results from the Reference Test (see 4.1).

4.2.1 Assumptions

In this control volume analysis, two assumptions were made regarding the convective losses of both fluid streams:

1. Since the hot stream flows through the entire TEG (and not simply the "top" as illustrated in Figures 4.1 and 4.2), the same hot stream convective loss term, $\dot{Q}_{H,L}$, therefore appeared in both CVs 1 and 2a (see Figure 4.1).
2. Since this analysis was based on the Reference Test which featured a low ambient temperature, the cold stream convective loss term, $\dot{Q}_{C,L}$, was assumed to be negligible, which facilitated the analysis.

4.2.2 Energy Balance Derivations of the Thermoelectric Generator

In this portion of the analysis, three separate control volumes were selected and used simultaneously: around the TEG itself between and excluding each of the streams (CV 1), around the hot stream alone (CV 2a), and finally around the cold stream alone (CV 2b).

4.2.2.1 Control Volume 1

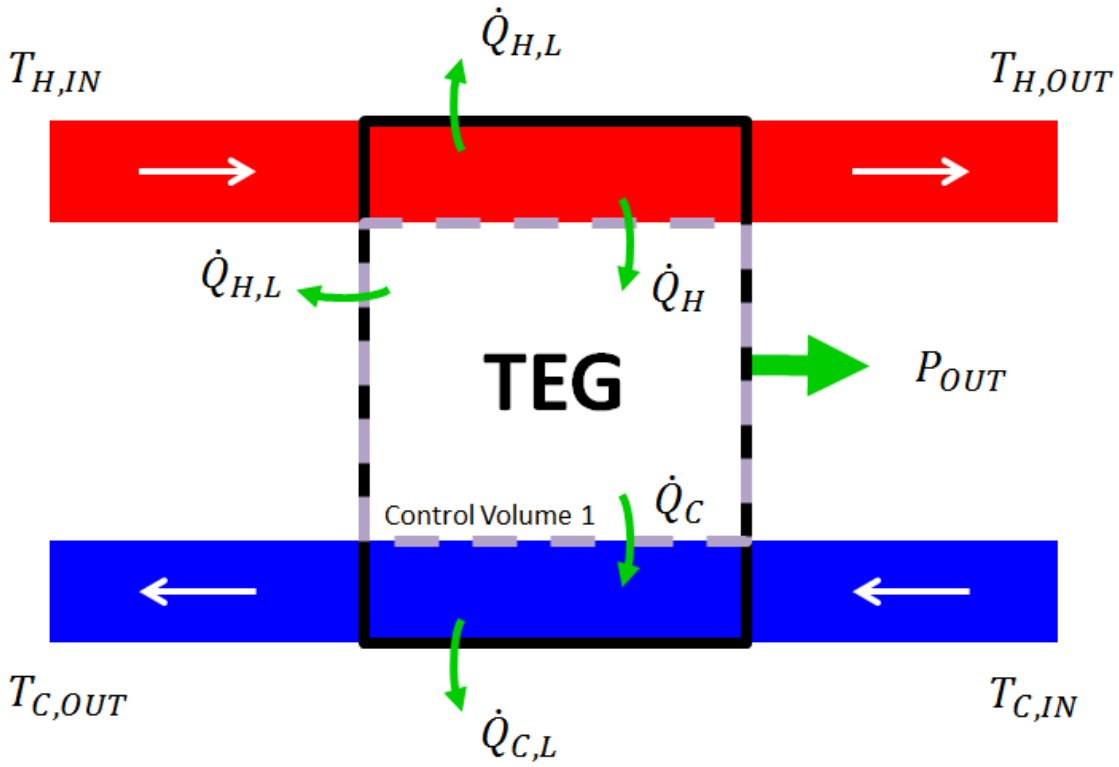

Figure 4.1: Control Volume 1 was the TEG itself, excluding the two streams. Note that the hot stream convective loss term appears twice as assumed (see 4.2.1).

Starting with the same energy balance equation for an open (control volume) system as used in 3.2.2,

$$\dot{E}_{IN} - \dot{E}_{OUT} = \dot{E}_{STOR} - \dot{E}_{GEN} \tag{3.2}$$

Here, the heat transfer into the control volume ($\dot{E}_{IN}$) is the heat transferred from the hot stream, $\dot{Q}_H$. Similarly, the heat transfer out of the control volume ($\dot{E}_{OUT}$) consists of the hot stream's convective loss term, $\dot{Q}_{H,L}$, the heat transferred to the cold stream, $\dot{Q}_C$, and the electrical power produced by the TEG, P_{OUT}. Further, there is no energy storage or generation over time:

$$\dot{Q}_H - \left(\dot{Q}_{H,L} + \dot{Q}_C + P_{OUT}\right) = 0 \tag{4.1}$$

Rearranging,

$$\dot{Q}_H - \dot{Q}_{H,L} = P_{OUT} + \dot{Q}_C \tag{4.2}$$

4.2.2.2 Control Volumes 2a & 2b

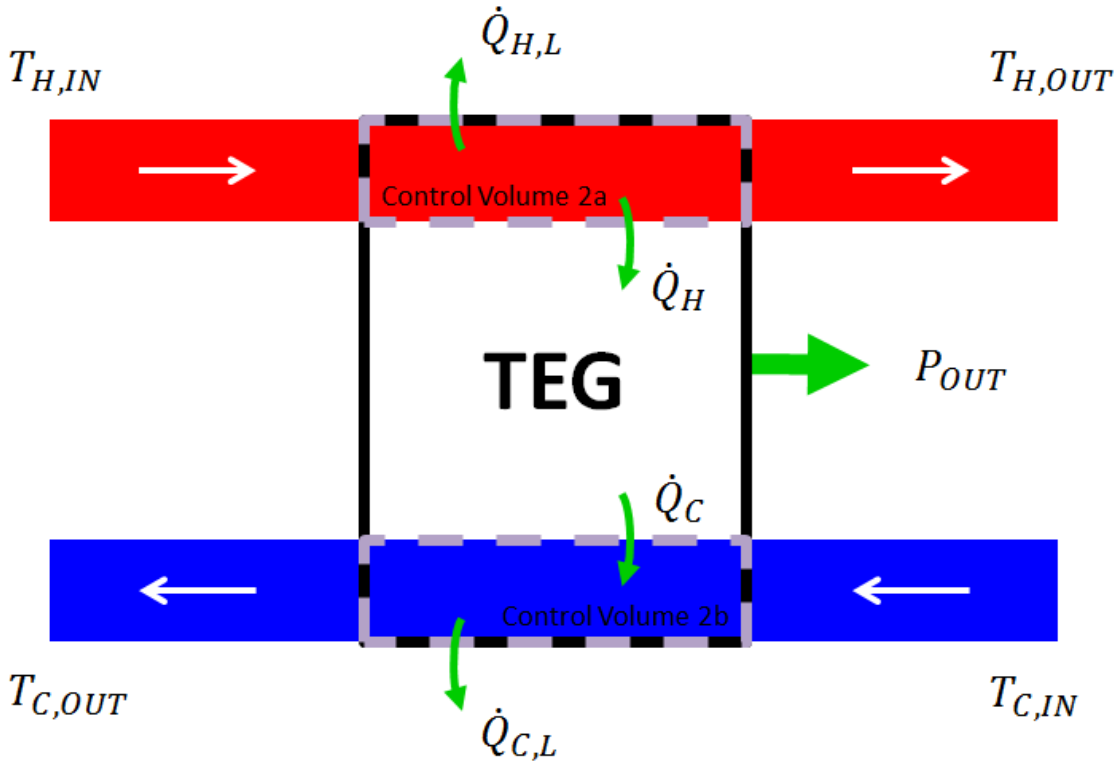

Figure 4.2: Control Volumes 2a and 2b were the hot and cold streams, respectively.

Control Volume 2a

Starting with the energy balance equation for an open (control volume) system once again,

$$\dot{E}_{IN} - \dot{E}_{OUT} = \dot{E}_{STOR} - \dot{E}_{GEN} \tag{3.2}$$

Here, the control volume applies to a single stream. Thus, the heat transfer input and output terms ($\dot{E}_{IN}$ and $\dot{E}_{OUT}$) are functions of the hot stream's mass flow rate and enthalpies. Additionally, the heat transferred from the hot stream, $\dot{Q}_H$, as well as the hot stream's convective losses, $\dot{Q}_{H,L}$, both contribute to the heat transfer output ($\dot{E}_{OUT}$). Finally, there was no energy storage or generation over time:

$$\dot{m}_H h_{H,IN} - \left(\dot{m}_H h_{H,OUT} + \dot{Q}_H + \dot{Q}_{H,L}\right) = 0 \tag{4.3}$$

Rearranging,

$$\dot{m}_H h_{H,IN} - \dot{m}_H h_{H,OUT} - \dot{Q}_H - \dot{Q}_{H,L} = 0 \tag{4.4}$$

$$-\dot{m}_H \Delta h_H - \dot{Q}_H - \dot{Q}_{H,L} = 0 \tag{4.5}$$

As done previously, the following relationship was assumed for the working fluid:

$$\Delta h = c_P \Delta T \tag{3.12}$$

Thus, the $\dot{m}_H \Delta h_H$ term was redefined and Equation 4.5 becomes:

$$-\dot{m}_H c_P \Delta T_H - \dot{Q}_H - \dot{Q}_{H,L} = 0 \tag{4.6}$$

Rearranging,

$$\dot{Q}_H + \dot{Q}_{H,L} = -\dot{m}_H c_P \Delta T_H \tag{4.7}$$

Control Volume 2b

Starting with the energy balance equation for an open (control volume) system once again,

$$\dot{E}_{IN} - \dot{E}_{OUT} = \dot{E}_{STOR} - \dot{E}_{GEN} \tag{3.2}$$

As in the previous energy balance, the control volume applies to a single stream. Thus, the heat transfer input and output terms ($\dot{E}_{IN}$ and $\dot{E}_{OUT}$) are functions of the cold stream's mass flow rate and enthalpies. Additionally, the heat transferred to the cold stream, $\dot{Q}_C$, was included as a heat transfer input term ($\dot{E}_{IN}$); similarly, the cold stream's

convective loss term, $\dot{Q}_{C,L}$, was included as a heat transfer output term ($\dot{E}_{OUT}$). Further, there was no energy storage or generation over time:

$$\left(\dot{m}_C h_{C,IN} + \dot{Q}_C\right) - \left(\dot{m}_C h_{C,OUT} + \dot{Q}_{C,L}\right) = 0 \tag{4.8}$$

Rearranging,

$$\dot{m}_C h_{C,IN} + \dot{Q}_C - \dot{m}_C h_{C,OUT} - \dot{Q}_{C,L} = 0 \tag{4.9}$$

Since the cold stream temperature was very nearly at ambient temperature during the Reference Test, it was assumed that the cold stream convective losses were negligible:

$$\dot{Q}_{C,L} \approx 0 \tag{4.10}$$

Thus,

$$\dot{m}_C h_{C,IN} + \dot{Q}_C - \dot{m}_C h_{C,OUT} = 0 \tag{4.11}$$

Rearranging,

$$-\dot{m}_C \Delta h_C + \dot{Q}_C = 0 \tag{4.12}$$

As done previously, the following relationship was assumed for the working fluid:

$$\Delta h = c_P \Delta T \tag{3.12}$$

Thus, the $\dot{m}_C \Delta h_C$ term was redefined and Equation 4.12 becomes:

$$-\dot{m}_C c_P \Delta T_C + \dot{Q}_C = 0 \tag{4.13}$$

Rearranging, the $\dot{Q}_C$ term is determined:

$$\dot{Q}_C = \dot{m}_C c_P \Delta T_C \tag{4.14}$$

4.2.2.3 Control Volumes 1 & 2a Combined

Here, Equations 4.2 and 4.7 will be used simultaneously to solve for the $\dot{Q}_H$ and $\dot{Q}_{H,L}$ terms:

$$\dot{Q}_H - \dot{Q}_{H,L} = P_{OUT} + \dot{Q}_C \tag{4.2}$$

$$\dot{Q}_H + \dot{Q}_{H,L} = -\dot{m}_H c_P \Delta T_H \tag{4.7}$$

Summing the two equations, $\dot{Q}_H$ is determined:

$$\dot{Q}_H = \frac{1}{2}\left(P_{OUT} + \dot{Q}_C - \dot{m}_H c_P \Delta T_H\right) \tag{4.15}$$

Rearranging Equation 4.7,

$$\dot{Q}_{H,L} = -\dot{Q}_H - \dot{m}_H c_P \Delta T_H \tag{4.16}$$

Substituting Equation 4.15 into 4.7 and solving for $\dot{Q}_{H,L}$, the following expression is obtained:

$$\dot{Q}_{H,L} = -\frac{1}{2}\left(P_{OUT} + \dot{Q}_C - \dot{m}_H c_P \Delta T_H\right) - \dot{m}_H c_P \Delta T_H \tag{4.17}$$

Simplifying,

$$\dot{Q}_{H,L} = -\frac{1}{2}\left(P_{OUT} + \dot{Q}_C + \dot{m}_H c_P \Delta T_H\right) \tag{4.18}$$

4.2.2.4 Determining the Overall Heat Transfer Coefficient and Operating Efficiency

Returning to Control Volume 1, Newton's Law of Cooling is used to define the hot stream convective loss term:

$$\dot{Q}_{H,L} = (UA)_{TEG,L} \Delta T_{TEG,LM} \tag{4.19}$$

Where the log mean temperature difference for a counterflow heat exchanger is defined as:

$$\Delta T_{TEG,LM} = \frac{(T_{H,OUT} - T_{C,IN}) - (T_{H,IN} - T_{C,OUT})}{ln\left(\frac{(T_{H,OUT} - T_{C,IN})}{(T_{H,IN} - T_{C,OUT})}\right)} \tag{4.20}$$

Rearranging,

$$(UA)_{TEG,L} = \frac{\dot{Q}_{H,L}}{\Delta T_{TEG,LM}} \tag{4.21}$$

Approximating the surface area of the TEG based on its physical dimensions,

$$A = 2(HW + WD + HD) \tag{4.22}$$

The overall heat transfer coefficient of the TEG is then estimated as:

$$U_{TEG,L} = \frac{\dot{Q}_{H,L}}{\Delta T_{TEG,LM} A} \tag{4.23}$$

Additionally, the operating efficiency of the TEG as a heat engine is defined as:

$$\eta_{TEG,HE} = \frac{P_{OUT}}{\dot{Q}_H} \tag{4.24}$$

The definition of efficiency, $\eta_{TEG,HE}$, derived here—in terms of it being a function of the net heat supplied to the TEG, $\dot{Q}_H$—is similar to the expression derived by Lampinen [13].

4.2.3 Summary of Important Equations Resulting from Energy Balances

From these three analyses, and with the assumption that $\dot{Q}_{C,L} \approx 0$, the three remaining heat transfer components in Figures 4.1 and 4.2 were calculated based on results from the Reference Test (see 4.1) [34]. The CV 2b analysis allowed determination of Equation 4.14, whereas CVs 1 and 2a allowed for simultaneous solution, yielding Equations 4.15 and 4.18:

$$\dot{Q}_C = \dot{m}_C c_P \Delta T_C \tag{4.14}$$

$$\dot{Q}_H = \frac{1}{2}\left(P_{OUT} + \dot{Q}_C - \dot{m}_H c_P \Delta T_H\right) \tag{4.15}$$

$$\dot{Q}_{H,L} = -\frac{1}{2}\left(P_{OUT} + \dot{Q}_C + \dot{m}_H c_P \Delta T_H\right) \tag{4.18}$$

Furthermore, the overall heat transfer coefficient and TEG efficiency were determined to be:

$$U_{TEG,L} = \frac{\dot{Q}_{H,L}}{\Delta T_{TEG,LM} A} \tag{4.23}$$

$$\eta_{TEG,HE} = \frac{P_{OUT}}{\dot{Q}_H} \tag{4.24}$$

4.3 Results of Analysis

In this section, experimental results from the Reference Test (see 4.1) were substituted into the preceding equations in order to quantify the equations above. As previously explained, the reader is strongly cautioned to note that these results were

quantified based on the Reference Test's conditions, which was a single test of the TEG conducted in an isolated environment (see 4.1). Recall that the Reference Test only served to provide a preliminary operating point of the TEG for this study. Of course, it would be scientifically preferred to have test data from many tests with the TEG operating in the built environment (as was expected with the upcoming Characterization Test), in order to empirically quantify these equations with greater accuracy. Therefore, it is understood that these parameters might change when more test data become available.

4.3.1 Quantifying the Internal Heat Transfer

Using the Reference Test (outlined in 4.1) and a constant specific heat capacity of water of $c_P = 4{,}190$ J/kg-K (see Nomenclature and 4.4.4), values were substituted into the equations outlined in 4.2.3 to determine each of the heat transfer parameters taking place within the TEG. This test produced the results shown in Table 4.2.

Parameter	Calculated Value
P_{OUT}	84 W
$\dot{m}_H c_P \Delta T_H = -(\dot{Q}_H + \dot{Q}_{H,L})$	-6,330 W
$\dot{Q}_C$	3,368 W
$\dot{Q}_{C,L}$	≈ 0 W (assumed)
$\dot{Q}_H$	4,891 W
$\dot{Q}_{H,L}$	1,439 W

Table 4.2: Modeling the TEG as a heat engine and using experimental data, each of the heat transfer components was calculated.

Thus, it was observed that the hot stream lost ($\dot{m}_H c_P \Delta T_H$) a total power of 6.3 kW, from which 4.9 kW served as power supplied to the TEG ($\dot{Q}_H$), and 1.4 kW were convective losses ($\dot{Q}_{H,L}$). And, it was observed that the cold stream picked up 3.4 kW of heat transfer from its inlet to outlet ($\dot{Q}_C$). These parameters served as a preliminary characterization of the TEG, albeit in an isolated environment with negligible cold stream convective losses.

What was particularly interesting was that per the specification sheet of the thermoelectric modules used in the TEG, a total heat input/source of 6.9 kW is required to drive the TEG at its nominal operating point—83 W. Here, it was observed that the actual heat input/source was calculated to be 4.9 kW—far short of the 6.9 kW. It was speculated that this seemingly advantageous discrepancy was the result of overestimation in the manufacturer's specification ratings, or perhaps that convective losses in the hot stream also served as extra "fuel" to the TEG's modules' required temperature differential.

4.3.2 Quantifying the Overall Heat Transfer Coefficient

This analysis allowed for estimation of the TEG's overall convective loss term, $(UA)_{TEG,L}$. Using Newton's Law of Cooling for $\dot{Q}_{H,L}$, and using the log mean temperature difference due to the counterflow heat exchange configuration within the TEG, $\dot{Q}_{H,L}$ was defined as:

$$\dot{Q}_{H,L} = (UA)_{TEG,L} \Delta T_{TEG,LM} \tag{4.25}$$

The log mean temperature difference was calculated to be:

$$\Delta T_{TEG,LM} = 98.0\ ℉ = 54.4\ ℃ \tag{4.26}$$

Knowing that $\dot{Q}_{H,L} = 1.4$ kW, it was concluded that:

$$(UA)_{TEG,L} = 26.43 \text{ W/℃} \quad (4.27)$$

Further, recalling the physical dimensions of the TEG, the surface area was approximated as $A_{TEG} \approx 2{,}684 \text{ in}^2$ (1.73 m^2). Therefore, the overall heat transfer coefficient of the TEG could be estimated as:

$$U_{TEG,L} = 15.26 \text{ W/m}^2\text{-℃} \quad (4.28)$$

However, it is understood that this value might possibly change under different operating conditions, as it was derived based on a single test.

4.3.3 The Operating Efficiency of the Thermoelectric Generator

Most importantly, these results allowed for a first-cut estimate of the instantaneous operating efficiency of the TEG as a heat engine:

$$\eta_{TEG,HE} = \frac{P_{OUT}}{\dot{Q}_H} = \frac{84 \text{ W}}{4.9 \text{ kW}} = 1.72\% \quad (4.29)$$

This efficiency was on par with thermoelectric devices in general [16, 18].

4.4 CHARACTERIZATION TEST

As described in the beginning of the chapter, the purpose for the upcoming Characterization Test was for the TEG to undergo lengthy, rigorous experimental characterization in order to understand and later be able to predict the TEG's performance during real-time operation. The Characterization Test will feature the TEG operating in the built environment in its default configuration per Figure 2.5. It is important to note that the numerical model of the solar collector-TEG coupled system (see 3.4) was constructed with this very test in mind. Finally, at the time of writing, the test was in its planning stages and was scheduled to take place later in 2011.

4.4.1 Location

This particular test will be hosted by *Nextek Power Systems* in Detroit, Michigan. The testing facility will be located at:

461 Burroughs St.
Detroit, MI 48202

However, since insolation and ambient temperature data obtained (see 3.3) were recorded at a station in the Detroit Metropolitan Airport (DTW), this particular airport location was instead used in the numerical model for consistency rather than the listed location. This airport location has geographic coordinates of $(LAT, LONG) = (42.215°, -83.349°)$ and is also identified as USAF #725370 and WBAN Station #94847. Additionally, since Detroit, MI falls in the North American Eastern Standard Time Zone (EST), its Standard Time Meridian is thus $STM = 75°$.

4.4.2 The Solar Collector System

In its default configuration in the built environment, the TEG uses a solar-thermal energy system as its hot stream source. This system will be an active, direct/open-loop system with 20 solar collectors and will consist entirely of *Power Panel Inc.* products (i.e., the solar collectors and thermal storage tank) [37]. The recommended operating heat transfer fluid of the *Power Panel Inc.* solar collector system was water.

It should be noted here that a solar collector system with 20 solar collectors does not easily lend itself to a residential application. Therefore, this type of test setup more closely resembles an industrial application, where a substantial number of panels and TEGs would be adopted. Should a residential application be desired, the reader should use the numerical model constructed in this study to simulate the effect of implementing fewer solar collectors.

4.4.2.1 Thermodynamic Properties of Water

Since the thermal properties of water remain relatively constant while in the liquid state (without undergoing a phase change), the specific heat capacity and density properties were therefore evaluated as constant values of $c_P = 4{,}190\ \mathrm{J/kg\text{-}K}$ and $\rho = 1{,}000\ \mathrm{kg/m^3}$, respectively.

4.4.2.2 Solar Collector Specifications

The solar collector system will employ 20 fixed-position, flat-plate photovoltaicthermal (PVT) panels, assembled in 2 arrays of 10 collectors. Each collector requires a volumetric flow rate of 1 gpm (gallons per minute); therefore, the required flow rate for the entire system is 20 gpm. (In terms of mass flow rates, each collector requires 0.063 kg/s, assuming a constant water density of $\rho = 1{,}000\ \mathrm{kg/m^3}$; for the entire system of 20 collectors, this corresponds to 1.262 kg/s.) With the lift height at the testing facility being approximately 32 feet, the corresponding total pumping electrical power requirement for the solar collector system (P_{SC} in Figure 3.3) will therefore approximately be 300 Watts [38].

Each collector features a thermal output of 450 Watts and has a gross collector area of $A_{SC} = 0.98\mathrm{m^2}$ [38]. Per ASHRAE Standard 93-77, each collector features a maximum efficiency of $\eta_0 = 67.5\%$ and a slope of $m_{SC} = $ -3.5 $\mathrm{W/m^2\text{-}℃}$ [38], illustrated in Figure 4.3.

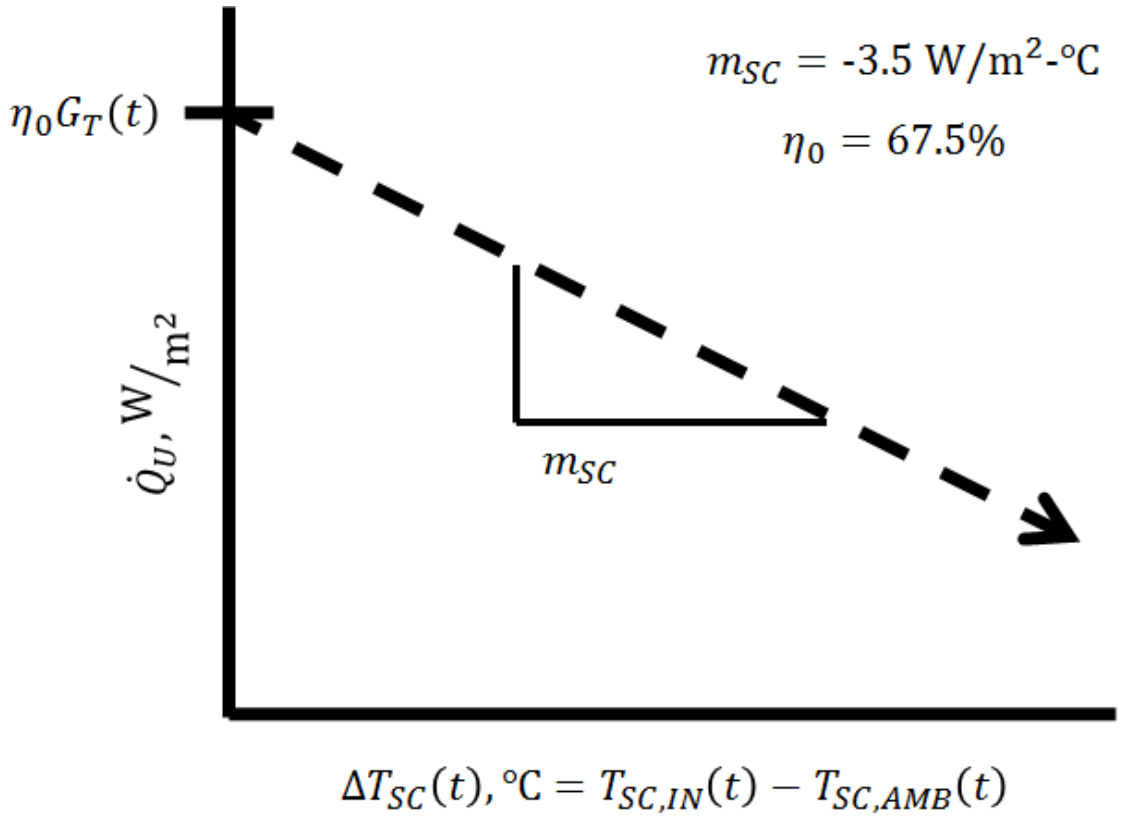

Figure 4.3: Solar collector efficiency curve for *Power Panel Inc.*'s PVT Panel, determined per ASHRAE 93-77 [38].

The solar collectors will be installed on the testing facility's rooftop at a collector tilt angle of $\beta = +45°$. The rooftop's skew from true south (i.e., collector azimuth angle) of $a_w = +22°$ (see 3.3.3).

4.4.2.3 Thermal Storage Tank Specifications

The system will feature *Power Panel Inc.*'s thermal storage tank, which has cylindrical dimensions of 60 inches in diameter and 48 inches in height [37], giving it a surface area of $A_S = 14{,}703$ in^2 (9.49 m^2). The storage tank has a volume capacity of $V_S = 1{,}250$ L. It is also insulated with 4 inch-thick EPP foam with an R-value of 4.2/inch

[21]; these two insulation values lead to a calculated overall convection coefficient of $U_S = 0.338\ \mathrm{W/m^2\text{-}K}$ for the storage tank, which were used to model the convective losses of the tank (appear in the $\dot{Q}_{S,LOSS}$ term in Equation 3.9).

The storage tank also features a maximum allowable water temperature of $T_{S,MAX} = 80\ ℃\ (176\ °\mathrm{F})$. Furthermore, the storage tank will be located in a building basement; it has been estimated that the ambient temperature will be a constant 75 °F during summer months (estimated to be May through August) and 55 °F during winter months (estimated to be September through April) [39].

4.4.3 The Geothermal Heat Pump System

In its default configuration in the built environment, the TEG uses a geothermal energy system as its cold stream source. As outlined in 3.6, a geothermal heat pump (GHP) system operating in reverse is typically employed.

Based on the results outlined in 4.3.1, the cold stream continuously absorbed heat at a rate of $\dot{Q}_C = 3.4\ \mathrm{kW}$. This was just under a ton of refrigeration (i.e., ton of cooling capacity). (Note: a ton of refrigeration is a capacity equivalent to 12,000 BTU/hr or approximately 3.52 kW [34].) Thus, a GHP system with a 1 ton refrigeration capacity would be sufficient to sustain the TEG's cold stream while operating in the built environment. (The only caveat here is that $\dot{Q}_C$ was derived based on the Reference Test outlined in 4.1, which was a single test conducted in an isolated environment rather than with the TEG operating in the built environment; see 4.3 for further information.) Such a small-scale system would therefore categorize it as a residential-scale system.

According to *Watts Thermoelectric LLC*, the original intent of the Characterization Test was to couple the TEG with a closed-loop system in particular,

primarily for their affordability over open-loop systems. Thus, ARI-330 or ARI-870 GHPs were therefore recommended by *Watts Thermoelectric LLC* (see 3.6.1). Further, a horizontal trench arrangement was recommended for the TEG for its efficient use of land area [21], regardless of which of the two GHPs is selected. In this arrangement, horizontal trenches are dug, usually with a 4–7 foot depth. (This is in contrast to digging vertical boreholes, whose depths go to several hundred feet below the surface.) Then, overlapping coils of polyethylene (PE) pipe are inserted in a stretched "slinky" arrangement, usually in 2–3 foot diameter circles [35]. The average reported output figure is 0.96 kW for every 10 meters (32.8 feet) of trench [35]. Thus, for a 1 ton capacity system (3.52 kW), approximately 120 feet of trench would be required to install a horizontally-trenched system.

However, due to limited resources in the upcoming Characterization Test, it was decided to install an above-surface closed loop using line water available at the testing facility rather than an actual subsurface GHP system. The actual temperature of the water was expected to be at approximately room temperature [39]. Nevertheless, the values cited here were later used when considering the economics of the system in 5.2.1.4.

4.4.4 Summary of Characterization Test Setup

Table 4.3 summarizes all parameters involved in the Characterization Test.

Parameter	Value
β	+45°
η_0	67.5%
ρ	1,000 kg/m^3
a_w	+22°
A_S	9.49 m^2
A_{SC}	0.98 m^2
c_P	4,190 J/kg-K
LAT	42.215°
$LONG$	-83.349°
m_{SC}	-3.5 W/m^2-℃
n_{SC}	20
P_{SC}	300 W (≈16 PSI)
P_{TEG}	28.8 W (6 PSI)
STM	75°
$T_{S,AMB,S}$	75 ℉
$T_{S,AMB,W}$	55 ℉
$T_{S,MAX}$	80 ℃ (176 ℉)
U_S	0.338 W/m^2-K
V_S	1,250 L

Table 4.3: Summary of all Characterization Test parameters.

4.4.5 Results

At the time of writing, this test was in its planning stages and had not yet commenced. Testing was expected to take place in later in 2011.

Chapter 5: Emissions and Economic Analyses of the Thermoelectric Generator in the Built Environment

This chapter first considers the environmental impact of operating the novel thermoelectric generator (TEG) in the built environment (Section 5.1). In particular, this analysis quantified the emissions avoided by implementing the TEG in place of a typical fossil fuel-burning energy generation technology. Then, the levelized cost of electricity of the TEG integrated into the built environment was estimated (Section 5.2).

5.1 EMISSIONS ANALYSIS

5.1.1 Data Source Used

The U.S. Environmental Protection Agency (EPA) regularly publishes the Emissions & Generation Resource Integrated Database (eGRID) [40], which is best described directly by the EPA:

> "The Emissions & Generation Resource Integrated Database (eGRID) is a comprehensive inventory of environmental attributes of electric power systems. The preeminent source of air emissions data for the electric power sector, eGRID is based on available plant-specific data for all U.S. electricity generating plants that provide power to the electric grid and report data to the U.S. government. eGRID integrates many different federal data sources on power plants and power companies, from three different federal agencies: EPA, the Energy Information Administration (EIA), and the Federal Energy Regulatory Commission (FERC). Emissions data from EPA are carefully integrated with generation data from EIA to produce useful values like pounds per megawatt-hour (lb/MWh) of emissions, which allows direct comparison of the environmental attributes of electricity generation. eGRID also provides aggregated data by state, U.S. total, company, and by three different sets of electric grid boundaries [40]."

The most recent database available by the EPA was eGRID2010 Version 1.1, which was published in February 2011 with year 2007 data. eGRID2010 served as an extremely useful database for this study in that it published annual aggregate figures such

as net electricity generation, emissions (total and per individual greenhouse gases), output emission rates, fuel/resource mix, and other figures for each of the 10 nationwide NERC[4] electric grid regions. Additionally, these figures could be filtered by subregion and even individual power plant.

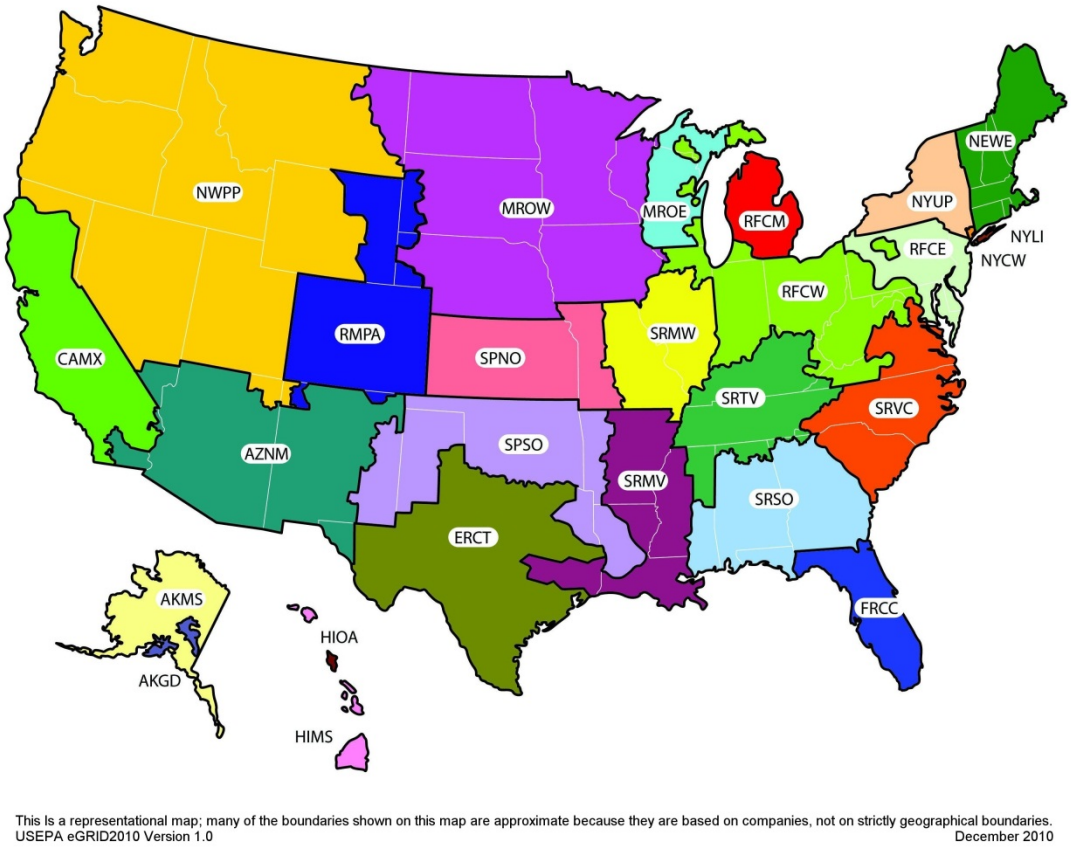

Figure 5.1: Geographic map of the 26 subregions of NERC [40]. NERC is constituted of 10 interconnected electric grid "regions," which are in turn subdivided into a total of 26 subregions (pictured). These 26 subregions have over 5,000 operating power plants, collectively. The RFCM subregion (in Michigan) was the primary focus of this study.

[4] NERC, the North American Electric Reliability Corporation, is the organization that oversees the 10 interconnected electric grid regions in the United States; see Figure 5.1.

The database proves useful when considering the environmental impact of any electricity generation technology on a certain electric grid. This can be accomplished by considering the generation offset by implementing that technology while intertied to the grid (for example, when installing solar panels in a residence), or by considering the generation avoided by *not* intertying that technology to a grid (for example, when using it as an auxiliary generator). And in either case, the electricity generation avoided results in emissions avoided, given that the technology is a zero-emission one.

Further, although eGRID published emissions for a wide range of greenhouse gases, in this particular case, only the all-encompassing carbon dioxide-equivalent (CO_2e) emissions were considered. CO_2e emissions are useful in that built in to them are the global warming potential for all greenhouse gas emissions, normalized with CO_2 as the reference gas. Per eGRID2010's Technical Support Document, CO_2e was calculated from the three electric power greenhouse gases: carbon dioxide (CO_2), methane (CH_4), and nitrous oxide (N_2O), which were assigned global warming potentials of 1, 23, and 296, respectively [40].

5.1.2 Motivation of Analysis

In this study, the thermoelectric generator (TEG) was the technology in focus. Regardless of what viewpoint is taken—whether the TEG is intertied to the local electric grid or not, the fact that the TEG was a zero-emission device led to this portion of the analysis—quantifying the emissions avoided by implementing the TEG.

5.1.3 The RFCM Electric Grid

Recall that the TEG will undergo its Characterization Test in Detroit, MI (see 4.4). As a result, this particular electric grid was considered.

5.1.3.1 Characterizing the RFCM Electric Grid

It is first important to characterize the electric grid in question. The electrical energy demand of Detroit, MI is supplied by the *Reliability First Corporation–Michigan* (RFCM) grid, which is one of three subregions in RFC. In 2007, RFCM produced a net electricity generation of 94,701,550.5 MWh and had carbon dioxide-equivalent emissions of 78,621,843.3 tons CO_2e. The resource mix of this particular subregion included coal (bituminous, lignite, et al.), oil (diesel, kerosene, et al.), gas (natural gas and propane gas), nuclear, hydro, biomass (which varied among solid, liquid, and gaseous biomass sources like hydrogen, methanol, et al.), wind, and other fossil fuels (also from solid, liquid, and gaseous sources like waste, methane, agricultural byproducts, et al.), as categorized by eGRID. (Note: although possible sources are listed in parentheses for each resource, not all of these sources were necessarily used in RFCM.) This resource mix is illustrated in Figure 5.2.

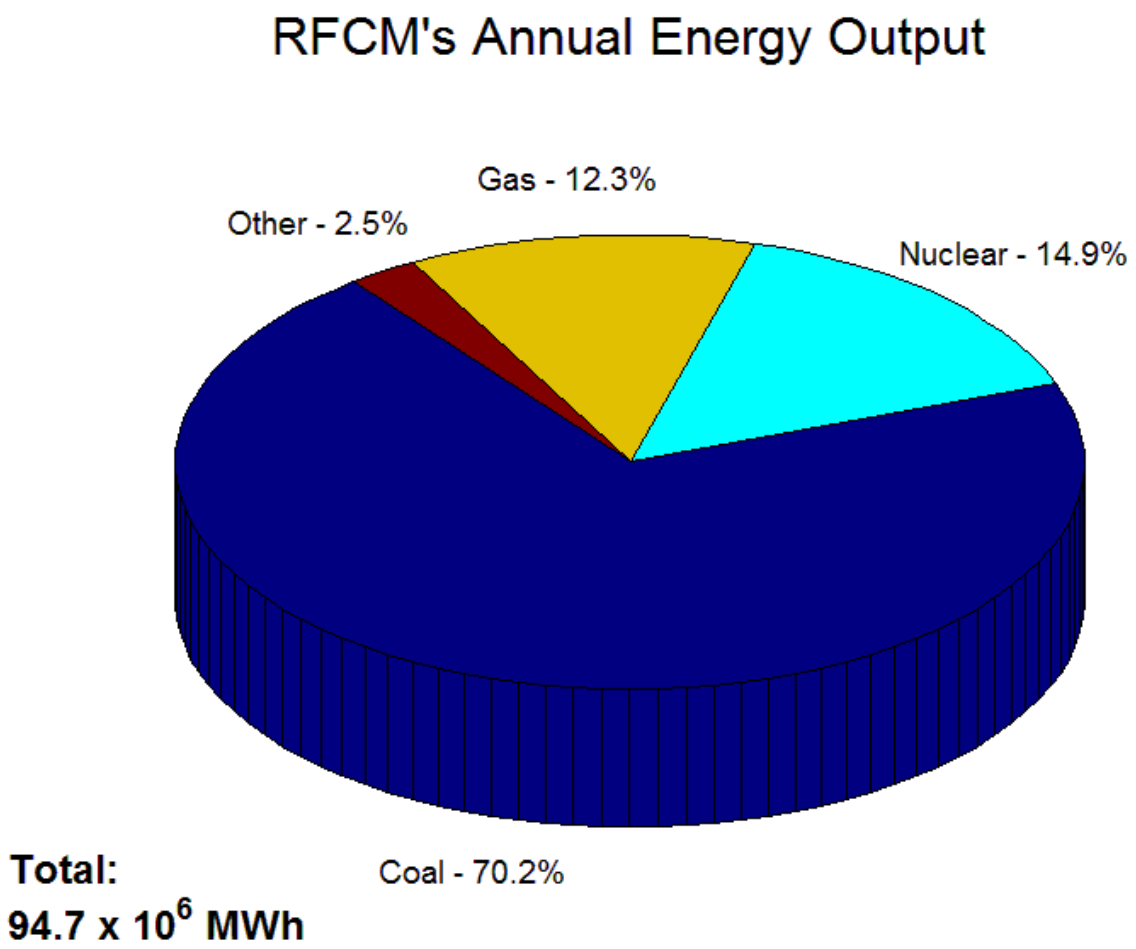

Figure 5.2: RFCM's resource mix for net annual electricity generation in 2007, which totaled 94,701,550.5 MWh [40]. The "Other" category was constituted of oil (0.7%), biomass (1.8%), hydro (-0.7%)[5], wind (<0.01%), and other fossil fuels (0.6%). Note that solar and geothermal energy sources were not part of RFCM's resource mix.

5.1.3.2 Quantifying the Emission Factor of the RFCM Electric Grid

The emission factor, (also known as the "emissions factor") is a ratio of emissions produced to electricity generated, typically expressed in unit weight of a pollutant

[5] Negative generation occurred when the energy consumed by a particular power plant was greater than the gross generation; see [40] for further information.

(greenhouse gas) per unit energy—here, the units used were in tons CO_2e/MWh. This ratio can be attributed to a fuel source, power plant, or even network of power plants constituting an electric grid, depending on what the system boundaries of the particular analysis are. Accordingly, a low-emission power plant will have a lower emission factor than a high-emission power plant generating the same amount of electricity. Reported emission factors for various fuel types can be found from a variety of sources, including governmental organizations like the EPA or EIA, as well as from studies published from academic institutions.

Although there are numerous methods and approaches to quantifying the emission factor, EF, in this study, a year-aggregate emission factor sufficed and was calculated using the following formula:

$$EF\ \left[\frac{\text{tons } CO_2\text{e}}{\text{MWh}}\right] = \frac{P_{TOT}\ [\text{tons } CO_2\text{e}]}{E_{TOT}\ [\text{MWh}]} \tag{5.1}$$

Here, note that a "ton" is the US Customary System unit of weight "ton," also known as a short ton, defined as 2,000 lbs. Substituting values based on RFCM's figures, the emission factor of RFCM was calculated as:

$$EF_{RFCM} = \frac{78{,}621{,}843.3 \text{ tons } CO_2\text{e}}{94{,}701{,}550.5 \text{ MWh}} = 0.830\ \frac{\text{tons } CO_2\text{e}}{\text{MWh}} \tag{5.2}$$

One knowledgeable in the field will observe that this is a relatively large EF—meaning that RFCM is a particularly high-polluting subregion. In fact, this EF made RFCM the 6th largest CO_2e-emitting subregion of the 26 subregions in the U.S. This was attributed to the fact that coal, a fossil fuel with one of the highest emission factors of fuel sources available [41], was used to generate more than 70% of the subregion's energy output, as seen in Figure 5.2.

5.1.4 Quantifying the Emissions Avoided

Recalling one of the results of Chapter 3, the net energy generated from operating the TEG over the course of a year (in this case, 2005 meteorological data were used) was 266.5 kWh, as listed in Equation 3.44. If the TEG's net annual energy output were to be used as a generation source rather than having that energy supplied by the local electric grid, 266.5 kWh (0.267 MWh) would thus translate into an annual energy savings in the electric grid. This value was used to calculate the annual emissions avoided via RFCM's emission factor:

$$P_{AVOIDED} = \left(E_{TEG,NET}\right)\left(EF_{RFCM}\right) = 0.221 \text{ tons } \mathrm{CO_2e/year} \tag{5.3}$$

Thus, operating the TEG over the course of the year would result in an annual emissions reduction of 0.221 tons CO_2e. However, note that these values correspond to installing and operating (in whatever the application or setting is) only a single TEG. While a single TEG admittedly had a minimal impact on emissions, implementing many TEGs resulted in considerable savings in emissions.

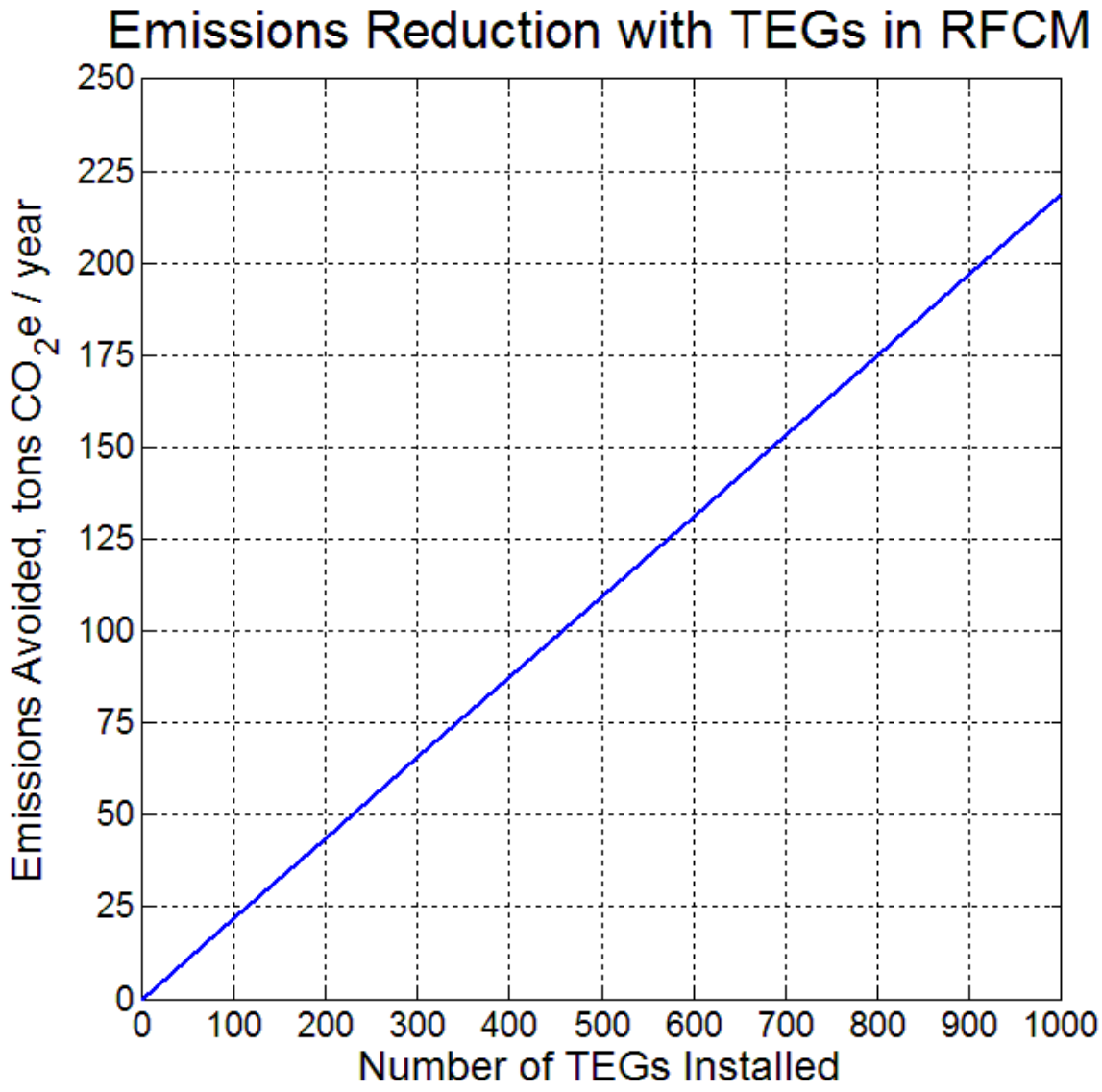

Figure 5.3: Implementing more than a single TEG can result in avoiding considerable emissions. Here, the reduction in emissions for the RFCM subregion are shown.

5.2 ECONOMIC ANALYSIS

This analysis considered the economics of the TEG by obtaining a first-cut estimate of the levelized cost of electricity of implementing the TEG in the built environment, as well as quantifying the economic benefits of the emissions avoided as a zero-emission energy generation technology.

5.2.1 The Levelized Cost of Electricity (LCOE)

The purpose of this analysis was to obtain a levelized cost of electricity of the TEG integrated into the built environment. Recalling 2.2.3, in its default configuration in the built environment, the TEG is integrated with a solar-thermal energy system as its hot stream source and a geothermal energy system as its cold stream source. Thus, there were three different subsystems to first consider: the solar collector system, the TEG itself, and the geothermal heat pump system.

5.2.1.1 Definition of the LCOE

The levelized cost of electricity ($LCOE$), sometimes referred to as the levelized cost of energy, is a standard way of quantitatively comparing the cost-effectiveness of implementing an energy generation technology (or system or plant). Essentially, the $LCOE$ is the total price paid to generate a unit of electricity (or energy) over the lifetime of the plant, and thus includes the time value of money and amortization of the capital investments. The total price is quantified by summing all required expenses, which are comprised of the capital expense, operational and maintenance expenses, and fuel costs. The $LCOE$ is a ratio of the monetary investment into a system to the annual amount of energy generated, typically expressed in dollars per unit energy *generated* per year (as in

$/MWh per year). Although there exist varying degrees of complexity and accuracy in calculating the $LCOE$ (like accounting for tax credits or other federal monetary incentives), in this context it will simply be defined as:

$$LCOE\left[\frac{\$}{\text{MWh}}\right] = \left(CAPEX\left[\frac{\$}{\text{year}}\right] + OPEX\left[\frac{\$}{\text{year}}\right] + Fuel\left[\frac{\$}{\text{year}}\right]\right) / \left(E_{GEN}\left[\frac{\text{MWh}}{\text{year}}\right]\right) \quad (5.4)$$

Each of these components that constitute the $LCOE$ will be explained in detail in the following paragraphs. The sum of components in the numerator in Equation 5.4 can be qualified as the annual Total Cost:

$$\text{Total Cost}\left[\frac{\$}{\text{year}}\right] = CAPEX\left[\frac{\$}{\text{year}}\right] + OPEX\left[\frac{\$}{\text{year}}\right] + Fuel\left[\frac{\$}{\text{year}}\right] \quad (5.5)$$

Thus, Equation 5.4 is rewritten as:

$$LCOE\left[\frac{\$}{\text{MWh}}\right] = \frac{\text{Total Cost}\left[\frac{\$}{\text{year}}\right]}{E_{GEN}\left[\frac{\text{MWh}}{\text{year}}\right]} \quad (5.6)$$

Further (just for reference), note that if the annual energy generated term, E_{GEN}, is distributed among all terms in the numerator, the following equation is obtained:

$$LCOE\left[\frac{\$}{\text{MWh}}\right] = CAPEX\left[\frac{\$}{\text{MWh}}\right] + OPEX\left[\frac{\$}{\text{MWh}}\right] + Fuel\left[\frac{\$}{\text{MWh}}\right] \quad (5.7)$$

Finally, to put into perspective, the $LCOE$ value can be thought of as an inverse efficiency value of a particular energy generation technology, since it is a ratio of the annual system cost ("what you pay") to its annual energy output ("what you get"). Thus, the lower the $LCOE$ is of a particular technology, the more appealing it is.

Capital Expenses

The first component in Equation 5.4 to consider is the capital expense, $CAPEX$. This term is the initial price necessary to acquire and implement an energy generation technology. Should this value be given as a $/MWh figure (which would be preferred), it is simply plugged into Equation 5.7. More often, however, the capital expense is known as a lump sum dollar [$] amount (the Installed Cost), since it is the initial investment

made on the system. It is typically in the range of thousands of dollars per kW of capacity and therefore not amortized over night but rather over the lifetime of the system (in decades). System lifetimes typically range between 20–40 years.

The Installed Cost (i.e., the principal amount) is annualized (i.e., calculated in a $/year amount) via a discount formula; here, the uniform capital recovery formula was selected in particular [31]. This formula is a function of the interest/discount rate, i, and total number of interest periods, n. In this study, all systems were amortized over a 20 year period (i.e., $n = 20$ years), with zero salvage value at the end of their lifetimes. Also, a typical interest/discount rate of $i = 5\%$ was chosen.

Altogether, the annual capital expense is calculated as:

$$CAPEX\left[\frac{\$}{\text{year}}\right] = (\text{Installed Cost }[\$]) \times \left\{\frac{i(1+i)^n}{(1+i)^n - 1}\right\} \tag{5.8}$$

At times, $CAPEX$ is also known as an annual price-per-unit-power value ($/MW-year) rather than as an upfront installed cost. In this case, the given value must be converted from a per-unit-power of *installed capacity* to a per-unit-energy *generated*. This is done by simply taking into account the system's capacity factor, CF, which is a measure of how often (as a percentage) the system is ON throughout the year:

$$CAPEX\left[\frac{\$}{\text{MWh}}\right] = CAPEX\left[\frac{\$}{\text{MW-year}}\right] \Big/ \left(CF \times \left|8{,}760\,\frac{\text{hr}}{\text{year}}\right|\right) \tag{5.9}$$

Operational and Maintenance (O&M) Expenses

Similarly, operational and maintenance (O&M) costs are typically given as values in units of either $/MWh, $/year, or $/(MW-year). In the first (and preferred) case, the $/MWh value is simply plugged into Equation 5.7. In the second (and still preferred) case, the $/year value is plugged into Equation 5.4. In the third case where $OPEX$ is reported in units of $/(MW-year), it must then be converted to a per-unit-energy *generated* value, just as done with $CAPEX$:

$$OPEX\left[\frac{\$}{\text{MWh}}\right] = OPEX\left[\frac{\$}{\text{MW-year}}\right] / \left(CF \times \left|8{,}760\,\frac{\text{hr}}{\text{year}}\right|\right) \tag{5.10}$$

Fuel Expenses

Fuel costs are also part of the $LCOE$ equation and are treated (in terms of units) just as $OPEX$ values are. However, should the system utilize an inexhaustible fuel source—as is commonly the case with renewable energy generation technologies—then fuel costs become zero. This is one of the greatest benefits of utilizing renewable energy sources like wind, solar, or geothermal energy. In this study, because the TEG was coupled with renewable energy sources (see 2.2.3.1), fuel expenses were consequently zero:

$$Fuel = \$0/\text{year} \tag{5.11}$$

Annual Energy Generation

The final term to consider is the annual energy generated by the system, E_{GEN}. At times, the annual energy generated is known explicitly known a priori or by some other means. For example, in thus study, the TEG's net annual electricity generation was determined via the numerical model (see Equation 3.44).

However, most times E_{GEN} is not explicitly known beforehand. In this case, E_{GEN} is calculated via the system or plant's capacity, CAP, capacity factor, CF (a measure of how often it is ON during the year), and a unit conversion factor to annualize the value:

$$E_{GEN}\left[\frac{\text{MWh}}{\text{year}}\right] = (CAP\ [\text{MW}] \times CF) \times \left|8{,}760\,\frac{\text{hr}}{\text{year}}\right| \tag{5.12}$$

Additionally, note that this equation is necessary only if Equation 5.4 is used (i.e., if either of the $CAPEX$, $OPEX$, or $Fuel$ terms were known in units of \$/year).

Most importantly, note that the annual energy generated can be in various forms—namely as electricity or thermal energy. In the case where electricity is used to

calculate the $LCOE$ of the subsystem, then $LCOE$ refers the levelized cost of *electricity*. In contrast, in the case where thermal energy is used to calculate the $LCOE$ of the subsystem, then $LCOE$ refers the levelized cost of *energy*. In either case, the $LCOE$ concept is the same, and they are only differentiated when considering the $LCOE$ of the integrated system (see the following section).

In this study, the solar-thermal energy and geothermal energy systems served to supply (or draw) the TEG with thermal energy; therefore, their $LCOE$s were calculated accordingly. In contrast, the TEG generated electricity, and its $LCOE$ was calculated using the TEG's electricity generation.

LCOE of Integrated Systems

Finally, for integrated systems, the $LCOE$ can be summed over each subsystem k to determine an $LCOE$ of the entire system:

$$LCOE_{TOT}\left[\frac{\$}{\text{MWh}}\right] = \sum_k \left(LCOE\left[\frac{\$}{\text{MWh}}\right]\right)_k \tag{5.13}$$

However, should each subsystem generate a different type of energy (as was the case here), then the $LCOE$ is calculated slightly differently. In this study, the $LCOE$ of the entire integrated system in the built environment as an electricity generation system was desired. Therefore, the expenses of each subsystem k were summed, but the net annual energy generated by the TEG (Equation 3.44) was used:

$$LCOE_{TOT}\left[\frac{\$}{\text{MWh}}\right] = \left(\sum_k \left(\text{Total Cost}\left[\frac{\$}{\text{year}}\right]\right)_k\right) \Big/ E_{TEG,OUT,NET}\left[\frac{\text{MWh}}{\text{year}}\right] \tag{5.14}$$

5.2.1.2 The LCOE of the Solar-Thermal Energy System

Here, since the solar collector system was used to supply the TEG with thermal energy, the levelized cost of *energy* was calculated.

Solar Collector System's Capital Cost

Because the solar collector system in the Characterization Test (see 4.4) will entirely be comprised *Power Panel Inc.* products, their price quotes were therefore used. *Power Panel Inc.* priced their system at $1,150 per collector, which included the thermal storage tank, ancillary equipment, and installation costs. With a system of 20 collectors, the total installed cost for the solar collector system was therefore:

$$\text{Installed Cost} = \left(1{,}150\ \frac{\$}{\text{collector}}\right)(20\ \text{collectors}) = \$23{,}000 \tag{5.15}$$

This installed cost is amortized over the lifespan of the system. Assuming a lifetime of $n = 20$ years (with zero salvage value) and an interest rate of $i = 5\%$, the installed cost of $23,000 was annualized via Equation 5.8:

$$CAPEX = (23{,}000\ [\$]) \times \left\{\frac{0.05 \times (1+0.05)^{20}}{(1+0.05)^{20}-1}\right\} = \$1{,}845.58/\text{year} \tag{5.16}$$

Solar Collector System's O&M and Fuel Costs

Next, the operational and maintenance costs were considered. Since they were not provided directly by *Power Panel Inc.* for this study, they were consequently estimated from literature. Howell et al. estimated maintenance costs of a solar collector system to be $25 every 5 years for the collector and $25/year for the thermal storage tank [31]. Over a system lifespan of 20 years, this value translated to an annual cost of $30/year. However, this was in 1982 dollars, and needed to be converted to a modern-day monetary value for fair comparison. To accomplish this, the U.S. annual inflation rate was taken into account by considering the consumer price index (CPI)—a value reported monthly by the U.S. Bureau of Labor Statistics—of both years. The average annual CPI of 1982 was 96.5, whereas the average annual CPI of 2010 was 218.1 [42]. The 1982 dollar value was converted into 2010 dollars by multiplying by the ratio of CPIs for both years. Thus, the O&M costs were calculated as:

$$OPEX = 30\ \left[\frac{\$}{\text{year}}\right] \times \frac{\text{CPI}_{2010}}{\text{CPI}_{1982}} = 30\ \left[\frac{\$}{\text{year}}\right] \times \frac{218.1}{96.5} = \$67.80/\text{year} \quad (5.17)$$

Finally, since fuel costs were zero for solar energy (a great benefit of utilizing renewable energies), the total annual cost was determined to be:

$$\text{Total Cost}_{SC} = CAPEX + OPEX = \$1{,}913.38/\text{year} \quad (5.18)$$

Solar Collector System's LCOE

Further, recall that the annual thermal energy collected by the system was obtained in 3.5.4:

$$E_{SC,C} = 39.73\ \text{MWh/year} \quad (3.49)$$

Thus, the levelized cost of *energy* of the solar collector system was calculated via Equation 5.4:

$$LCOE_{SC} = \left(1{,}913.38\ \frac{\$}{\text{year}}\right)/\left(39.73\ \frac{\text{MWh}}{\text{year}}\right) = \$48.16/\text{MWh} \quad (5.19)$$

Here, it should be noted that this value fell considerably short of the $LCOE$ values reported by the U.S. Department of Energy's Office of Energy Efficiency and Renewable Energy (EERE), which ranged from \$90–\$145/MWh for solar-thermal systems [43], as well as those reported by the EIA, which averaged \$311.8/MWh [9]. Table 6.1 lists these reported values. The reason for this discrepancy is that the EERE and EIA reported $LCOE$ values based on electricity generation (i.e., levelized cost of *electricity*) rather than thermal energy output (i.e., levelized cost of *energy*) as done here.

5.2.1.3 The LCOE of the Novel Thermoelectric Generator

Contrary to the solar collector and geothermal heat pump systems, since the TEG generated electricity, the levelized cost of *electricity* was calculated here.

TEG's Capital Cost

According to *Watts Thermoelectric LLC*, the capital cost to build a bank at mass-production price rates is projected to be $60.31/bank (at a rate of $1.00/thermoelectric module) [21]. (Recall from 2.2.1 that these were bismuth telluride modules.) Recalling that a single rack has 16 banks, and incorporating the price of the other rack components and labor costs needed to assemble the rack, the total capital cost per rack was reported by *Watts Thermoelectric LLC* to be [21]:

$$\text{Installed Cost} = \$1{,}553.66/\text{rack} \tag{5.20}$$

While the fuel is free for the TEG system, this price of $1,554 per 83 Watts of capacity is quite expensive compared with conventional power plant options. This price per Watt effectively comes out to:

$$P_{TEG}\left[\frac{\$}{\text{W}}\right] = \left(1{,}553.66\,\frac{\$}{\text{rack}}\right)/\left(83\,\frac{\text{W}}{\text{rack}}\right) = \$18.72/\text{W} \tag{5.21}$$

However, this value is an underestimation, as it does not account for the costs necessary to supply the TEG with the thermal energy required to operate. That is, it does not include the system costs for the solar-thermal energy system and geothermal energy system. (A more accurate price-per-Watt value is given in 5.2.1.5 as Equation 5.36.)

Continuing, it might be difficult at first glance to accept that a price of $1,554 need be amortized over the TEG's lifetime. In fact, it might be decided that such a cost could in fact be amortized "over night" (thereby making it the capital expense, $CAPEX$), and in the process avoid paying unnecessary interest. However, such a thought process does not consider the time value of money; that is, it neglects to account for the fact that by paying the installed cost in one lump sum, that money is consequently not allowed to increase in value by being placed into a type of savings account where interest is compounded over the system's lifetime. Thus, it is important to point out that whether the installed cost is amortized over its lifetime at a certain interest rate, or paid in one lump

sum (and thus not allowed to accrue interest), the end result is effectively the same, and the same amount of money is ultimately paid. Thus, the installed cost was amortized over the TEG's lifetime, as standardly done with calculating the $LCOE$.

Next, the expected lifetime of the TEG was considered. The first item to consider was the lifetime of the TEG's components. With exception of two components, all components of the TEG had lifetimes of 200,000–300,000 hours. Recalling Equation 3.40, the TEG only operated for 56.1% of the year while coupled with a solar collector system (based on the results of the numerical model), which could theoretically give the TEG a lifetime of 40–60 years. However, the TEG's operational lifetime may be significantly lower than this, since failure is not likely to be the result of component failure. Rather, for the TEG in particular, the expected modes of failure would be fouling of the heat exchanger passages (channels within the heat spreaders, as outlined in 2.2.1) and corrosion of mechanical and electrical connections over time. Fouling of passages is the result of fluid streams picking up impurities over time, which stick to the inner surface of passages and increase their thermal resistance, thereby gradually degrading performance. Therefore, the lifetime of the TEG was set to 20 years in this analysis as done with the other systems. (Of course, it is possible that the TEG may have a longer operational lifetime.)

Thus, with a lifetime of $n = 20$ years (with zero salvage value) and assuming an interest rate of $i = 5\%$, the installed cost was annualized via Equation 5.8. The resulting value was, as expected, extremely small when compared to the solar collector system:

$$CAPEX = (1{,}553.66\ [\$]) \times \left\{\frac{0.05 \times (1+0.05)^{20}}{(1+0.05)^{20}-1}\right\} = \$124.67/\text{year} \qquad (5.22)$$

TEG's O&M and Fuel Costs

Next, the operation and maintenance (O&M) costs of the TEG were considered. In order to estimate the O&M costs for the TEG, the two components most likely to fail during its 20-year lifetime were considered. There were only two components in the TEG without the 200,000–300,000 hour lifetime described previously; replacing these two components were the only O&M costs attributed to the TEG. These components were the two recirculation pumps at the inlet of each stream, which only had 20,000 hour lifetimes. Although the TEG only operated 56.1% of the year per Equation 3.40 (4,917.70 hours/year), in this portion of the analysis, it was assumed that the pumps operated continually (i.e., operated 100% of the year), thereby giving these pumps a conservative 2 year lifetime. With a price of $9 per pump [21], the O&M costs for the entire TEG over the 20 year period would therefore be:

$$OPEX = \$9/\text{year} \tag{5.23}$$

Since fuel costs were zero (because it used solar-thermal energy and geothermal energy systems as its hot and cold sources), the total annual cost was calculated to be:

$$\text{Total Cost}_{TEG} = CAPEX + OPEX = \$133.67/\text{year} \tag{5.24}$$

TEG's LCOE

Further, recall that the net annual electrical energy produced by the TEG (single rack) was quantified in 3.5.3:

$$E_{TEG,OUT,NET} = 266.5\ \text{kWh/year} \tag{3.44}$$

Thus, the levelized cost of electricity of the TEG was calculated via Equation 5.4:

$$LCOE_{TEG} = \left(133.67\ \frac{\$}{\text{year}}\right)/\left(0.267\ \frac{\text{MWh}}{\text{year}}\right) = \$501.50/\text{MWh} \tag{5.25}$$

However, this value is not particularly useful, since it assumes that the required thermal energy (for both the hot and cold streams) is supplied for free. Consequently, the levelized cost of electricity for the entire integrated system must be calculated.

5.2.1.4 The LCOE of the Geothermal Energy System

Similar to the solar collector system, since the geothermal heat pump system was used to draw thermal energy from the TEG, the levelized cost of *energy* was calculated here.

Further, since the Characterization Test (see 4.4) did not employ an actual geothermal heat pump (GHP) system, there was no specific manufacturer to contact regarding the economics of the system. As a result, both capital and O&M expenses of implementing such a system were estimated for this study.

Geothermal Heat Pump System's Capital Cost

Recall that it was concluded in 4.4.3 that only 1 ton of continuous cooling (3.52 kW) was a sufficient capacity for the TEG's GHP system; there, it was also indicated that a horizontal "slinky" trench closed-loop system was the recommended GHP system with which to couple the TEG. As Banks reports, the installed cost of a 3.5 kW horizontal system is approximately $950 [35]. However, it is pointed out that this is a nominal value and does not include additional costs like taxes and consultants' fees that are associated with actually commissioning a GHP system, and therefore underestimates the cost by roughly 50% [35]. Adjusting for these ancillary expenses, the installed cost was therefore estimated as:

$$\text{Installed Cost} = \$1{,}425 \tag{5.26}$$

Note that this cost was substantially lower than installed costs of a general GHP system for the residential market reported by the EERE, which ranged from $5,000–$6,000 per ton of cooling [43]. It is speculated that the reason for this discrepancy is that the EERE likely considered open-loop systems with vertical boreholes (which are substantially more expensive) rather than closed-loop systems with horizontal trenches.

Continuing, this cost was amortized over a 20 year period ($n = 20$ years) with zero salvage value and an interest rate of $i = 5\%$. The capital expense was calculated via Equation 5.8 to be:

$$CAPEX = (1{,}425\ [\$]) \times \left\{\frac{0.05 \times (1+0.05)^{20}}{(1+0.05)^{20}-1}\right\} = \$114.35/\text{year} \tag{5.27}$$

Geothermal Heat Pump System's O&M and Fuel Costs

Unfortunately, explicitly-reported values for operation and maintenance (O&M) costs for small-scale, residential systems were found to be scant. The few reported O&M costs for GHP systems found pertained only to very large scale GHP systems—binary cycle and flash steam geothermal power plants, which have capacities in the MW ranges. Here, the goal was simply obtain an approximate $LCOE$ value of a closed-loop GHP system for purpose of this study. Because binary cycle geothermal power plants generally feature lower O&M costs than flash steam geothermal power plants, they were consequently selected to represent the O&M costs for the GHP system. According to the California Energy Commission, the variable O&M costs for such plants are [44]:

$$OPEX = \$4.55/\text{MWh} \tag{5.28}$$

Here, note that $OPEX$ was not given in units of $/year as before, but rather $/MWh. In order to convert this into a $/year value, it was first necessary to estimate the GHP system's annual thermal energy generated, E_{GEN}. Having E_{GEN}, $OPEX$ could be determined via the following equation:

$$OPEX\left[\frac{\$}{\text{year}}\right] = OPEX\left[\frac{\$}{\text{MWh}}\right] \times E_{GEN}\left[\frac{\text{MWh}}{\text{year}}\right] \quad (5.29)$$

There were two different methods of estimating E_{GEN} for the GHP system:

- Via Equation 5.12, where the system's capacity, CAP, and capacity factor, CF, must be assumed. In this approach, the system capacity would be 1 ton of refrigeration ($CAP = 3.52$ kW) as outlined in 4.4.3, and the commonly assumed capacity factor for geothermal power plants, $CF = 90\%$, would be assumed.
- Via Equation 5.30 below, where the capacity factor, although not shown, essentially reflects the TEG's "capacity factor" reported earlier based on the numerical model (see Equation 3.40). Here, the same capacity is used (1 ton of cooling), but the time that the TEG was ON throughout the year is used in place of CF. That is:

$$E_{GEN,GHP}\left[\frac{\text{MWh}}{\text{year}}\right] = (CAP\ [\text{MW}])\left(\text{Time TEG ON } [^{\text{hours}}/_{\text{year}}]\right) \quad (5.30)$$

The second approach was taken, since it was a more accurate representation of the GHP operating in conjunction with the TEG. That is, it uses a capacity factor that was more closely aligned with the TEG's annual performance rather than that of a generic geothermal power plant. Note that regardless of which approach were taken, the overall $LCOE$ of the integrated system would not be affected, since $LCOE_{TOT}$ accounted for the TEG's electricity generation (this is explained later in 5.2.1.5).

Thus, the GHP system's annual energy generated was calculated to be:

$$E_{GEN,GHP} = (3.52\text{ kW})\left(4{,}917.70\ ^{\text{hours}}/_{\text{year}}\right) = 17.29\text{ MWh/year} \quad (5.31)$$

Using Equation 5.29, the annual O&M costs were calculated:

$$OPEX\left[\frac{\$}{\text{year}}\right] = \$78.69/\text{year} \quad (5.32)$$

Thus, with the cost of fuel being zero as before, the total cost was calculated to be:

$$\text{Total Cost}_{GHP} = CAPEX + OPEX = \$193.04/\text{year} \quad (5.33)$$

Geothermal Heat Pump System's LCOE

Therefore, the levelized cost of *energy* of the GHP system was calculated to be:

$$LCOE_{GHP} = \left(193.04\ \frac{\$}{\text{year}}\right)/\left(17.29\ \frac{\text{MWh}}{\text{year}}\right) = \$11.16/\text{MWh} \quad (5.34)$$

Similar to the solar collector system's $LCOE$, this value was considerably less than values reported by EERE, which ranged from \$42–\$69/MWh for geothermal systems [43], as well as those reported by the EIA, which averaged \$101.7/MWh [9].

As with the solar collector system's $LCOE$, the reason for this discrepancy is that the EERE and EIA reported $LCOE$ values based on electricity generation rather than thermal output.

5.2.1.5 The LCOE of the Integrated System in the Built Environment

Finally, the $LCOE$ of the integrated system was able to be quantified. Here, as explained in the final section of 5.2.1.1, the goal of this analysis was to estimate the levelized cost of *electricity* for the integrated system. Thus, using 266.5 kWh of net annual electricity generated by the TEG (see Equation 3.44) and Equation 5.14, the $LCOE$ was estimated as:

$$LCOE_{TOT}\left[\frac{\$}{\text{MWh}}\right] = (\text{Total Cost}_{SC} + \text{Total Cost}_{TEG} + \text{Total Cost}_{GHP})/E_{TEG,OUT,NET}$$

$$= (\$2{,}240.09/\text{year})/(266.5\ \text{kWh/year}) = \$8{,}404.18/\text{MWh} \quad (5.35)$$

This value is equivalent to \$8.40/kWh. This value is compared to other generation technologies in 6.2.2.

Additionally, the price per Watt of the integrated system was estimated using the Installed Cost of each of the three subsystems. This value supersedes Equation 5.21 and came to:

$$P_{TOT}\left[\frac{\$}{\mathrm{W}}\right] = (\text{Installed Cost}_{SC} + \text{Installed Cost}_{TEG} + \text{Installed Cost}_{GHP})/P_{OUT}$$
$$= \left(25{,}979\,\frac{\$}{\text{system}}\right)/\left(83\,\frac{\mathrm{W}}{\text{system}}\right) = \$313/\mathrm{W} \quad (5.36)$$

However, the greatest caveat here is that these two prices—$LCOE_{TOT}$ and P_{TOT}—only apply to this particular test setup of the upcoming Characterization Test. That is, it applies only to an integrated system consisting of the following: a solar collector system of 20 solar collectors with a single thermal storage tank; a single TEG; and a GHP system sized for 1 ton of cooling. Note that this study did not include an optimization of any sort, particularly of the solar collector system size (i.e., number of solar collectors and storage tanks) for which to couple with the TEG. Should an optimization analysis of the coupled system be performed in order to ascertain a more appropriate solar collector system size (see 3.5.2.2)—i.e., one that would result in the TEG being ON for longer throughout the year (see Equation 3.40) and thus improve its net annual electricity output (see Equation 3.44)—then these two values would change accordingly (and would likely improve substantially). (A more suitable solar collector system size is suggested in 6.1.1.2.)

5.2.2 Considering Federal Greenhouse Gas Emissions Policy

The final consideration in the economic analysis of the TEG was the potential cost savings in implementing the TEG in face of a carbon tax. Here, no specific policy is considered but rather a generic federal policy taxing greenhouse gas emissions. Figure 5.4 shows the annual cost savings for a range of potential carbon taxes by implementing the TEG.

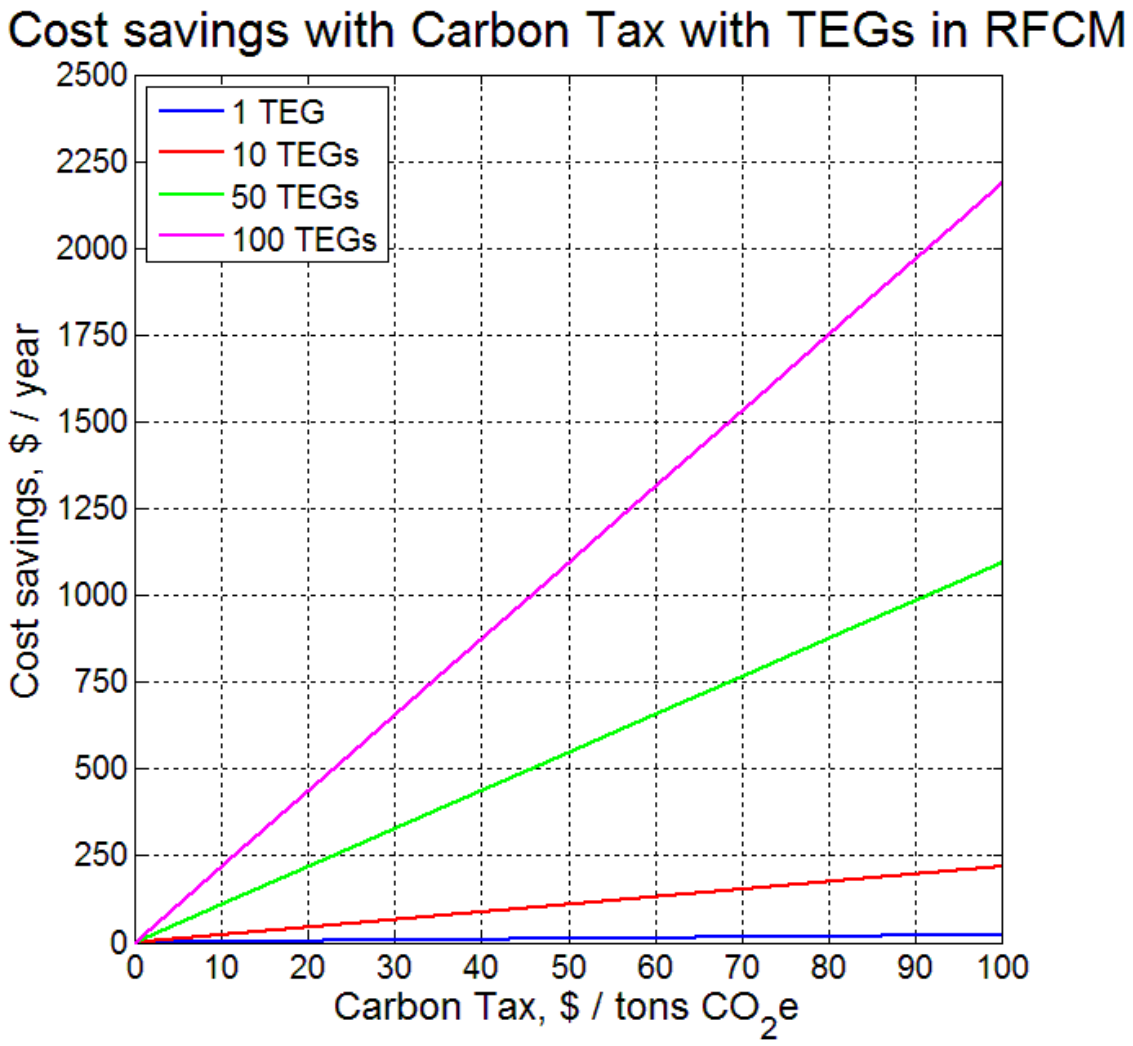

Figure 5.4: The annual cost savings due to a carbon tax play an important role in implementing TEGs.

Chapter 6: Summary of Analyses and Conclusions

The purpose of this chapter is to summarize the procedures and results obtained from each analysis of this study, as well as to draw conclusions from each analysis. A roadmap of the study was originally illustrated in Figure 1.4.

6.1 THERMODYNAMIC ANALYSES

Chapters 3 and 4 each presented a different systems-level thermodynamic analysis conducted in this study. These two analyses' results are summarized here. Figure 6.1 summarizes at a high-level the results of each analysis and their relation to one other, similar to Figure 3.6.

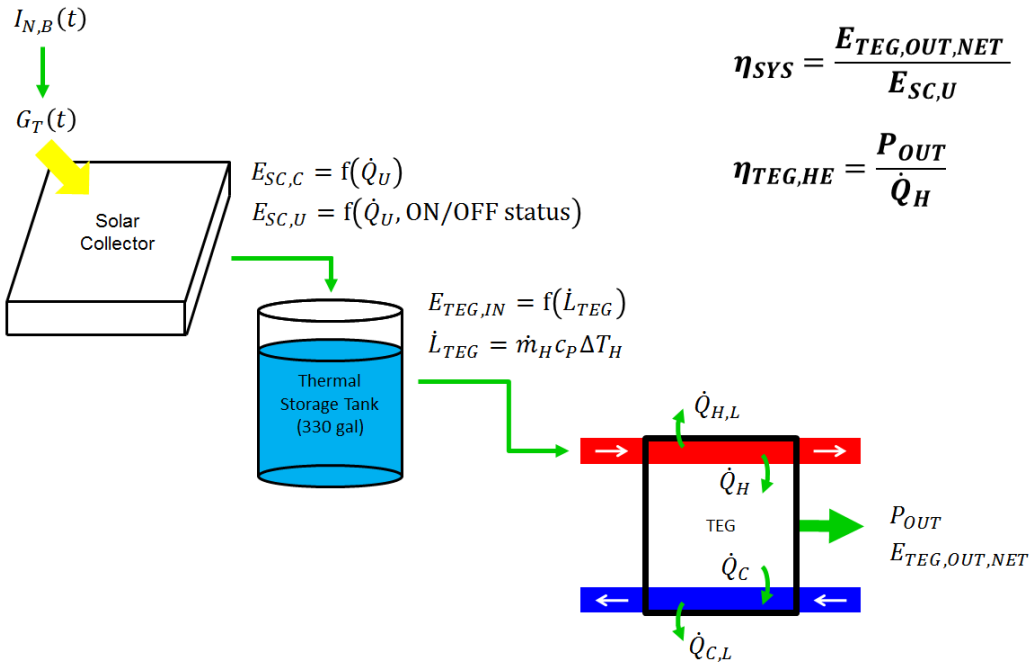

Figure 6.1: High-level flow chart of results of the two thermodynamic analyses presented in Chapters 3 and 4. The numerical model of Chapter 3 included all three components, but the analysis of Chapter 4 studied the TEG more in-depth.

6.1.1 Thermodynamic Analysis of the Solar Collector-Thermoelectric Generator Coupled System Operating in the Built Environment

6.1.1.1 Summary of Procedure and Results

The first analysis in this study (see Chapter 3) focused on the thermoelectric generator (TEG) coupled with a solar collector system as its hot stream source. The goal of this analysis was to estimate the coupled system's annual energetic performance as it operated in the built environment. A control volume analysis was performed on the solar collector system's thermal storage tank, as it was necessary to observe how the storage tank temperature, T_S, fluctuated over the course of a day. The storage tank temperature was of particular importance because this governed the TEG's hot stream inlet temperature, $T_{H,IN}$. From the energy balance of the storage tank, the governing equation for T_S was found to be a first-order ordinary differential equation (ODE). It was a function of solar insolation incident on the tilted collector, G_T, and ambient temperature, $T_{SC,AMB}$. Because these two terms were only available as discrete data, the ODE was therefore solved numerically via a forward Euler explicit finite-difference scheme. Further, the numerical model incorporated the test conditions of the TEG's upcoming Characterization Test.

In the end, the following parameters were quantified: the TEG's annual thermal energy consumption, $E_{TEG,IN}$; the TEG's net annual electricity generation, $E_{TEG,OUT,NET}$; annual thermal energy collected by the solar collector system, $E_{SC,C}$; annual thermal energy actually used by the solar collector system, $E_{SC,U}$; and finally the coupled system's operating efficiency, η_{SYS}. (Recall that the TEG was modeled as fully self-autonomous by having it power its two recirculation pumps; this effectively reduced its power output from 83 Watts to 54.2 Watts, as explained in 3.5.3.2.) These energies were illustrated in Figure 3.13.

To summarize (note the difference in units between these parameters),

$$E_{TEG,IN} = 34.06 \text{ MWh/year} \tag{3.41}$$

$$E_{TEG,OUT,NET} = 266.5 \text{ kWh/year} \tag{3.44}$$

$$E_{SC,C} = 39.73 \text{ MWh/year} \tag{3.49}$$

$$E_{SC,U} = 35.46 \text{ MWh/year} \tag{3.50}$$

$$\eta_{SYS} = 0.75\% \tag{3.53}$$

6.1.1.2 Conclusions

Here, the immediate observation is that the electrical energy produced by the TEG is two orders of magnitude less than the thermal energy collected by the solar collectors, as originally indicated in 3.5.6. Accordingly, the efficiency of the coupled system was low, being less than 1%.

The first observation is that the TEG's hot stream continually requires a huge input of thermal energy in order to operate, per Equations 3.28 and 3.41. This is directly because of its design, where fluid flow supplies the TEG's temperature differential.

The second observation is that coupling a solar collector system with the TEG as its hot stream source does not make for an efficient system from an operational standpoint. This is because the TEG generates a small amount of electricity (characteristic of thermoelectrics in general) while consuming a substantial amount of thermal energy from the thermal storage tank. Nevertheless, the solar collector system is able to sustain the TEG during daylight hours—that is, it is can feed it with the thermal energy it needs. In short, solar-thermal energy is a renewable energy source that serves as a starting point for the TEG operating in the built environment.

More importantly, based on the thermal storage tank temperature's behavior over the course of a sample representative day (see Figure 3.10) and the resulting annual energetic performance of the coupled system per the numerical model, it is pointed out that the solar collector system in this study (i.e., the Characterization Test) is not the optimal size for a single TEG, as originally discussed in 3.5.2.2. This conclusion was arrived to directly from two observations: first, the storage tank temperature reached the TEG's minimum hot inlet temperature in less than a day, and even reached the storage tank's maximum storage temperature on most days modeled thereby forcing the solar collector system to shut OFF—both of which are a function of utilizing 20 solar collectors; second, the single storage tank could not sustain the TEG over night. As a result, it is suggested that the TEG be coupled with fewer solar collectors but a larger (or more than a single) storage tank. This would mean that the initial charging days in the year would be longer, but the TEG would likely be sustained for longer throughout the year—perhaps even over night, thus improving its annual energetic performance. As pointed out in 5.2.1.5, an optimization analysis of the coupled system was not part of the study. Instead, this is recommended as a follow-on study.

Finally, it is pointed out that thermal storage (or any other fluid) is not necessarily a requirement for the novel TEG. That is, the TEG need not require a hot water reservoir from which to draw thermal energy from as it did in this analysis. Similar to the cold stream source (in which a horizontally-trenched closed-loop GHP system was assumed), the TEG's hot stream source can conceivably be supplied by running a closed-loop system through any hot source—granted that the appropriate materials and thermal analysis has validated such a configuration.

6.1.2 Thermodynamic Analysis and Characterization of the Thermoelectric Generator during Operation

6.1.2.1 Summary of Procedure and Results

The second analysis (see Chapter 4) focused on the TEG itself. This analysis aimed at characterizing the internal thermodynamics occurring within the TEG during operation. Treating the TEG as a heat engine, three separate control volume analyses were performed on different sections of the TEG. The resulting energy balance equations were solved simultaneously and mathematical expressions for the heat transfer components were obtained. These components were: the rate at which the TEG's cold stream absorbs heat, $\dot{Q}_C$; the rate at which the TEG's hot stream supplies heat, $\dot{Q}_H$; and the hot stream's convective losses, $\dot{Q}_{H,L}$.

In order to quantify each of the individual heat transfer components taking place within the TEG during operation, experimental data were needed. However, the primary difficulty encountered in this study was that the novel TEG had not yet undergone any thorough, rigorous experimental testing, and therefore no data of the TEG in operation were available. In fact, such a test—called the Characterization Test (see 4.4)—was being planned at the time of writing and was expected to take place later in 2011. As a result, this analysis revolved around the Reference Test (see 4.1), which supplied this analysis with the necessary experimental data. The Reference Test, conducted by *Watts Thermoelectric LLC*, was a single experiment of the TEG in operation in an isolated environment on the benchtop—not in the built environment. Ultimately, this analysis provided a preliminary empirical thermodynamic characterization of the TEG. As outlined in Table 4.3,

- $\dot{Q}_C = 3{,}368$ W
- $\dot{Q}_{C,L} \approx 0$ W (assumed)

- $\dot{Q}_H = 4{,}891$ W
- $\dot{Q}_{H,L} = 1{,}439$ W
- $P_{OUT} = 84$ W

In addition to quantifying the heat transfer parameters (see 4.3.1), the overall heat transfer coefficient of the TEG, $U_{TEG,L}$, was derived based on the hot stream's convective loss term, $\dot{Q}_{H,L}$. This required calculating the log mean temperature difference (due to the heat exchanger design of the TEG), $\Delta T_{TEG,LM}$, and the TEG's surface area as $A_{TEG} \approx$ 2,684 in^2 (1.73 m^2). In all,

$$\Delta T_{TEG,LM} = 98.0\ ℉ = 54.4\ ℃ \tag{4.26}$$

$$(UA)_{TEG,L} = 26.43\ \text{W/℃} \tag{4.27}$$

$$U_{TEG,L} = 15.26\ \text{W/m}^2\text{-℃} \tag{4.28}$$

Most importantly, this analysis allowed for a first-cut estimate of the instantaneous operating efficiency of the TEG (as a heat engine):

$$\eta_{TEG,HE} = 1.72\% \tag{4.29}$$

6.1.2.2 Conclusions

The low operational efficiency calculated was expected and is on par with thermoelectric generation devices in general [15, 16, 18, 19, 23]. It is important to realize that this low efficiency should not be attributed to the novel TEG but rather the low operational efficiencies inherent to thermoelectric materials and the small temperature differences that drove the system. As a starting point, these results were a good preliminary thermodynamic characterization of the TEG, having never been studied before. The upcoming Characterization Test is expected to provide more experimental

data in order to better understand the operational characteristics of the TEG in the built environment.

6.2 EMISSIONS AND ECONOMIC ANALYSES OF THE THERMOELECTRIC GENERATOR IN THE BUILT ENVIRONMENT

Chapter 5 presented the emissions and economic analyses performed in this study. These analyses' results are summarized here.

6.2.1 Emissions Analysis

6.2.1.1 Summary of Procedure and Results

The emissions analysis (see Section 5.1) had the goal of quantifying the carbon dioxide-equivalent (CO_2e) emissions avoided by implementing the novel, zero-emission TEG in place of a traditional, fossil fuel-burning electricity generation technology. This analysis entailed studying the electric grid of where the Characterization Test was located. Because it was expected to take place in Detroit, MI, the *Reliability First Corporation–Michigan* (RFCM) electric grid was considered.

The first step involved characterizing the electric grid by determining what its emission factor, EF, was. The emission factor is a ratio of the emissions produced by all the power plants in the electric grid (in tons CO_2e) to the grid's total electricity generation (in MWh). Using year-aggregate data from the U.S. Environmental Protection Agency for all the operating power plants in the RFCM electric grid, the emission factor was quantified for RFCM:

$$EF_{RFCM} = 0.830 \ \frac{\text{tons } CO_2e}{\text{MWh}} \tag{5.2}$$

As a result, this value was multiplied by the net annual electrical energy generation by the TEG, $E_{TEG,OUT,NET}$, which was obtained from the numerical model (see 6.1.1). This step quantified the emissions avoided, $P_{AVOIDED}$:

$$P_{AVOIDED} = 0.221 \text{ tons } CO_2e/\text{year} \tag{5.3}$$

6.2.1.2 Conclusions

Although RFCM's emission factor was particularly high—the 6th largest of all 26 NERC subregions in the nation—the TEG's low annual energy generation resulted in a low avoidance of emissions. Nevertheless, 0.221 tons CO_2e only corresponded to a single TEG, and implementing more than a single TEG—which is a more practical scenario—would result in significant annual savings of emissions, as Figure 5.3 demonstrated.

6.2.2 Economic Analysis

6.2.2.1 Summary of Procedure and Results

The final analysis (see Section 5.2) dealt with the economics of this study—in particular, determining the levelized cost of electricity (LCOE) of the TEG integrated into the built environment. Recall that the TEG uses solar-thermal energy and geothermal energy as its hot and cold stream sources, respectively (see 2.2.3.1). Further, recall that a solar collector system with 20 flat-plate solar collectors was planned for the upcoming Characterization Test (see 4.4.2), and that a horizontally-trenched closed-loop geothermal heat pump (GHP) system was assumed in this analysis.

In order to estimate the LCOE of the integrated system, the capital, operating & maintenance (O&M), and fuel costs of each subsystem were considered. For the solar collector system, capital costs were obtained from a price quote provided directly by

Power Panel Inc., the system's manufacturer in the upcoming Characterization Test [38]; O&M costs were estimated from figures reported by Howell et al. [31]. For the TEG itself, all costs were obtained directly from *Watts Thermoelectric LLC* [21]. For the GHP system, all costs were estimated from Banks [35]. Each subsystem's installed cost was amortized over a 20 year lifetime with zero salvage value. In the end, the following annual costs were estimated for the three subsystems:

$$\text{Total Cost}_{SC} = \$1{,}913.38/\text{year} \tag{5.18}$$

$$\text{Total Cost}_{TEG} = \$133.67/\text{year} \tag{5.24}$$

$$\text{Total Cost}_{GHP} = \$193.04/\text{year} \tag{5.33}$$

Then, using the TEG's net annual electricity generation, the LCOE and price per Watt of the integrated system were calculated:

$$LCOE_{TOT} = \$8{,}404.18/\text{MWh}\ (\$8.40/\text{kWh}) \tag{5.35}$$

$$P_{TOT}\left[\frac{\$}{\text{W}}\right] = \$313/\text{W} \tag{5.36}$$

Both of these prices are much higher than competitive power-generation options. As noted in 5.2.1.5, however, these estimates are the consequences of the particular design assumptions for this specific study, and are not intended to be a general conclusion about the TEG overall, or this particular TEG design. In particular, the solar collectors are the most expensive contributor to the overall cost, followed by the GHP system. Thus, the TEG is the smaller cost of the three major subsystems. Subsequently, finding a way to use the TEG without the expensive solar-thermal and GHP subsystems would improve its overall financial outlook.

6.2.2.2 Conclusions

First, the annual cost of the TEG, Total Cost_{TEG}, was calculated based on capital and O&M costs reported directly from *Watts Thermoelectric LLC*. Should these figures

be optimistic (see 5.2.1.3), the LCOE of the integrated system would increase accordingly.

Second, the total annual cost of the solar collector system, Total Cost_{SC}, was found to be much greater than that of the TEG, Total Cost_{TEG}, or the geothermal heat pump system, Total Cost_{GHP}. Furthermore, each of the three subsystems featured low O&M costs. Thus, the solar collector system was much more capital-intensive than any of the other subsystems.

In their *Annual Energy Outlook 2011* publication, the U.S. Department of Energy's Energy Information Administration (EIA) reported levelized cost figures for a variety of energy generation technologies [9]. The only caveat here is that these estimates apply for utility-scale generation technologies, whereas the systems analyzed here were small-scale systems (with the exception of the solar collector system). Similarly, the U.S. Department of Energy's Office of Energy Efficiency and Renewable Energy (EERE) also reported levelized cost of energy figures in their *2008 Geothermal Technologies Market Report* publication [43]. These values are listed in Table 6.1 and can be used as a point of comparison for the LCOE of the TEG integrated into the built environment.

Generation Technology	LCOE, Reported by EIA [2009 $/MWh] [9]	LCOE, Reported by EERE [2008 $/MWh] [43]
TEG integrated into the built environment ($LCOE_{TOT}$ per Equation 5.35)	8,404.18	
Conventional Coal	94.8	74 – 135
Natural Gas: Conventional Combined Cycle	66.1	73 – 100
Nuclear	113.9	98 – 126
Wind	97.0	44 – 91
Solar Photovoltaic	210.7	96 – 154
Solar-Thermal	311.8	90 – 145
Geothermal	101.7	42 – 69
Biomass	112.5	50 – 94
Hydro	86.4	—

Table 6.1: Levelized costs for various electricity generation technologies, as reported by the EIA [9] and EERE [43]. The EIA figures refer to large-scale plants entering service in 2016, whereas the EERE figures do not specify what size systems were analyzed. While the two sources matched for fossil fuel sources, there were significant discrepancies observed for renewable sources, particularly solar technologies.

When comparing levelized costs of various energy generation sources, it is clear that the integrated system's levelized cost is substantially greater than the others, primarily due to the solar collector system's high annual cost, Total Cost_{SC}, and the integrated system's low annual energy output (characteristic of thermoelectrics).

In order for any generation technology to be a viable option, it must be economically competitive with the electric grid. Although the benefits of a renewable energy source like the novel TEG are certainly present—namely the fact that is has zero emissions—the average customer or any end user will have no incentive to purchase and implement such systems until they become economically competitive with other generation sources. Based on EIA figures, the average U.S. retail price of electricity to residential- or commercial-sector customers has been between 10–12 cents/kWh since 2008; for industrial-sector customers, this price drops to less than 7 cents/kWh [45]. Therefore, the integrated system's $8.40/kWh is roughly 70 times more expensive than electric utility prices.

Finally, as originally outlined in 5.2.1.5, the $LCOE_{TOT}$ and P_{TOT} prices pertain directly to the Characterization Test setup. The size of the solar collector system (which was coupled with the TEG) was not optimized for performance from the TEG. A suggestion for a more suitable solar collector system size was made in 6.1.1.2. A solar collector system reflecting this suggestion would likely result in significantly lower prices.

6.3 FINAL CONCLUSIONS: THE BOTTOM LINE AND WASTE HEAT RECOVERY CONSIDERATIONS

This study found that the TEG would likely work as promised, is an emissions-free source of energy, is compatible with renewable energy sources, and has a robust method of generating electricity. However, it also continuously requires a substantial amount of thermal energy to operate due to its design and a low overall efficiency. As this study demonstrated, a solar collector system can supply the TEG's hot stream with the thermal energy needed, but such systems are extremely capital-intensive; in fact, the

solar collector system was largely responsible for the enormous LCOE of the integrated system. In contrast, recall that the TEG itself and GHP system each had low annual costs, thus making the GHP system an economically suitable source for the TEG's cold stream. In the end, having such a large LCOE will make the integrated system economically infeasible. Therefore, a replacement for the solar collector system is recommended—the TEG would be more cost-competitive if it were coupled with systems that not only have low-cost fuel sources, but also minimal capital costs.

Accordingly, a recommendation of this study is that a more promising energy source for the TEG's hot stream potentially lies in waste heat recovery. This topic was briefly surveyed in 2.2.3.2. Waste heat may be a more symbiotic source for the TEG's hot stream than solar-thermal energy, assuming that the capital costs of recovering waste heat and implementing it to the TEG are comparatively low. In the end (and in addition to the optimization analysis discussed in 6.1.1.2 and 6.2.2.2), thorough evaluation of potential waste heat sources in industrial, commercial, and residential settings is also recommended as a follow-on study.

Appendix A: Insolation

A.1: Measured/Recorded Insolation Data

Two sets of extraterrestrial insolation data were available [28]: insolation incident on a horizontal surface $I_{H,B}$ and insolation incident on a surface normal to the sun $I_{N,B}$, herein referred to as "horizontal insolation data" and "normal insolation data," respectively. These data sets were recorded at nearly the exact same location (in terms of geographic coordinates) as listed in 4.4.1. Rather than tabulating these data (96 data points for each of the 12 representative days), they were plotted in the following sections.

Note that although figures list months, data correspond to the 12 representative days in 2005 (i.e., January refers to 01/20/2005, etc.; see 3.3.1).

A.1.1 Extraterrestrial Insolation Incident on a Horizontal Surface, $I_{H,B}$

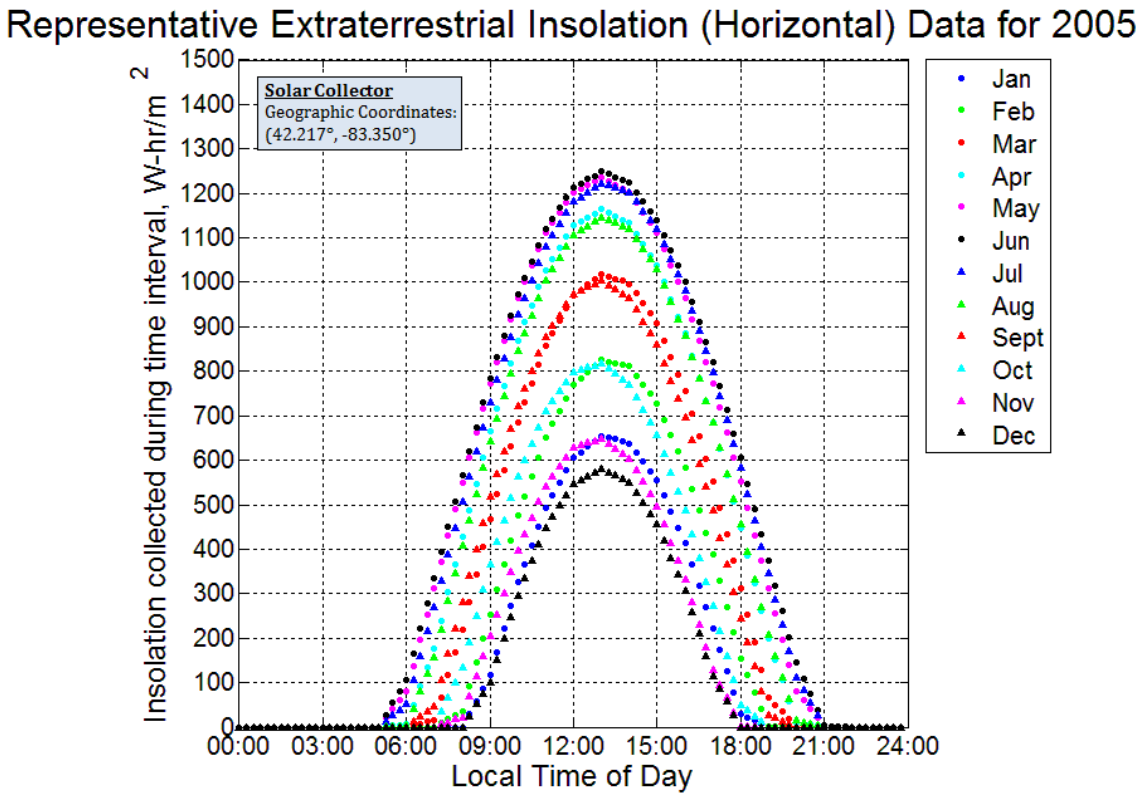

Figure A.1: Representative extraterrestrial insolation incident on a horizontal surface for the 12 representative days. As discussed in 3.3, data were linearly interpolated to obtain quarter-hourly data (shown). Further, as discussed in the following derivation, these data sets were ultimately not used; instead, normal insolation data were used.

A.1.2 Extraterrestrial Insolation Incident on a Surface Normal to the Sun, $I_{N,B}$

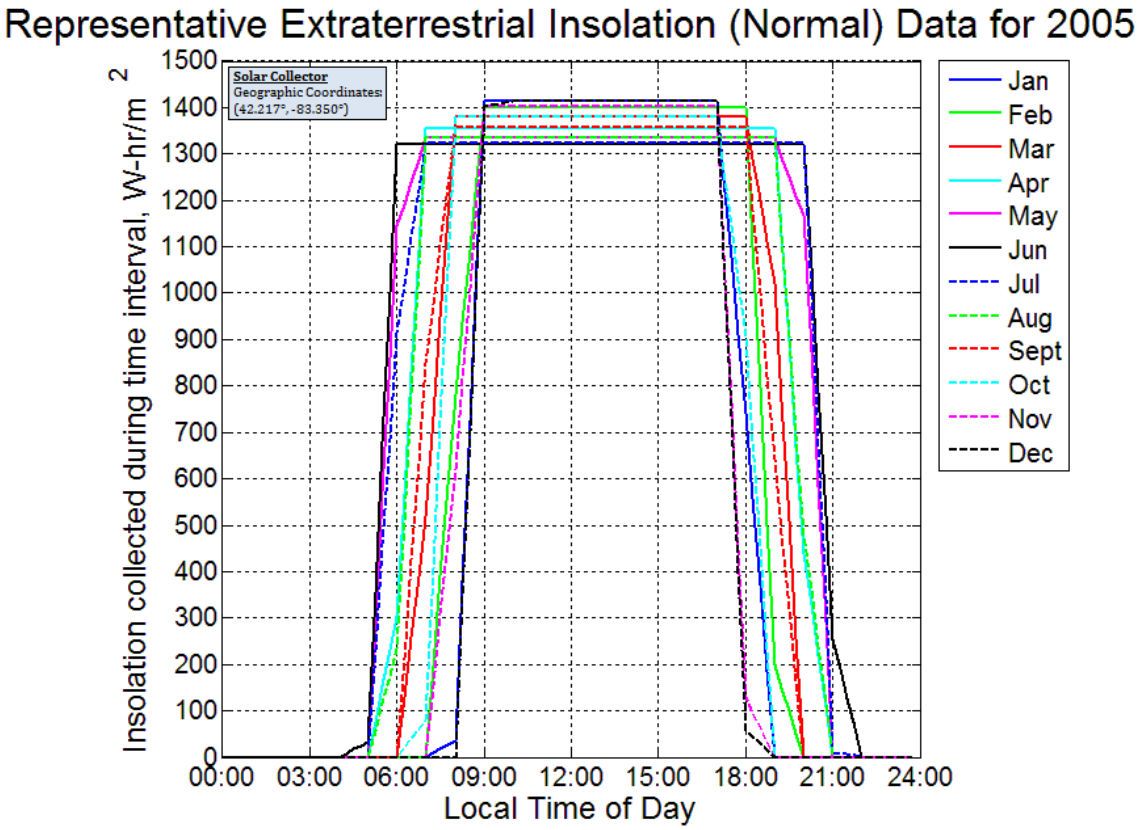

Figure A.2: Representative extraterrestrial insolation incident on a surface normal to the sun for the 12 representative days. Here, note that data are still in quarter-hourly format; however, lines rather than data points make it easier to distinguish at the nominal peak levels.

A.2: CALCULATING INSOLATION INCIDENT ON A TILTED SURFACE FROM MEASURED INSOLATION DATA

The solar trigonometric equations presented here were used to convert extraterrestrial insolation data—both incident on a horizontal surface, $I_{H,B}$, and on a surface normal to the sun, $I_{N,B}$—into insolation incident on a tilted surface, G_T. This derivation primarily follows Goswami et al. [30]; Howell et al. [31] was also used as a reference.

Note that the terms G and I are interchangeable and both refer to insolation in units of $[\mathrm{W/m^2}]$.

A.2.1 Derivation

A.2.1.1 Using Normal Insolation Data

The insolation incident on a tilted surface is the sum of the beam/direct, diffuse, and reflected radiation components incident on the tilted surface:

$$G_T = I_{T,B} + I_{T,D} + I_{T,R}$$

Where each component is defined as:

$$\begin{aligned} I_{T,B} &= I_{N,B}\cos(i) \\ I_{T,D} &= I_{H,D}\cos^2\left(\frac{\beta}{2}\right) \\ &= \left(CI_{N,B}\right)\cos^2\left(\frac{\beta}{2}\right) \\ I_{T,R} &= \rho_{SC} I_H \sin^2\left(\frac{\beta}{2}\right) \\ &= \rho_{SC}\left(I_{N,B}(\sin(\alpha)+C)\right)\sin^2\left(\frac{\beta}{2}\right) \end{aligned}$$

Together,

$$\boldsymbol{G_T = I_{N,B}\left(\cos(i) + C\cos^2\left(\frac{\beta}{2}\right) + \rho_{SC}(\sin(\alpha)+C)\sin^2\left(\frac{\beta}{2}\right)\right)} \qquad \text{(A.1)}$$

Where:

$$\cos(i) = \cos(\alpha)\cos(a_s - a_w)\sin(\beta) + \sin(\alpha)\cos(\beta)$$

All parameters are known (constant) except for the solar angles, which are defined as:

$$a_s = \sin^{-1}\left\{\frac{\cos(\delta_s)\sin(h_s)}{\cos(\alpha)}\right\}$$
$$\alpha = \sin^{-1}\{\sin(LAT)\sin(\delta_s) + \cos(LAT)\cos(\delta_s)\cos(h_s)\}$$
$$\delta_s = \sin^{-1}\left\{\sin(23.45°)\sin\left(\frac{360}{365°}(284+n)\right)\right\}$$

Note angle restrictions:

$$0° \leq \alpha \leq 90°$$
$$0° \leq i \leq 90°$$

Continuing,

$$h_s = \frac{\text{Minutes from local solar noon}}{4\ \text{min/deg}}$$
$$\text{Minutes from local solar noon} = \text{Solar Time} - \text{Local Solar Noon}$$
$$\text{Solar Time} = LST + ET + (STM - |LONG|)\cdot 4\ \text{min/deg}$$
$$ET = 9.87\sin(2B) - 7.53\cos(B) - 1.5\sin(B)$$
$$B = \frac{360}{364}(n-81)$$

Furthermore, it is standard in the field to express Equation A.1 in terms of each insolation component's tilt factors [30]:

$$G_T = I_{N,B}(R_b + CR_d + (\sin(\alpha) + C)R_r)$$

Where the tilt factors are defined as:

$$R_b = \cos(i)$$
$$R_d = \cos^2\left(\frac{\beta}{2}\right)$$
$$R_r = \rho_{SC}\sin^2\left(\frac{\beta}{2}\right)$$

However, this author decided to express Equation A.1 using overall multipliers rather than tilt factors to simplify the analysis (note: this is the only deviation from Goswami et al. in this derivation):

$$G_T = I_{N,B}(R_b + F_d + F_r)$$

Where the author-defined "insolation multipliers" are defined as:

$$F_d = CR_d = C\cos^2\left(\frac{\beta}{2}\right)$$
$$F_r = (\sin(\alpha) + C)R_r = \rho_{SC}(\sin(\alpha) + C)\sin^2\left(\frac{\beta}{2}\right)$$

Continuing, the beam/direct tilt factor, R_b, and insolation multipliers, F_d and F_r, can be summed into a single, overall "insolation factor," F_{TOT}:

$$F_{TOT} = R_b + F_d + F_r \tag{A.2}$$

Thus, Equation A.1 can be simplified as:

$$\boldsymbol{G_T = I_{N,B} F_{TOT}} \tag{A.3}$$

A.2.1.2 An Additional Step: Using Horizontal Insolation Data

Horizontal insolation data can be used in place of normal insolation data via the following relation [30]:

$$I_{N,B} = \frac{I_{H,B}}{\sin(\alpha)} \tag{A.4}$$

Here, the sine term in the denominator affects all parameters. Equation A.1 therefore becomes:

$$G_T = I_{H,B} \frac{\left(\cos(i) + C\cos^2\left(\frac{\beta}{2}\right) + \rho_{SC}(\sin(\alpha) + C)\sin^2\left(\frac{\beta}{2}\right)\right)}{\sin(\alpha)} \tag{A.5}$$

The insolation factor F_{TOT} is also obviously affected, resulting in the definition of an insolation factor strictly for horizontal insolation data, which incorporates the sine term in the denominator:

$$F'_{TOT} = \frac{F_{TOT}}{\sin(\alpha)} \tag{A.6}$$

thereby making Equation A.3:

$$G_T = I_{H,B} F'_{TOT} \tag{A.7}$$

A.2.2 Known Values (Constants) and Calculated Values

A.2.2.1 Known Values (Constants)

This section outlines the known values (constants) that were substituted into the equations during calculations. Recall that only a single representative day from each month was selected (see 3.3.1); however, for simplicity, the month is listed as the head row.

	Jan	Feb	Mar	Apr	May	Jun	Jul	Aug	Sept	Oct	Nov	Dec
n	20	49	79	110	141	172	203	234	265	295	325	355
C	0.058	0.06	0.071	0.097	0.121	0.134	0.136	0.122	0.092	0.073	0.063	0.057

Table A.1: n, the day number of the year 2005 (as shown in 3.3.1), and C, the sky diffuse factor, which was taken as constant for each month [30].

Parameter	Value
ρ_{SC}	0.2
β	+45°
a_w	+22°
LAT	42.215°
$LONG$	-83.349°
STM	75°

Table A.2: List of parameters used in calculating the insolation incident on the tilted collector, which reflect the Characterization Test (see 4.4). The value for radiation reflectance, ρ_{SC}, was based on the urban location of the testing facility (see 4.4.1) [30].

A.2.2.2 Calculated Values

This section lists the parameters calculated from the equations outlined in A.2.1.

	Jan	**Feb**	**Mar**	**Apr**	**May**	**Jun**	**Jul**	**Aug**	**Sept**	**Oct**	**Nov**	**Dec**
B [deg]	-60.3	-31.6	-2.0	28.7	59.3	90.0	120.7	151.3	182.0	211.6	241.3	271.0
ET [min]	-10.9	-14.4	-8.2	1.0	3.5	-1.5	-6.1	-2.4	8.3	16.0	13.2	1.0
δ_s [deg]	-20.2	-12.0	-0.8	11.0	20.0	23.4	20.1	11.2	-0.6	-11.9	-20.3	-23.4

Table A.3: List of calculated parameters that were constant throughout the representative day selected of the month.

The remainder of the parameters (Solar Time, Minutes from Local Solar Noon, h_s, α, a_s, and i) varied per quarter-hour, as they are functions of the local standard time, LST. As a result, tabulated values of said parameters have been excluded for brevity. Instead, plots of only the most important parameters have been included in the proceeding section.

A.2.3 Plots

A.2.3.1 Calculated Insolation Factor, F_{TOT}

The overall insolation factor was calculated two different ways—using horizontal insolation data $I_{H,B}$ (via Equation A.6) and normal insolation data $I_{N,B}$ (via Equation A.2).

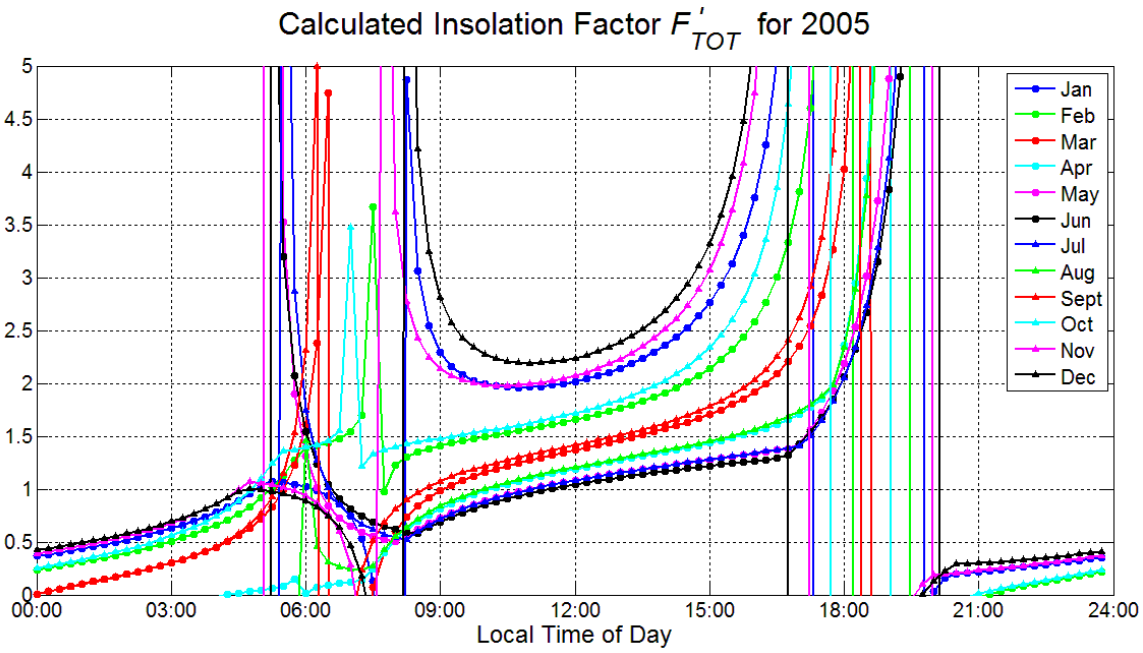

Figure A.3: Insolation factor F'_{TOT}, calculated from horizontal insolation data and presented for the 12 representative days of 2005.

As seen in Figure A.3, F'_{TOT} exhibits asymptotic behavior due to the $\sin(\alpha)$ term (see Equation A.6) at $\alpha = 0°$, which occurs at sunrise and sunset of each day. Had restrictions for α and i been placed (see A.2.1), each factor would simply increase to infinity at sunrise and sunset (plots excluded for brevity). Thus, F'_{TOT} is only valid between sunrise and sunset (i.e., between the two asymptotes of each day).

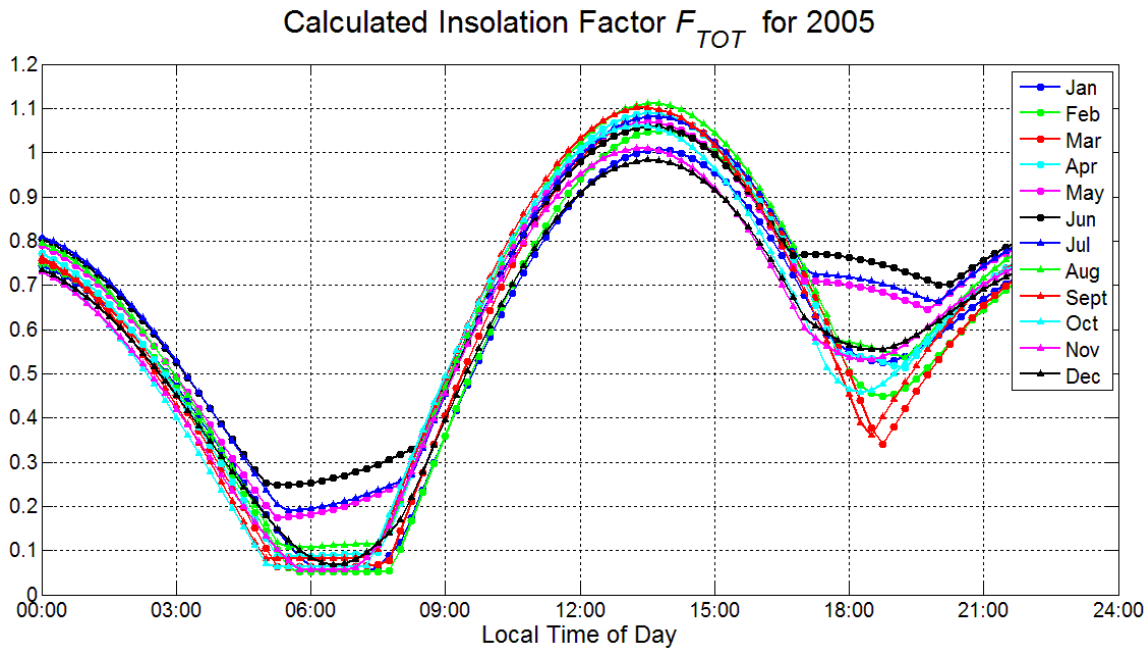

Figure A.4: Insolation factor F_{TOT}, calculated from normal insolation data and presented for the 12 representative days of 2005.

Without the sine term in the denominator, the calculated insolation factor F_{TOT} for each day exhibited much smoother behavior, even at sunrise and sunset (i.e., $\alpha = 0°$). (Here, the appropriate restrictions for α and i were placed.)

A.2.3.2 Calculated Insolation, G_T

The insolation incident on a tilted surface G_T was also calculated two different ways—using horizontal insolation data $I_{H,B}$ (via Equation A.7) and normal insolation data $I_{N,B}$ (via Equation A.3).

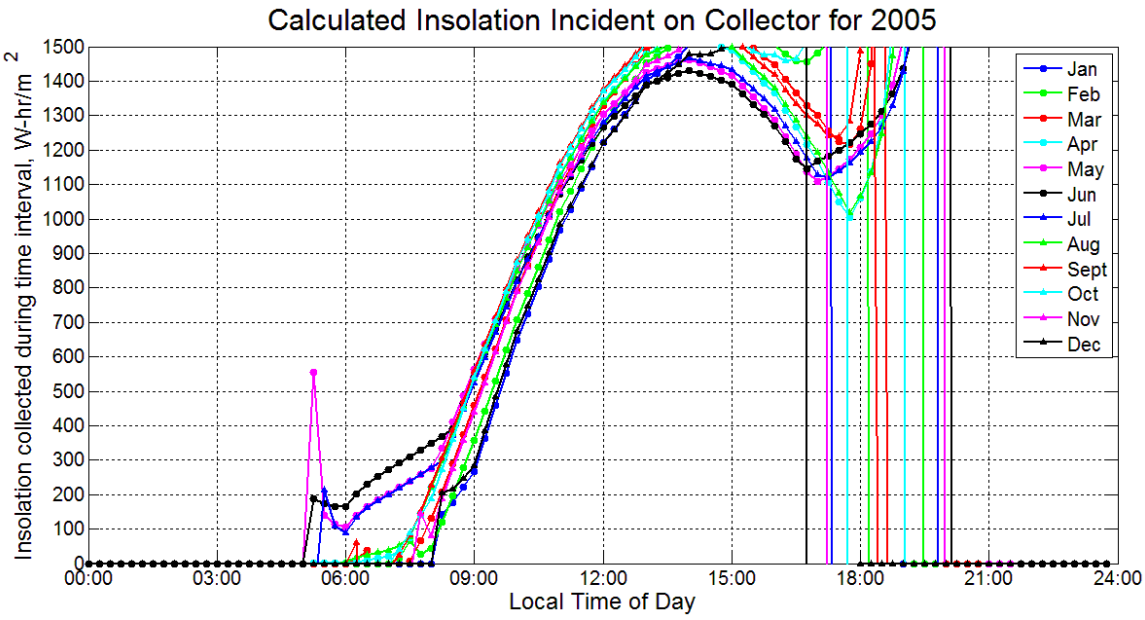

Figure A.5: Insolation incident on a tilted surface, calculated from horizontal insolation data and presented for the 12 representative days of 2005.

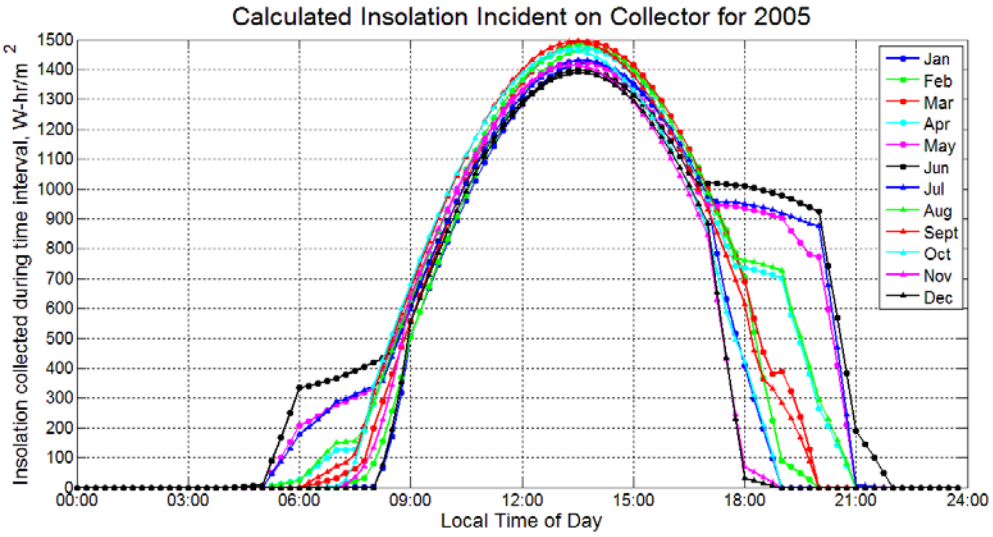

Figure A.6: Insolation incident on a tilted surface, calculated from normal insolation data and presented for the 12 representative days of 2005. (This figure was originally shown as Figure 3.5.)

The two plots were compared, and it was ultimately decided to use normal insolation data $I_{N,B}$ rather than horizontal insolation data $I_{H,B}$ for determination of insolation incident on the tilted collector G_T. In fact, the mere observation that $F'_{TOT} > 2$ for certain days, whereas $F_{TOT} < 1.12$ (collectively), resulted in the decision to instead use normal insolation data.

Appendix B: Numerical Model

B.1: SOLUTION PLOTS FOR ALL 12 REPRESENTATIVE DAYS

This section includes the following 5 solution plots for each of the 12 representative days:

- Solar collector's $\dot{Q}_U$ and ON/OFF status
- Insolation incident on the tilted collector, G_T, which were calculated from normal insolation data
- Beam/direct tilt factor R_b and insolation factors F_d and F_r (see Appendix A.2.1), which were calculated from normal insolation data
- Storage tank temperature, T_S, over the course of the day
- TEG's ON/OFF status

Recall that results for only 3 consecutive days are presented (see 3.5.2.1). Note: solutions plots have been included without labels or captions.

B.1.1 January (01/20/2005)

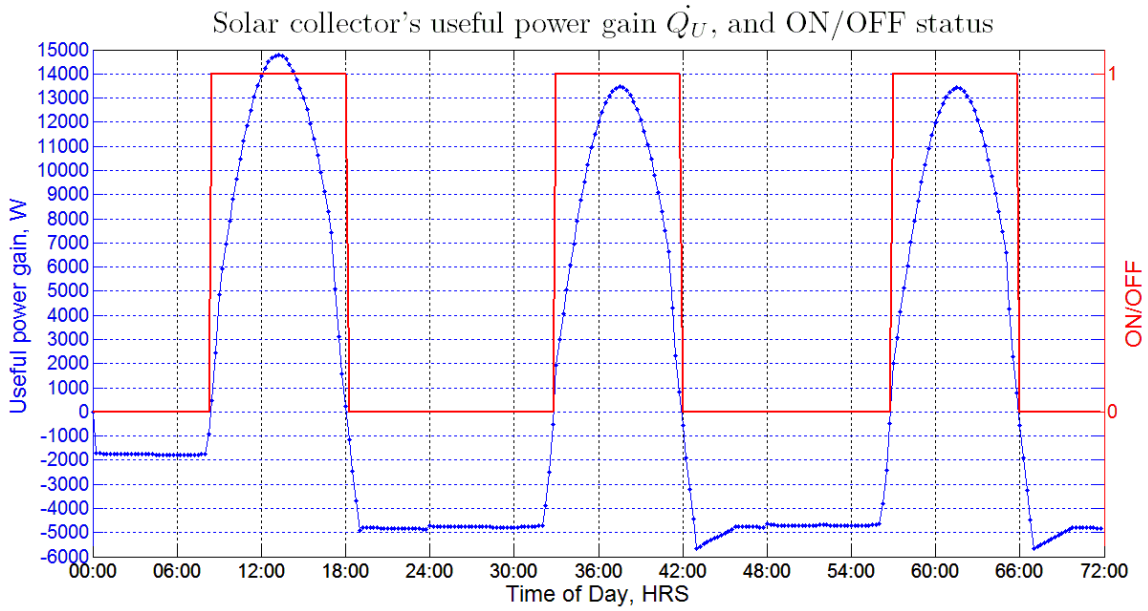

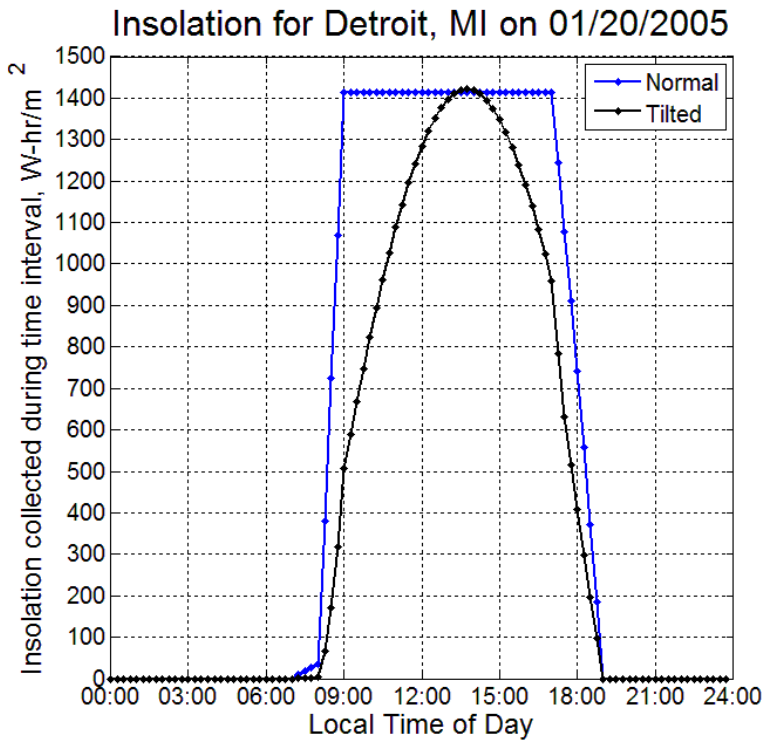

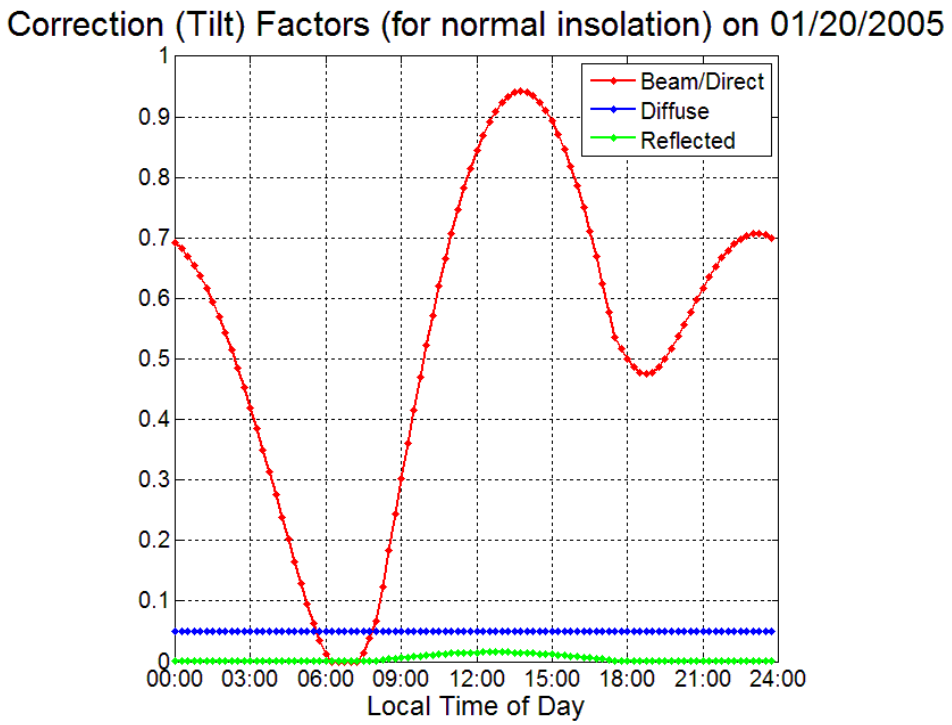
Correction (Tilt) Factors (for normal insolation) on 01/20/2005
Beam/Direct
Diffuse
Reflected
1
0.9
0.8
0.7
0.6
0.5
0.4
0.3
0.2
0.1
0
00:00 03:00 06:00 09:00 12:00 15:00 18:00 21:00 24:00
Local Time of Day

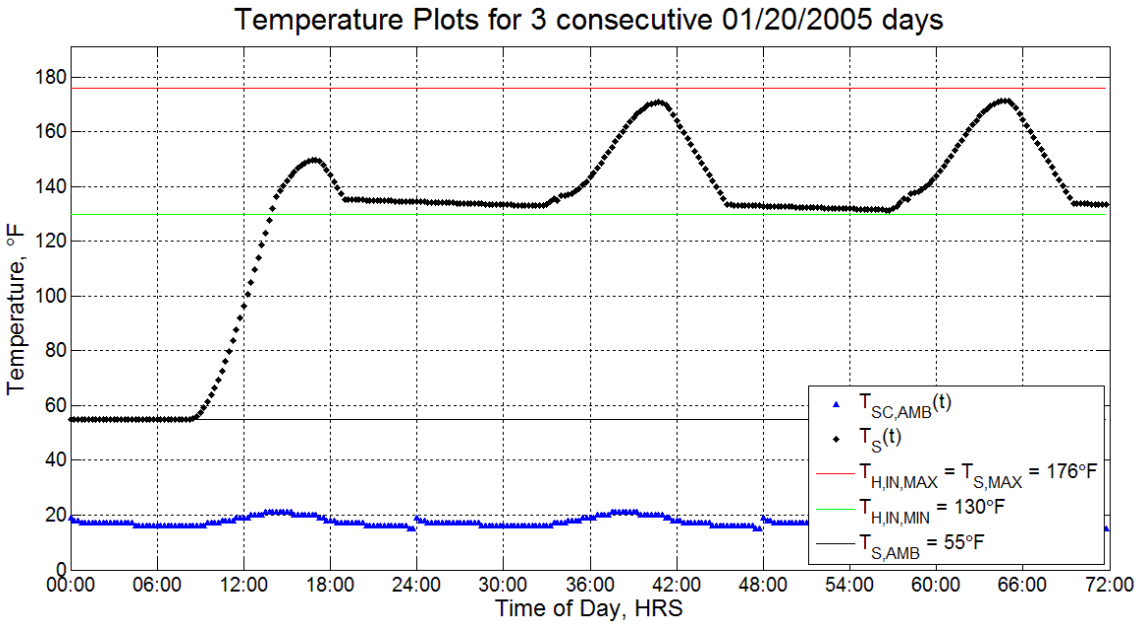
Temperature Plots for 3 consecutive 01/20/2005 days
Temperature, °F
180
160
140
120
100
80
60
40
20
0
00:00 06:00 12:00 18:00 24:00 30:00 36:00 42:00 48:00 54:00 60:00 66:00 72:00
Time of Day, HRS
T_SC,AMB(t)
T_S(t)
T_H,IN,MAX = T_S,MAX = 176°F
T_H,IN,MIN = 130°F
T_S,AMB = 55°F

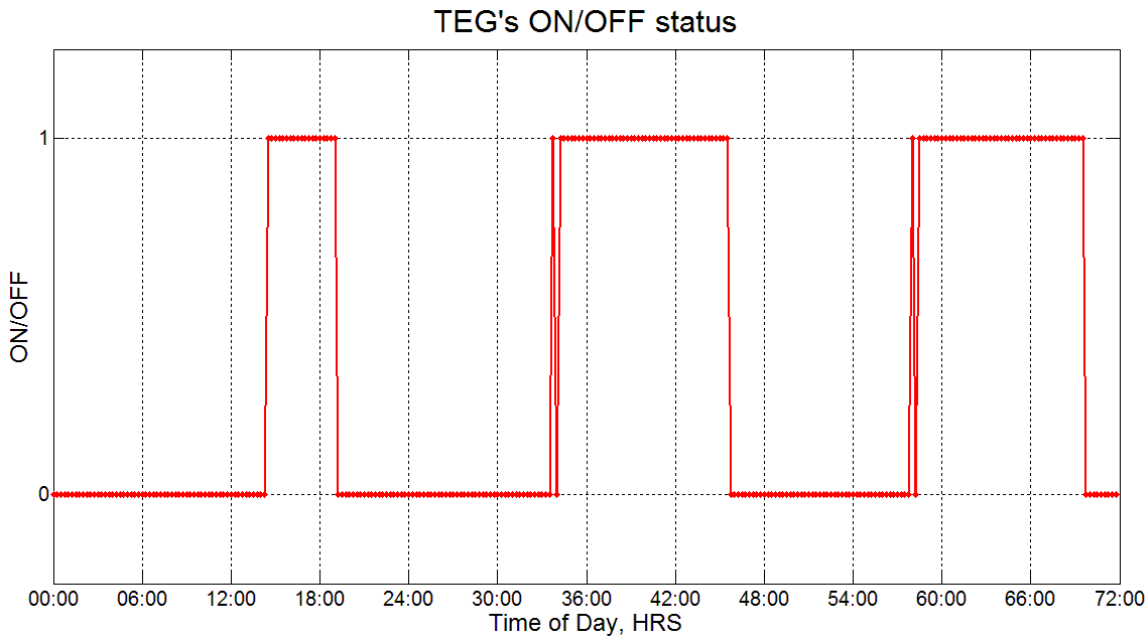
TEG's ON/OFF status
ON/OFF
1
0
00:00
06:00
12:00
18:00
24:00
30:00
36:00
42:00
48:00
54:00
60:00
66:00
72:00
Time of Day, HRS

B.1.2 February (02/18/2005)

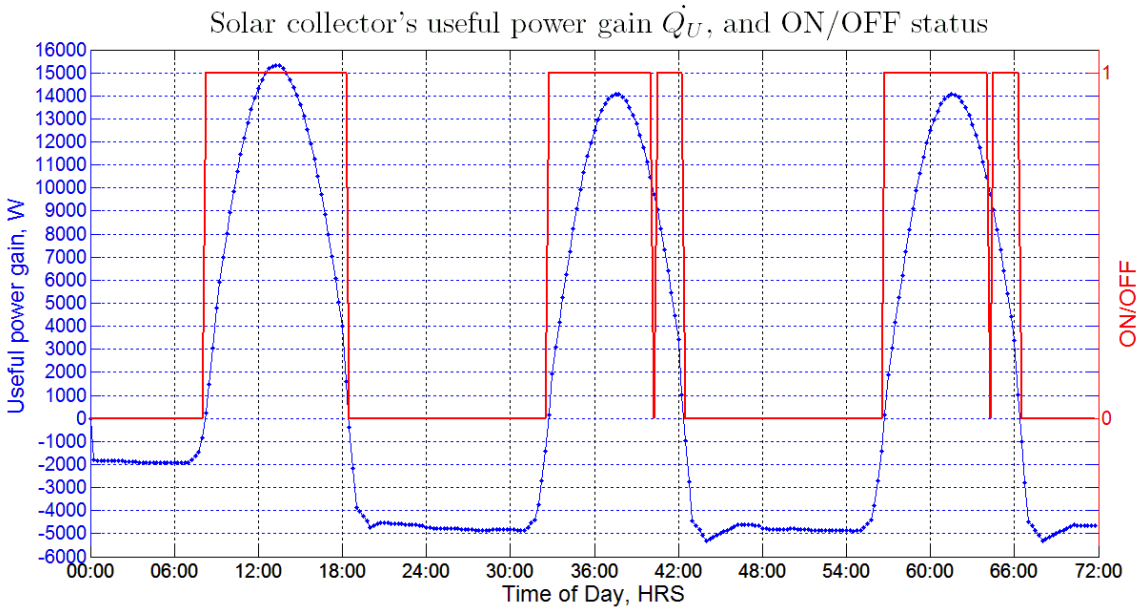

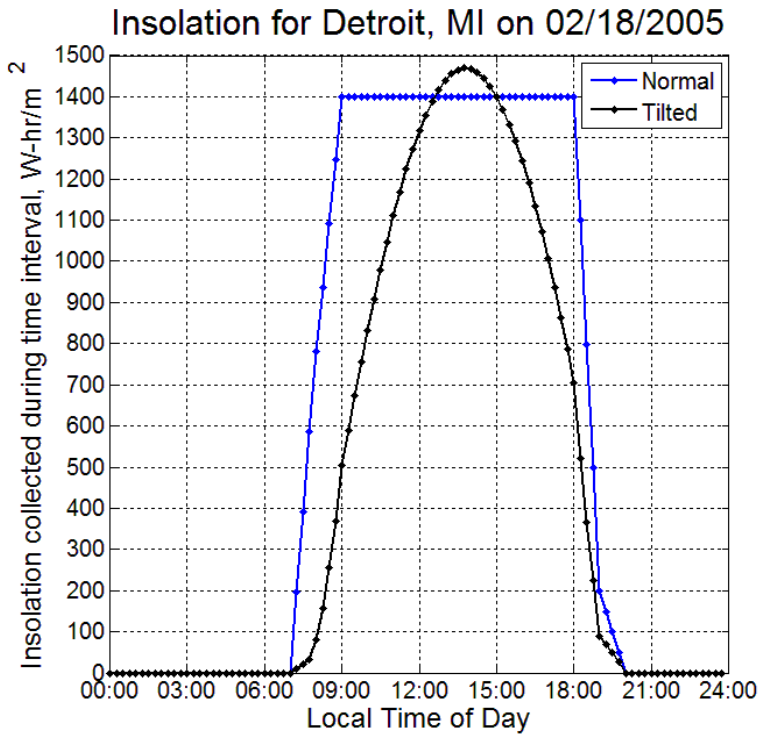

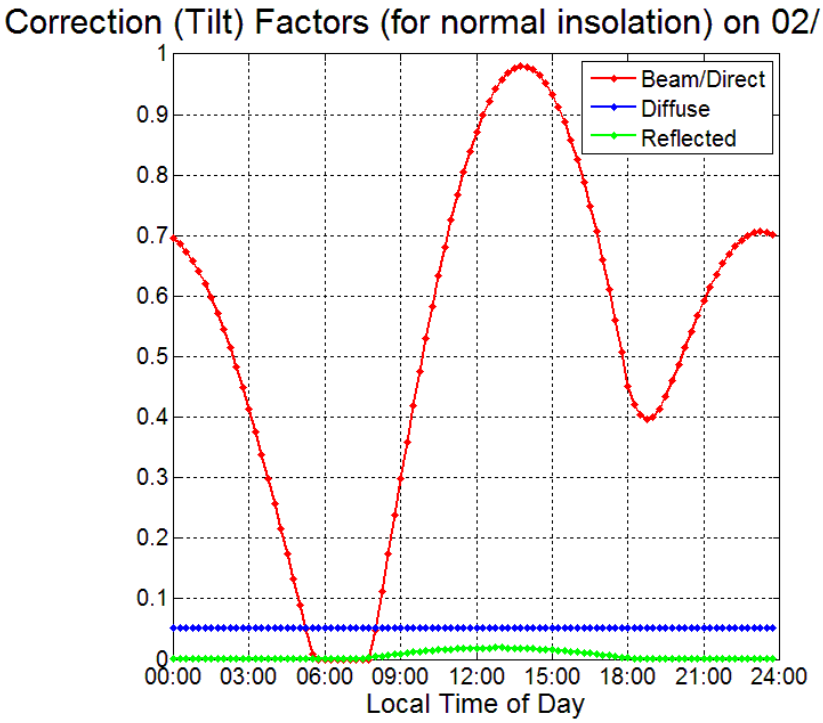
Correction (Tilt) Factors (for normal insolation) on 02/18/2005
Beam/Direct
Diffuse
Reflected
1
0.9
0.8
0.7
0.6
0.5
0.4
0.3
0.2
0.1
0
00:00 03:00 06:00 09:00 12:00 15:00 18:00 21:00 24:00
Local Time of Day

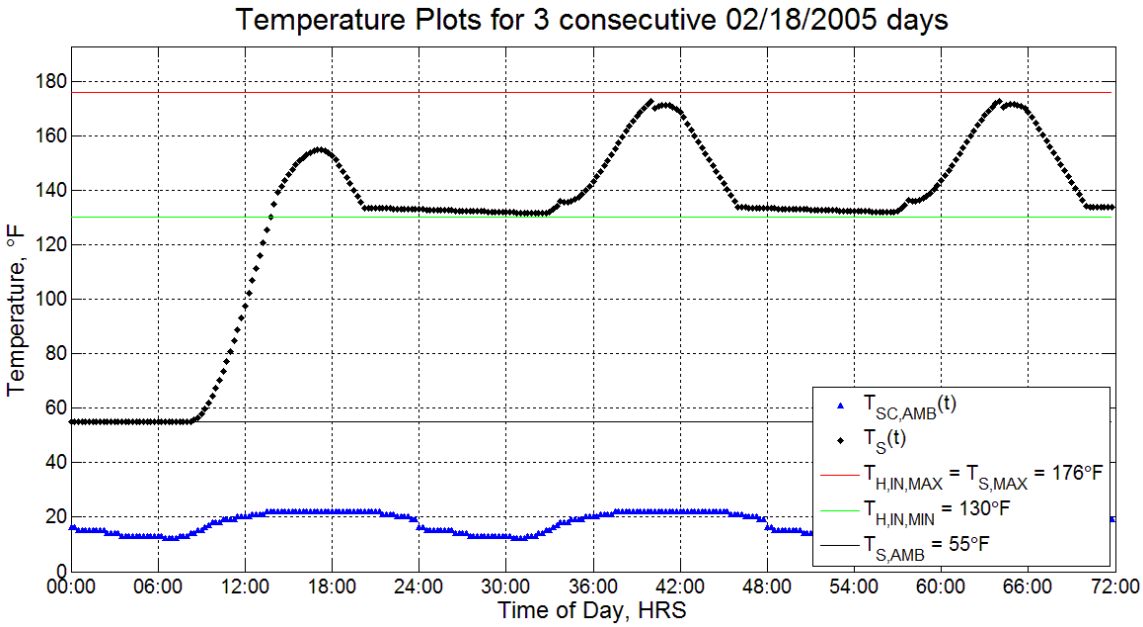
Temperature Plots for 3 consecutive 02/18/2005 days
Temperature, °F
180
160
140
120
100
80
60
40
20
0
00:00 06:00 12:00 18:00 24:00 30:00 36:00 42:00 48:00 54:00 60:00 66:00 72:00
Time of Day, HRS
T_SC,AMB(t)
T_S(t)
T_H,IN,MAX = T_S,MAX = 176°F
T_H,IN,MIN = 130°F
T_S,AMB = 55°F

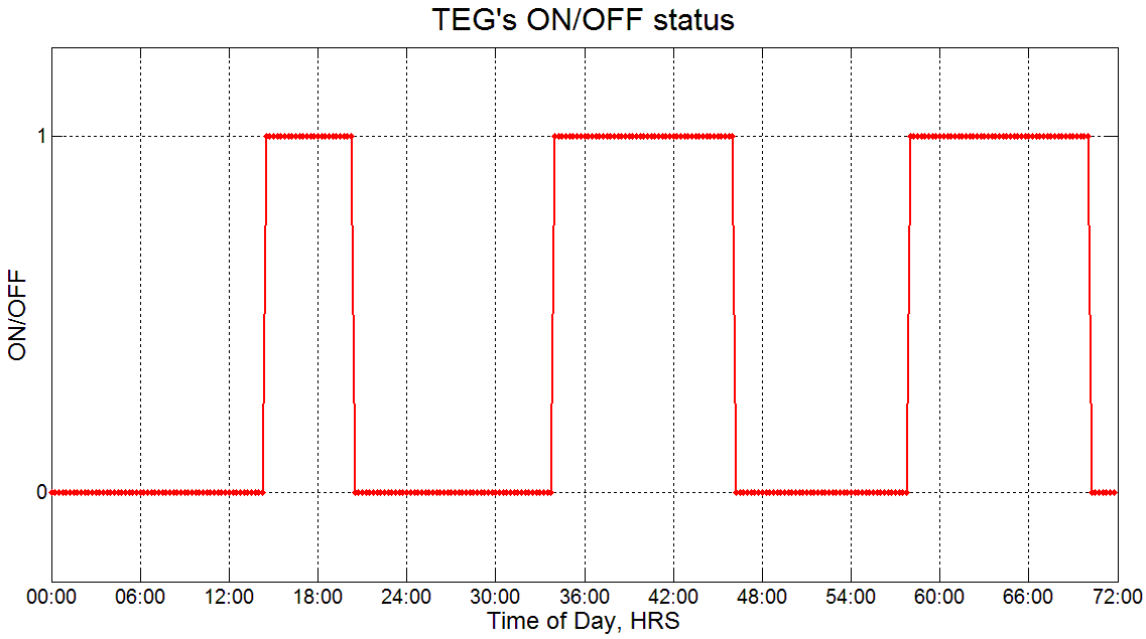
TEG's ON/OFF status
ON/OFF
1
0
00:00
06:00
12:00
18:00
24:00
30:00
36:00
42:00
48:00
54:00
60:00
66:00
72:00
Time of Day, HRS

B.1.3 March (03/20/2005)

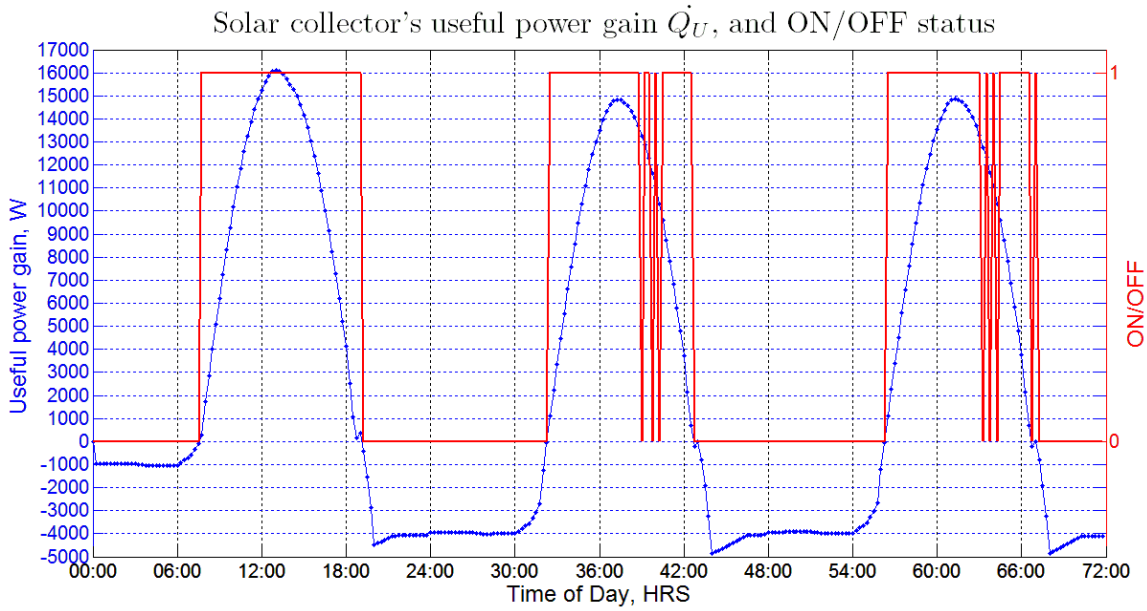

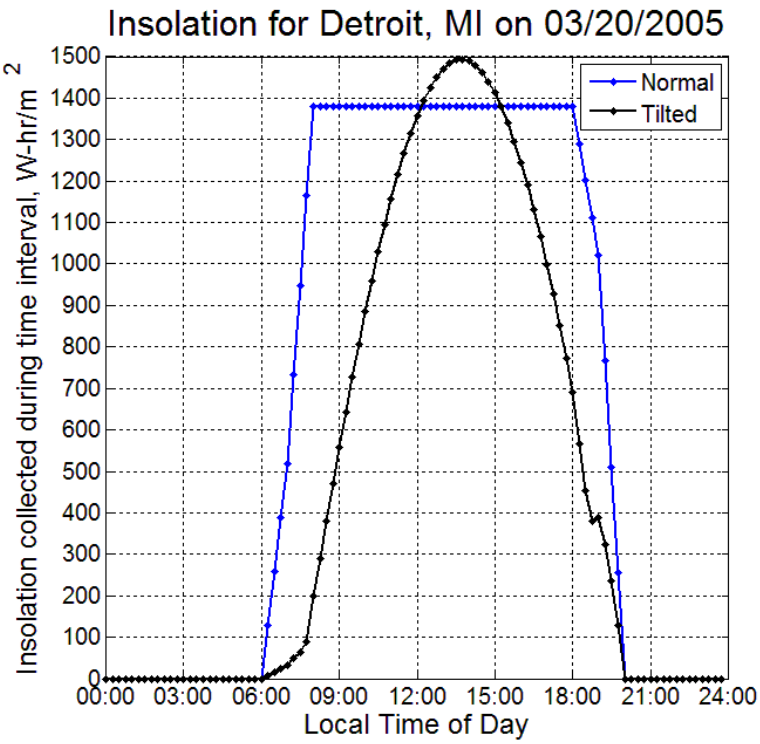

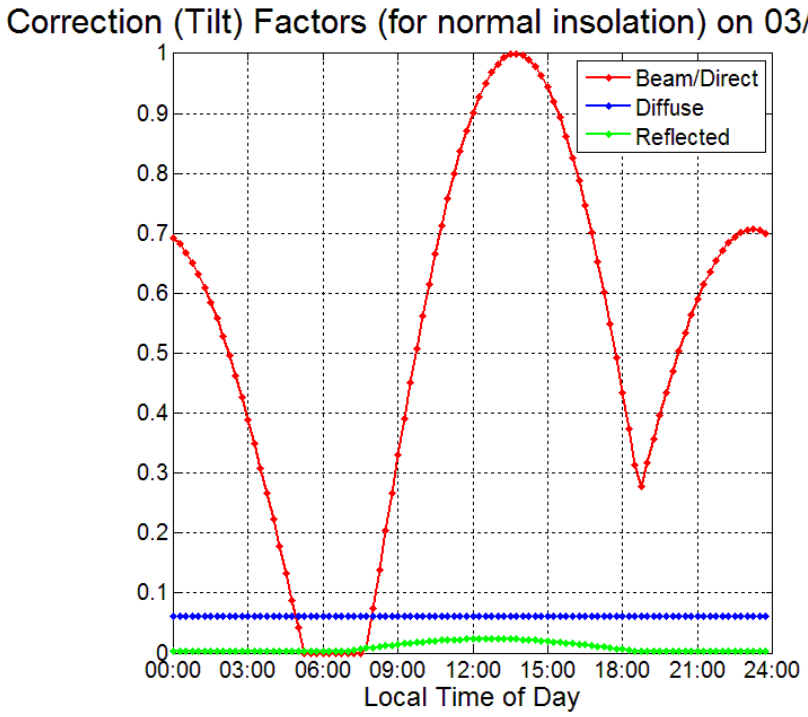
Correction (Tilt) Factors (for normal insolation) on 03/20/2005
Beam/Direct
Diffuse
Reflected
1
0.9
0.8
0.7
0.6
0.5
0.4
0.3
0.2
0.1
0
00:00 03:00 06:00 09:00 12:00 15:00 18:00 21:00 24:00
Local Time of Day

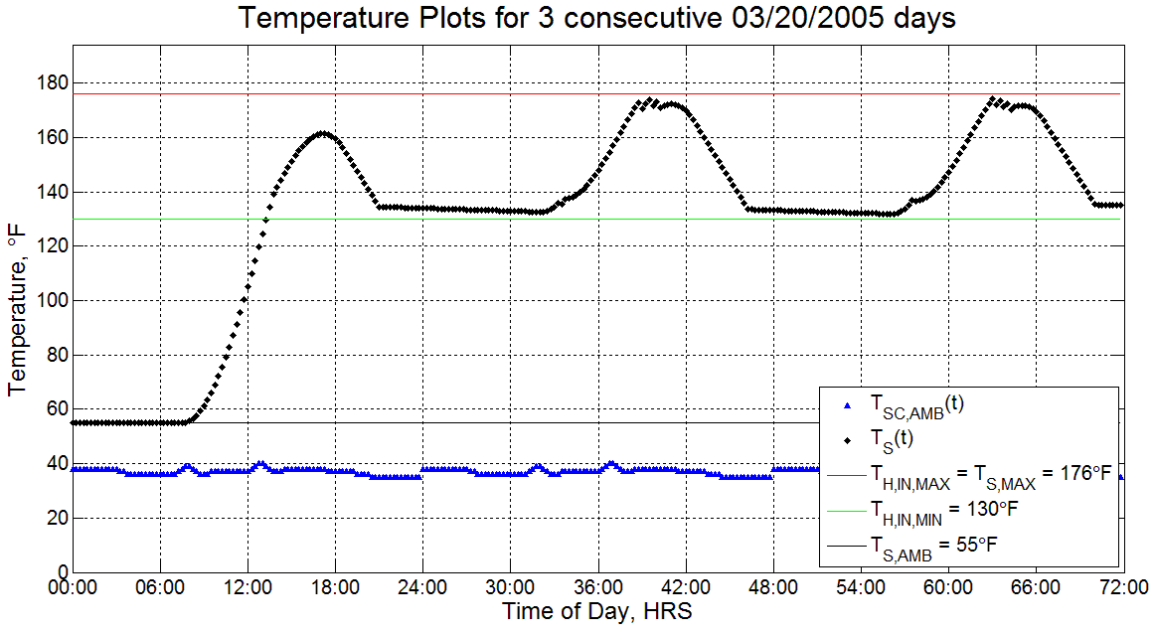
Temperature Plots for 3 consecutive 03/20/2005 days
Temperature, °F
180
160
140
120
100
80
60
40
20
0
00:00 06:00 12:00 18:00 24:00 30:00 36:00 42:00 48:00 54:00 60:00 66:00 72:00
Time of Day, HRS
T_SC,AMB(t)
T_S(t)
T_H,IN,MAX = T_S,MAX = 176°F
T_H,IN,MIN = 130°F
T_S,AMB = 55°F

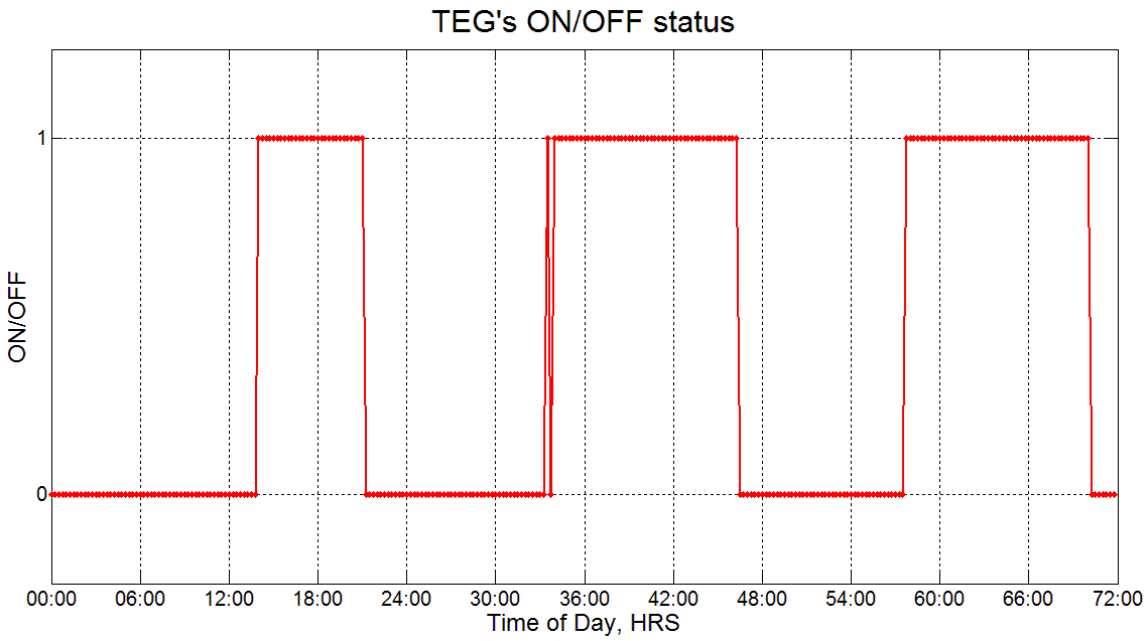
TEG's ON/OFF status
ON/OFF
1
0
00:00
06:00
12:00
18:00
24:00
30:00
36:00
42:00
48:00
54:00
60:00
66:00
72:00
Time of Day, HRS

B.1.4 April (04/20/2005)

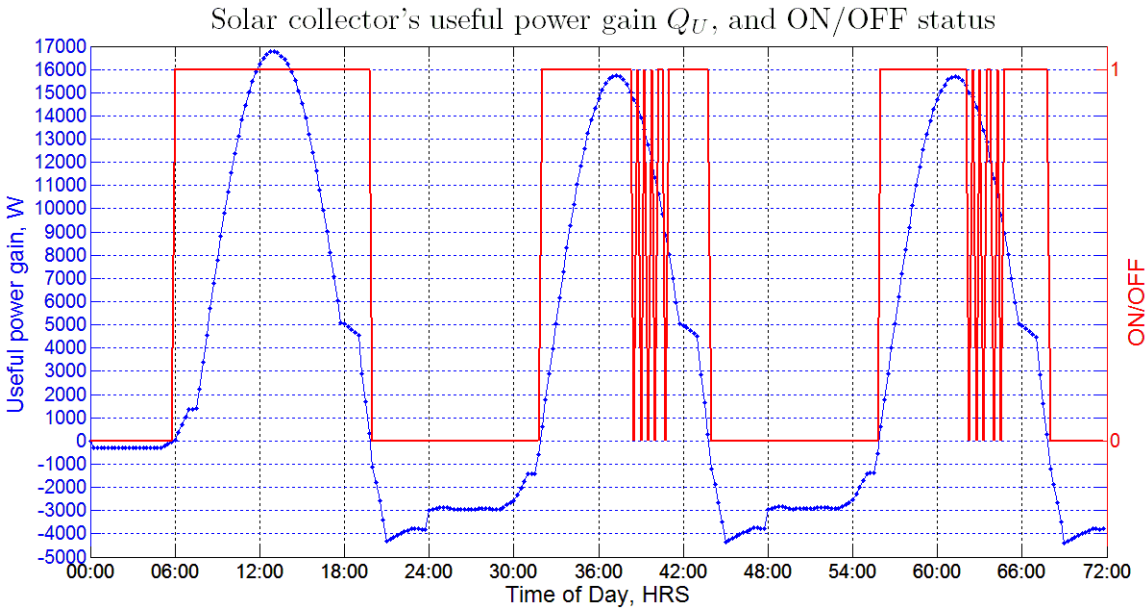

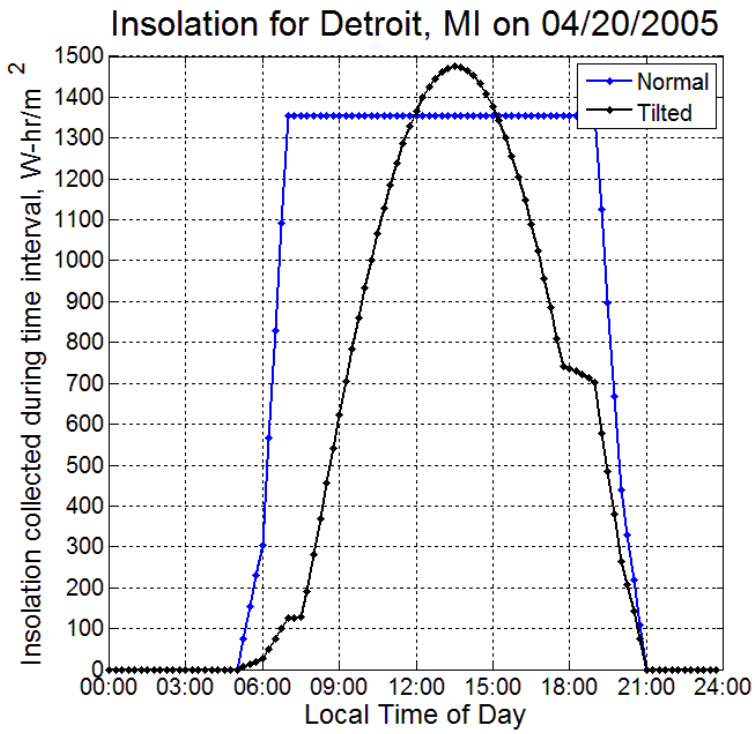

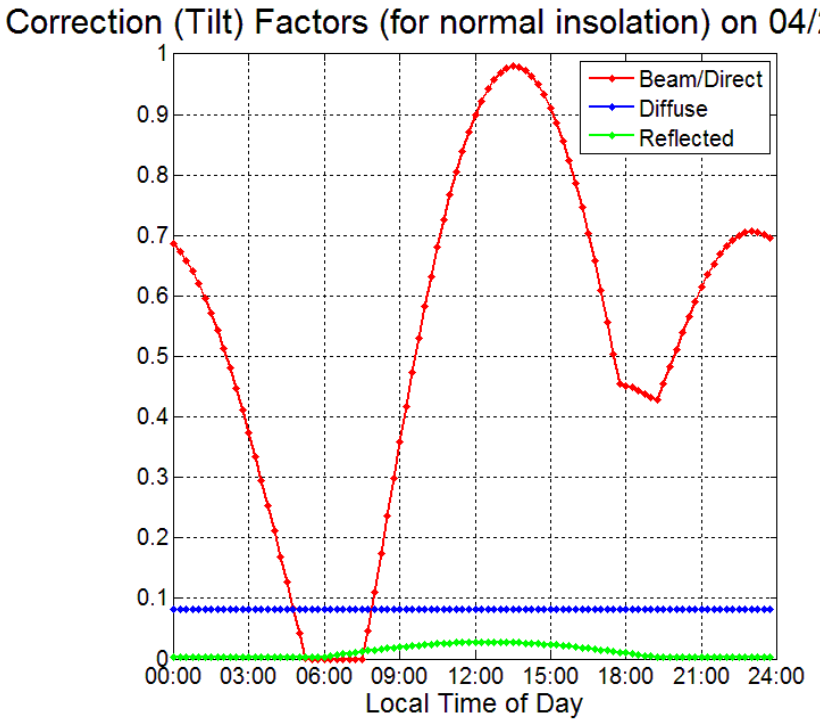
Correction (Tilt) Factors (for normal insolation) on 04/20/2005
Beam/Direct
Diffuse
Reflected
1
0.9
0.8
0.7
0.6
0.5
0.4
0.3
0.2
0.1
0
00:00
03:00
06:00
09:00
12:00
15:00
18:00
21:00
24:00
Local Time of Day

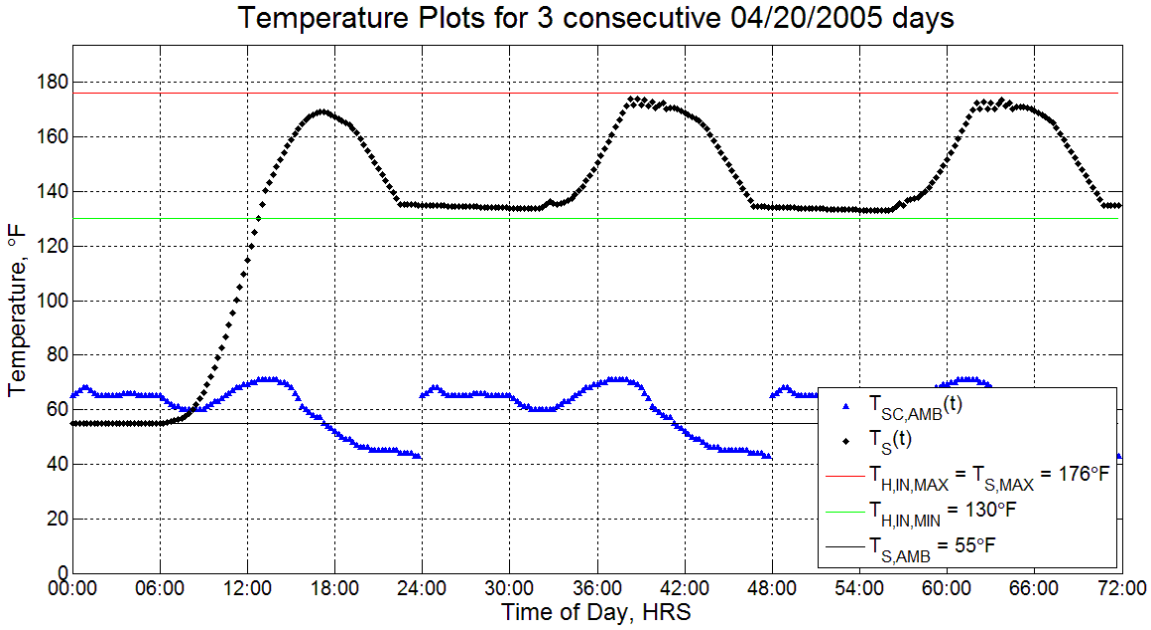
Temperature Plots for 3 consecutive 04/20/2005 days
Temperature, °F
180
160
140
120
100
80
60
40
20
0
00:00
06:00
12:00
18:00
24:00
30:00
36:00
42:00
48:00
54:00
60:00
66:00
72:00
Time of Day, HRS
T_SC,AMB(t)
T_S(t)
T_H,IN,MAX = T_S,MAX = 176°F
T_H,IN,MIN = 130°F
T_S,AMB = 55°F

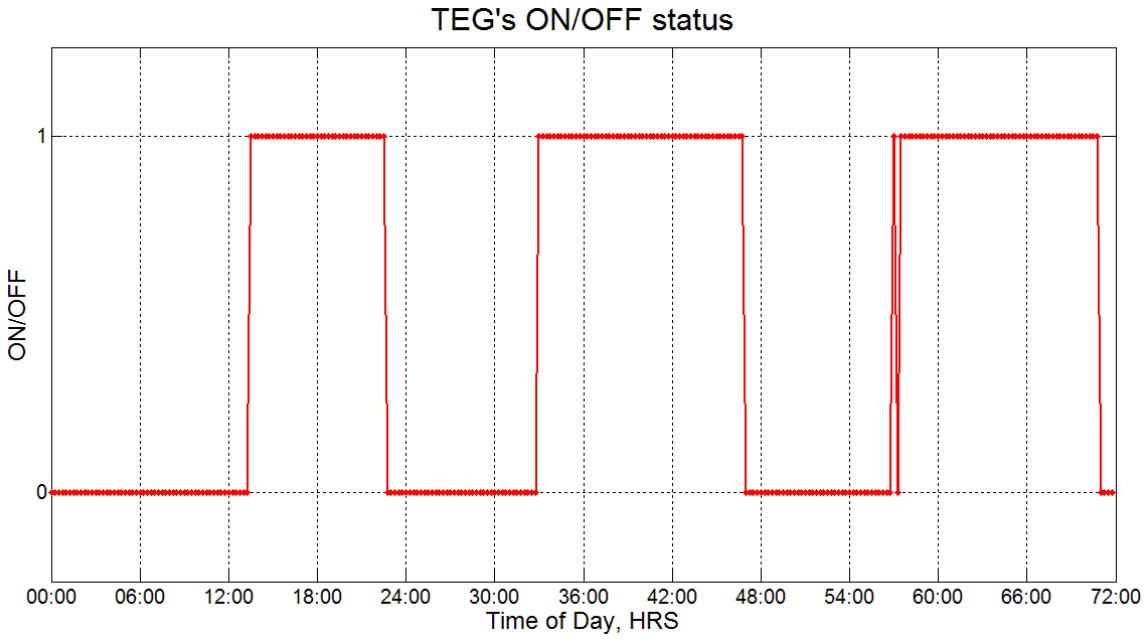
TEG's ON/OFF status
ON/OFF
1
0
00:00
06:00
12:00
18:00
24:00
30:00
36:00
42:00
48:00
54:00
60:00
66:00
72:00
Time of Day, HRS

B.1.5 May (05/21/2005)

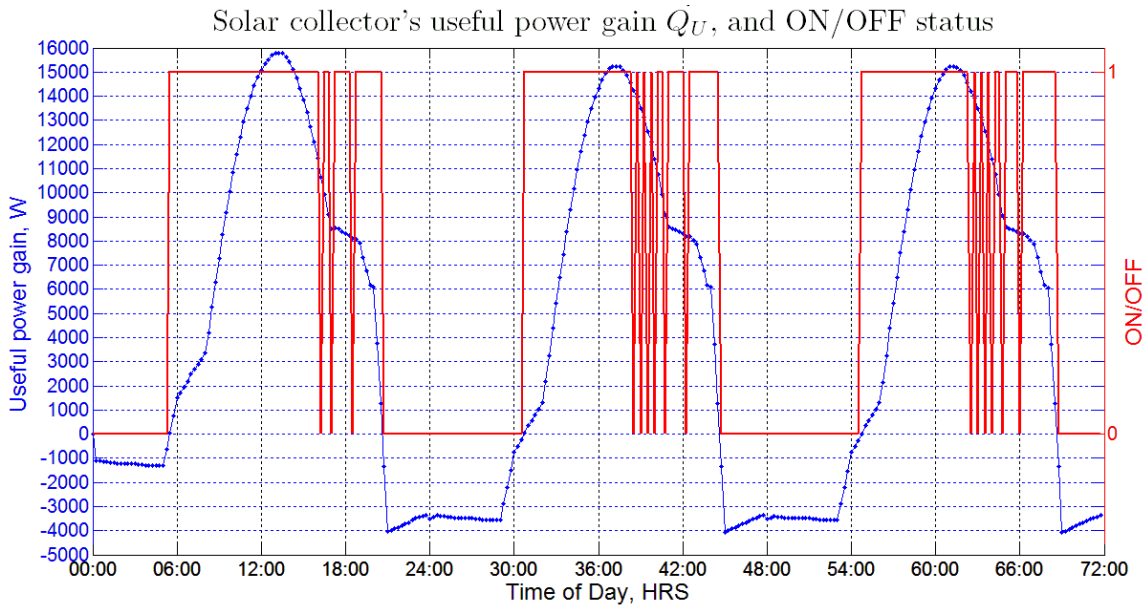

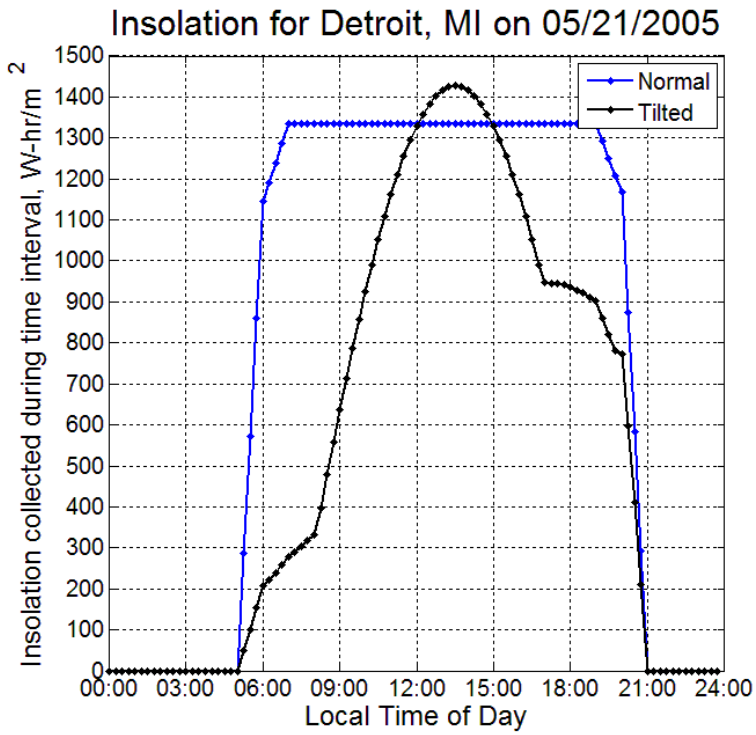

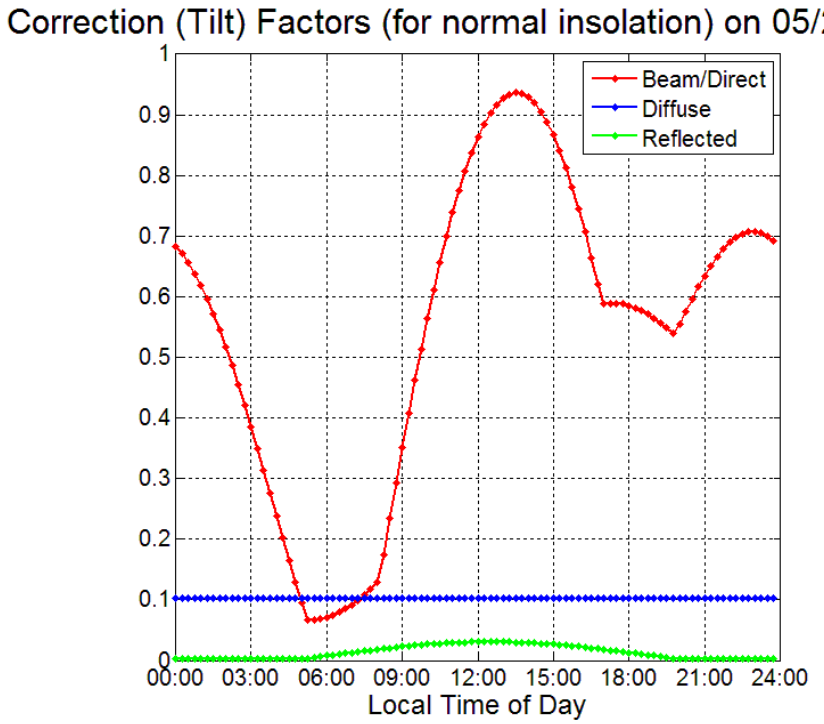
Correction (Tilt) Factors (for normal insolation) on 05/21/2005
Beam/Direct
Diffuse
Reflected
1
0.9
0.8
0.7
0.6
0.5
0.4
0.3
0.2
0.1
0
00:00
03:00
06:00
09:00
12:00
15:00
18:00
21:00
24:00
Local Time of Day

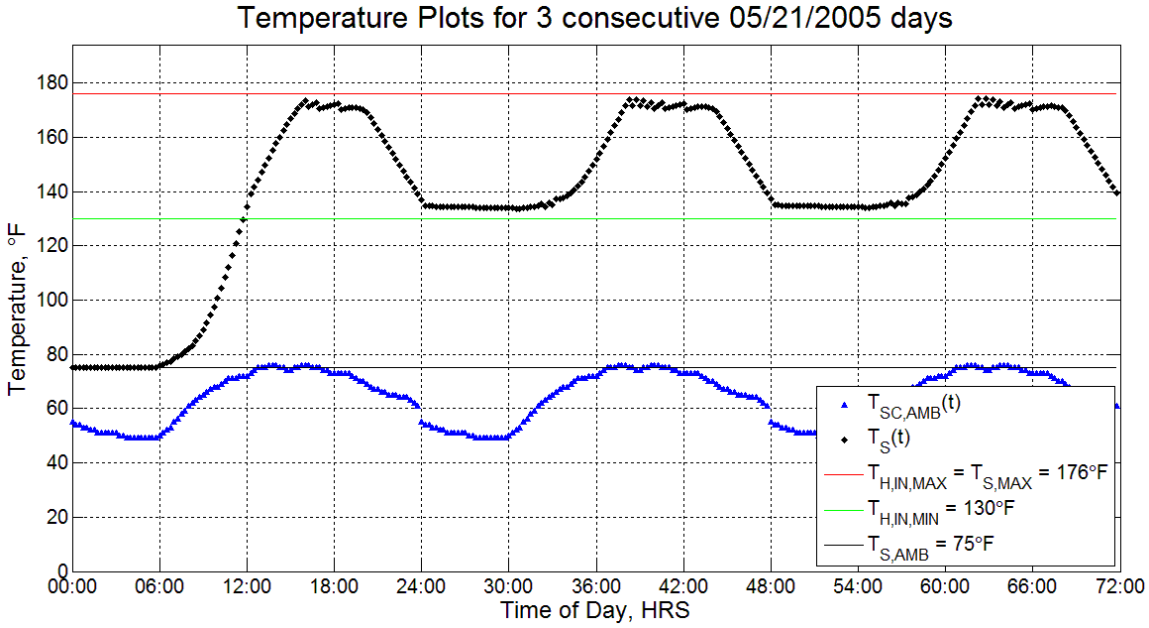
Temperature Plots for 3 consecutive 05/21/2005 days
Temperature, °F
180
160
140
120
100
80
60
40
20
0
00:00
06:00
12:00
18:00
24:00
30:00
36:00
42:00
48:00
54:00
60:00
66:00
72:00
Time of Day, HRS
T_SC,AMB(t)
T_S(t)
T_H,IN,MAX = T_S,MAX = 176°F
T_H,IN,MIN = 130°F
T_S,AMB = 75°F

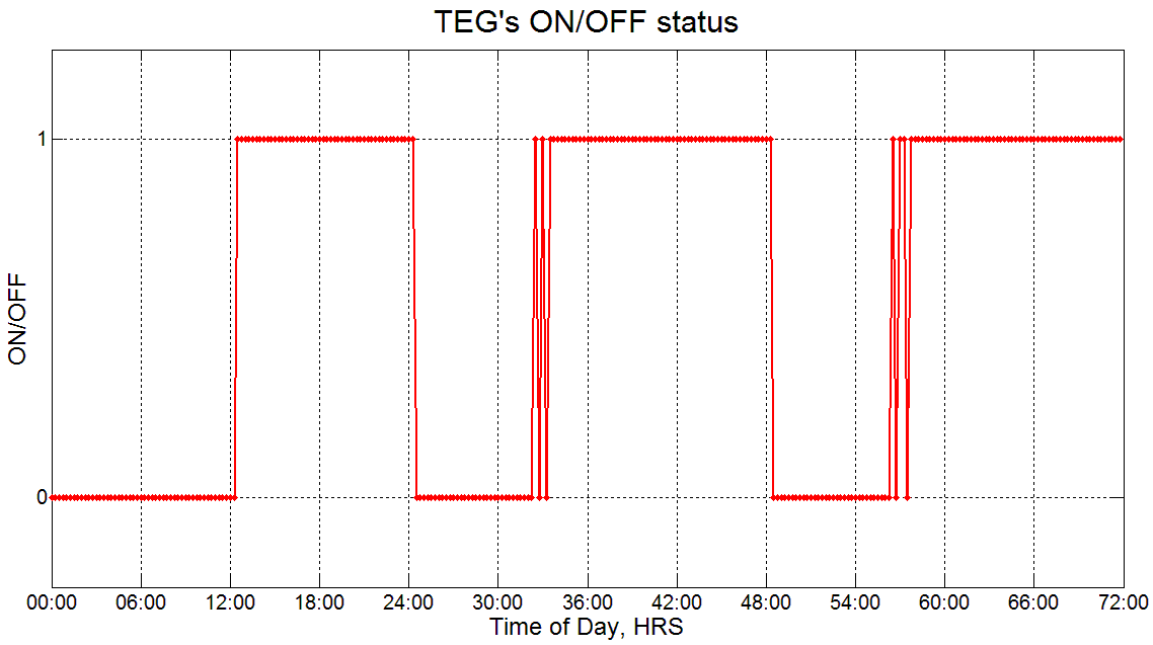
TEG's ON/OFF status
ON/OFF
1
0
00:00
06:00
12:00
18:00
24:00
30:00
36:00
42:00
48:00
54:00
60:00
66:00
72:00
Time of Day, HRS

B.1.6 June (06/21/2005)

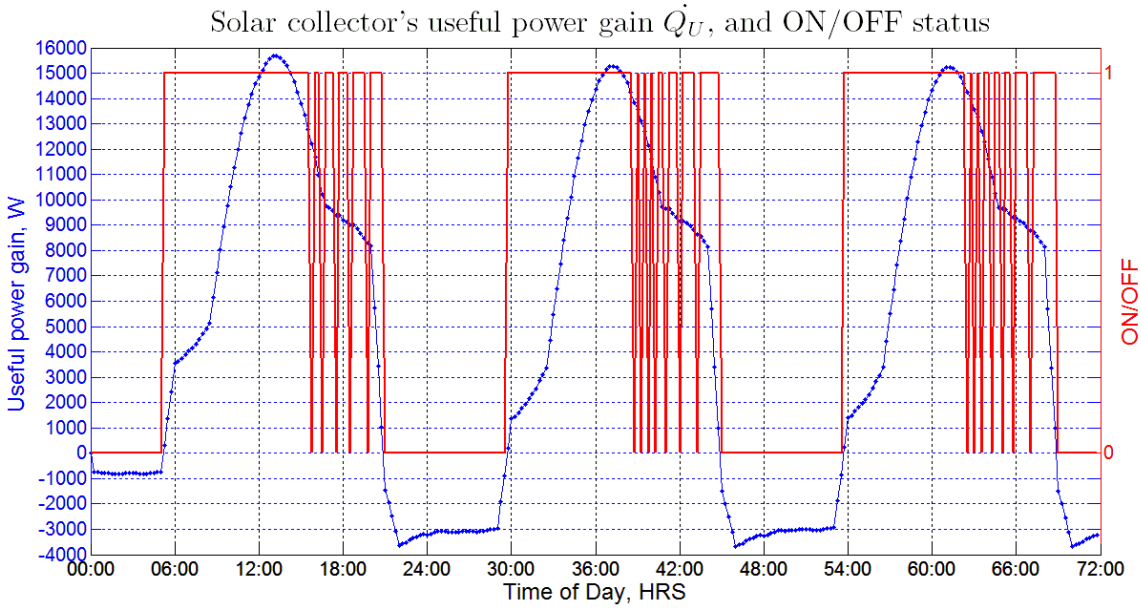

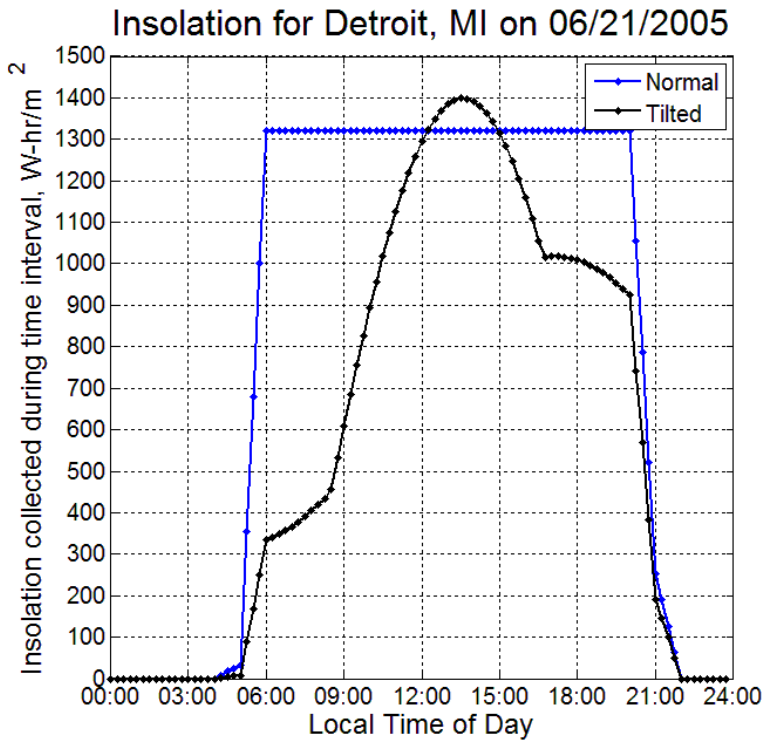

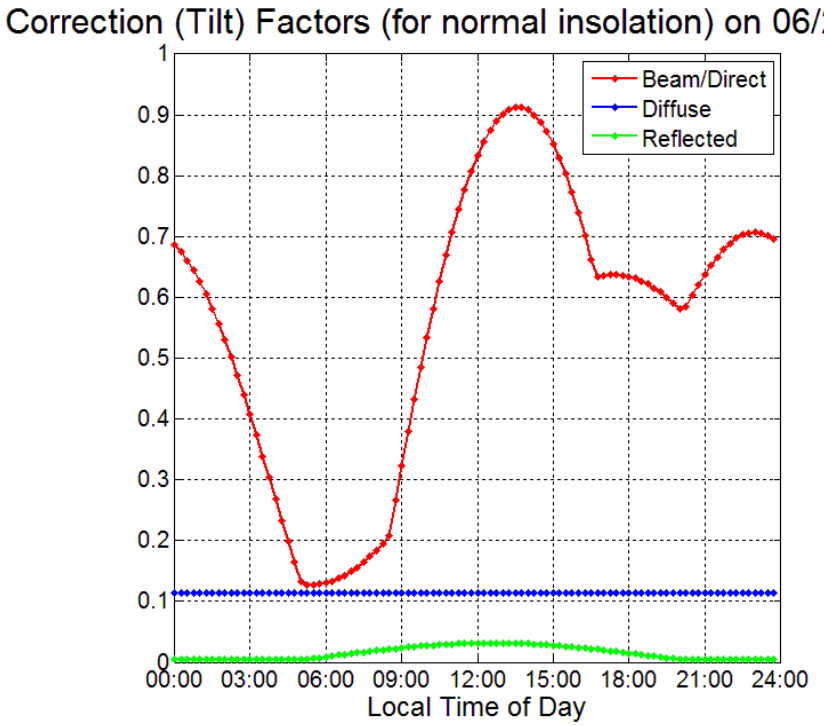
Correction (Tilt) Factors (for normal insolation) on 06/21/2005
Beam/Direct
Diffuse
Reflected
1
0.9
0.8
0.7
0.6
0.5
0.4
0.3
0.2
0.1
0
00:00 03:00 06:00 09:00 12:00 15:00 18:00 21:00 24:00
Local Time of Day

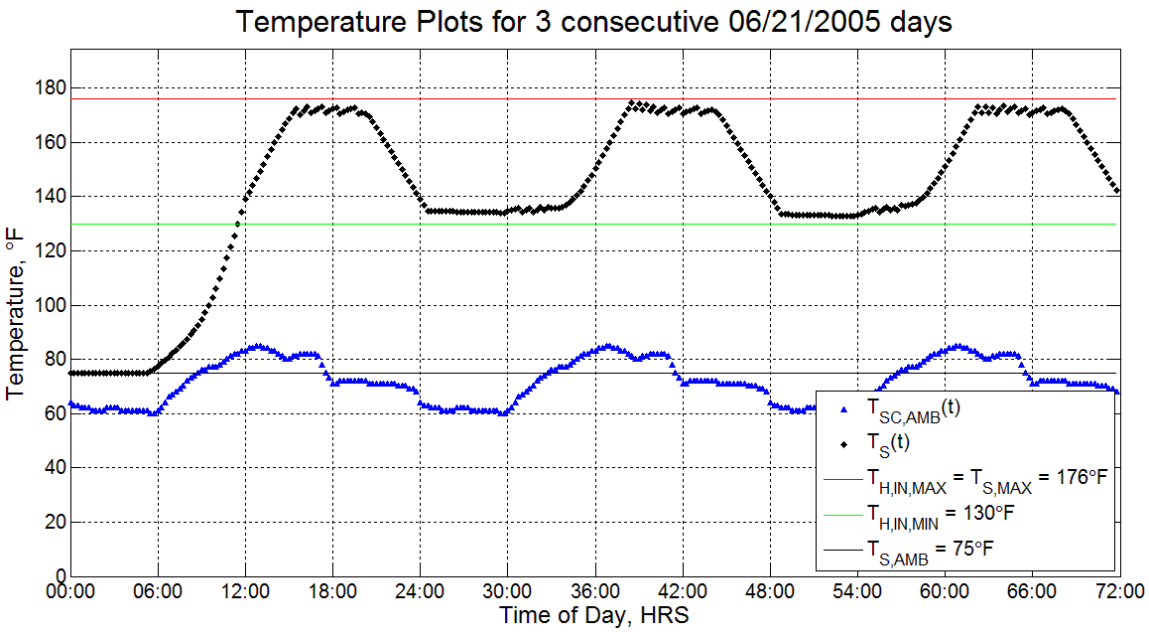
Temperature Plots for 3 consecutive 06/21/2005 days
Temperature, °F
180
160
140
120
100
80
60
40
20
0
00:00 06:00 12:00 18:00 24:00 30:00 36:00 42:00 48:00 54:00 60:00 66:00 72:00
Time of Day, HRS
T_SC,AMB(t)
T_S(t)
T_H,IN,MAX = T_S,MAX = 176°F
T_H,IN,MIN = 130°F
T_S,AMB = 75°F

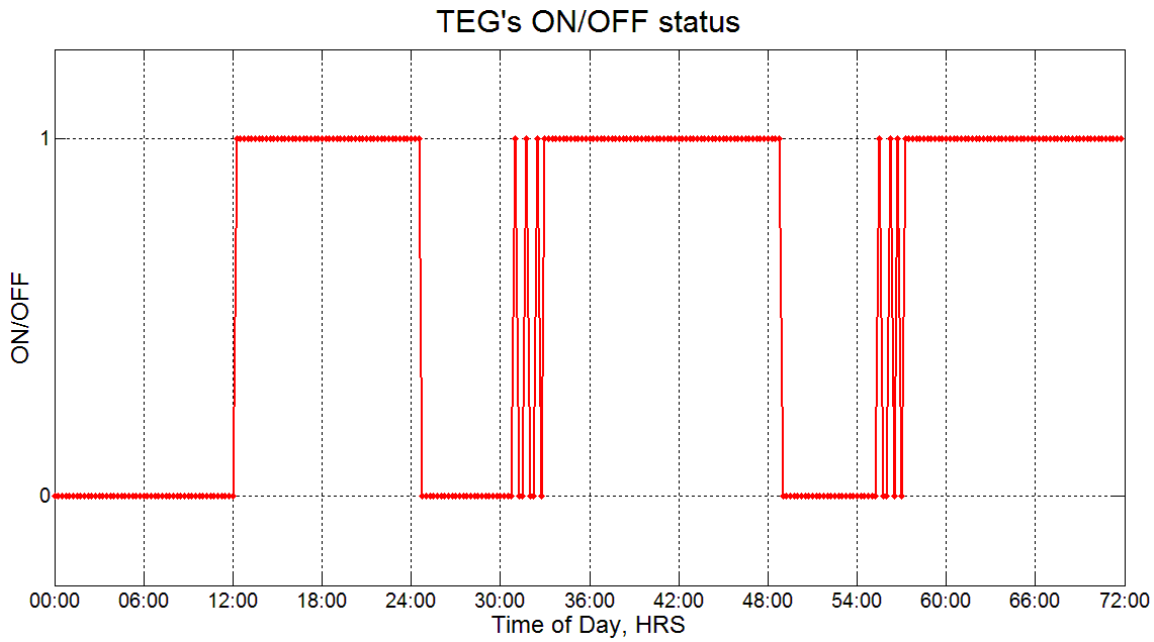
TEG's ON/OFF status
ON/OFF
1
0
00:00
06:00
12:00
18:00
24:00
30:00
36:00
42:00
48:00
54:00
60:00
66:00
72:00
Time of Day, HRS

B.1.7 July (07/22/2005)

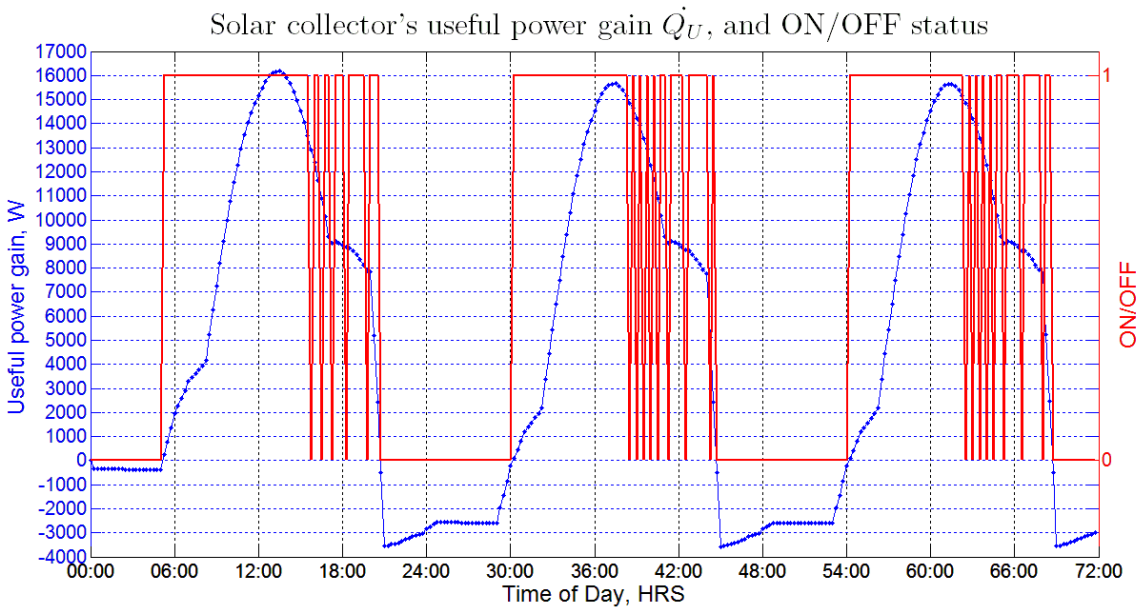

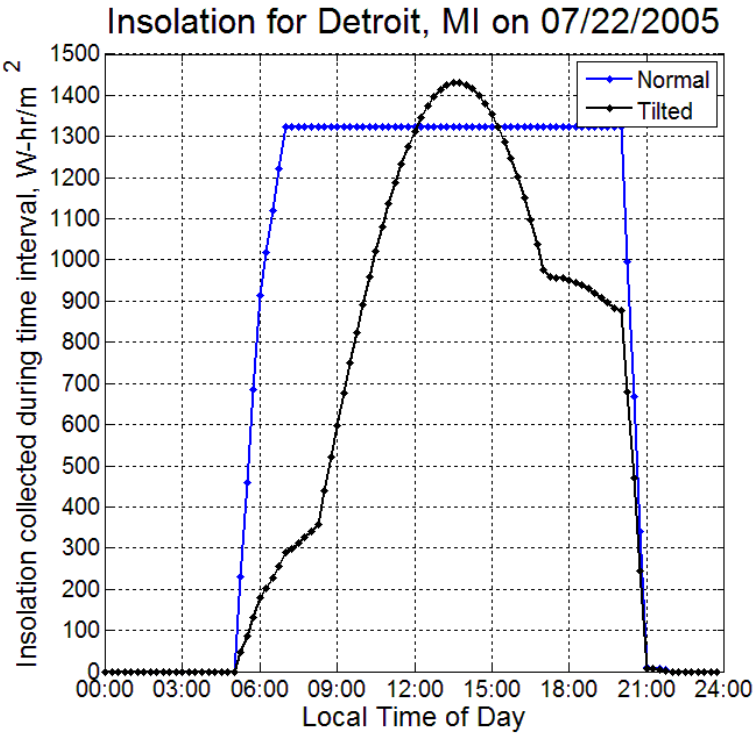

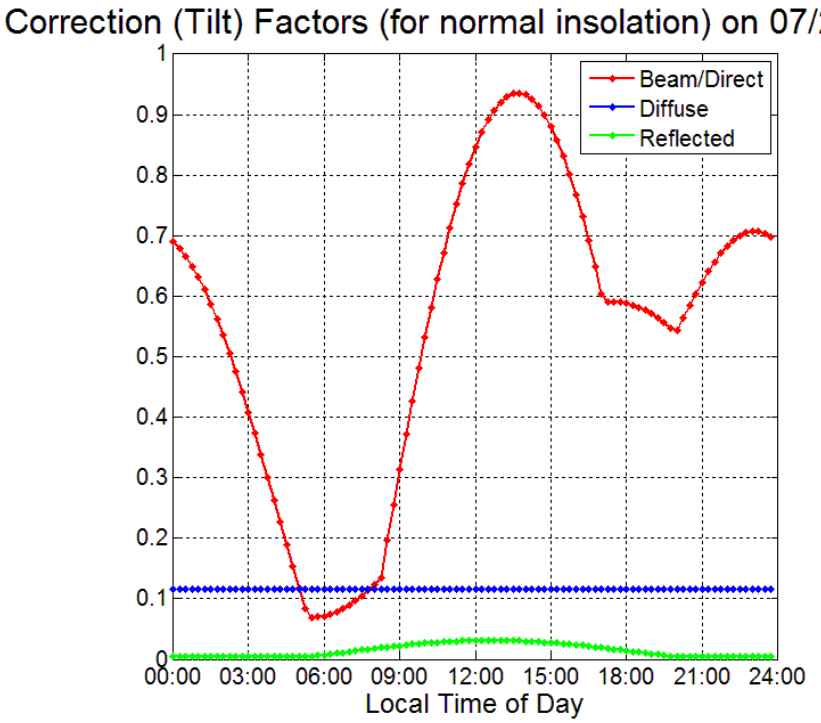
Correction (Tilt) Factors (for normal insolation) on 07/22/2005
Beam/Direct
Diffuse
Reflected
1
0.9
0.8
0.7
0.6
0.5
0.4
0.3
0.2
0.1
0
00:00
03:00
06:00
09:00
12:00
15:00
18:00
21:00
24:00
Local Time of Day

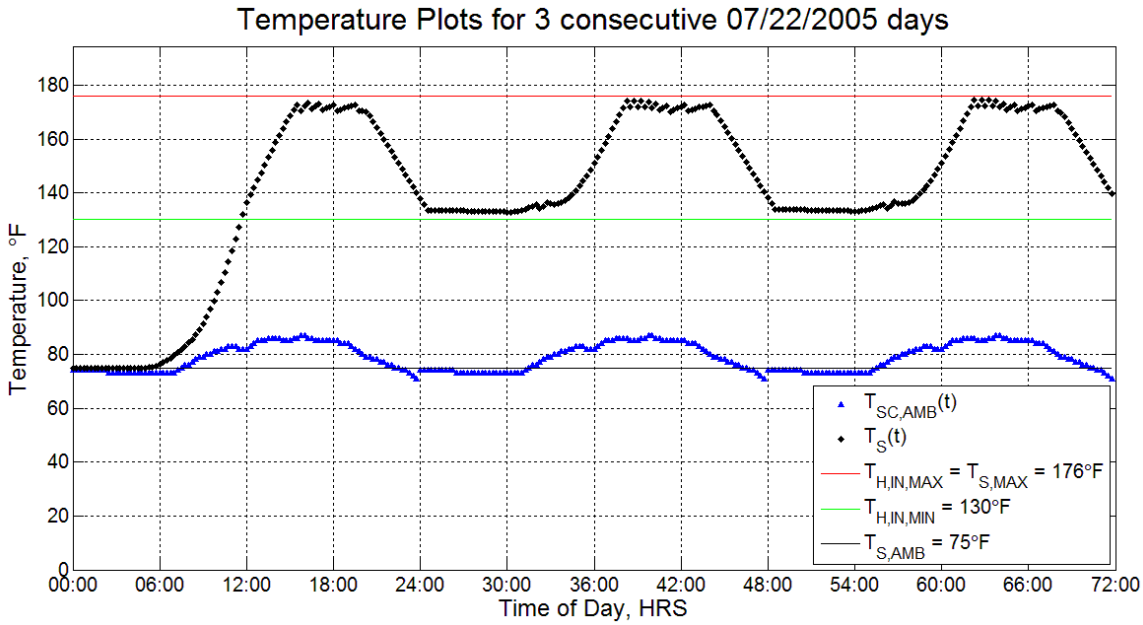
Temperature Plots for 3 consecutive 07/22/2005 days
Temperature, °F
180
160
140
120
100
80
60
40
20
0
00:00
06:00
12:00
18:00
24:00
30:00
36:00
42:00
48:00
54:00
60:00
66:00
72:00
Time of Day, HRS
T_SC,AMB(t)
T_S(t)
T_H,IN,MAX = T_S,MAX = 176°F
T_H,IN,MIN = 130°F
T_S,AMB = 75°F

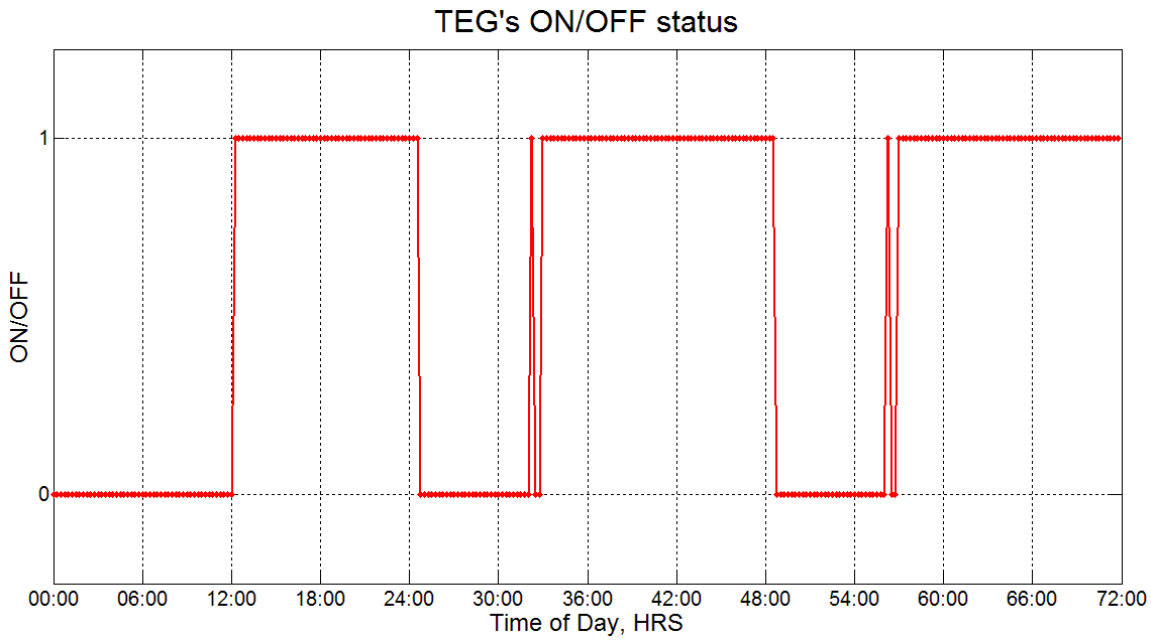
TEG's ON/OFF status
ON/OFF
1
0
00:00
06:00
12:00
18:00
24:00
30:00
36:00
42:00
48:00
54:00
60:00
66:00
72:00
Time of Day, HRS

B.1.8 August (08/22/2005)

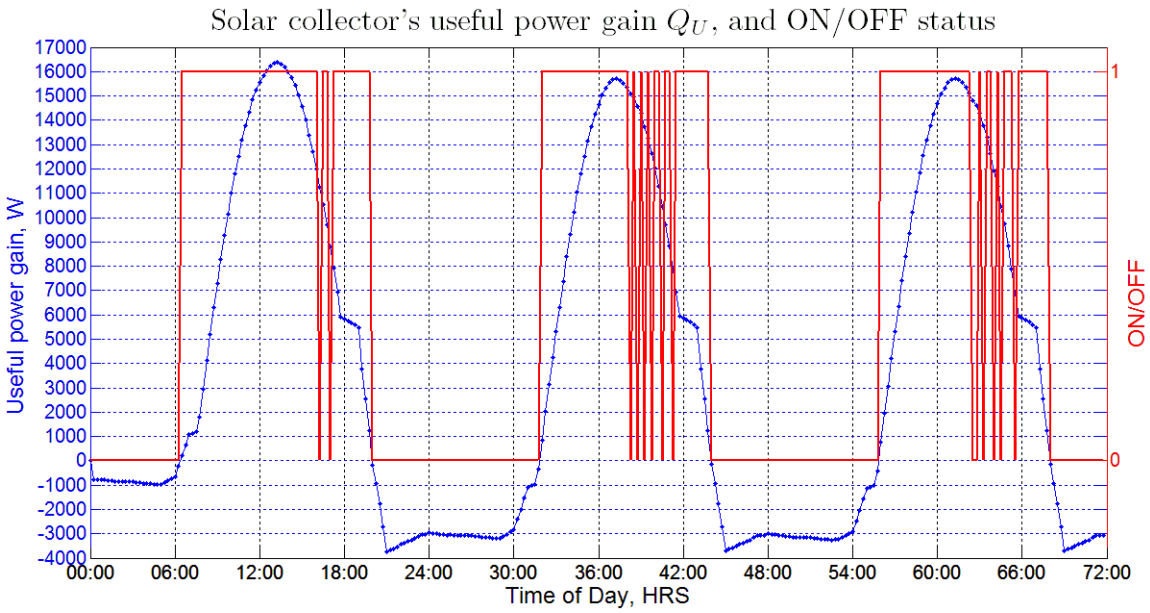

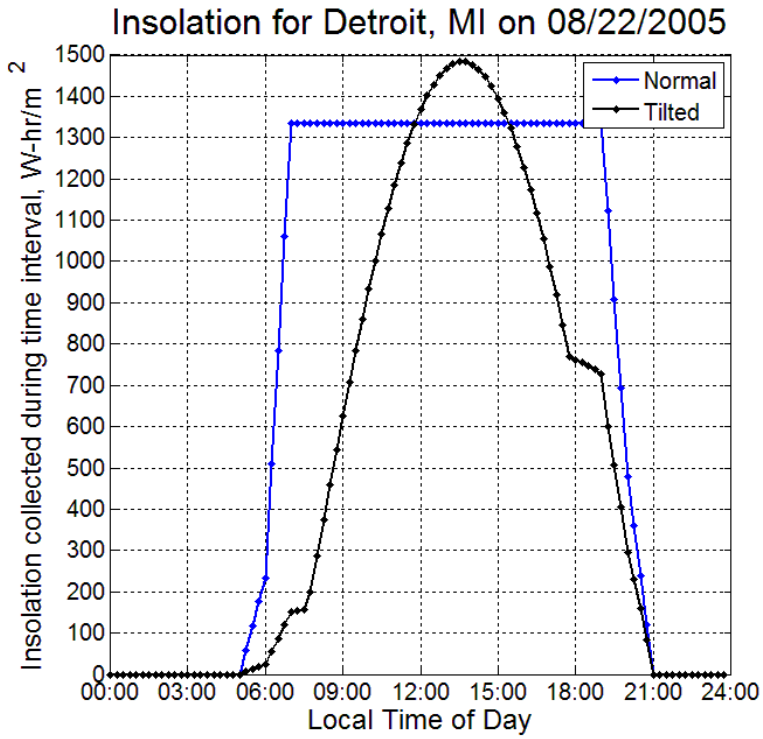

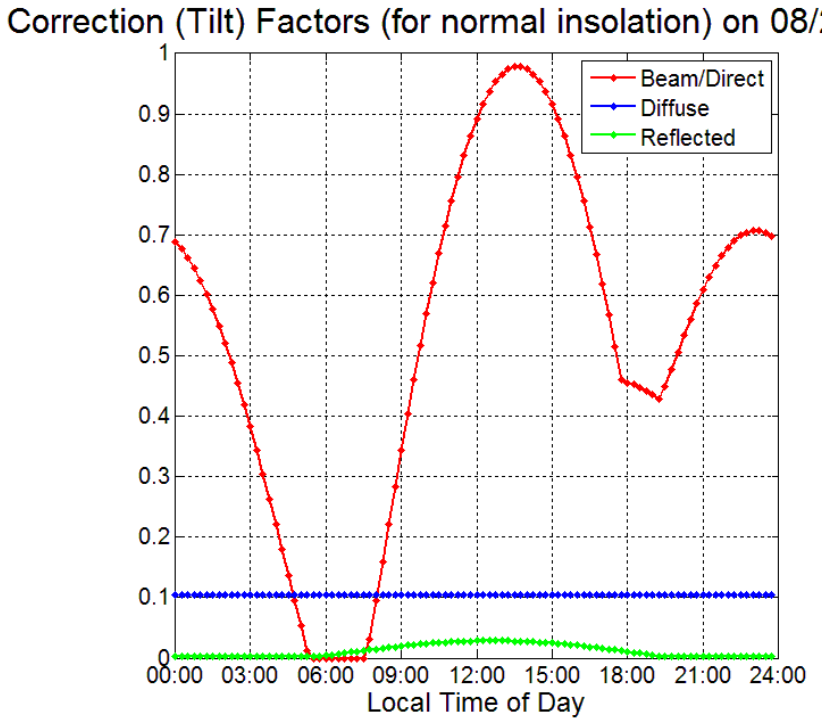
Correction (Tilt) Factors (for normal insolation) on 08/22/2005
Beam/Direct
Diffuse
Reflected
1
0.9
0.8
0.7
0.6
0.5
0.4
0.3
0.2
0.1
0
00:00
03:00
06:00
09:00
12:00
15:00
18:00
21:00
24:00
Local Time of Day

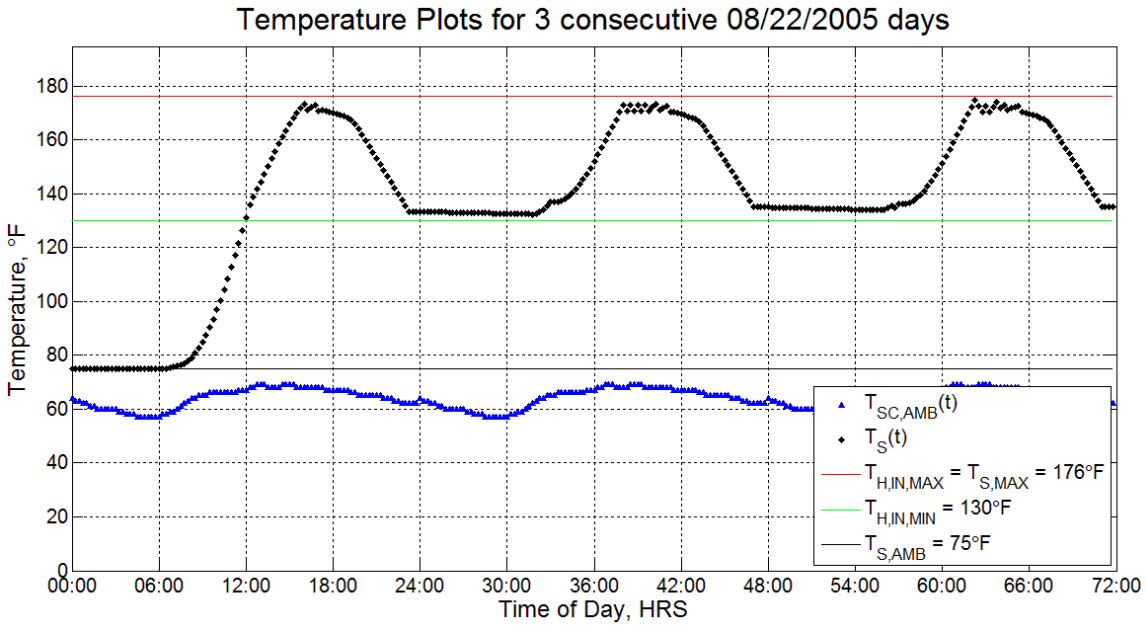
Temperature Plots for 3 consecutive 08/22/2005 days
Temperature, °F
180
160
140
120
100
80
60
40
20
0
00:00
06:00
12:00
18:00
24:00
30:00
36:00
42:00
48:00
54:00
60:00
66:00
72:00
Time of Day, HRS
T_SC,AMB(t)
T_S(t)
T_H,IN,MAX = T_S,MAX = 176°F
T_H,IN,MIN = 130°F
T_S,AMB = 75°F

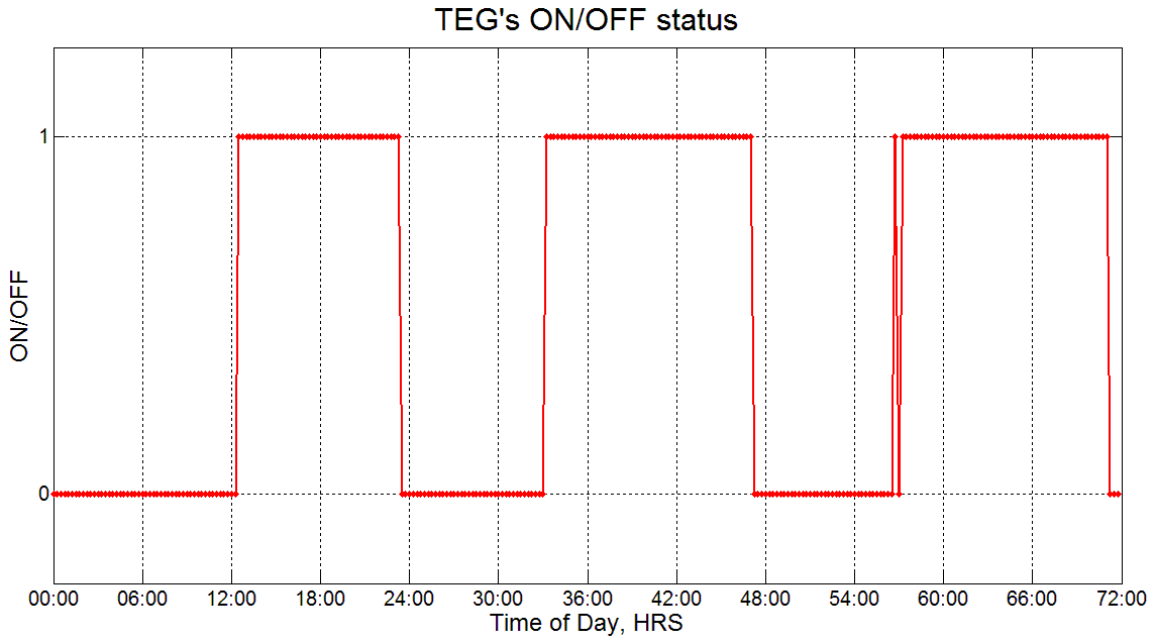
TEG's ON/OFF status
ON/OFF
1
0
00:00
06:00
12:00
18:00
24:00
30:00
36:00
42:00
48:00
54:00
60:00
66:00
72:00
Time of Day, HRS

B.1.9 September (09/22/2005)

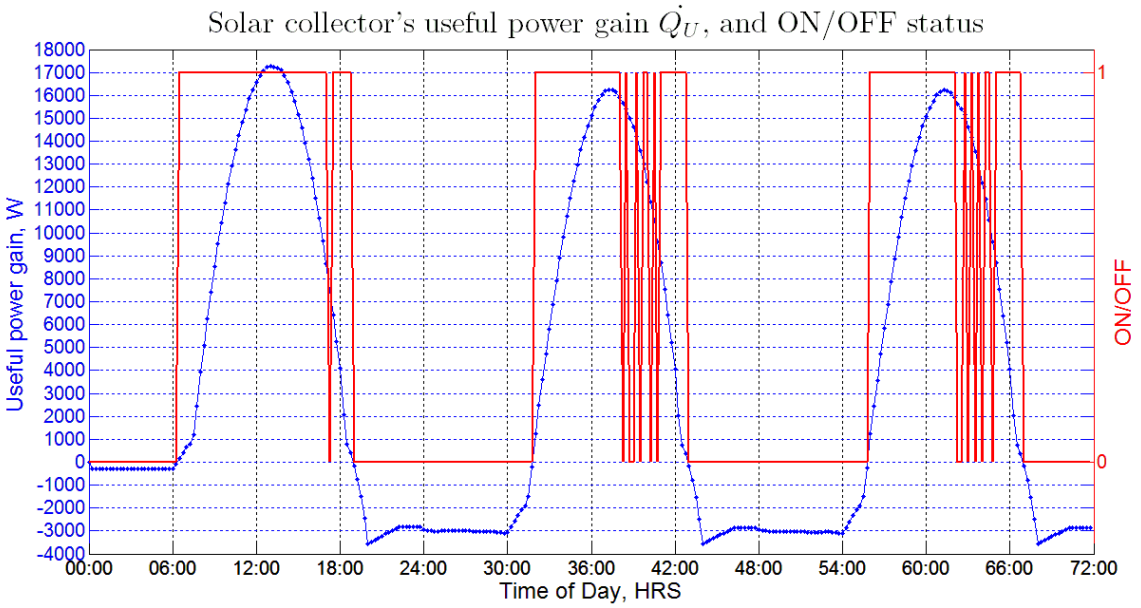

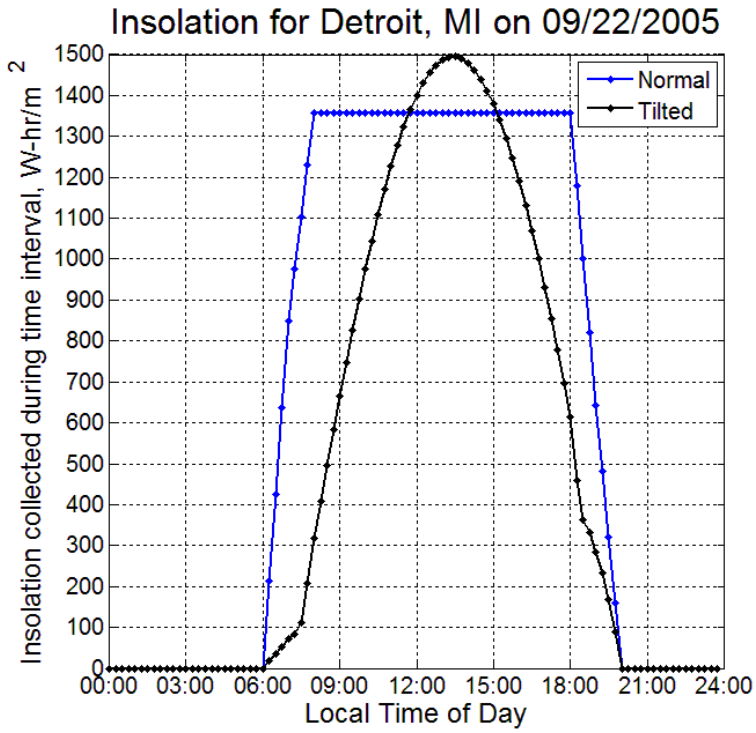

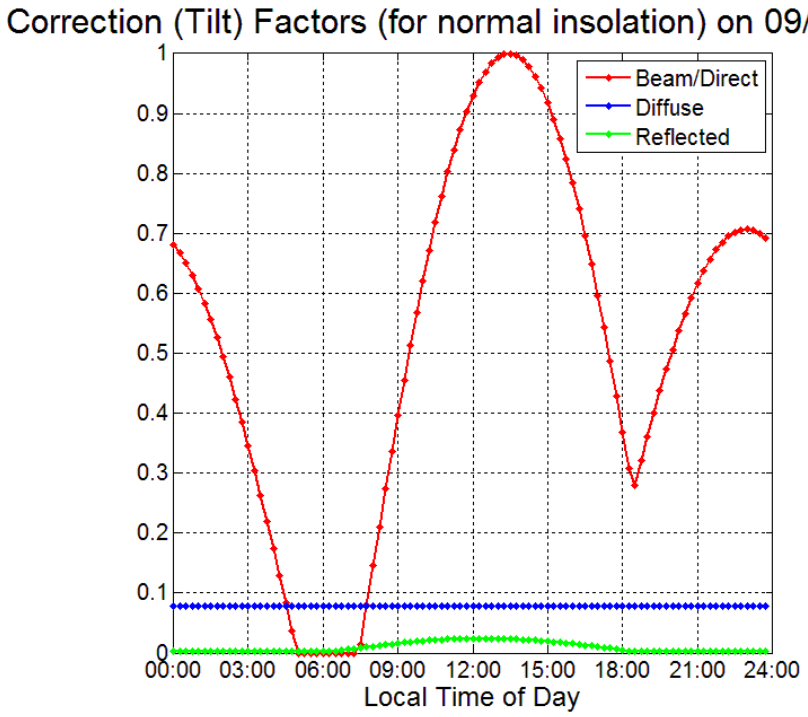
Correction (Tilt) Factors (for normal insolation) on 09/22/2005
Beam/Direct
Diffuse
Reflected
1
0.9
0.8
0.7
0.6
0.5
0.4
0.3
0.2
0.1
0
00:00 03:00 06:00 09:00 12:00 15:00 18:00 21:00 24:00
Local Time of Day

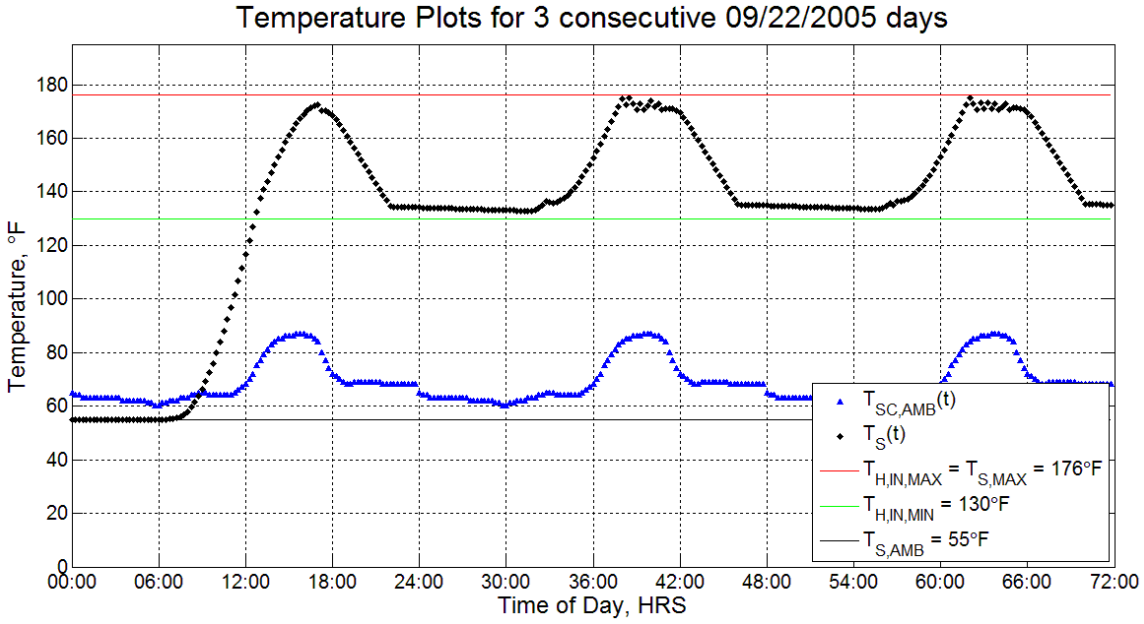
Temperature Plots for 3 consecutive 09/22/2005 days
Temperature, °F
180
160
140
120
100
80
60
40
20
0
00:00 06:00 12:00 18:00 24:00 30:00 36:00 42:00 48:00 54:00 60:00 66:00 72:00
Time of Day, HRS
T_SC,AMB(t)
T_S(t)
T_H,IN,MAX = T_S,MAX = 176°F
T_H,IN,MIN = 130°F
T_S,AMB = 55°F

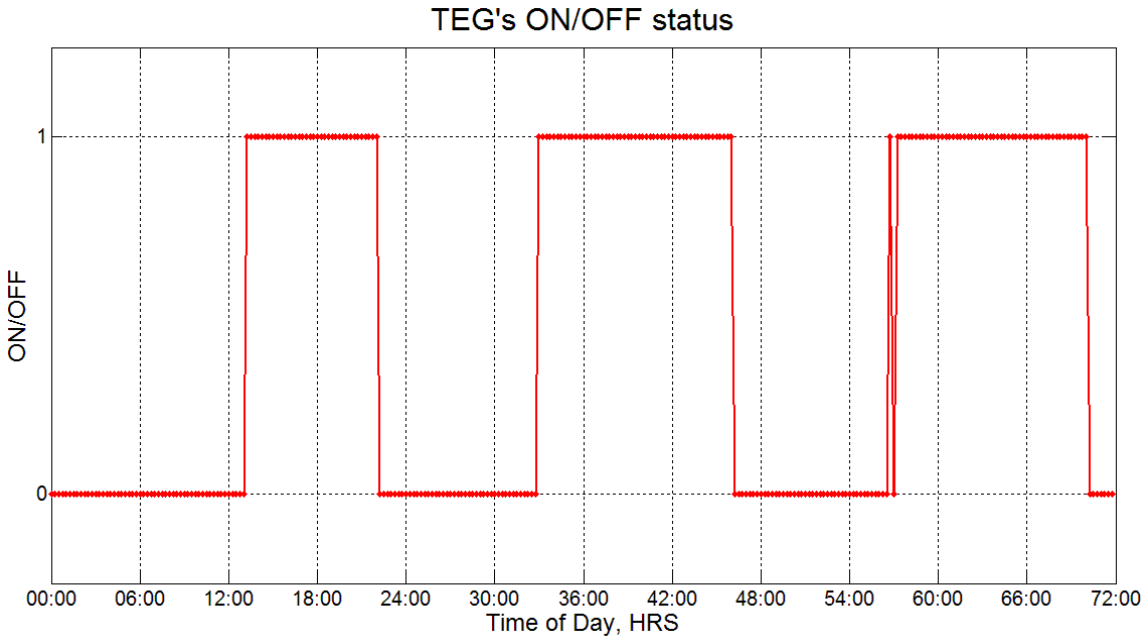
TEG's ON/OFF status
ON/OFF
1
0
00:00
06:00
12:00
18:00
24:00
30:00
36:00
42:00
48:00
54:00
60:00
66:00
72:00
Time of Day, HRS

B.1.10 October (10/22/2005)

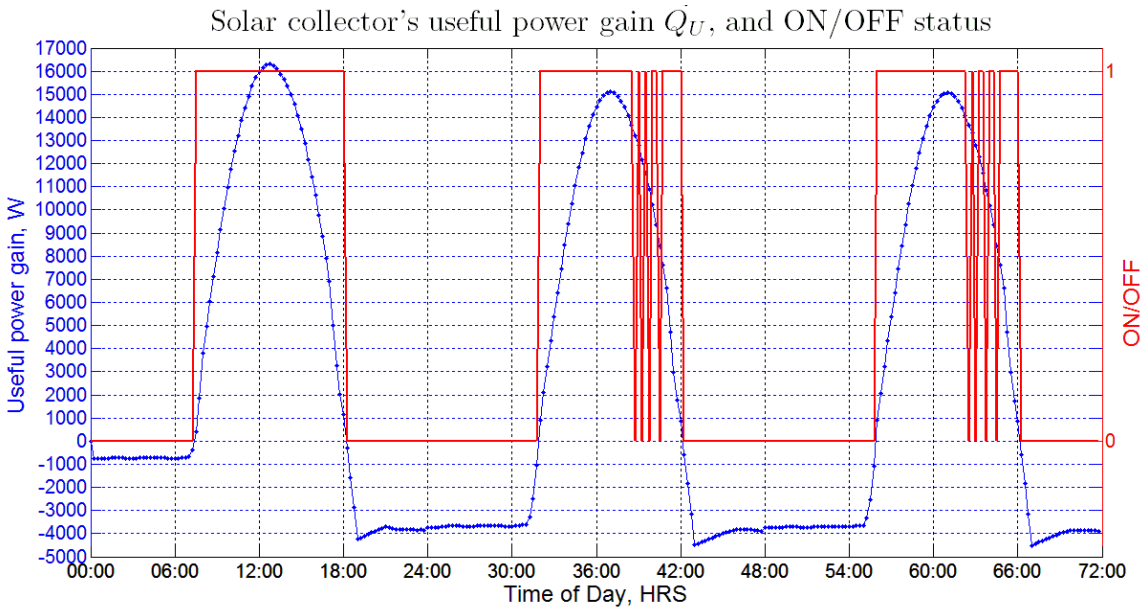

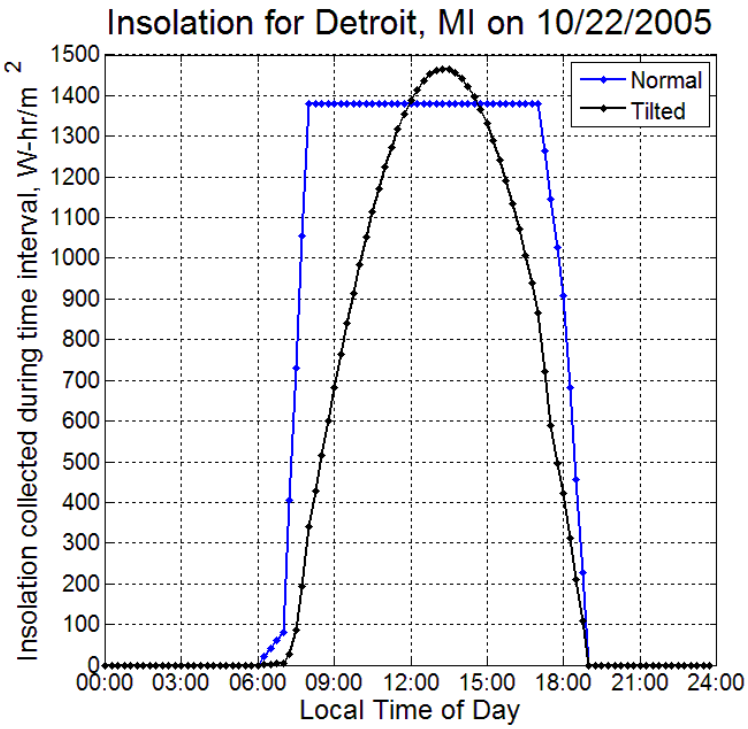

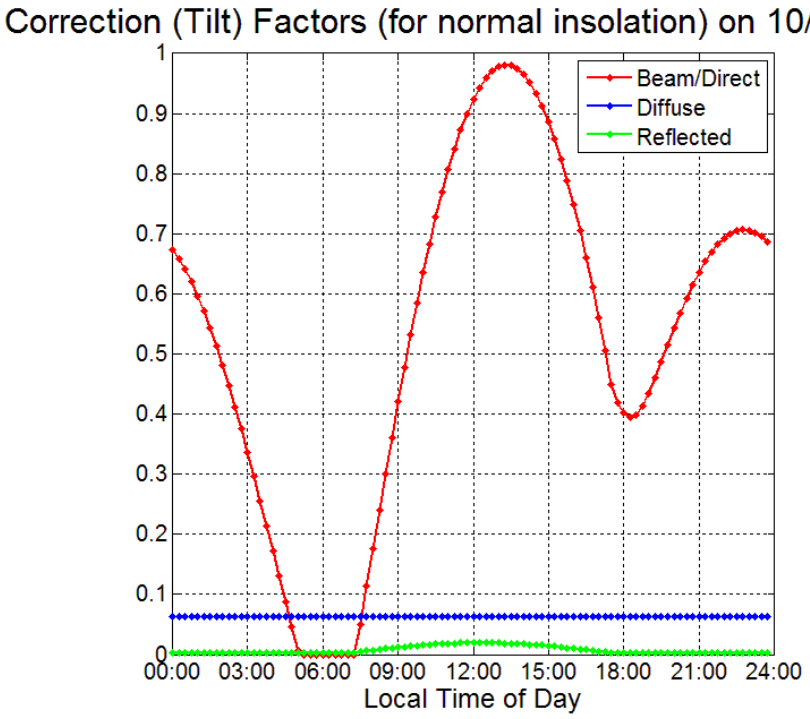
Correction (Tilt) Factors (for normal insolation) on 10/22/2005
Beam/Direct
Diffuse
Reflected
1
0.9
0.8
0.7
0.6
0.5
0.4
0.3
0.2
0.1
0
00:00 03:00 06:00 09:00 12:00 15:00 18:00 21:00 24:00
Local Time of Day

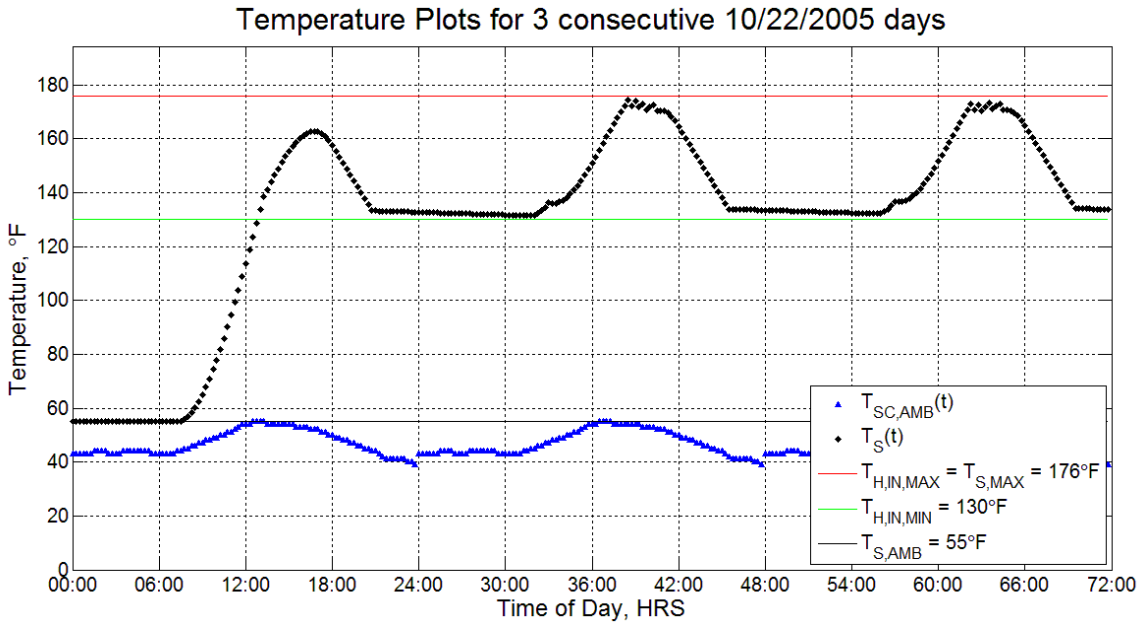
Temperature Plots for 3 consecutive 10/22/2005 days
Temperature, °F
180
160
140
120
100
80
60
40
20
0
00:00 06:00 12:00 18:00 24:00 30:00 36:00 42:00 48:00 54:00 60:00 66:00 72:00
Time of Day, HRS
T_SC,AMB(t)
T_S(t)
T_H,IN,MAX = T_S,MAX = 176°F
T_H,IN,MIN = 130°F
T_S,AMB = 55°F

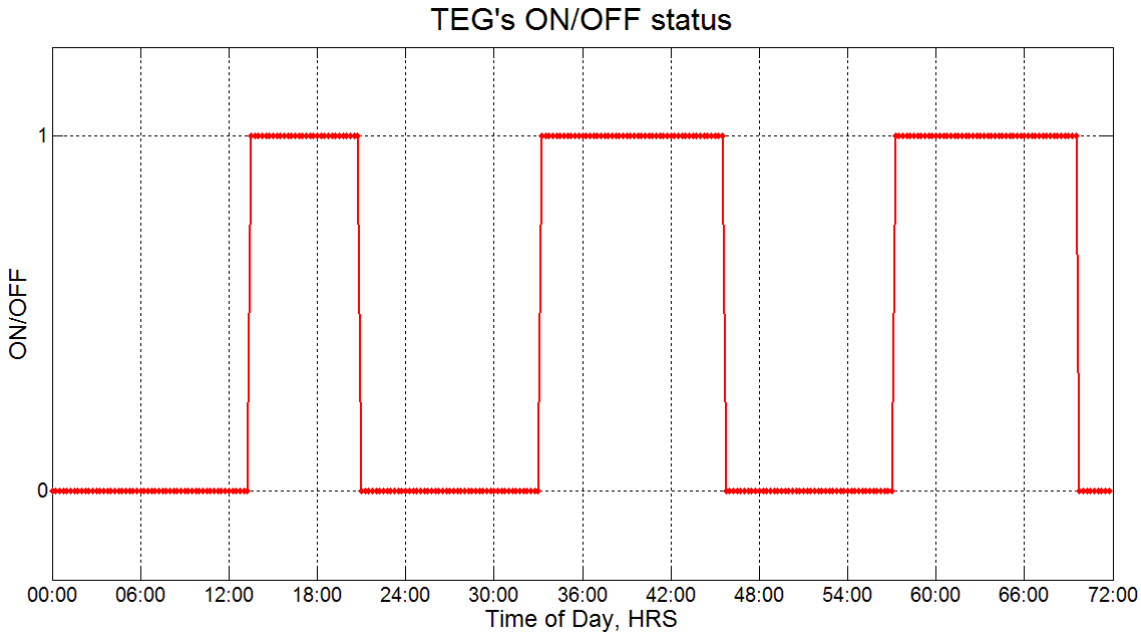
TEG's ON/OFF status
ON/OFF
1
0
00:00
06:00
12:00
18:00
24:00
30:00
36:00
42:00
48:00
54:00
60:00
66:00
72:00
Time of Day, HRS

B.1.11 November (11/21/2005)

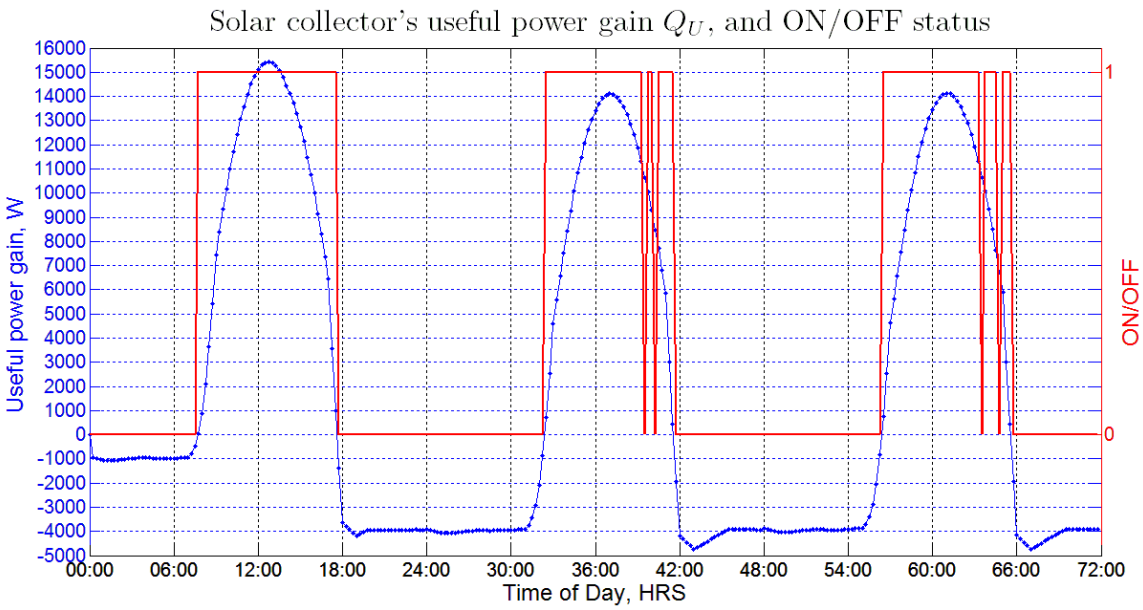

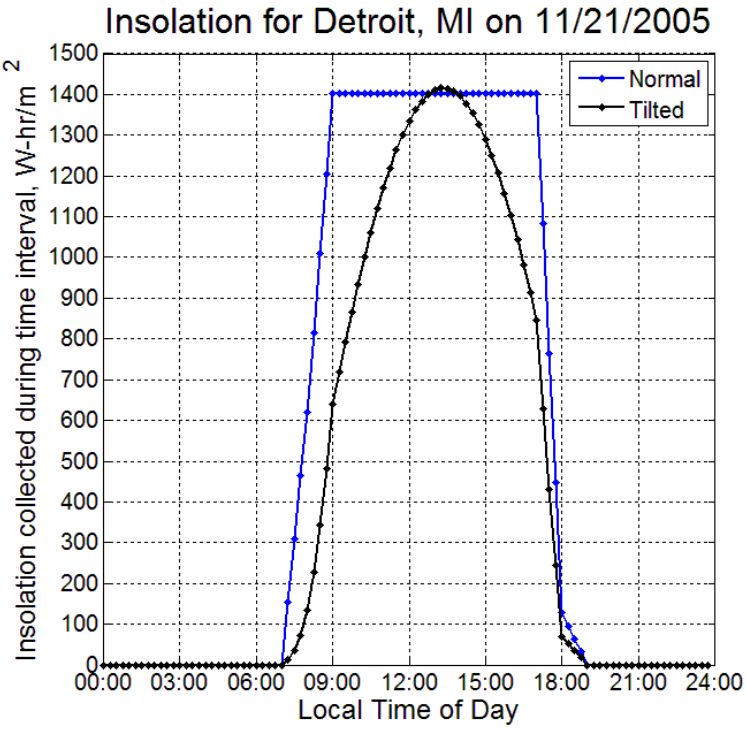

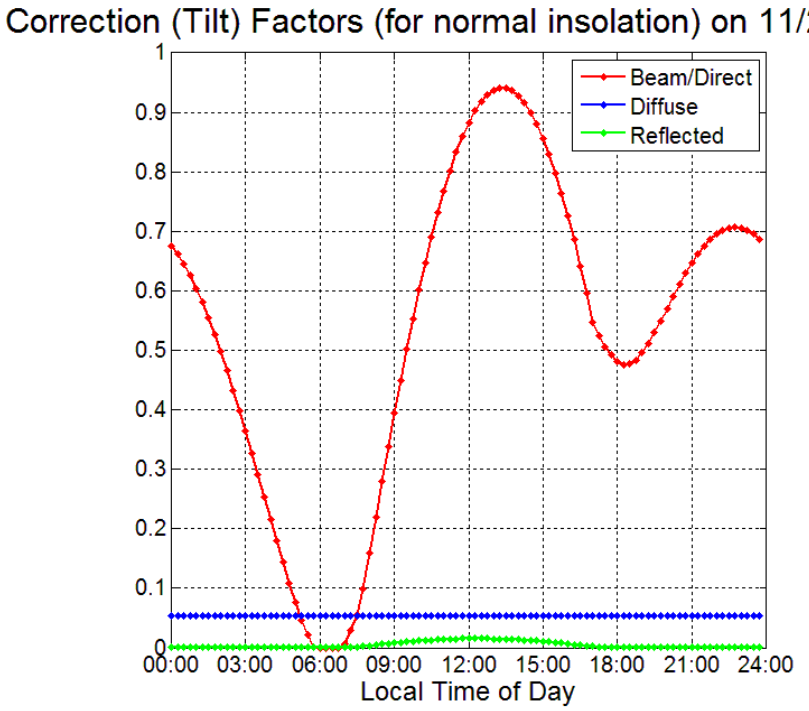
Correction (Tilt) Factors (for normal insolation) on 11/21/2005
Beam/Direct
Diffuse
Reflected
1
0.9
0.8
0.7
0.6
0.5
0.4
0.3
0.2
0.1
0
00:00
03:00
06:00
09:00
12:00
15:00
18:00
21:00
24:00
Local Time of Day

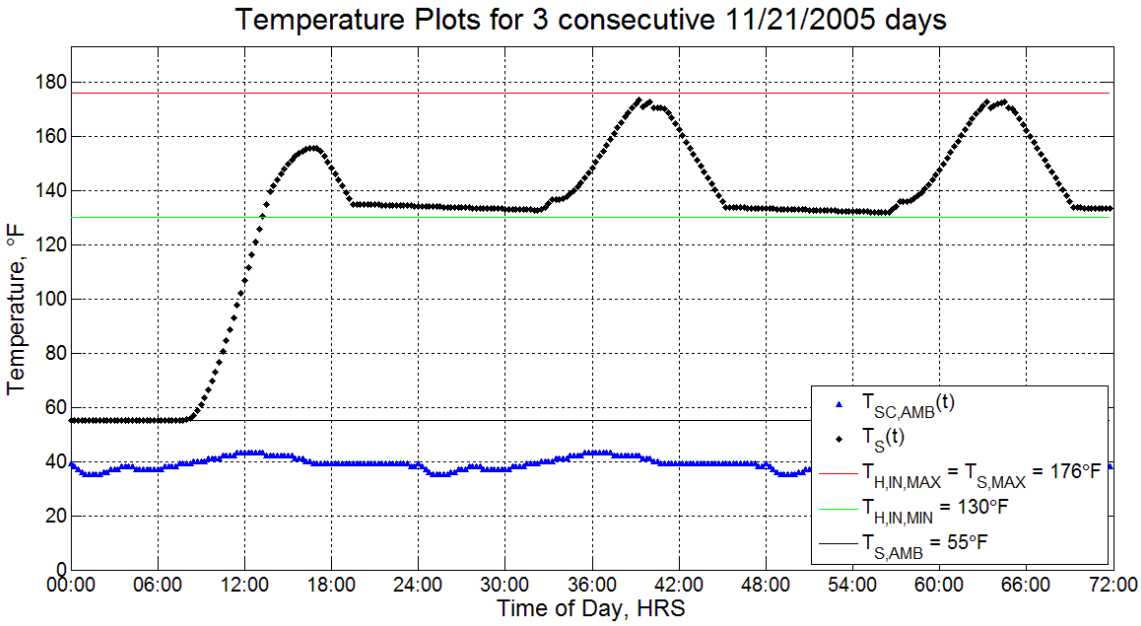
Temperature Plots for 3 consecutive 11/21/2005 days
Temperature, °F
180
160
140
120
100
80
60
40
20
0
00:00
06:00
12:00
18:00
24:00
30:00
36:00
42:00
48:00
54:00
60:00
66:00
72:00
Time of Day, HRS
T_SC,AMB(t)
T_S(t)
T_H,IN,MAX = T_S,MAX = 176°F
T_H,IN,MIN = 130°F
T_S,AMB = 55°F

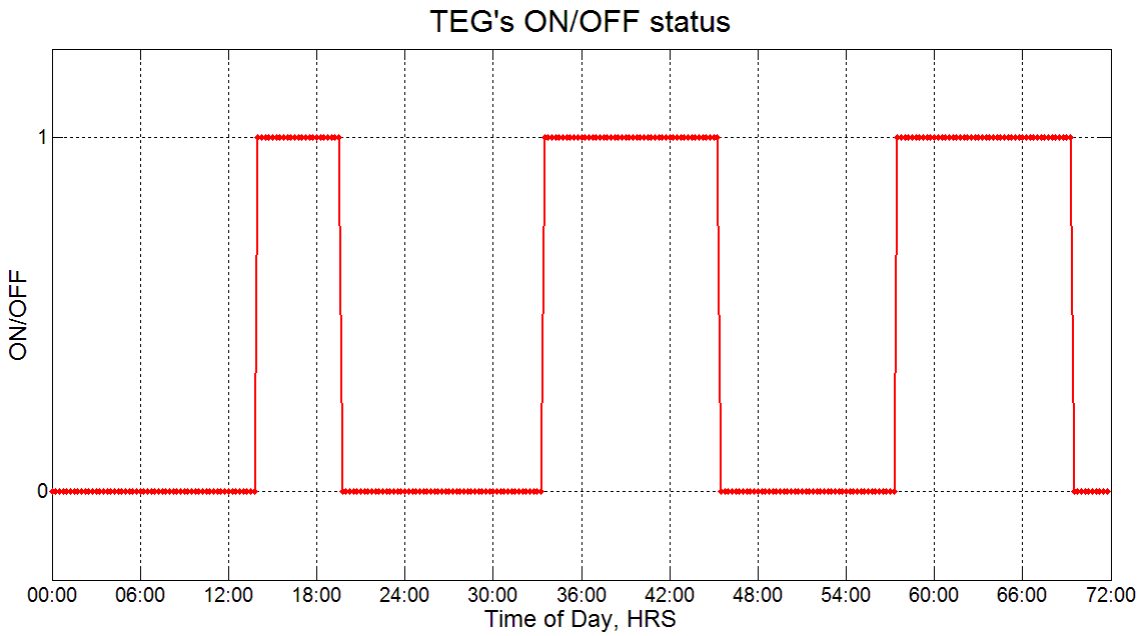
TEG's ON/OFF status
ON/OFF
1
0
00:00
06:00
12:00
18:00
24:00
30:00
36:00
42:00
48:00
54:00
60:00
66:00
72:00
Time of Day, HRS

B.1.12 December (12/21/2005)

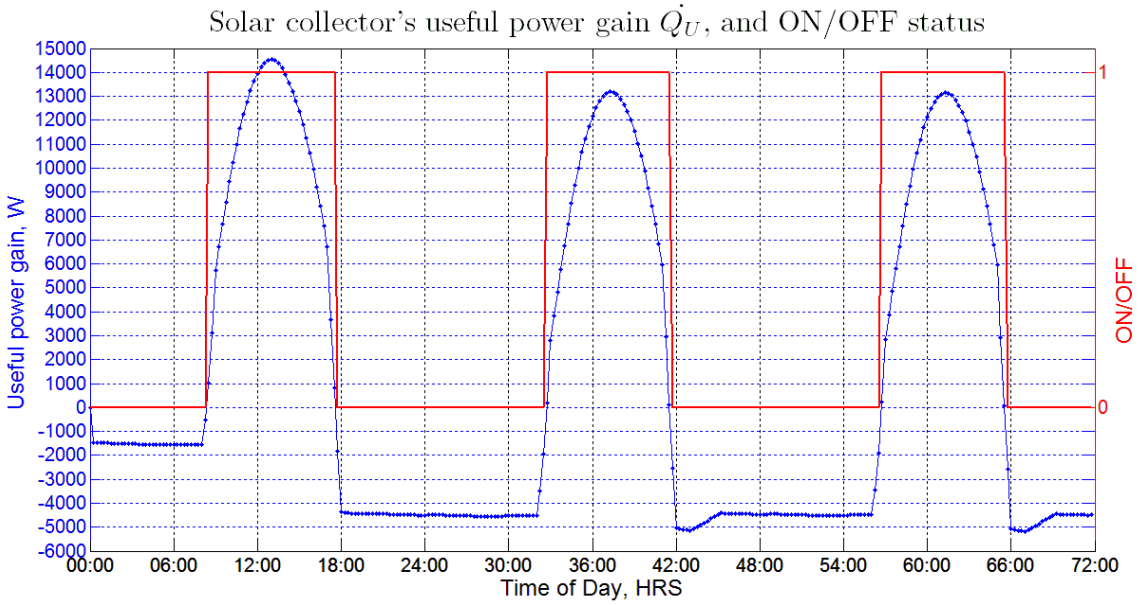

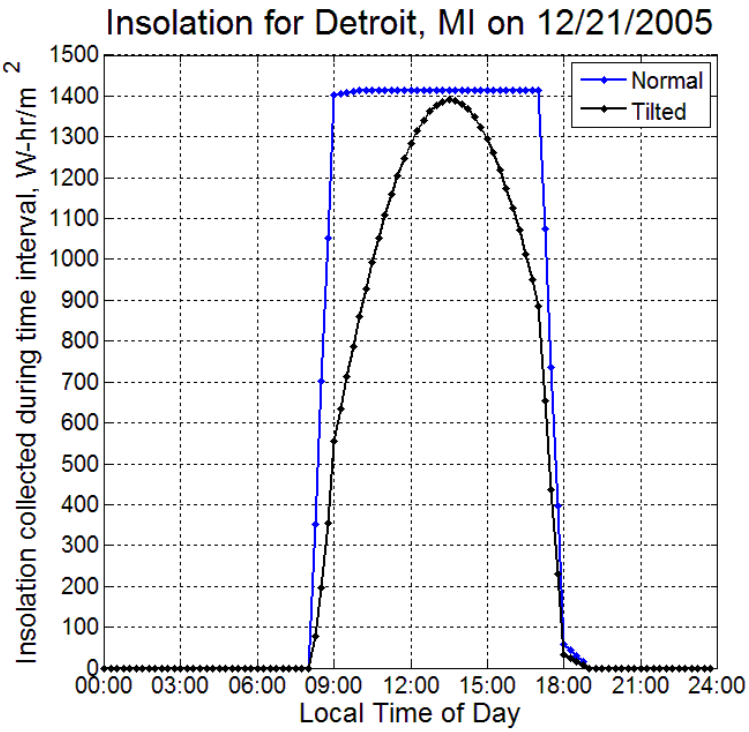

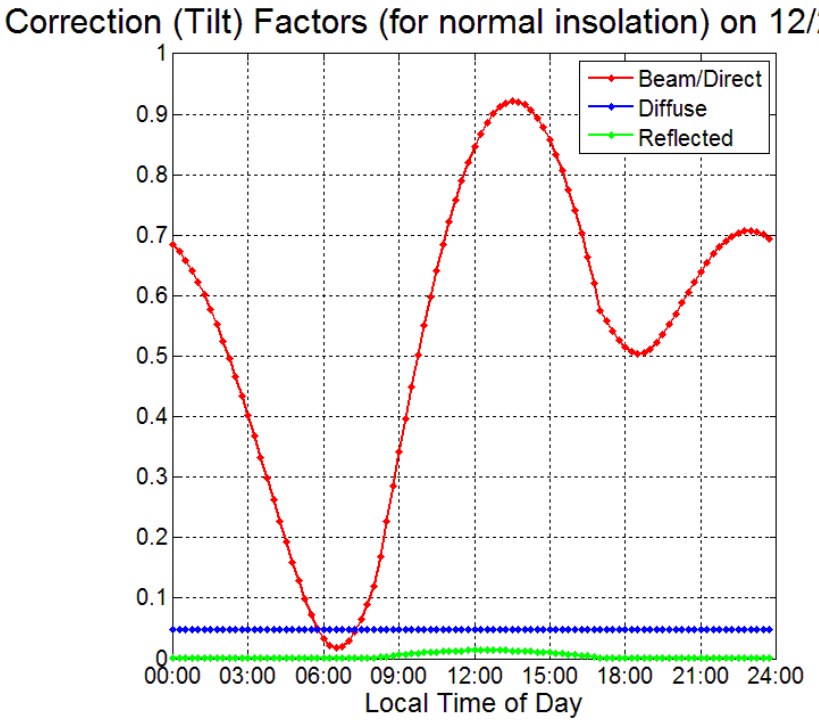
Correction (Tilt) Factors (for normal insolation) on 12/21/2005
Beam/Direct
Diffuse
Reflected
1
0.9
0.8
0.7
0.6
0.5
0.4
0.3
0.2
0.1
0
00:00 03:00 06:00 09:00 12:00 15:00 18:00 21:00 24:00
Local Time of Day

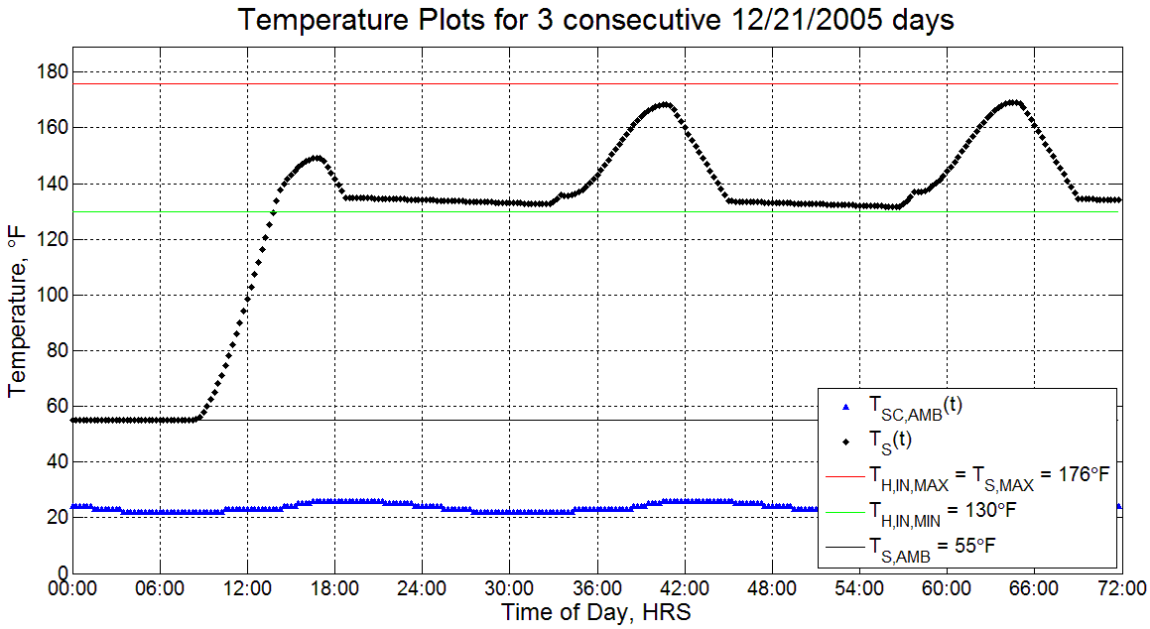
Temperature Plots for 3 consecutive 12/21/2005 days
Temperature, °F
180
160
140
120
100
80
60
40
20
0
00:00 06:00 12:00 18:00 24:00 30:00 36:00 42:00 48:00 54:00 60:00 66:00 72:00
Time of Day, HRS
T_SC,AMB(t)
T_S(t)
T_H,IN,MAX = T_S,MAX = 176°F
T_H,IN,MIN = 130°F
T_S,AMB = 55°F

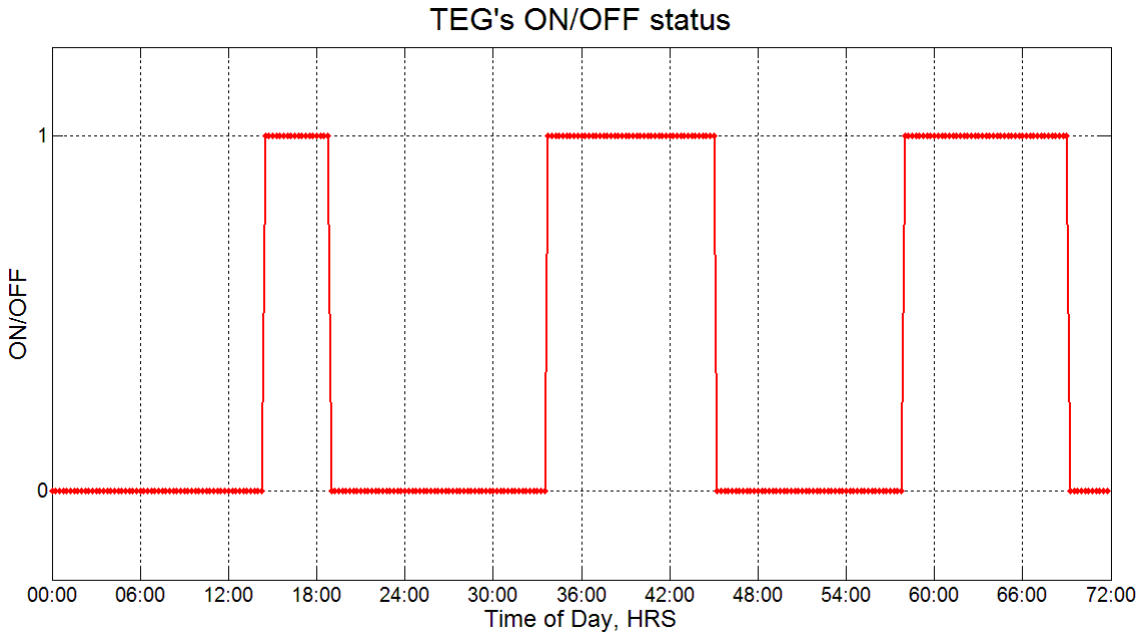
TEG's ON/OFF status
ON/OFF
1
0
00:00
06:00
12:00
18:00
24:00
30:00
36:00
42:00
48:00
54:00
60:00
66:00
72:00
Time of Day, HRS

B.2: MATLAB SCRIPTS

The MATLAB script, developed by the author, is included here in its entirety.

B.2.1 Main Program

```
%{
Adolfo Lozano, Webber Energy Group
Numerical Analysis of a Solar Collector
Original created 04/01/2011
Revision created 06/21/2011
%}

clear all;

% ------------------------------------------------------------------
% Numerical model parameters (user-selected)
    % Number of days simulated (1-7 only); keep semicolon off!
        N = 7
    % Choose representative month to simulate (1-12); 6 for June (SS), 12 for December
(WS), etc.; keep semicolon off!
        MONTH = 1
% ------------------------------------------------------------------

% Import all data used, and convert to [C]
    ImportAllData;

% Input parameters (fixed)

[I,Z,rho,cp,A_c,eta_0,n_p,slope_c,a_w,beta,lat,long,STM,rho_c,R_s,t_s,D_s,H_s,V_s,T_s_amb
_F_SS,T_s_amb_F_WS,T_s_max_C,Vdot_TEG,deltaT_TEG_C,TEG_height,TEG_width,TEG_length,T_TEG_
in_min_F,T_TEG_in_max_F,Edot_TEG_nominal] = InputParameters;

% Calculated/Converted Parameters
    [M,dt,t_end_axis,Z_v,U_s,A_s,V_s,Vdot_TEG,mdot_TEG,TEG_SA] =
CalculatedInputParameters(N,I,R_s,t_s,D_s,H_s,V_s,Vdot_TEG,rho,TEG_height,TEG_width,TEG_l
ength);

% Temperature Conversion
    % Analyses must be done in Celsius!
    TempData_1_C = Convert_F_to_C(TempData_1_F);
    TempData_2_C = Convert_F_to_C(TempData_2_F);
    TempData_3_C = Convert_F_to_C(TempData_3_F);
    TempData_4_C = Convert_F_to_C(TempData_4_F);
    TempData_5_C = Convert_F_to_C(TempData_5_F);
    TempData_6_C = Convert_F_to_C(TempData_6_F);
    TempData_7_C = Convert_F_to_C(TempData_7_F);
    TempData_8_C = Convert_F_to_C(TempData_8_F);
    TempData_9_C = Convert_F_to_C(TempData_9_F);
    TempData_10_C = Convert_F_to_C(TempData_10_F);
    TempData_11_C = Convert_F_to_C(TempData_11_F);
    TempData_12_C = Convert_F_to_C(TempData_12_F);
    T_s_max_F = Convert_C_to_F(T_s_max_C);  % for plotting purposes only
    T_TEG_in_min_C = Convert_F_to_C(T_TEG_in_min_F);
    T_TEG_in_max_C = Convert_F_to_C(T_TEG_in_max_F);


% NUMERICAL ANALYSIS -----------------------------------------------
% Initialize Vectors

[T_s_C,Qdot_u,Q_loss,T_c_amb_C,t,G_vector,C_c,C_TEG,Collector_status,TEG_status,E_c_colle
cted,E_c_used,Qdot_u_real_collected,Qdot_u_real_used,Energy_from_Collector_Collected_per_
Day_in_kWh,Energy_from_Collector_Used_per_Day_in_kWh] = InitializeAsZeroVectors(N,M);
```

```
    % X-Axis increment definition, for plotting purposes only (Solution Plot)
    [dt_axis,aa,bb,cc,dd,ee,ff,gg,hh,ii,jj,kk,ll,mm,nn,oo,pp,qq] = XAxisIncrement(N);

    % Define necessary 1-day discrete-data-vectors (choose month)
    [G_hor,G_normal,T,Label,T_s_amb_F] =
AssignParametersBasedOnMonth(MONTH,InsolationData_normal_1,InsolationData_normal_2,Insola
tionData_normal_3,InsolationData_normal_4,InsolationData_normal_5,InsolationData_normal_6
,InsolationData_normal_7,InsolationData_normal_8,InsolationData_normal_9,InsolationData_n
ormal_10,InsolationData_normal_11,InsolationData_normal_12,InsolationData_hor_1,Insolatio
nData_hor_2,InsolationData_hor_3,InsolationData_hor_4,InsolationData_hor_5,InsolationData
_hor_6,InsolationData_hor_7,InsolationData_hor_8,InsolationData_hor_9,InsolationData_hor_
10,InsolationData_hor_11,InsolationData_hor_12,TempData_1_C,TempData_2_C,TempData_3_C,Tem
pData_4_C,TempData_5_C,TempData_6_C,TempData_7_C,TempData_8_C,TempData_9_C,TempData_10_C,
TempData_11_C,TempData_12_C,T_s_amb_F_WS,T_s_amb_F_SS);
    T_s_amb_C = Convert_F_to_C(T_s_amb_F); % Convert from F to [C], because analysis done
only in [C]; since use [F] later, leave this line and don't bury it in another function

% Convert G_hor to G_t (horizontal to tilted insolation); This approach wasn't used!

%[B,ET,SolarTimeDiff,d_s,SolarTime,MFLSN,h_s,alpha,a_s,i,R_h_b,R_h_d,R_h_r,R_h_tot,G_t_h_
b,G_t_h_d,G_t_h_r,G_t_h,C,G_hor_master] =
Convert_Insolation_hor(TimesVector,MONTH,SkyDiffuseFactorPerMonth,Z,Z_v,I,STM,lat,long,be
ta,a_w,rho_c,G_hor,Label,InsolationData_hor_1,InsolationData_hor_2,InsolationData_hor_3,I
nsolationData_hor_4,InsolationData_hor_5,InsolationData_hor_6,InsolationData_hor_7,Insola
tionData_hor_8,InsolationData_hor_9,InsolationData_hor_10,InsolationData_hor_11,Insolatio
nData_hor_12);

% Convert G_normal to G_t (normal to tilted insolation)

[B,ET,SolarTimeDiff,d_s,SolarTime,MFLSN,h_s,alpha,a_s,i,R_n_b,R_n_d,R_n_r,R_n_tot,G_t_n_b
,G_t_n_d,G_t_n_r,G_t_n,C,G_normal_master] =
Convert_Insolation_normal(TimesVector,MONTH,SkyDiffuseFactorPerMonth,Z,Z_v,I,STM,lat,long
,beta,a_w,rho_c,G_normal,Label,InsolationData_normal_1,InsolationData_normal_2,Insolation
Data_normal_3,InsolationData_normal_4,InsolationData_normal_5,InsolationData_normal_6,Ins
olationData_normal_7,InsolationData_normal_8,InsolationData_normal_9,InsolationData_norma
l_10,InsolationData_normal_11,InsolationData_normal_12);
%{
% Compare all 4 insolation plots (in PER MONTH basis): horizontal data, normal data,
tilted (calc from hor), tilted (calc from normal)
    Plot_Calculated_Insolation(TimesVector,G_hor,G_t_h,G_normal,G_t_n,Label);
%}
% Extend vectors appropriately based on number of days N
    t = 0:dt:(t_end_axis-dt);  % Each day is defined from 00:00 - 23:45 rather than 00:00
- 24:00; "t" is just a dummy variable for x-axis
    t=t';
    for n=1:N
        G_vector((I*(n-1)+1):n*I)=G_t_n;  % G_vector is an N-day vector, whereas G is a
1-day vector
        T_c_amb_C((I*(n-1)+1):n*I)=T;  % T_c_amb_C is an N-day vector, whereas T is a 1-
day vector
    end

% Initial conditions
    T_s_C(1) = T_s_amb_C; % Initialize T_s to ambient temperature
    X_TEG = 0; % Start with load (TEG) off initially
% ON/OFF Vectors
    C_c(1)=0; % Collector ON/OFF Vector
    C_TEG(1)=0; % TEG ON/OFF Vector


% Heart of Numerical Model; NOTE: T_s_C is solution vector!
for n=2:M
% I. CALCULATIONS ------------------------------------------------------
% Solar Collector
    % Control (ON/OFF) factor for solar collector --------------------
```

```
    % Note: need to break apart as two separate control factors because need to calculate
Qdot(u) at each iteration
    if T_s_C(n-1)<T_c_amb_C(n)  % 1a) deltaT in Qdot_u must be positive (in nature); this
is necessary even with (1b) condition to ensure it's not negative (- and - = +)
        X_c_b=0; % Collector doesn't convect (physically can't in nature)
    else
        X_c_b=1; % Collector convects
    end

    % Calculate Qdot_u at each n
    Qdot_u(n) = n_p * A_c * (G_vector(n)*eta_0 - X_c_b*slope_c*(T_s_C(n-1)-
T_c_amb_C(n))); % This is in [W]; see above for explanation/significance of Qdot_u
    Qdot_u(n) = Qdot_u(n) - 300; % This simulates the pump's power requirement of 300 W

% Storage Tank Convective Losses -------------------------------------
    % Calculate Q_loss
    Q_loss(n) = U_s*A_s*(T_s_C(n-1) - T_s_amb_C); % This is in [W]
    if Q_loss(n)<0  % 2) Q_loss must be positive (in nature)
        Q_loss(n)=0;
    end

% II. CONTROLS -------------------------------------------------------
% Collector Control
    % Don't run collector unless it benefits you!
    if Qdot_u(n)<=0  % 1b) Qdot_u must be positive (can't hurt you), in spite of (1a)
condition; i.e. run collector only if Qdot_u positive
        X_c_a=0; % To ensure it doesn't convect at night (because it shouldn't be
running)
    else
        X_c_a=1;
    end

    % Collector's max storage temperature
    if T_s_C(n-1)>=(T_s_max_C-2) % Max storage temp
        X_c_a=0;
    end

% TEG Control
    if T_s_C(n-1) < (T_TEG_in_min_C+3)  % Should TEG's ON/OFF control be coupled with
Collector being ON/OFF? They're really independent of each other...
        X_TEG = 0;
    else
        X_TEG = 1;
    end

% Store values into ON/OFF Control Vectors at current iteration
    C_c(n) = X_c_a;
    C_TEG(n) = X_TEG;

% III. ITERATION -----------------------------------------------------
% Calculate new T_s_C at that time step n
    T_s_C(n) = T_s_C(n-1) + (3600*dt)*(1/(rho*V_s*cp))*(X_c_a*Qdot_u(n) +
X_TEG*mdot_TEG*cp*deltaT_TEG_C - Q_loss(n));
end

% Temperature Conversion
    % Convert temperature vectors from [C] back to [F] (for plotting purposes)
    T_s_F = Convert_C_to_F(T_s_C);
    T_c_amb_F = Convert_C_to_F(T_c_amb_C);

% POST-ANALYSIS ------------------------------------------------------
% Quantify number of times Collector and TEG ON/OFF in month selected
    for n=1:N
        Collector_status(n) = sum(C_c((I*(n-1)+1):n*I));
        TEG_status(n) = sum(C_TEG((I*(n-1)+1):n*I));
    end
```

```
    % Output on main MATLAB screen (see Thesis text for methodology; this section works
best for N = 7 days)
    Time_Collector_ON_during_Selected_Month_in_HRS = (Collector_status(1)*0.25)*1 +
(mean(Collector_status(2:N)*0.25))*29.4375
    Time_TEG_ON_during_Selected_Month_in_HRS = (TEG_status(1)*0.25)*1 +
(mean(TEG_status(2:N)*0.25))*29.4375
    Percent_Time_Collector_ON_during_Selected_Month =
Time_Collector_ON_during_Selected_Month_in_HRS / 24 / 30.4375 * 100;
    Percent_Time_TEG_ON_during_Selected_Month = Time_TEG_ON_during_Selected_Month_in_HRS
/ 24 / 30.4375 * 100;

% Calculate the energy collected by the solar collector in N days selected
    % Define "real" Qdots (neither have any negatives)
    Qdot_u_real_collected = Qdot_u;
    Qdot_u_real_used = Qdot_u;
    for n=1:M
        if Qdot_u(n) < 0
            Qdot_u_real_collected(n) = 0;  % Qdot_u_real_collected is the physical energy
collected (no negatives)
            Qdot_u_real_used(n) = 0;
        end
        if C_c(n) == 0
            Qdot_u_real_used(n) = 0;  % Qdot_u_real_used is the actual energy used (based
on collector ON/OFF)
        end
    end
    % Integrate via trapezoids to quantify energy collected in N days (in [kWh])
    for n=1:M
        if n<=(M-1)
            E_c_collected(n) = (mean([Qdot_u_real_collected(n)
Qdot_u_real_collected(n+1)]))*0.25/1000;
            E_c_used(n) = (mean([Qdot_u_real_used(n) Qdot_u_real_used(n+1)]))*0.25/1000;
        end
    end

    % Quantify energy collected per day
    for n=1:N
        Energy_from_Collector_Collected_per_Day_in_kWh(n) = sum(E_c_collected((I*(n-
1)+1):n*I));
        Energy_from_Collector_Used_per_Day_in_kWh(n) = sum(E_c_used((I*(n-1)+1):n*I));
    end

% Output energy collected and used by solar collector in that month
    Energy_from_Collector_Collected_during_Selected_Month_in_kWh =
Energy_from_Collector_Collected_per_Day_in_kWh(1)*1 +
mean(Energy_from_Collector_Collected_per_Day_in_kWh(2:N))*29.4375
    Energy_from_Collector_Used_during_Selected_Month_in_kWh =
Energy_from_Collector_Used_per_Day_in_kWh(1)*1 +
mean(Energy_from_Collector_Used_per_Day_in_kWh(2:N))*29.4375

figure(200);
plot(t,Qdot_u_real_collected,'-db','MarkerFaceColor','b','MarkerSize',5)
hold on
plot(t,Qdot_u_real_used,'-dr','MarkerFaceColor','r','MarkerSize',5)
legend('Qdot collected','Qdot used')
figure(201);
plot(t,E_c_collected,'-dg','MarkerFaceColor','g','MarkerSize',5)
hold on
plot(t,E_c_used,'-dm','MarkerFaceColor','m','MarkerSize',5)
legend('E_c collected','E_c used')

% Output energy produced by TEG in that month
    Energy_Produced_by_TEG_during_Selected_Month_in_kWh =
Time_TEG_ON_during_Selected_Month_in_HRS * Edot_TEG_nominal / 1000
```

```
% Plots ------------------------------------------------------------------
figure(1); % Insolation Plot for single month
Plot_Insolation_SingleDay(TimesVector,G_t_n,Label);

figure(2); % Horizontal Insolation data for all 12 months
Plot_Insolation_hor_All(TimesVector,InsolationData_hor_1,InsolationData_hor_2,InsolationD
ata_hor_3,InsolationData_hor_4,InsolationData_hor_5,InsolationData_hor_6,InsolationData_h
or_7,InsolationData_hor_8,InsolationData_hor_9,InsolationData_hor_10,InsolationData_hor_1
1,InsolationData_hor_12);

figure(3); % Normal Insolation data for all 12 months
Plot_Insolation_normal_All(TimesVector,InsolationData_normal_1,InsolationData_normal_2,In
solationData_normal_3,InsolationData_normal_4,InsolationData_normal_5,InsolationData_norm
al_6,InsolationData_normal_7,InsolationData_normal_8,InsolationData_normal_9,InsolationDa
ta_normal_10,InsolationData_normal_11,InsolationData_normal_12);

figure(4); % Ambient Temperature data for all 12 months
Plot_Temperature_All(TimesVector,TempData_1_F,TempData_2_F,TempData_3_F,TempData_4_F,Temp
Data_5_F,TempData_6_F,TempData_7_F,TempData_8_F,TempData_9_F,TempData_10_F,TempData_11_F,
TempData_12_F);

figure(5); % Temperature Plots in Fahrenheit
Plot_Solution(t,T_c_amb_F,T_s_F,M,T_s_max_F,T_TEG_in_min_F,T_s_amb_F,N,Label,t_end_axis,d
t_axis,MONTH,aa,bb,cc,dd,ee,ff,gg,hh,ii,jj,kk,ll,mm,nn,oo,pp,qq);

figure(6); % Collector's Qdot_u & ON/OFF
Plot_Collector_Results(t,Qdot_u,C_c,t_end_axis,dt_axis,aa,bb,cc,dd,ee,ff,gg,hh,ii,jj,kk,l
l,mm,nn,oo,pp,qq,N);

figure(7); % TEG's ON/OFF
Plot_TEG_Results(t,C_TEG,t_end_axis,dt_axis,N,aa,bb,cc,dd,ee,ff,gg,hh,ii,jj,kk,ll,mm,nn,o
o,pp,qq);
```

B.2.2 ImportAllData.m

```
function ImportAllData
%User-defined function:
%This function uses the pre-defined "importfile" function, obtained online at:
%    http://www.mathworks.com/help/techdoc/import_export/br5wz4t.html#bsc58dc
%Note: Each text file has 96 data points, from 00:00-23:45 (in 00:15 intervals)

importfile('TimesVector.txt');

% Insolation Data (note: Extraterrestrial solar radiation received on a HORIZONTAL
surface; will be corrected for a TILTED surface later)
importfile('InsolationData_hor_1.txt');   % January 2005
importfile('InsolationData_hor_2.txt');   % February 2005
importfile('InsolationData_hor_3.txt');   % March 2005
importfile('InsolationData_hor_4.txt');   % April 2005
importfile('InsolationData_hor_5.txt');   % May 2005
importfile('InsolationData_hor_6.txt');   % June 2005
importfile('InsolationData_hor_7.txt');   % July 2005
importfile('InsolationData_hor_8.txt');   % August 2005
importfile('InsolationData_hor_9.txt');   % September 2005
importfile('InsolationData_hor_10.txt');   % October 2005
importfile('InsolationData_hor_11.txt');   % November 2005
importfile('InsolationData_hor_12.txt');   % December 2005

% Insolation Data (note: Extraterrestrial solar radiation received on a HORIZONTAL
surface; will be corrected for a TILTED surface later)
importfile('InsolationData_normal_1.txt');   % January 2005
importfile('InsolationData_normal_2.txt');   % February 2005
importfile('InsolationData_normal_3.txt');   % March 2005
importfile('InsolationData_normal_4.txt');   % April 2005
importfile('InsolationData_normal_5.txt');   % May 2005
importfile('InsolationData_normal_6.txt');   % June 2005
importfile('InsolationData_normal_7.txt');   % July 2005
importfile('InsolationData_normal_8.txt');   % August 2005
importfile('InsolationData_normal_9.txt');   % September 2005
importfile('InsolationData_normal_10.txt');   % October 2005
importfile('InsolationData_normal_11.txt');   % November 2005
importfile('InsolationData_normal_12.txt');   % December 2005

% Ambient Temperature Data (convert to [C] later)
importfile('TempData_1_F.txt');   % January 2005
importfile('TempData_2_F.txt');   % February 2005
importfile('TempData_3_F.txt');   % March 2005
importfile('TempData_4_F.txt');   % April 2005
importfile('TempData_5_F.txt');   % May 2005
importfile('TempData_6_F.txt');   % June 2005
importfile('TempData_7_F.txt');   % July 2005
importfile('TempData_8_F.txt');   % August 2005
importfile('TempData_9_F.txt');   % September 2005
importfile('TempData_10_F.txt');   % October 2005
importfile('TempData_11_F.txt');   % November 2005
importfile('TempData_12_F.txt');   % December 2005

% Other
importfile('SkyDiffuseFactorPerMonth.txt');    % Sky Diffuse Factors, C, for each months
```

B.2.3 InputParameters.m

```
function
[I,Z,rho,cp,A_c,eta_0,n_p,slope_c,a_w,beta,lat,long,STM,rho_c,R_s,t_s,D_s,H_s,V_s,T_s_amb
_F_SS,T_s_amb_F_WS,T_s_max_C,Vdot_TEG,deltaT_TEG_C,TEG_height,TEG_width,TEG_length,T_TEG_
in_min_F,T_TEG_in_max_F,Edot_TEG_nominal] = InputParameters
%User-defined function:
%This function lists all input parameters needed in numerical model.

% Number of data points [in imported text file] per day (96 for quarter-hourly data)
    I = 96;
% Number of test dates (i.e. number of months in a year)
    Z = 12;

% Fluid Parameters
    rho = 1000; % Fluid density (water) [kg/m^3]
    cp = 4190; % Specific heat (water) [J/kg-K]; Average value for [75-175F] temp range

% Solar Collector Parameters
    %Vdot_c = 1; % Volumetric flow rate through collector [gpm]; never use explicitly--
probably embedded in eta_0 & slope_c values
    A_c = 0.98; % Aperture area [m^2]
    eta_0 = 0.675; % Max panel efficiency
    n_p = 20; % Number of panels installed
    slope_c = 3.5; % Collector Efficiency Curve Slope [W/C]

% Convert Insolation Parameters
    a_w = 22; % Panel azimuth angle; panel's skew from south
    beta = 45; % Panel tilt angle
    lat = 42.215; % Latitude of solar panel location (taken from NOAA temp data)
    long = -83.349; % Longitude of solar panel location (taken from NOAA temp data)
    STM = 75; % Standard time meridian (75 deg for EST time zone)
    rho_c = 0.2;

% Storage Tank Parameters
    R_s = 4.2;  % R-value [/in]
    t_s = 4; % Insulation thickness [in]
    D_s = 60; % Tank diameter [in]
    H_s = 48; % Tank height [in]
    V_s = 1250; % Tank volume capacity [liters]
    T_s_amb_F_SS = 75; % Room temperature [F]
    T_s_amb_F_WS = 55; % Room temperature [F]
    T_s_max_C = 80; % Max temp in [C]!

% TEG Parameters
    Vdot_TEG = 1.31; % Volumetric flow rate [gpm] (for HOT loop only; COLD loop reqiures
6 gpm)
    deltaT_TEG_C = -20; % Temp drop across TEG's hot stream in [C]; nominally ~36 F delta
T
    TEG_height = 31; % Height in [in]
    TEG_width = 13.5; % Width in [in]
    TEG_length = 19.5; % Length in [in]
    T_TEG_in_min_F = 130; % In [F]...leave a buffer zone!
    T_TEG_in_max_F = 176; % In [F].......change plot legend!!
    Edot_TEG_nominal = 83;
```

B.2.4 CalculatedInputParameters.m

```
function [M,dt,t_end_axis,Z_v,U_s,A_s,V_s,Vdot_TEG,mdot_TEG,TEG_SA] =
CalculatedInputParameters(N,I,R_s,t_s,D_s,H_s,V_s,Vdot_TEG,rho,TEG_height,TEG_width,TEG_l
ength)
%User-defined function:
%This function calculates/converts the input parameters to whatever units
%are required in the numerical model.

    M = N*I; % No. iterations per day
    dt = 0.25; % Time step (quarter-hours)
    t_end_axis = N*24; % Used for plotting purposes only
    Z_v = [20;49;79;110;141;172;203;234;265;295;325;355];  % Vector with Day Number Of
Year for 12 chosen dates

% Solar Collector Parameters (don't need; inherent in solar efficiency curve)
    %Vdot_c = Vdot_c * 6.30901964E-5; % Convert volumetric flow rate to [m^3/s]
    %mdot_c = Vdot_c * rho; % Mass flow rate in [kg/s]

% Storage Tank Parameters
    U_s = (R_s * t_s / 5.678)^-1; % Calculated U value [W/m2-K]
    A_s = (2*pi()*D_s^2/4 + pi()*D_s*H_s) * 0.0254^2; % Calculated Surface Area [m^2]
    V_s = V_s * 0.001; % Convert volume to [m^3]

% TEG Parameters
    %Vdot_TEG = Vdot_TEG*(5/3)*1E-5; % Convert [liters/min] to [m^3/s]
    Vdot_TEG = Vdot_TEG * 6.30901964E-5; % Convert [gpm] to [m^3/s]
    mdot_TEG = Vdot_TEG * rho; % Mass flow rate in [kg/s]
    TEG_SA =
(2*((TEG_height*TEG_width)+(TEG_height*TEG_length)+(TEG_width*TEG_length)))*1.6387064E-5;
% Calculate surface area in [m^3]
```

B.2.5 Convert_F_to_C.m

```
function Temp_C = Convert_F_to_C(Temp_F)
%User-defined function:
%This function converts a value from [F] to [C]

Temp_C = (Temp_F-32)*5/9;
```

B.2.6 InitializeAsZeroVectors.m

```
function
[T_s_C,Qdot_u,Q_loss,T_c_amb_C,t,G_vector,C_c,C_TEG,Collector_status,TEG_status,E_c_colle
cted,E_c_used,Qdot_u_real_collected,Qdot_u_real_used,Energy_from_Collector_Collected_per_
Day_in_kWh,Energy_from_Collector_Used_per_Day_in_kWh] = InitializeAsZeroVectors(N,M)
%User-defined function:
%This function simply initializes all vectors needed in numerical model as null vectors.

    T_s_C = zeros(M,1);  % The solution vector (thermal storage tank temperature) in [C]
    Qdot_u = zeros(M,1);  % Qdot_u is the Useful thermal energy collected/gained from
collector (notation standard in the field)
    Q_loss = zeros(M,1);  % Storage tank heat loss
    %G = zeros(M,1);
    T_c_amb_C = zeros(M,1);
    t = zeros(M,1);
    G_vector = zeros(M,1);
    C_c = zeros(M,1);  % Binary (ON/OFF) vector for collector
    C_TEG = zeros(M,1);  % Binary (ON/OFF) vector for TEG

    Collector_status = zeros(N,1);
    TEG_status = zeros(N,1);
    E_c_collected = zeros(M,1);
    E_c_used = zeros(M,1);
    Qdot_u_real_collected = zeros(M,1);
    Qdot_u_real_used = zeros(M,1);
    Energy_from_Collector_Collected_per_Day_in_kWh = zeros(N,1);
    Energy_from_Collector_Used_per_Day_in_kWh = zeros(N,1);
```

B.2.7 XAxisIncrement.m

```
function [dt_axis,aa,bb,cc,dd,ee,ff,gg,hh,ii,jj,kk,ll,mm,nn,oo,pp,qq] = XAxisIncrement(N)
%User-defined function:
%This function is purely for plotting purposes (x-axis), based on N chosen.

switch N>0  %X-axis increments change based on number of days plotting
    case N==1
        dt_axis = 1.5;
        aa = '00:00'; bb = '01:30'; cc = '03:00';
        dd = '04:30'; ee = '06:00'; ff = '07:30';
        gg = '09:00'; hh = '10:30'; ii = '12:00';
        jj = '13:30'; kk = '15:00'; ll = '16:30';
        mm = '18:00'; nn = '19:30'; oo = '21:00';
        pp = '22:30'; qq = '24:00';
    case N==2
        dt_axis = 3;
        aa = '00:00'; bb = '03:00'; cc = '06:00';
        dd = '09:00'; ee = '12:00'; ff = '15:00';
        gg = '18:00'; hh = '21:00'; ii = '24:00';
        jj = '27:00'; kk = '30:00'; ll = '33:00';
        mm = '36:00'; nn = '39:00'; oo = '42:00';
        pp = '45:00'; qq = '48:00';
    case N==3
        dt_axis = 6;
        aa = '00:00'; bb = '06:00'; cc = '12:00';
        dd = '18:00'; ee = '24:00'; ff = '30:00';
        gg = '36:00'; hh = '42:00'; ii = '48:00';
        jj = '54:00'; kk = '60:00'; ll = '66:00';
        mm = '72:00'; nn = 0; oo = 0;
        pp = 0; qq = 0;
    case N==4
        dt_axis = 6;
        aa = '00:00'; bb = '06:00'; cc = '12:00';
        dd = '18:00'; ee = '24:00'; ff = '30:00';
        gg = '36:00'; hh = '42:00'; ii = '48:00';
        jj = '54:00'; kk = '60:00'; ll = '66:00';
        mm = '72:00'; nn = '78:00'; oo = '84:00';
        pp = '90:00'; qq = '96:00';
    case N==5
        dt_axis = 12;
        aa = '00:00'; bb = '12:00'; cc = '24:00';
        dd = '36:00'; ee = '48:00'; ff = '60:00';
        gg = '72:00'; hh = '84:00'; ii = '96:00';
        jj = '108:00'; kk = '120:00'; ll = 0;
        mm = 0; nn = 0; oo = 0;
        pp = 0; qq = 0;
    case N==6
        dt_axis = 12;
        aa = '00:00'; bb = '12:00'; cc = '24:00';
        dd = '36:00'; ee = '48:00'; ff = '60:00';
        gg = '72:00'; hh = '84:00'; ii = '96:00';
        jj = '108:00'; kk = '120:00'; ll = '132:00';
        mm = '144:00'; nn = 0; oo = 0;
        pp = 0; qq = 0;
    case N==7
        dt_axis = 12;
        aa = '00:00'; bb = '12:00'; cc = '24:00';
        dd = '36:00'; ee = '48:00'; ff = '60:00';
        gg = '72:00'; hh = '84:00'; ii = '96:00';
        jj = '108:00'; kk = '120:00'; ll = '132:00';
        mm = '144:00'; nn = '156:00'; oo = '168:00';
        pp = 0; qq = 0;
end
```

B.2.8 AssignParametersBasedOnMonth.m

```
function [G_hor,G_normal,T,Label,T_s_amb_F] =
AssignParametersBasedOnMonth(MONTH,InsolationData_normal_1,InsolationData_normal_2,Insola
tionData_normal_3,InsolationData_normal_4,InsolationData_normal_5,InsolationData_normal_6
,InsolationData_normal_7,InsolationData_normal_8,InsolationData_normal_9,InsolationData_n
ormal_10,InsolationData_normal_11,InsolationData_normal_12,InsolationData_hor_1,Insolatio
nData_hor_2,InsolationData_hor_3,InsolationData_hor_4,InsolationData_hor_5,InsolationData
_hor_6,InsolationData_hor_7,InsolationData_hor_8,InsolationData_hor_9,InsolationData_hor_
10,InsolationData_hor_11,InsolationData_hor_12,TempData_1_C,TempData_2_C,TempData_3_C,Tem
pData_4_C,TempData_5_C,TempData_6_C,TempData_7_C,TempData_8_C,TempData_9_C,TempData_10_C,
TempData_11_C,TempData_12_C,T_s_amb_F_WS,T_s_amb_F_SS)
%User-defined function:
%Parameters used in numerical model are defined here for the chosen month.
%Note: T_s_amb_F determination is a guess (per Mike Helms), based on test conditions in
Detroit.

switch MONTH>0
    case MONTH==1
        G_hor = InsolationData_hor_1;
        G_normal = InsolationData_normal_1;
        T = TempData_1_C;
        Label = '01/20/2005';
        T_s_amb_F = T_s_amb_F_WS;  % Convert to [C] later
    case MONTH==2
        G_hor = InsolationData_hor_2;
        G_normal = InsolationData_normal_2;
        T = TempData_2_C;
        Label = '02/18/2005';
        T_s_amb_F = T_s_amb_F_WS;
    case MONTH==3
        G_hor = InsolationData_hor_3;
        G_normal = InsolationData_normal_3;
        T = TempData_3_C;
        Label = '03/20/2005';
        T_s_amb_F = T_s_amb_F_WS;
    case MONTH==4
        G_hor = InsolationData_hor_4;
        G_normal = InsolationData_normal_4;
        T = TempData_4_C;
        Label = '04/20/2005';
        T_s_amb_F = T_s_amb_F_WS;  % if change this, change Plot_Solution too
    case MONTH==5
        G_hor = InsolationData_hor_5;
        G_normal = InsolationData_normal_5;
        T = TempData_5_C;
        Label = '05/21/2005';
        T_s_amb_F = T_s_amb_F_SS;
    case MONTH==6
        G_hor = InsolationData_hor_6;
        G_normal = InsolationData_normal_6;
        T = TempData_6_C;
        Label = '06/21/2005';
        T_s_amb_F = T_s_amb_F_SS;
    case MONTH==7
        G_hor = InsolationData_hor_7;
        G_normal = InsolationData_normal_7;
        T = TempData_7_C;
        Label = '07/22/2005';
        T_s_amb_F = T_s_amb_F_SS;
    case MONTH==8
        G_hor = InsolationData_hor_8;
        G_normal = InsolationData_normal_8;
        T = TempData_8_C;
        Label = '08/22/2005';
        T_s_amb_F = T_s_amb_F_SS;
```

```
    case MONTH==9
        G_hor = InsolationData_hor_9;
        G_normal = InsolationData_normal_9;
        T = TempData_9_C;
        Label = '09/22/2005';
        T_s_amb_F = T_s_amb_F_WS;
    case MONTH==10
        G_hor = InsolationData_hor_10;
        G_normal = InsolationData_normal_10;
        T = TempData_10_C;
        Label = '10/22/2005';
        T_s_amb_F = T_s_amb_F_WS;
    case MONTH==11
        G_hor = InsolationData_hor_11;
        G_normal = InsolationData_normal_11;
        T = TempData_11_C;
        Label = '11/21/2005';
        T_s_amb_F = T_s_amb_F_WS;
    case MONTH==12
        G_hor = InsolationData_hor_12;
        G_normal = InsolationData_normal_12;
        T = TempData_12_C;
        Label = '12/21/2005';
        T_s_amb_F = T_s_amb_F_WS;
end
```

B.2.9 Convert_Insolation_hor.m

```
function
[B,ET,SolarTimeDiff,d_s,SolarTime,MFLSN,h_s,alpha,a_s,i,R_h_b,R_h_d,R_h_r,R_h_tot,G_t_h_b
,G_t_h_d,G_t_h_r,G_t_h,C,G_hor_master] =
Convert_Insolation_hor(TimesVector,MONTH,SkyDiffuseFactorPerMonth,Z,Z_v,I,STM,lat,long,be
ta,a_w,rho_c,G_hor,Label,InsolationData_hor_1,InsolationData_hor_2,InsolationData_hor_3,I
nsolationData_hor_4,InsolationData_hor_5,InsolationData_hor_6,InsolationData_hor_7,Insola
tionData_hor_8,InsolationData_hor_9,InsolationData_hor_10,InsolationData_hor_11,Insolatio
nData_hor_12)
%User-defined function:
% This function converts insolation data from a horizontal surface to a
% tilted surface.
% G_t_h is the tilted insolation calculated from horizontal data

TimesVector_min = TimesVector*60;
G_hor_master = zeros(I,Z);

% CHOOSE TOP HALF (ALL 12 MONTHS) OR BOTTOM HALF (PER MONTH)

%{
% All 12 months ------------------------------------------------------------
    % Initialize vectors/matrices as needed
    C = SkyDiffuseFactorPerMonth';
    B = zeros(Z,1)';
    ET = zeros(Z,1)';
    d_s = zeros(Z,1)';
    SolarTimeDiff = zeros(Z,1)';
    SolarTime = zeros(I,Z);
    MFLSN = zeros(I,Z);
    h_s = zeros(I,Z);
    alpha = zeros(I,Z);
    a_s = zeros(I,Z);
    i = zeros(I,Z);
    R_h_b = zeros(I,Z);
    R_h_d = zeros(I,Z);
    R_h_r = zeros(I,Z);
    R_h_tot = zeros(I,Z);
    G_hor_master = zeros(I,Z);
    G_t_h_b = zeros(I,Z);
    G_t_h_d = zeros(I,Z);
    G_t_h_r = zeros(I,Z);
    G_t_h = zeros(I,Z);

% Define master insolation (hor) matrix
    G_hor_master(:,1) = InsolationData_hor_1;  % January data - horizontal insolation
    G_hor_master(:,2) = InsolationData_hor_2;  % February data - horizontal insolation
    G_hor_master(:,3) = InsolationData_hor_3;  % March data - horizontal insolation
    G_hor_master(:,4) = InsolationData_hor_4;  % April data - horizontal insolation
    G_hor_master(:,5) = InsolationData_hor_5;  % May data - horizontal insolation
    G_hor_master(:,6) = InsolationData_hor_6;  % June data - horizontal insolation
    G_hor_master(:,7) = InsolationData_hor_7;  % July data - horizontal insolation
    G_hor_master(:,8) = InsolationData_hor_8;  % August data - horizontal insolation
    G_hor_master(:,9) = InsolationData_hor_9;  % September data - horizontal insolation
    G_hor_master(:,10) = InsolationData_hor_10;  % October data - horizontal insolation
    G_hor_master(:,11) = InsolationData_hor_11;  % November data - horizontal insolation
    G_hor_master(:,12) = InsolationData_hor_12;  % December data - horizontal insolation

% Vectors (scalars per month) (1 x N)
for n=1:Z
    B(n) = 360/364*(Z_v(n)-81);
    ET(n) = 9.87*sind(2*B(n))-7.53*cosd(B(n))-1.5*sind(B(n));
    SolarTimeDiff(n) = ET(n)+(STM - abs(long))*4;
    d_s(n) = asind(sind(23.45)*sind(360/365*(284+Z_v(n))));
end
```

```
% Matrices (vectors per month) (I=96 x N)
for n=1:Z
    SolarTime(:,n) = TimesVector_min+SolarTimeDiff(n);
    MFLSN(:,n) = SolarTime(:,n)-720;
    h_s(:,n) = MFLSN(:,n)/4;
    alpha(:,n) = asind(sind(lat).*sind(d_s(n))+cosd(lat)*cosd(d_s(n)).*cosd(h_s(:,n)));
%{
    % RESTRICTION 1: After calculate alpha, make sure alpha>=0
        for jjj=1:I
            if alpha(jjj,n)<0
                alpha(jjj,n) = 0;
            end
        end
%}
    a_s(:,n) = asind(cosd(d_s(n))*sind(h_s(:,n))./cosd(alpha(:,n)));
    i(:,n) = acosd(cosd(alpha(:,n)).*cosd(a_s(:,n)-
a_w).*sind(beta)+sind(alpha(:,n))*cosd(beta));
%{
    % RESTRICTION 2: After calculate i, make sure i<=90 (because cos(i) cannot be
negative)
        for jjj=1:I
            if i(jjj,n)>90
                i(jjj,n) = 90;
            end
        end
%}

% Insolation Tilt Factors
    R_h_b(:,n) = cosd(i(:,n))./sind(alpha(:,n));
    R_h_d(:,n) = C(n)*(cosd(beta/2))^2./sind(alpha(:,n));
    R_h_r(:,n) = rho_c*((sind(alpha(:,n))+C(n))*(sind(beta/2))^2)./sind(alpha(:,n));
    R_h_tot (:,n) = R_h_b(:,n) + R_h_d(:,n) + R_h_r(:,n);

% Insolation Components
    G_t_h_b(:,n) = G_hor_master(:,n) .* R_h_b(:,n);
    G_t_h_d(:,n) = G_hor_master(:,n) .* R_h_d(:,n);
    G_t_h_r(:,n) = G_hor_master(:,n) .* R_h_r(:,n);
end

G_t_h = G_t_h_b + G_t_h_d + G_t_h_r;


figure(60);
plot(TimesVector,G_t_h(:,1),'-ob','LineWidth',2,'MarkerSize',5,'MarkerFaceColor','b')
hold on
plot(TimesVector,G_t_h(:,2),'-og','LineWidth',2,'MarkerSize',5,'MarkerFaceColor','g')
hold on
plot(TimesVector,G_t_h(:,3),'-or','LineWidth',2,'MarkerSize',5,'MarkerFaceColor','r')
hold on
plot(TimesVector,G_t_h(:,4),'-oc','LineWidth',2,'MarkerSize',5,'MarkerFaceColor','c')
hold on
plot(TimesVector,G_t_h(:,5),'-om','LineWidth',2,'MarkerSize',5,'MarkerFaceColor','m')
hold on
plot(TimesVector,G_t_h(:,6),'-ok','LineWidth',2,'MarkerSize',5,'MarkerFaceColor','k')
hold on
plot(TimesVector,G_t_h(:,7),'-^b','LineWidth',2,'MarkerSize',5,'MarkerFaceColor','b')
hold on
plot(TimesVector,G_t_h(:,8),'-^g','LineWidth',2,'MarkerSize',5,'MarkerFaceColor','g')
hold on
plot(TimesVector,G_t_h(:,9),'-^r','LineWidth',2,'MarkerSize',5,'MarkerFaceColor','r')
hold on
plot(TimesVector,G_t_h(:,10),'-^c','LineWidth',2,'MarkerSize',5,'MarkerFaceColor','c')
hold on
plot(TimesVector,G_t_h(:,11),'-^m','LineWidth',2,'MarkerSize',5,'MarkerFaceColor','m')
hold on
plot(TimesVector,G_t_h(:,12),'-^k','LineWidth',2,'MarkerSize',5,'MarkerFaceColor','k')
```

```
title(['Calculated Insolation Incident on Collector for 2005'],'fontsize',23)
xlabel('Local Time of Day','fontsize',18)
ylabel('Insolation collected during time interval, W-hr/m^2','fontsize',18)
%axis square
axis([0 24 0 1500])
set(gca,'YTick',0:100:1500)
set(gca,'XTick',0:3:24)
set(gca,'XTickLabel',{'00:00','03:00','06:00','09:00','12:00','15:00','18:00','21:00','24
:00'},'fontsize',15)
legend('Jan','Feb','Mar','Apr','May','Jun','Jul','Aug','Sept','Oct','Nov','Dec','Location
','NorthEast')
grid on

figure(61);
plot(TimesVector,R_h_tot(:,1),'-ob','LineWidth',2,'MarkerSize',5,'MarkerFaceColor','b')
hold on
plot(TimesVector,R_h_tot(:,2),'-og','LineWidth',2,'MarkerSize',5,'MarkerFaceColor','g')
hold on
plot(TimesVector,R_h_tot(:,3),'-or','LineWidth',2,'MarkerSize',5,'MarkerFaceColor','r')
hold on
plot(TimesVector,R_h_tot(:,4),'-oc','LineWidth',2,'MarkerSize',5,'MarkerFaceColor','c')
hold on
plot(TimesVector,R_h_tot(:,5),'-om','LineWidth',2,'MarkerSize',5,'MarkerFaceColor','m')
hold on
plot(TimesVector,R_h_tot(:,6),'-ok','LineWidth',2,'MarkerSize',5,'MarkerFaceColor','k')
hold on
plot(TimesVector,R_h_tot(:,7),'-^b','LineWidth',2,'MarkerSize',5,'MarkerFaceColor','b')
hold on
plot(TimesVector,R_h_tot(:,8),'-^g','LineWidth',2,'MarkerSize',5,'MarkerFaceColor','g')
hold on
plot(TimesVector,R_h_tot(:,9),'-^r','LineWidth',2,'MarkerSize',5,'MarkerFaceColor','r')
hold on
plot(TimesVector,R_h_tot(:,10),'-^c','LineWidth',2,'MarkerSize',5,'MarkerFaceColor','c')
hold on
plot(TimesVector,R_h_tot(:,11),'-^m','LineWidth',2,'MarkerSize',5,'MarkerFaceColor','m')
hold on
plot(TimesVector,R_h_tot(:,12),'-^k','LineWidth',2,'MarkerSize',5,'MarkerFaceColor','k')

title(['Calculated Insolation Factor \itF^''_T_O_T \rm for 2005'],'fontsize',23)
xlabel('Local Time of Day','fontsize',18)
%ylabel('','fontsize',18)
%axis square
bla=5;
axis([0 24 0 bla])
set(gca,'XTick',0:3:24)
set(gca,'YTick',0:0.5:bla)
set(gca,'XTickLabel',{'00:00','03:00','06:00','09:00','12:00','15:00','18:00','21:00','24
:00'},'fontsize',15)
legend('Jan','Feb','Mar','Apr','May','Jun','Jul','Aug','Sept','Oct','Nov','Dec','Location
','NorthEast')
grid on

%}

% Per month basis ------------------------------------------------------
    % Note: Necessary angle restrictions not placed
C = SkyDiffuseFactorPerMonth(MONTH);
B = 360/364*(Z_v(MONTH)-81);
ET = 9.87*sind(2*B)-7.53*cosd(B)-1.5*sind(B);
SolarTimeDiff = ET+(STM - abs(long))*4;
SolarTime = TimesVector_min+SolarTimeDiff;
MFLSN = SolarTime-720;  % vector
h_s = MFLSN/4;  % vector
d_s = asind(sind(23.45)*sind(360/365*(284+Z_v(MONTH))));
alpha = asind(sind(lat)*sind(d_s)+cosd(lat)*cosd(d_s)*cosd(h_s));
```

```
a_s = asind(cosd(d_s)*sind(h_s)./cosd(alpha));
i = acosd(cosd(alpha).*cosd(a_s-a_w).*sind(beta)+sind(alpha)*cosd(beta));

% Insolation Tilt Factors (from horizontal data)
R_h_b = cosd(i)./sind(alpha);
R_h_d = C*(cosd(beta/2))^2./sind(alpha);
R_h_r = rho_c*((sind(alpha)+C)*(sind(beta/2))^2)./sind(alpha);
R_h_tot = R_h_b + R_h_d + R_h_r;

% Insolation components (from horizontal data)
G_t_h_b = G_hor.*R_h_b;
G_t_h_d = G_hor.*R_h_d;
G_t_h_r = G_hor.*R_h_r;
G_t_h = G_t_h_b + G_t_h_d + G_t_h_r;
%}

% Plots
figure(10);
plot(TimesVector,R_h_b,'-rd','LineWidth',2,'MarkerSize',4,'MarkerFaceColor','r')
hold on
plot(TimesVector,R_h_d,'-bd','LineWidth',2,'MarkerSize',4,'MarkerFaceColor','b')
hold on
plot(TimesVector,R_h_r,'-gd','LineWidth',2,'MarkerSize',4,'MarkerFaceColor','g')

title(['Correction (Tilt) Factors (for horizontal insolation) on
',num2str(Label)],'fontsize',23)
xlabel('Local Time of Day','fontsize',18)
axis square
%axis([0 24 0 1300])
%set(gca,'YTick',0:100:1300)
set(gca,'XTick',0:3:24)
set(gca,'XTickLabel',{'00:00','03:00','06:00','09:00','12:00','15:00','18:00','21:00','24
:00'},'fontsize',15)
legend('Beam/Direct','Diffuse','Reflected','Location','NorthEastOutside')
grid on


figure(11);
plot (TimesVector,G_hor,'-bd','LineWidth',2,'MarkerSize',4,'MarkerFaceColor','b')
hold on
plot (TimesVector,G_t_h,'-kd','LineWidth',2,'MarkerSize',4,'MarkerFaceColor','k')

title(['Insolation for Detroit, MI on ',num2str(Label)],'fontsize',23)  % Don't forget
the damn brackets around the title's text!
xlabel('Local Time of Day','fontsize',18)
ylabel('Insolation collected during time interval, W-hr/m^2','fontsize',18)
axis square
%axis([0 24 0 1300])
%set(gca,'YTick',0:100:1300)
set(gca,'XTick',0:3:24)
set(gca,'XTickLabel',{'00:00','03:00','06:00','09:00','12:00','15:00','18:00','21:00','24
:00'},'fontsize',15)
legend('Horizontal','Tilted','Location','NorthEastOutside')
grid on
%}
```

B.2.10 Convert_Insolation_normal.m

```
function
[B,ET,SolarTimeDiff,d_s,SolarTime,MFLSN,h_s,alpha,a_s,i,R_n_b,R_n_d,R_n_r,R_n_tot,G_t_n_b
,G_t_n_d,G_t_n_r,G_t_n,C,G_normal_master] =
Convert_Insolation_normal(TimesVector,MONTH,SkyDiffuseFactorPerMonth,Z,Z_v,I,STM,lat,long
,beta,a_w,rho_c,G_normal,Label,InsolationData_normal_1,InsolationData_normal_2,Insolation
Data_normal_3,InsolationData_normal_4,InsolationData_normal_5,InsolationData_normal_6,Ins
olationData_normal_7,InsolationData_normal_8,InsolationData_normal_9,InsolationData_norma
l_10,InsolationData_normal_11,InsolationData_normal_12)
%User-defined function:
% This function converts insolation data from a normal surface to a
% tilted surface.
% G_t_n is the tilted insolation calculated from normal data

TimesVector_min = TimesVector*60;
G_normal_master = zeros(I,Z);

% CHOOSE TOP HALF (ALL 12 MONTHS) OR BOTTOM HALF (PER MONTH)

%{
% All 12 months ------------------------------------------------------------
    % Initialize vectors/matrices as needed
    C = SkyDiffuseFactorPerMonth';
    B = zeros(Z,1)';
    ET = zeros(Z,1)';
    d_s = zeros(Z,1)';
    SolarTimeDiff = zeros(Z,1)';
    SolarTime = zeros(I,Z);
    MFLSN = zeros(I,Z);
    h_s = zeros(I,Z);
    alpha = zeros(I,Z);
    a_s = zeros(I,Z);
    i = zeros(I,Z);
    R_n_b = zeros(I,Z);
    R_n_d = zeros(I,Z);
    R_n_r = zeros(I,Z);
    R_n_tot = zeros(I,Z);
    G_normal_master = zeros(I,Z);
    G_t_n_b = zeros(I,Z);
    G_t_n_d = zeros(I,Z);
    G_t_n_r = zeros(I,Z);
    G_t_n = zeros(I,Z);

% Define master insolation (hor) matrix
    G_normal_master(:,1) = InsolationData_normal_1;  % January data - normal insolation
    G_normal_master(:,2) = InsolationData_normal_2;  % February data - normal insolation
    G_normal_master(:,3) = InsolationData_normal_3;  % March data - normal insolation
    G_normal_master(:,4) = InsolationData_normal_4;  % April data - normal insolation
    G_normal_master(:,5) = InsolationData_normal_5;  % May data - normal insolation
    G_normal_master(:,6) = InsolationData_normal_6;  % June data - normal insolation
    G_normal_master(:,7) = InsolationData_normal_7;  % July data - normal insolation
    G_normal_master(:,8) = InsolationData_normal_8;  % August data - normal insolation
    G_normal_master(:,9) = InsolationData_normal_9;  % September data - normal insolation
    G_normal_master(:,10) = InsolationData_normal_10;  % October data - normal insolation
    G_normal_master(:,11) = InsolationData_normal_11;  % November data - normal
insolation
    G_normal_master(:,12) = InsolationData_normal_12;  % December data - normal
insolation

% Vectors (scalars per month) (1 x N)
for n=1:Z
    B(n) = 360/364*(Z_v(n)-81);
    ET(n) = 9.87*sind(2*B(n))-7.53*cosd(B(n))-1.5*sind(B(n));
    SolarTimeDiff(n) = ET(n)+(STM - abs(long))*4;
    d_s(n) = asind(sind(23.45)*sind(360/365*(284+Z_v(n))));
```

```
end

% Matrices (vectors per month) (I=96 x N)
for n=1:Z
    SolarTime(:,n) = TimesVector_min+SolarTimeDiff(n);
    MFLSN(:,n) = SolarTime(:,n)-720;
    h_s(:,n) = MFLSN(:,n)/4;
    alpha(:,n) = asind(sind(lat).*sind(d_s(n))+cosd(lat)*cosd(d_s(n)).*cosd(h_s(:,n)));
    % RESTRICTION 1: After calculate alpha, make sure alpha>=0
        for jjj=1:I
            if alpha(jjj,n)<0
                alpha(jjj,n) = 0;
            end
        end
    a_s(:,n) = asind(cosd(d_s(n))*sind(h_s(:,n))./cosd(alpha(:,n)));
    i(:,n) = acosd(cosd(alpha(:,n)).*cosd(a_s(:,n)-
a_w).*sind(beta)+sind(alpha(:,n))*cosd(beta));
    % RESTRICTION 2: After calculate i, make sure i<=90 (because cos(i) cannot be
negative)
        for jjj=1:I
            if i(jjj,n)>90
                i(jjj,n) = 90;
            end
        end

% Insolation Tilt Factors
    R_n_b(:,n) = cosd(i(:,n));
    R_n_d(:,n) = C(n)*(cosd(beta/2))^2;
    R_n_r(:,n) = rho_c*((sind(alpha(:,n))+C(n))*(sind(beta/2))^2);
    R_n_tot (:,n) = R_n_b(:,n) + R_n_d(:,n) + R_n_r(:,n);

% Insolation Components
    G_t_n_b(:,n) = G_normal_master(:,n) .* R_n_b(:,n);
    G_t_n_d(:,n) = G_normal_master(:,n) .* R_n_d(:,n);
    G_t_n_r(:,n) = G_normal_master(:,n) .* R_n_r(:,n);
end

G_t_n = G_t_n_b + G_t_n_d + G_t_n_r;


figure(50);
plot(TimesVector,G_t_n(:,1),'-ob','LineWidth',2,'MarkerSize',5,'MarkerFaceColor','b')
hold on
plot(TimesVector,G_t_n(:,2),'-og','LineWidth',2,'MarkerSize',5,'MarkerFaceColor','g')
hold on
plot(TimesVector,G_t_n(:,3),'-or','LineWidth',2,'MarkerSize',5,'MarkerFaceColor','r')
hold on
plot(TimesVector,G_t_n(:,4),'-oc','LineWidth',2,'MarkerSize',5,'MarkerFaceColor','c')
hold on
plot(TimesVector,G_t_n(:,5),'-om','LineWidth',2,'MarkerSize',5,'MarkerFaceColor','m')
hold on
plot(TimesVector,G_t_n(:,6),'-ok','LineWidth',2,'MarkerSize',5,'MarkerFaceColor','k')
hold on
plot(TimesVector,G_t_n(:,7),'-^b','LineWidth',2,'MarkerSize',5,'MarkerFaceColor','b')
hold on
plot(TimesVector,G_t_n(:,8),'-^g','LineWidth',2,'MarkerSize',5,'MarkerFaceColor','g')
hold on
plot(TimesVector,G_t_n(:,9),'-^r','LineWidth',2,'MarkerSize',5,'MarkerFaceColor','r')
hold on
plot(TimesVector,G_t_n(:,10),'-^c','LineWidth',2,'MarkerSize',5,'MarkerFaceColor','c')
hold on
plot(TimesVector,G_t_n(:,11),'-^m','LineWidth',2,'MarkerSize',5,'MarkerFaceColor','m')
hold on
plot(TimesVector,G_t_n(:,12),'-^k','LineWidth',2,'MarkerSize',5,'MarkerFaceColor','k')

title(['Calculated Insolation Incident on Collector for 2005'],'fontsize',23)
```

```
xlabel('Local Time of Day','fontsize',18)
ylabel('Insolation collected during time interval, W-hr/m^2','fontsize',18)
%axis square
axis([0 24 0 1500])
set(gca,'YTick',0:100:1500)
set(gca,'XTick',0:3:24)
set(gca,'XTickLabel',{'00:00','03:00','06:00','09:00','12:00','15:00','18:00','21:00','24
:00'},'fontsize',15)
legend('Jan','Feb','Mar','Apr','May','Jun','Jul','Aug','Sept','Oct','Nov','Dec','Location
','NorthEast')
grid on

figure(51);
plot(TimesVector,R_n_tot(:,1),'-ob','LineWidth',2,'MarkerSize',5,'MarkerFaceColor','b')
hold on
plot(TimesVector,R_n_tot(:,2),'-og','LineWidth',2,'MarkerSize',5,'MarkerFaceColor','g')
hold on
plot(TimesVector,R_n_tot(:,3),'-or','LineWidth',2,'MarkerSize',5,'MarkerFaceColor','r')
hold on
plot(TimesVector,R_n_tot(:,4),'-oc','LineWidth',2,'MarkerSize',5,'MarkerFaceColor','c')
hold on
plot(TimesVector,R_n_tot(:,5),'-om','LineWidth',2,'MarkerSize',5,'MarkerFaceColor','m')
hold on
plot(TimesVector,R_n_tot(:,6),'-ok','LineWidth',2,'MarkerSize',5,'MarkerFaceColor','k')
hold on
plot(TimesVector,R_n_tot(:,7),'-^b','LineWidth',2,'MarkerSize',5,'MarkerFaceColor','b')
hold on
plot(TimesVector,R_n_tot(:,8),'-^g','LineWidth',2,'MarkerSize',5,'MarkerFaceColor','g')
hold on
plot(TimesVector,R_n_tot(:,9),'-^r','LineWidth',2,'MarkerSize',5,'MarkerFaceColor','r')
hold on
plot(TimesVector,R_n_tot(:,10),'-^c','LineWidth',2,'MarkerSize',5,'MarkerFaceColor','c')
hold on
plot(TimesVector,R_n_tot(:,11),'-^m','LineWidth',2,'MarkerSize',5,'MarkerFaceColor','m')
hold on
plot(TimesVector,R_n_tot(:,12),'-^k','LineWidth',2,'MarkerSize',5,'MarkerFaceColor','k')

title(['Calculated Insolation Factor \itF_T_O_T\rm for 2005'],'fontsize',23)
xlabel('Local Time of Day','fontsize',18)
%ylabel('','fontsize',18)
%axis square
axis([0 24 0 1.2])
set(gca,'XTick',0:3:24)
set(gca,'YTick',0:0.1:1.2)
set(gca,'XTickLabel',{'00:00','03:00','06:00','09:00','12:00','15:00','18:00','21:00','24
:00'},'fontsize',15)
legend('Jan','Feb','Mar','Apr','May','Jun','Jul','Aug','Sept','Oct','Nov','Dec','Location
','NorthEast')
grid on

%}

% Per month basis ------------------------------------------------------
C = SkyDiffuseFactorPerMonth(MONTH);
B = 360/364*(Z_v(MONTH)-81);
ET = 9.87*sind(2*B)-7.53*cosd(B)-1.5*sind(B);
SolarTimeDiff = ET+(STM - abs(long))*4;
SolarTime = TimesVector_min+SolarTimeDiff;
MFLSN = SolarTime-720;  % vector
h_s = MFLSN/4;  % vector
d_s = asind(sind(23.45)*sind(360/365*(284+Z_v(MONTH))));
alpha = asind(sind(lat)*sind(d_s)+cosd(lat)*cosd(d_s)*cosd(h_s));
    % RESTRICTION 1: After calculate alpha, make sure alpha>=0
    for jjj=1:I
            if alpha(jjj)<0
                alpha(jjj) = 0;
```

```
            end
    end
a_s = asind(cosd(d_s)*sind(h_s)./cosd(alpha));
i = acosd(cosd(alpha).*cosd(a_s-a_w).*sind(beta)+sind(alpha)*cosd(beta));
    % RESTRICTION 2: After calculate i, make sure i<=90 (because cos(i) cannot be
negative)
        for jjj=1:I
            if i(jjj)>90
                i(jjj) = 90;
            end
        end

% Insolation Tilt Factors (from normal data)
R_n_b = cosd(i);
R_n_d = C*(cosd(beta/2))^2;
R_n_r = rho_c*((sind(alpha)+C)*(sind(beta/2))^2);
R_n_tot = R_n_b + R_n_d + R_n_r;

% Insolation components (from normal data)
G_t_n_b = G_normal.*R_n_b;
G_t_n_d = G_normal.*R_n_d;
G_t_n_r = G_normal.*R_n_r;
G_t_n = G_t_n_b + G_t_n_d + G_t_n_r;
%}

% Plots
figure(20);
plot(TimesVector,R_n_b,'-dr','LineWidth',2,'MarkerSize',4,'MarkerFaceColor','r')
hold on
plot(TimesVector,R_n_d,'-db','LineWidth',2,'MarkerSize',4,'MarkerFaceColor','b')
hold on
plot(TimesVector,R_n_r,'-dg','LineWidth',2,'MarkerSize',4,'MarkerFaceColor','g')

title(['Correction (Tilt) Factors (for normal insolation) on
',num2str(Label)],'fontsize',23)
xlabel('Local Time of Day','fontsize',18)
axis square
axis([0 24 0 1])
set(gca,'XTick',0:3:24)
set(gca,'XTickLabel',{'00:00','03:00','06:00','09:00','12:00','15:00','18:00','21:00','24
:00'},'fontsize',15)
legend('Beam/Direct','Diffuse','Reflected','Location','NorthEast')
grid on
%}

figure(21);
plot (TimesVector,G_normal,'-bd','LineWidth',2,'MarkerSize',4,'MarkerFaceColor','b')
hold on
plot (TimesVector,G_t_n,'-kd','LineWidth',2,'MarkerSize',4,'MarkerFaceColor','k')

title(['Insolation for Detroit, MI on ',num2str(Label)],'fontsize',23)  % Don't forget
the damn brackets around the title's text!
xlabel('Local Time of Day','fontsize',18)
ylabel('Insolation collected during time interval, W-hr/m^2','fontsize',18)
axis square
axis([0 24 0 1500])
set(gca,'YTick',0:100:1500)
set(gca,'XTick',0:3:24)
set(gca,'XTickLabel',{'00:00','03:00','06:00','09:00','12:00','15:00','18:00','21:00','24
:00'},'fontsize',15)
legend('Normal','Tilted','Location','NorthEast')
grid on
%}
```

B.2.11 Plot_Calculated_Insolation.m

```
function Plot_Calculated_Insolation(TimesVector,G_hor,G_t_h,G_normal,G_t_n,Label)
%User-defined function:
%This function plots the tilted insolation for all 12 representative days,
%calculated from the horizontal and normal insolation data. This only
%applies on a PER MONTH basis.

figure(30);
plot (TimesVector,G_hor,'-bd','LineWidth',2,'MarkerSize',4,'MarkerFaceColor','b')
hold on
plot (TimesVector,G_t_h,'-kd','LineWidth',2,'MarkerSize',4,'MarkerFaceColor','k')
hold on
plot (TimesVector,G_normal,'-gd','LineWidth',2,'MarkerSize',4,'MarkerFaceColor','g')
hold on
plot (TimesVector,G_t_n,'-rd','LineWidth',2,'MarkerSize',4,'MarkerFaceColor','r')


title(['Calculated tilted insolation on ',num2str(Label)],'fontsize',23)
xlabel('Local Time of Day','fontsize',18)
ylabel('Insolation collected during time interval, W-hr/m^2','fontsize',18)
axis square
axis([0 24 0 1600])
set(gca,'YTick',0:100:1600)
set(gca,'XTick',0:3:24)
set(gca,'XTickLabel',{'00:00','03:00','06:00','09:00','12:00','15:00','18:00','21:00','24
:00'},'fontsize',15)
legend('Horizontal','Tilted (H)','Normal','Tilted (N)','Location','NorthEastOutside')
grid on
```

B.2.12 Convert_C_to_F.m

```
function Temp_F = Convert_C_to_F(Temp_C)
%User-defined function:
%This funtion converts a temperature from [C] to [F]

Temp_F = (Temp_C*9/5)+32;
```

B.2.13 Plot_Insolation_SingleDay.m

```
function Plot_Insolation_SingleDay(TimesVector,G,Label)
%User-defined function:
%This function plots Insolation for a single day, based on month chosen.

%plot(Vector1_X,Vector1_Y,'bd','MarkerSize',5,'MarkerFaceColor','b')
plot(TimesVector,G,'-bd','MarkerSize',5,'MarkerFaceColor','b')
title(['Insolation Incident on Collector for Detroit, MI on
',num2str(Label)],'fontsize',23)  % Don't forget the damn brackets around the title's
text!
xlabel('Local Time of Day','fontsize',18)
ylabel('Insolation collected during time interval, W-hr/m^2','fontsize',18)
axis square
axis([0 24 0 1500])
set(gca,'YTick',0:100:1500)
set(gca,'XTick',0:3:24)
set(gca,'XTickLabel',{'00:00','03:00','06:00','09:00','12:00','15:00','18:00','21:00','24
:00'},'fontsize',15)
%legend('Ambient Temperature Data Data', 'Location','NorthWest')
%legend('SS','WS')
grid on
```

B.2.14 Plot_Insolation_hor_All.m

```
function
Plot_Insolation_hor_All(TimesVector,InsolationData_hor_1,InsolationData_hor_2,InsolationD
ata_hor_3,InsolationData_hor_4,InsolationData_hor_5,InsolationData_hor_6,InsolationData_h
or_7,InsolationData_hor_8,InsolationData_hor_9,InsolationData_hor_10,InsolationData_hor_1
1,InsolationData_hor_12)
%User-defined function:
%This function plots Insolation for all 12 representative days

plot(TimesVector,InsolationData_hor_1,'ob','MarkerSize',4,'MarkerFaceColor','b')
hold on
plot(TimesVector,InsolationData_hor_2,'og','MarkerSize',4,'MarkerFaceColor','g')
hold on
plot(TimesVector,InsolationData_hor_3,'or','MarkerSize',4,'MarkerFaceColor','r')
hold on
plot(TimesVector,InsolationData_hor_4,'oc','MarkerSize',4,'MarkerFaceColor','c')
hold on
plot(TimesVector,InsolationData_hor_5,'om','MarkerSize',4,'MarkerFaceColor','m')
hold on
plot(TimesVector,InsolationData_hor_6,'ok','MarkerSize',4,'MarkerFaceColor','k')
hold on
plot(TimesVector,InsolationData_hor_7,'^b','MarkerSize',5,'MarkerFaceColor','b')
hold on
plot(TimesVector,InsolationData_hor_8,'^g','MarkerSize',5,'MarkerFaceColor','g')
hold on
plot(TimesVector,InsolationData_hor_9,'^r','MarkerSize',5,'MarkerFaceColor','r')
hold on
plot(TimesVector,InsolationData_hor_10,'^c','MarkerSize',5,'MarkerFaceColor','c')
hold on
plot(TimesVector,InsolationData_hor_11,'^m','MarkerSize',5,'MarkerFaceColor','m')
hold on
plot(TimesVector,InsolationData_hor_12,'^k','MarkerSize',5,'MarkerFaceColor','k')
hold on

title(['Representative Extraterrestrial Insolation (Horizontal) Data for
2005'],'fontsize',23)
xlabel('Local Time of Day','fontsize',18)
ylabel('Insolation collected during time interval, W-hr/m^2','fontsize',18)
axis square
axis([0 24 0 1500])
set(gca,'YTick',0:100:1500)
set(gca,'XTick',0:3:24)
set(gca,'XTickLabel',{'00:00','03:00','06:00','09:00','12:00','15:00','18:00','21:00','24
:00'},'fontsize',15)
legend('Jan','Feb','Mar','Apr','May','Jun','Jul','Aug','Sept','Oct','Nov','Dec','Location
','NorthEastOutside')
%legend('January','February','March','April','May','June','July','August','September','Oc
tober','November','December','Location','NorthWest')
%legend('1/20','2/18','3/20','4/20','5/21','6/21','7/22','8/22','9/22','10/22','11/21','1
2/21')
grid on
```

B.2.15 Plot_Insolation_normal_All.m

```
function
Plot_Insolation_normal_All(TimesVector,InsolationData_normal_1,InsolationData_normal_2,In
solationData_normal_3,InsolationData_normal_4,InsolationData_normal_5,InsolationData_norm
al_6,InsolationData_normal_7,InsolationData_normal_8,InsolationData_normal_9,InsolationDa
ta_normal_10,InsolationData_normal_11,InsolationData_normal_12)
%User-defined function:
%This function plots Insolation for all 12 representative days

%plot(TimesVector,InsolationData_normal_1,'-ob','MarkerSize',4,'MarkerFaceColor','b')
plot(TimesVector,InsolationData_normal_1,'-b','LineWidth',2)
hold on
%plot(TimesVector,InsolationData_normal_2,'-og','MarkerSize',4,'MarkerFaceColor','g')
plot(TimesVector,InsolationData_normal_2,'-g','LineWidth',2)
hold on
%plot(TimesVector,InsolationData_normal_3,'-or','MarkerSize',4,'MarkerFaceColor','r')
plot(TimesVector,InsolationData_normal_3,'-r','LineWidth',2)
hold on
%plot(TimesVector,InsolationData_normal_4,'-oc','MarkerSize',4,'MarkerFaceColor','c')
plot(TimesVector,InsolationData_normal_4,'-c','LineWidth',2)
hold on
%plot(TimesVector,InsolationData_normal_5,'-om','MarkerSize',4,'MarkerFaceColor','m')
plot(TimesVector,InsolationData_normal_5,'-m','LineWidth',2)
hold on
%plot(TimesVector,InsolationData_normal_6,'-ok','MarkerSize',4,'MarkerFaceColor','k')
plot(TimesVector,InsolationData_normal_6,'-k','LineWidth',2)
hold on
%plot(TimesVector,InsolationData_normal_7,'-db','MarkerSize',5,'MarkerFaceColor','b')
plot(TimesVector,InsolationData_normal_7,'--b','LineWidth',2)
hold on
%plot(TimesVector,InsolationData_normal_8,'-dg','MarkerSize',5,'MarkerFaceColor','g')
plot(TimesVector,InsolationData_normal_8,'--g','LineWidth',2)
hold on
%plot(TimesVector,InsolationData_normal_9,'-dr','MarkerSize',5,'MarkerFaceColor','r')
plot(TimesVector,InsolationData_normal_9,'--r','LineWidth',2)
hold on
%plot(TimesVector,InsolationData_normal_10,'-dc','MarkerSize',5,'MarkerFaceColor','c')
plot(TimesVector,InsolationData_normal_10,'--c','LineWidth',2)
hold on
%plot(TimesVector,InsolationData_normal_11,'-dm','MarkerSize',5,'MarkerFaceColor','m')
plot(TimesVector,InsolationData_normal_11,'--m','LineWidth',2)
hold on
%plot(TimesVector,InsolationData_normal_12,'-dk','MarkerSize',5,'MarkerFaceColor','k')
plot(TimesVector,InsolationData_normal_12,'--k','LineWidth',2)
hold on

title(['Representative Extraterrestrial Insolation (Normal) Data for
2005'],'fontsize',23)
xlabel('Local Time of Day','fontsize',18)
ylabel('Insolation collected during time interval, W-hr/m^2','fontsize',18)
axis square
axis([0 24 0 1500])
set(gca,'YTick',0:100:1500)
set(gca,'XTick',0:3:24)
set(gca,'XTickLabel',{'00:00','03:00','06:00','09:00','12:00','15:00','18:00','21:00','24
:00'},'fontsize',15)
legend('Jan','Feb','Mar','Apr','May','Jun','Jul','Aug','Sept','Oct','Nov','Dec','Location
','NorthEastOutside')
%legend('January','February','March','April','May','June','July','August','September','Oc
tober','November','December','Location','NorthWest')
%legend('1/20','2/18','3/20','4/20','5/21','6/21','7/22','8/22','9/22','10/22','11/21','1
2/21')
grid on
```

B.2.16 Plot_Temperature_All.m

```
function
Plot_Temperature_All(TimesVector,TempData_1_F,TempData_2_F,TempData_3_F,TempData_4_F,Temp
Data_5_F,TempData_6_F,TempData_7_F,TempData_8_F,TempData_9_F,TempData_10_F,TempData_11_F,
TempData_12_F)
%User-defined function:
%This function plots Ambient Temperature for all 12 representative days

plot(TimesVector,TempData_1_F,'-ob','MarkerSize',4,'MarkerFaceColor','b')
hold on
plot(TimesVector,TempData_2_F,'-og','MarkerSize',4,'MarkerFaceColor','g')
hold on
plot(TimesVector,TempData_3_F,'-or','MarkerSize',4,'MarkerFaceColor','r')
hold on
plot(TimesVector,TempData_4_F,'-oc','MarkerSize',4,'MarkerFaceColor','c')
hold on
plot(TimesVector,TempData_5_F,'-om','MarkerSize',4,'MarkerFaceColor','m')
hold on
plot(TimesVector,TempData_6_F,'-ok','MarkerSize',4,'MarkerFaceColor','k')
hold on
plot(TimesVector,TempData_7_F,'-^b','MarkerSize',5,'MarkerFaceColor','b')
hold on
plot(TimesVector,TempData_8_F,'-^g','MarkerSize',5,'MarkerFaceColor','g')
hold on
plot(TimesVector,TempData_9_F,'-^r','MarkerSize',5,'MarkerFaceColor','r')
hold on
plot(TimesVector,TempData_10_F,'-^c','MarkerSize',5,'MarkerFaceColor','c')
hold on
plot(TimesVector,TempData_11_F,'-^m','MarkerSize',5,'MarkerFaceColor','m')
hold on
plot(TimesVector,TempData_12_F,'-^k','MarkerSize',5,'MarkerFaceColor','k')
hold on

title(['Representative Ambient Temperature Data for 2005'],'fontsize',23)
xlabel('Local Time of Day','fontsize',18)
ylabel('Ambient Temperature, \circF','fontsize',18)
axis square
axis([0 24 0 90])
set(gca,'YTick',0:5:90)
set(gca,'XTick',0:3:24)
set(gca,'XTickLabel',{'00:00','03:00','06:00','09:00','12:00','15:00','18:00','21:00','24
:00'},'fontsize',15)
legend('Jan','Feb','Mar','Apr','May','Jun','Jul','Aug','Sept','Oct','Nov','Dec','Location
','NorthEastOutside')
%legend('January','February','March','April','May','June','July','August','September','Oc
tober','November','December','Location','NorthWest')
%legend('1/20','2/18','3/20','4/20','5/21','6/21','7/22','8/22','9/22','10/22','11/21','1
2/21')
grid on
```

B.2.17 Plot_Solution.m

```
function
Plot_Solution(t,T_c_amb_F,T_s_F,M,T_s_max_F,T_TEG_in_min_F,T_s_amb_F,N,Label,t_end_axis,d
t_axis,MONTH,aa,bb,cc,dd,ee,ff,gg,hh,ii,jj,kk,ll,mm,nn,oo,pp,qq)
%User-defined function:
%This function is the solution plot!

plot(t,T_c_amb_F,'b^','MarkerSize',5,'MarkerFaceColor','b')
hold on
plot(t,T_s_F,'kd','MarkerSize',5,'MarkerFaceColor','k')
line([0 t(M)],[T_s_max_F T_s_max_F],'Color','r')  % Storage maximum temp
%line([0 t(M)],[T_TEG_in_max_F T_TEG_in_max_F],'Color','r')  % TEG's HOT IN maximum temp
(same as T_s_max_F)
line([0 t(M)],[T_TEG_in_min_F T_TEG_in_min_F],'Color','g')  % TEG's HOT IN temp (based on
TEG's spec sheet)
line([0 t(M)],[T_s_amb_F T_s_amb_F],'Color','k')

title(['Temperature Plots for ',num2str(N),' consecutive ',num2str(Label),'
days'],'fontsize',23)
xlabel('Time of Day, HRS','fontsize',18)
ylabel('Temperature, \circF','fontsize',18)
axis([0 t_end_axis 0 max(T_s_F)+20])
set(gca,'XTick',0:dt_axis:t_end_axis)
set(gca,'YTick',0:20:max(T_s_F)+20)
grid on

% Legend (two cases since T_S_AMB varies based on month)
if MONTH==5 || MONTH==6 || MONTH==7 || MONTH==8
    legend('T_S_C_,_A_M_B(t)','T_S(t)','T_H_,_I_N_,_M_A_X = T_S_,_M_A_X =
176\circF','T_H_,_I_N_,_M_I_N = 130\circF','T_S_,_A_M_B =
75\circF','Location','SouthEast')
end
if MONTH==1 || MONTH==2 || MONTH==3 || MONTH==4 || MONTH==9 || MONTH==10 || MONTH==11 ||
MONTH==12
    legend('T_S_C_,_A_M_B(t)','T_S(t)','T_H_,_I_N_,_M_A_X = T_S_,_M_A_X =
176\circF','T_H_,_I_N_,_M_I_N = 130\circF','T_S_,_A_M_B =
55\circF','Location','SouthEast')
end

% X-Axis stuff
if N==1

set(gca,'XTickLabel',{aa,bb,cc,dd,ee,ff,gg,hh,ii,jj,kk,ll,mm,nn,oo,pp,qq},'fontsize',15)
end
if N==2

set(gca,'XTickLabel',{aa,bb,cc,dd,ee,ff,gg,hh,ii,jj,kk,ll,mm,nn,oo,pp,qq},'fontsize',15)
end
if N==3
    set(gca,'XTickLabel',{aa,bb,cc,dd,ee,ff,gg,hh,ii,jj,kk,ll,mm},'fontsize',15)
end
if N==4

set(gca,'XTickLabel',{aa,bb,cc,dd,ee,ff,gg,hh,ii,jj,kk,ll,mm,nn,oo,pp,qq},'fontsize',15)
end
if N==5
    set(gca,'XTickLabel',{aa,bb,cc,dd,ee,ff,gg,hh,ii,jj,kk},'fontsize',15)
end
if N==6
    set(gca,'XTickLabel',{aa,bb,cc,dd,ee,ff,gg,hh,ii,jj,kk,ll,mm},'fontsize',15)
end
if N==7
    set(gca,'XTickLabel',{aa,bb,cc,dd,ee,ff,gg,hh,ii,jj,kk,ll,mm,nn,oo},'fontsize',15)
end
```

B.2.18 Plot_Collector_Results.m

```
function
Plot_Collector_Results(t,Qdot_u,C_c,t_end_axis,dt_axis,aa,bb,cc,dd,ee,ff,gg,hh,ii,jj,kk,l
l,mm,nn,oo,pp,qq,N)
%User-defined function:
%This plot applies to the solar collector.
%Note: The function “round2” used here was obtained from:
http://www.mathworks.com/matlabcentral/fileexchange/4261-round2

% AX(1) is x-axis and left y-axis; AX(2) is x-axis and right y-axis; H's are graphics
[AX,H1,H2] = plotyy(t,Qdot_u,t,C_c*round2(max(Qdot_u)-500,1000),'plot');
title('Solar collector''s useful power gain $\dot{Q_U}$, and ON/OFF
status','interpreter','latex','fontsize',23)
axis([0 t_end_axis round2(min(Qdot_u)-500,1000) round2(max(Qdot_u)+500,1000)])
xlabel('Time of Day, HRS','fontsize',18)
set(AX(1),'XTick',0:dt_axis:t_end_axis)
set(AX(2),'XTick',0:dt_axis:t_end_axis)
set(AX(1),'YTick',round2(min(Qdot_u)-500,1000):1000:round2(max(Qdot_u)+500,1000))
set(AX(1),'YColor','b','fontsize',15)
set(AX(2),'YTick', 0:round2(max(Qdot_u)-500,1000):round2(max(Qdot_u)-500,1000))
set(AX(2),'YTickLabel',{'0','1'},'YColor','r','fontsize',15)
set(get(AX(1),'Ylabel'),'String','Useful power gain, W','fontsize',18,'Color','b')  % I
think you "get" the axis when editing the labels only
set(get(AX(2),'Ylabel'),'String','ON/OFF','fontsize',18,'Color','r')
linkaxes(AX,'x');
linkaxes(AX,'y');
set(H1,'Color','b','Marker','d','MarkerSize',4,'MarkerFaceColor','b')
set(H2,'Color','r','LineStyle','-','LineWidth',2)
grid on

% X-Axis stuff
if N==1

set(AX(1),'XTickLabel',{aa,bb,cc,dd,ee,ff,gg,hh,ii,jj,kk,ll,mm,nn,oo,pp,qq},'fontsize',15
)

set(AX(2),'XTickLabel',{aa,bb,cc,dd,ee,ff,gg,hh,ii,jj,kk,ll,mm,nn,oo,pp,qq},'fontsize',15
)
end
if N==2

set(AX(1),'XTickLabel',{aa,bb,cc,dd,ee,ff,gg,hh,ii,jj,kk,ll,mm,nn,oo,pp,qq},'fontsize',15
)

set(AX(2),'XTickLabel',{aa,bb,cc,dd,ee,ff,gg,hh,ii,jj,kk,ll,mm,nn,oo,pp,qq},'fontsize',15
)
end
if N==3
    set(AX(1),'XTickLabel',{aa,bb,cc,dd,ee,ff,gg,hh,ii,jj,kk,ll,mm},'fontsize',15)
    set(AX(2),'XTickLabel',{aa,bb,cc,dd,ee,ff,gg,hh,ii,jj,kk,ll,mm},'fontsize',15)
end
if N==4

set(AX(1),'XTickLabel',{aa,bb,cc,dd,ee,ff,gg,hh,ii,jj,kk,ll,mm,nn,oo,pp,qq},'fontsize',15
)

set(AX(2),'XTickLabel',{aa,bb,cc,dd,ee,ff,gg,hh,ii,jj,kk,ll,mm,nn,oo,pp,qq},'fontsize',15
)
end
if N==5
    set(AX(1),'XTickLabel',{aa,bb,cc,dd,ee,ff,gg,hh,ii,jj,kk},'fontsize',15)
    set(AX(2),'XTickLabel',{aa,bb,cc,dd,ee,ff,gg,hh,ii,jj,kk},'fontsize',15)
end
if N==6
    set(AX(1),'XTickLabel',{aa,bb,cc,dd,ee,ff,gg,hh,ii,jj,kk,ll,mm},'fontsize',15)
```

```
    set(AX(2),'XTickLabel',{aa,bb,cc,dd,ee,ff,gg,hh,ii,jj,kk,ll,mm},'fontsize',15)
end
if N==7
    set(AX(1),'XTickLabel',{aa,bb,cc,dd,ee,ff,gg,hh,ii,jj,kk,ll,mm,nn,oo},'fontsize',15)
    set(AX(2),'XTickLabel',{aa,bb,cc,dd,ee,ff,gg,hh,ii,jj,kk,ll,mm,nn,oo},'fontsize',15)
end
```

B.2.19 Plot_TEG_Results.m

```
function
Plot_TEG_Results(t,C_TEG,t_end_axis,dt_axis,N,aa,bb,cc,dd,ee,ff,gg,hh,ii,jj,kk,ll,mm,nn,o
o,pp,qq)
%User-defined function:
%This plot applies to the TEG, when it is ON/OFF.

plot(t,C_TEG,'-rd','LineWidth',2,'MarkerSize',4,'MarkerFaceColor','r')
title('TEG''s ON/OFF status','fontsize',23)
axis([0 t_end_axis -0.25 1.25])
xlabel('Time of Day, HRS','fontsize',18)
ylabel('ON/OFF','fontsize',18)
set(gca,'XTick',0:dt_axis:t_end_axis)
set(gca,'YTick',0:1:1)
grid on

% X-Axis stuff
if N==1

set(gca,'XTickLabel',{aa,bb,cc,dd,ee,ff,gg,hh,ii,jj,kk,ll,mm,nn,oo,pp,qq},'fontsize',15)
end
if N==2

set(gca,'XTickLabel',{aa,bb,cc,dd,ee,ff,gg,hh,ii,jj,kk,ll,mm,nn,oo,pp,qq},'fontsize',15)
end
if N==3
    set(gca,'XTickLabel',{aa,bb,cc,dd,ee,ff,gg,hh,ii,jj,kk,ll,mm},'fontsize',15)
end
if N==4

set(gca,'XTickLabel',{aa,bb,cc,dd,ee,ff,gg,hh,ii,jj,kk,ll,mm,nn,oo,pp,qq},'fontsize',15)
end
if N==5
    set(gca,'XTickLabel',{aa,bb,cc,dd,ee,ff,gg,hh,ii,jj,kk},'fontsize',15)
end
if N==6
    set(gca,'XTickLabel',{aa,bb,cc,dd,ee,ff,gg,hh,ii,jj,kk,ll,mm},'fontsize',15)
end
if N==7
    set(gca,'XTickLabel',{aa,bb,cc,dd,ee,ff,gg,hh,ii,jj,kk,ll,mm,nn,oo},'fontsize',15)
end
```

References

[1] U.S. Energy Information Administration, "Renewable Energy Explained," 2011, URL: http://www.eia.gov/energyexplained/index.cfm?page=renewable_home [cited 08 June 2011].

[2] U.S. Department of Energy, Office of Energy Efficiency and Renewable Energy, "Renewable Energy Technologies," 31 May 2011, URL: http://www.eere.energy.gov/basics/renewable_energy/ [cited 12 July 2011].

[3] Selley, R. C., *Elements of Petroleum Geology*, 2nd ed., Academic Press, California, 1998, Chapter 5, Figure 5.11.

[4] Gluyas, J., and Swarbrick, R., *Petroleum Geoscience*, 1st ed., Blackwell Publishing, Massachusetts, 2004, Chapter 4, Figure 4.13.

[5] U.S. Environmental Protection Agency, "Greenhouse Gas Emissions," 20 April 2011, URL: http://epa.gov/climatechange/emissions/ [cited 25 July 2011].

[6] U.S. Energy Information Administration, "Environment: Emissions of Greenhouse Gases," *Annual Energy Review 2009*, Chapter 12, Table & Figure 12.1, 19 August 2010, URL: http://www.eia.gov/emeu/aer/envir.html; PDF: http://www.eia.gov/emeu/aer/pdf/pages/sec12.pdf [cited 16 May 2011].

[7] U.S. Energy Information Administration, "Energy Explained: Coal – Coal and the Environment," 08 July 2011, URL: http://www.eia.gov/energyexplained/index.cfm?page=coal_environment [cited 25 July 2011].

[8] U.S. Environmental Protection Agency, "Climate Change: Science – State of Knowledge," 14 April 2011, URL: http://www.epa.gov/climatechange/science/stateofknowledge.html [cited 25 July 2011].

[9] U.S. Energy Information Administration, "Levelized Cost of New Generation Resources in the Annual Energy Outlook 2011," *Annual Energy Outlook 2011*, Table 1, 26 April 2011, URL: http://www.eia.gov/oiaf/aeo/electricity_generation.html; PDF: http://www.eia.gov/oiaf/aeo/pdf/2016levelized_costs_aeo2011.pdf [cited 10 July 2011].

[10] U.S. Energy Information Administration, "Energy Explained: Electricity – Electricity in the United States," 21 July 2011, URL: http://www.eia.gov/energyexplained/index.cfm?page=electricity_in_the_united_states [cited 25 July 2011].

[11] U.S. Energy Information Administration, "Market Trends," *Annual Energy Outlook 2011*, Section IV, 26 April 2011, URL: http://www.eia.gov/forecasts/aeo/index.cfm; PDF: http://www.eia.gov/forecasts/aeo/pdf/0383%282011%29.pdf [cited 08 July 2011].

[12] Chen, G., *Nanoscale Energy Transport and Conversion: A Parallel Treatment of Electrons, Molecules, Phonons, and Photons*, 1st ed., Oxford University Press, New York, 2005, Chapter 8.

[13] Lampinen, M. J., "Thermodynamic Analysis of a Thermoelectric Generator," *Journal of Applied Physics*, Vol. 69, No. 8, 1991, pp. 4318-4323.

[14] Figliola, R. S., and Beasley, D. E., *Theory and Design for Mechanical Measurements*, 3rd ed., John Wiley & Sons, Inc., 2000, Chapter 8.

[15] Bell, L. E., "Cooling, Heating, Generating Power, and Recovering Waste Heat with Thermoelectric Systems," *Science*, Vol. 321, No. 5895, 2008, pp. 1457-1461.

[16] Sales, B. C., "Thermoelectric Materials – Smaller is Cooler," *Science*, Vol. 295, No. 5558, 2002, pp. 1248-1249.

[17] Deng, Y. G., and Liu, J., "Recent Advances in Direct Solar Thermal Power Generation," *Journal of Renewable and Sustainable Energy*, Vol. 1, No. 5, 2009.

[18] Rowe, D. M., "Thermoelectrics, An Environmentally-Friendly Source of Electrical Power," *Renewable Energy*, Vol. 16, No. 1-4, 1999, pp. 1251-1256.

[19] DiSalvo, F. J., "Thermoelectric Cooling and Power Generation," *Science*, Vol. 285, No. 5428, 1999, pp. 703-706.

[20] Watts, P. C., Townsend and Townsend and Crew LLP, San Francisco, CA, U.S. Patent Application for a "Thermoelectric Generator," Patent Application No. 20090301541, published 10 Dec. 2009.

[21] Watts, P. C., Watts Thermoelectric LLC, Private communication.

[22] Saqr, K. M., and Musa, M. N., "Critical Review of Thermoelectrics in Modern Power Generation Applications," *Thermal Science*, Vol. 13, No. 3, 2009, pp. 165-174.

[23] Hendricks, T., and Choate, W. T., "Engineering Scoping Study of Thermoelectric Generator Systems for Industrial Waste Heat Recovery," Industrial Technologies Program, U.S. Department of Energy, November 2006.

[24] Kalogirou, S. A., "Solar thermal collectors and applications," *Progress in Energy and Combustion Science*, Vol. 30, No. 3, 2004, pp. 231-295.

[25] U.S. Department of Energy, Office of Energy Efficiency and Renewable Energy, "Energy Savers: Solar Water Heaters," URL: http://www.energysavers.gov/your_home/water_heating/index.cfm/mytopic=12850 [cited 09 January 2011].

[26] Solene Solar Hot Water Systems, URL: http://www.solene.com/ [cited 20 January 2011].

[27] California Center for Sustainable Energy, "Solar Water Heating: Basics for Homeowners," URL: https://energycenter.org/index.php/incentive-programs/self-generation-incentive-program/sgip-documents/doc_download/6-solar-water-heating-basics-for-homeowners [cited 20 January 2011].

[28] National Renewable Energy Laboratory RREDC, USAF #725370 – Detroit Metropolitan Airport (DTW), *National Solar Radiation Data Base* [online database], URL: http://rredc.nrel.gov/solar/old_data/nsrdb/1991-2005/ [cited 07 March 2011].

[29] National Oceanic and Atmospheric Administration NESDIS, WBAN Station #94847 – Detroit Metro Wayne County Airport (DTW), *Online Climate Data Directory: U.S.--Local Climatological Data* [online database], URL: http://www.ncdc.noaa.gov/oa/climate/climatedata.html#hourly [cited 17 March 2011].

[30] Goswami, D. Y., Kreith, F., and Kreider, J. F., *Principles of Solar Engineering*, 2nd ed., Taylor & Francis, Pennsylvania, 1999, Chapter 2.

[31] Howell, J. R., Bannerot, R. B., and Vliet, G. C., *Solar-Thermal Energy Systems: Analysis and Design*, 1st ed., McGraw-Hill, Inc., New York, 1982, Chapters 3, 10.

[32] Moin, P., *Fundamentals of Engineering Numerical Analysis*, 1st ed., Cambridge University Press, New York, 2001, Chapters 2, 4.

[33] Duffie, J. A., and Beckman, W. A., *Solar Engineering of Thermal Processes*, 2nd ed., John Wiley & Sons, Inc., New York, 1991, Chapter 8.

[34] Schmidt, P. S., Ezekoye, O. A., Howell, J. R., Baker, D. K., *Thermodynamics: An Integrated Learning System*, 1st ed., John Wiley & Sons, Inc., 2006, Chapters 8, 11.

[35] Banks, D., *An Introduction to Thermogeology: Ground Source Heating and Cooling*. 1st ed., Blackwell Publishing, Oxford UK, 2008, Chapters 3, 4, 6, 8.

[36] U.S. Energy Information Administration, "Geothermal Heat Pump Manufacturing Activities 2009," *Renewable Energy Annual 2009*, December 2010, URL: http://www.eia.gov/cneaf/solar.renewables/page/ghpsurvey/ghpssurvey.html; PDF: http://www.eia.gov/cneaf/solar.renewables/page/ghpsurvey/geothermalrpt.pdf [cited 11 July 2011].

[37] Power Panel Inc., URL: http://www.powerpanel.com/.

[38] Schultz, G., Power Panel Inc., Private communication.

[39] Helms, M., Nextek Power Systems, Private communication.

[40] U.S. Environmental Protection Agency, "eGRID2010 Version 1.1," *The Emissions & Generation Resource Integrate Database (eGRID)* [online database], URL: http://www.epa.gov/cleanenergy/energy-resources/egrid/index.html [cited 24 May 2011].

[41] U.S. Energy Information Administration, "Voluntary Reporting of Greenhouse Gas Programs: Emission Factors and Global Warming Potentials," Table 1, 28 April 2011, URL: http://www.eia.gov/oiaf/1605/emission_factors.html; XLS: http://www.eia.gov/oiaf/1605/excel/Fuel_Emission_Factors.xls [cited 21 June 2011].

[42] U.S. Department of Labor, Bureau of Labor Statistics, Consumer Price Index: CPI Databases, *All Urban Consumers: CPI* [online database], URL: http://www.bls.gov/cpi/data.htm [cited 15 July 2011]

[43] U.S. Department of Energy, Office of Energy Efficiency and Renewable Energy, "2008 Geothermal Technologies Market Report," Figure 20, July 2009, URL: http://www.nrel.gov/analysis/pdfs/46022.pdf [cited 12 July 2011].

[44] California Energy Commission, "Renewable Energy Cost of Generation Update," Table 14, August 2009, URL: http://www.energy.ca.gov/2009publications/CEC-500-2009-084/CEC-500-2009-084.PDF [cited 13 July 2011].

[45] U.S. Energy Information Administration, *Electric Power Monthly: July 2011 Edition*, Chapter 5, Table 5.3, 20 July 2011, URL: http://www.eia.gov/cneaf/electricity/epm/epm_sum.html; PDF: http://www.eia.gov/cneaf/electricity/epm/epm.pdf [cited 23 July 2011].

Vita

Adolfo Lozano III graduated from the Science Academy of South Texas in May 2004. He pursued his undergraduate studies at the University of Texas Pan American under the full tuition and fees *University Scholars Program*, graduating summa cum laude with a Bachelor of Science in Mechanical Engineering in May 2008. He worked as a mathematics tutor at the university's Learning Assistance Center throughout his undergraduate career. In August 2009, he commenced his graduate studies at the University of Texas at Austin with the *South Texas Graduate School Fellowship*, where during his first year he served as a teaching assistant for ME 326 Thermodynamics under Dr. Philip S. Schmidt, and was awarded the *H. Grady Rylander Longhorn Mechanical Engineering Club Excellence in Teaching Fellowship* in May 2010. In August 2010, he joined the Webber Energy Group, headed by Dr. Michael E. Webber. He is expected to graduate with a Master of Science in Engineering in August 2011. His past professional experience includes a summer internship with Ford Motor Company in Dearborn, MI, a two-term cooperative education assignment (co-op) with Northrop Grumman – Electronic Systems in Linthicum, MD, and a summer internship with the Air Force Research Laboratory at Wright-Patterson Air Force Base, OH. Upon graduation, he is expected to begin working for Raytheon – Space and Airborne Systems in El Segundo, CA.

Permanent email: adolfo.lozano@utexas.edu; adolfo.lozano@live.com

This thesis was typed by the author.